

---

# **Characterisation of Inter-subunit Interactions within Cardiac Ryanodine Receptor**

**Monika Seidel**

Thesis submitted for the award of Philosophiae Doctor

Institute of Molecular & Experimental Medicine  
Cardiff University School of Medicine

## **DECLARATION**

This work has not been submitted in substance for any other degree or award at this or any other university or place of learning, nor is being submitted concurrently in candidature for any degree or other award.

Signed .....

Date .....

## **STATEMENT 1**

This thesis is being submitted in partial fulfilment of the requirements for the degree of PhD

Signed .....

Date .....

## **STATEMENT 2**

This thesis is the result of my own independent work/investigation, except where otherwise stated. Other sources are acknowledged by explicit references. The views expressed are my own.

Signed .....

Date .....

## **STATEMENT 3**

I hereby give consent for my thesis, if accepted, to be available for photocopying and for inter-library loan, and for the title and summary to be made available to outside organisations.

Signed .....

Date .....

## **ACKNOWLEDGMENTS**

First and foremost I would like to thank my supervisors Professor F. Anthony Lai and Doctor Spyros Zissimopoulos for providing me with the opportunity to conduct this work. I am very grateful to Prof Anthony Lai for his support during writing of this thesis, mainly for his countless efforts to persuade me into staying calm (very challenging) and carrying on. Neither the work presented here nor the completion of this thesis itself would have been possible without Dr Spyros Zissimopoulos. I am greatly indebted to him for his scientific expertise which was invaluable, time and for never-ending enthusiasm. His optimism was contagious and kept me going in times when results of my experiments were uninterpretable. I would also like to thank him for his maddening attention to detail which made me just a bit closer to conceiving the concept of using articles in English. And finally, for being my friend.

I would also like to thank Dr Lowri Thomas for her input into my research, Dr Christopher H. George for his kind help and Dr Philip James for his support and invaluable advice.

I am very grateful to all the people that made my everyday life in the laboratory pleasurable and filled with laughter; Vryonia Vasilakopoulou, Chloe Maxwell, Joao Bigares, Sara Seifan, Cedric Viero, Rienk Doetjes, Peter Willson, Ioannis Ladas, Brian Calver, Katherine Connolly, Gareth Willis, Phillip Freeman and many more. I would also like to thank Ewelina Sagan with whom I shared my moments of joy and despair and who became my close friend. I am also greatly indebted to Magdalena Laugsch.

Finally I would like to thank my family for their continuous support. I am very grateful to my partner Mark for his help, infinite amount of patience and his ability to withstand my countless psychotic episodes. Most of all, I would like to thank my beloved daughter Katja for making me leave all my problems behind, back in the laboratory.

## SUMMARY

Ryanodine receptors (RyRs) are the largest known ion channels composed of four identical subunits. Interactions between structural/functional domains have been proposed to regulate channel activity and play an important role in the pathogenesis of RyR-associated disorders. RyR2 mediates the release of calcium from sarcoplasmic reticulum of cardiac myocytes and its dysfunction is associated with life-threatening arrhythmias.

The principal aim of this study was to characterise the self-association of the RyR2 N-terminus biochemically and evaluate its impact on channel function. Moreover, its role in channel dysfunction observed in arrhythmia-susceptible individuals was tested together with dantrolene's ability to rescue the disease phenotype.

RyR2 N-terminus self-association is mediated by multiple sites with two critical oligomerisation determinants located in the loops connecting strands  $\beta$ 8- $\beta$ 9 and  $\beta$ 20- $\beta$ 21, predicted to reside at the inter-subunit interface. N-terminus self-association is further stabilised by disulphide bonds most likely involving multiple cysteine residues with cysteine 361 contributing to this process.

Normal N-terminal inter-subunit interactions within the full-length RyR2 appear to prevent spontaneous activation of the channel at diastolic calcium. Channel hypersensitivity is a common feature of the arrhythmia-associated phenotype suggesting that abnormal N-terminus self-interaction might be involved in RyR2 pathology. Indeed the presence of arrhythmia-linked mutations (L433P and R176Q) compromises the ability of the RyR2 N-terminus to oligomerise.

Defective N-terminus self-association appears to underlie the functional impairment of RyR2<sup>L433P</sup>. The mutated channel displays compromised [<sup>3</sup>H]ryanodine binding and reduced stability of tetrameric assembly, both of which can be rescued by dantrolene at clinically relevant concentrations. Notably, dantrolene's primary mode of action appears to involve stabilisation of the N-terminal inter-subunit interactions.

In summary, the work presented here provides important insights into a novel domain-domain interaction and its role in the regulation of RyR2 function.

# Contents

Title.....	I
Declaration.....	II
Acknowledgements.....	III
Summary.....	IV
Table of contents.....	V

## Table of contents

1 General Introduction .....	2
1.1 Calcium signalling components .....	2
1.2 Ryanodine receptor isoforms.....	6
1.3 Ryanodine receptor structure.....	8
1.3.1 Primary sequence motifs .....	9
1.3.2 Three-dimensional architecture.....	12
1.3.3 Transmembrane domains and the pore region .....	14
1.4 RyR and excitation-contraction coupling .....	16
1.5 RyR regulation .....	19
1.5.1 Calcium, magnesium and ATP .....	19
1.5.2 Calmodulin.....	22
1.5.3 Other EF-hand proteins: sorcin and S100A1 .....	23
1.5.4 SR proteins: calsequestrin, triadin and junctin.....	24
1.5.5 FK506-Binding Proteins (FKBP).....	25
1.5.6 Phosphorylation .....	27

1.5.7	Redox modifications .....	28
1.5.8	Pharmacological modulation of RyR .....	33
1.6	RyR-associated disorders .....	37
1.6.1	RyR1-associated disorders .....	37
1.6.2	RyR2-associated disorders .....	41
1.6.2.1	Mechanism of channel dysfunction .....	50
1.6.2.2	Existing therapies.....	54
1.7	RyR – an allosteric protein.....	57
1.7.1	N-terminal – central domain interactions.....	58
1.7.2	Interactions within central domains .....	61
1.7.3	Central and C-terminal domain interface .....	62
1.7.4	Interaction within C-terminal domains .....	64
1.7.5	Interaction between RyR tetrameric complexes .....	66
1.8	Hypothesis and Aims.....	68
2	Materials and Methods.....	71
2.1	Materials .....	71
2.1.1	Molecular biology .....	71
2.1.2	Protein biochemistry .....	72
2.1.2.1	Sucrose density gradient ultracentrifugation .....	74
2.1.2.2	[ <sup>3</sup> H]ryanodine binding .....	74
2.1.3	Yeast culture.....	75
2.1.4	Bacterial culture .....	76
2.1.5	Mammalian cell culture.....	76
2.1.6	Oligonucleotides .....	77
2.1.7	Plasmid Vectors .....	77
2.2	Methods .....	86
2.2.1	Molecular biology methods .....	86

2.2.1.1	Standard PCR.....	86
2.2.1.2	DNA sequencing.....	87
2.2.1.3	DNA digestion with restriction endonucleases.....	88
2.2.1.4	DNA ligation.....	88
2.2.1.5	Agarose gel electrophoresis .....	89
2.2.1.6	Mutagenesis .....	89
2.2.1.7	Introducing deletions into plasmid DNA.....	90
2.2.1.8	Electroporation of bacteria.....	93
2.2.1.9	Chemical transformation of bacteria.....	94
2.2.1.10	Colony screen and plasmid isolation .....	94
2.2.2	Protein Biochemistry Methods.....	95
2.2.2.1	Mammalian cell homogenisation.....	95
2.2.2.2	Determination of protein concentration.....	96
2.2.2.3	Chemical crosslinking.....	96
2.2.2.4	Polyacrylamide gel electrophoresis .....	96
2.2.2.5	Western blotting.....	98
2.2.2.6	Sub-cellular fractionation .....	98
2.2.2.7	Co-immunoprecipitation.....	99
2.2.2.8	Sucrose density gradient ultracentrifugation .....	99
2.2.2.9	[ <sup>3</sup> H]ryanodine binding .....	100
2.2.3	Yeast two-hybrid system.....	101
2.2.3.1	Yeast Culture .....	101
2.2.3.2	Yeast transformation.....	101
2.2.3.3	$\beta$ -galactosidase colony-lift filter assay .....	102
2.2.3.4	Quantitative liquid $\beta$ -galactosidase assay .....	102
2.2.3.5	Cell homogenisation and protein extraction .....	103
2.2.4	Bacterial Culture .....	104

2.2.4.1	Culture maintenance .....	104
2.2.4.2	Liquid cultures for plasmid isolation.....	104
2.2.4.3	Generation of electrocompetent cells .....	105
2.2.5	Mammalian Cell Culture.....	105
2.2.5.1	HEK293 cell maintenance .....	105
2.2.5.2	Transfection .....	106
2.2.5.3	Long term storage .....	106
3	Identification of cysteines involved in the tetramerisation of the RyR2 N-terminus.....	109
3.1	Introduction .....	109
3.2	Methods .....	115
3.2.1	Site-directed mutagenesis approach.....	115
3.2.1.1	Chemical crosslinking.....	117
3.2.2	Mass spectrometry approach.....	118
3.2.2.1	Immunoprecipitation.....	118
3.2.2.2	Sample preparation for mass spectrometry.....	120
3.3	Results .....	121
3.3.1	Site-directed mutagenesis.....	121
3.3.1.1	Cysteines: 36, 244, 548, 577, 633, 736, 757 and 758 are not involved in disulphide bond formation .....	122
3.3.1.2	Cysteines mutants BT4L <sup>C361S</sup> , BT4L <sup>C501S</sup> and BT4L <sup>C615/618/620S</sup> display variable behaviour .....	124
3.3.1.3	The combined mutants suggest an important role of cysteine 361 in the formation of disulphide bond-mediated tetramers .....	124
3.3.1.4	Chemical crosslinking of BT4L <sup>C361S</sup> suggests additional disulphide-independent role of cysteine 361in tetramer formation .....	126
3.3.2	Mass spectrometry .....	128
3.3.2.1	Immunoprecipitation.....	128

3.3.2.2	Spectral analysis .....	131
3.4	Discussion .....	134
3.4.1	Cysteines involved in disulphide bond formation do not reside in the BT4L N- and C-terminus .....	134
3.4.2	The elusive role of cysteine 361 in the oligomerisation process .....	135
3.4.3	DTT-sensitive tetramers – alternative models of interaction .....	136
3.4.4	Location of putative cysteine residues – feasibility of disulphide bond formation.....	138
3.4.5	Disulphide bond formation – experimental artifact? .....	141
3.4.6	Concluding remarks .....	143
4	Determinants of RyR2 N-terminus tetramerisation .....	145
4.1	Introduction .....	145
4.2	Methods .....	151
4.2.1	Generation of the truncated BT4Δ12 construct.....	151
4.2.2	Generation of internal deletion mutants.....	152
4.2.3	Chemical crosslinking.....	152
4.2.4	Co-immunoprecipitation .....	153
4.3	Results .....	154
4.3.1	The BT4Δ12 displays a unique oligomerisation pattern.....	155
4.3.2	Deletion of the SPRY β5-β6 loop has no effect on the tetramerisation process	156
4.3.3	Deletion of the β22-β23 loop has no effect on the tetramerisation process	157
4.3.4	Deletion of the β8-β9 loop impairs oligomerisation .....	159
4.3.5	Deletion of the β20-β21 loop changes oligomerisation pattern .....	162
4.4	Discussion .....	163
4.4.1	The elusive role of SPRY domain in the inter-subunit interaction ....	164
4.4.2	Oligomerisation intermediates .....	166

4.4.3	The role of the loops located at the putative inter-subunit interface...	167
4.4.4	Final remarks.....	169
5	Dissecting the role of N-terminus in RyR2 function .....	172
5.1	Introduction .....	172
5.2	Methods .....	173
5.2.1	Sub-cellular fractionation.....	173
5.2.2	[ <sup>3</sup> H]ryanodine binding assay .....	174
5.3	Results .....	175
5.3.1	The BT4L fragment interacts with the full length RyR2 .....	175
5.3.2	The BT4L fragment activates RyR2 at diastolic Ca <sup>2+</sup> .....	176
5.4	Discussion .....	177
6	The effect of arrhythmia-linked mutations on RyR2 N-terminus self-association	
	181	
6.1	Introduction .....	181
6.2	Methods .....	185
6.2.1	Generation of the BT4L <sup>R176Q</sup> and the BT4L <sup>L433P</sup> .....	185
6.2.2	Chemical crosslinking.....	186
6.2.3	Co-immunoprecipitation .....	187
6.2.4	Yeast two-hybrid system.....	187
6.2.5	Sub-cellular fractionation.....	188
6.3	Results .....	189
6.3.1	Arrhythmia-linked mutations reduce N-terminus self-association ....	190
6.3.2	The formation of mixed oligomers is severely compromised in the presence of the L433P mutation .....	193
6.3.3	The L433P mutation perturbs RyR2 N-terminus oligomerisation <i>in situ</i> (yeast two-hybrid system).....	195
6.3.4	Dantrolene partially reverses the effects of the L433P mutation.....	198

6.3.5	Arrhythmia-linked mutations affect BT4L interaction with the full length channel .....	202
6.4	Discussion .....	204
6.4.1	Oligomerisation of RyR2 N-terminus is affected by arrhythmia-linked mutations.....	205
6.4.2	Dantrolene .....	208
6.4.3	Compromised association between exogenous N-terminus and RyR2 containing arrhythmia-linked mutations .....	210
6.4.4	Final remarks.....	210
7	Further insights into the L443P mutation .....	213
7.1	Introduction .....	213
7.2	Methods .....	214
7.2.1	[ <sup>3</sup> H]ryanodine binding assay – RyR2 <sup>WT</sup> versus RyR2 <sup>L433P</sup> .....	214
7.2.2	[ <sup>3</sup> H]ryanodine binding assay – evaluating the effect of the BT4L fragment	215
7.2.3	Sucrose density gradient ultracentrifugation.....	215
7.2.4	[ <sup>3</sup> H]ryanodine binding assay - dantrolene effect.....	216
7.3	Results .....	216
7.3.1	RyR2 <sup>L433P</sup> displays unique calcium dependence of [ <sup>3</sup> H]ryanodine binding	216
7.3.2	RyR2 <sup>L433P</sup> calcium sensitivity remains unchanged in the presence of the BT4L fragment .....	219
7.3.3	RyR2 <sup>L433P</sup> channels dissociate into monomers upon sucrose density gradient centrifugation.....	221
7.3.4	Dantrolene increases tetramer stability .....	222
7.3.5	Dantrolene changes RyR <sup>L433P</sup> ryanodine binding profile.....	224
7.4	Discussion .....	225
8	Closing remarks .....	229

I	Appendix: List of abbreviations .....	235
II	Appendix: Bibliography .....	239

# Chapter 1

## General Introduction

# 1 General Introduction

Calcium ions ( $\text{Ca}^{2+}$ ) constitute one of the most versatile signalling molecules in living systems. The ability of  $\text{Ca}^{2+}$  to fulfil its diverse functions lies upon the fact that its concentration exhibits high level of spatial and temporal dynamics within the cell. In multicellular organisms, the versatility of calcium signals is further expanded by a unique expression profile of calcium signalling proteins within each cell type. Physiological signals involving calcium are characterised by brief pulses of  $\text{Ca}^{2+}$  generated in the cytoplasm by ion fluxes from the extracellular medium and/or intracellular stores. Transient increase in the cytoplasmic calcium triggers a signalling cascade which regulates many different cellular functions (Berridge *et al.* 2003). The triggered response directly depends on the duration, amplitude, frequency and the location of the calcium transient (Taylor and Tovey 2010). The ultimate challenge is to assure that calcium levels are under rigorous control. This is pivotal for calcium to perform its signalling role and to prevent cell damage associated with prolonged calcium elevation.

## 1.1 Calcium signalling components

The extracellular medium of multicellular organism contains free calcium at the concentration four orders of magnitude higher than the level found within the cell cytoplasm. The low intracellular level of  $\text{Ca}^{2+}$  prevents its precipitation in the form of phosphate salts and allows small changes of calcium levels to fulfil its signalling role with minimal expenditure of cell energy.

Eukaryotic cells contain a number of molecules which are able to bind calcium ions and therefore regulate its intracellular concentration. These include non-specific calcium buffers such as membrane phospholipids and inorganic phosphates and a discrete group of proteins evolved to bind calcium in a highly selective manner. Within this specialised class of proteins, only a small minority function as calcium buffers *per se* (e.g. parvalbumin, calbindin, calretinin (Krebs and Michalak 2007)), the majority regulates calcium levels by actively transporting the ions between extracellular and intracellular compartments. The removal of  $\text{Ca}^{2+}$  from the cytoplasm

into the extracellular space or/and intracellular stores is performed by calcium pumps and exchangers. Calcium ATPase pumps are characterised by relatively low transport rates but high affinities allowing them to respond to modest elevations in  $\text{Ca}^{2+}$  levels (Berridge et al. 2003). These pumps reside in the plasma membrane (PMCA, plasma membrane  $\text{Ca}^{2+}$ -ATPase), in the membrane of sarco/endoplasmic reticulum (SERCA, sarco/endoplasmic reticulum  $\text{Ca}^{2+}$ -ATPase) and in the Golgi membranes (SPCA, secretory pathway  $\text{Ca}^{2+}$ -ATPase) (Krebs and Michalak 2007). In the circumstances when large quantities of calcium are released in the cytoplasm,  $\text{Ca}^{2+}$  removal is undertaken by plasma membrane sodium/calcium exchanger (NCX) which exhibits a low affinity for  $\text{Ca}^{2+}$  but a very high transport rate (Berridge 2012). NCX extrudes one calcium ion in exchange for three sodium ions; however, in specific conditions such as high cytoplasmic sodium concentration and positive membrane potential, the exchanger can work in an opposite direction allowing calcium inward transient (Bers 2002). Calcium influx is also mediated by a distinct type of sodium/calcium exchanger (NCLX; sodium/calcium/lithium exchanger) located in the inner membrane of mitochondria and suggested to be critically involved in calcium shuttling between intracellular compartments (Palty et al. 2012). Calcium influx into mitochondria is supported by mitochondrial calcium uniporter (MCU) which has been proposed to have a substantial contribution into  $\text{Ca}^{2+}$  extrusion pathway in the event of prolong and superphysiological  $\text{Ca}^{2+}$  elevations (Williams et al. 2013).

The rise in cytoplasmic calcium triggers a number of cellular responses and therefore in physiological conditions, calcium influx is rigorously controlled and occurs only in response to a specific stimulus. One of such stimuli is a change in the cell membrane potential which activates calcium channels located in the plasma membrane (VGCC, voltage-gated calcium channels). These channels transfer  $\text{Ca}^{2+}$  from extracellular space and regulate a number of downstream events including cell excitability, contraction, hormonal secretion and gene transcription. Voltage-gated calcium channels are divided into five groups displaying not only different pharmacological and biophysical properties but also developmental and tissue-specific expression pattern (Krebs and Michalak 2007). The L-type  $\text{Ca}^{2+}$  channels, which are activated by high voltage, are major players in the excitation-contraction (EC) coupling triggering the release of calcium from sarcoplasmic reticulum of skeletal and cardiac myocytes thus enabling muscle contraction. In some cell types however the primary role of L-

type channels is to provide an inward calcium transient for the generation and/or regulation of action potentials (Krebs and Michalak 2007). T-type  $\text{Ca}^{2+}$  channels are characterised by low voltage activation profile, transient nature and small amplitude of the produced calcium current. They significantly contribute to cardiac automaticity, excitation-contraction coupling and have been shown to play a crucial role in cardiac hypertrophy (Ono and Iijima 2010). The remaining three groups, i.e. N, P/Q, and R-type channels are primarily expressed in neurons and regulate neurotransmitter release (Catterall 2000).

Calcium entry via plasma membrane is also triggered by signalling molecules including extracellular ligands binding to receptor-operated channels and internal messengers which activate second-messenger-operated channels (Berridge *et al.* 2003). The influx of calcium from the extracellular space remains tightly coupled to the intracellular availability of  $\text{Ca}^{2+}$  in internal stores, i.e. sarcoplasmic/endoplasmic reticulum (ER/SR). This so called store-operated  $\text{Ca}^{2+}$  entry (SOCE) is the major mechanism of calcium entry in nearly all non-excitable cells which primary role is to rapidly refill depleted ER (Collins *et al.* 2013). However, SOCE has been now recognised to exist in excitable cells and proposed to play an important role in skeletal and cardiac muscle pathologies (Hunton *et al.* 2002; Eltit *et al.* 2013). The two components of SOCE pathway include stromal interaction protein 1 (STIM1) which resides in the SR/ER and Orai1 forming a highly selective calcium channel within the plasma membrane (Muik *et al.* 2012). Upon internal store depletion, STIM1 oligomerises and translocates to the cell periphery in close proximity to the plasma membrane where it activates Orai channels.

In addition to the extracellular medium, cells also use internal sources for calcium signalling. The principal intracellular calcium store is located in the endoplasmic/sarcoplasmic reticulum, where total  $\text{Ca}^{2+}$  is estimated to be in excess of 2mM. The free calcium concentration is considerably lower due to the buffering properties of ER/SR-resident proteins including calreticulin, glucose-regulated protein 94, immunoglobulin binding protein and calsequestrin (Krebs and Michalak 2007). Calcium release is mediated through two types of calcium-sensitive channels: inositol 1,4,5-trisphosphate receptors ( $\text{IP}_3\text{R}$ ) and ryanodine receptors (RyR). The two types of receptors, although only ~30% identical in primary sequence, share substantial structural homology and display surprisingly high conservation of

structure-function relationship (Seo *et al.* 2012). Ryanodine receptors, which exist as large homotetrameric complexes, are essential determinants of excitation-contraction coupling in skeletal and heart muscle and will be discussed in detail in subsequent sections. IP<sub>3</sub> receptors are ubiquitously expressed and control a variety of calcium-dependent processes including cell proliferation and differentiation, fertilisation, immune responses, brain function etc. (Mikoshiba 2007). IP<sub>3</sub> receptors are activated by inositol 1,4,5 triphosphate (IP<sub>3</sub>) produced by phospholipase C in response to the stimulation of G protein-coupled receptors or tyrosine kinase receptors located at the plasma membrane (Patterson *et al.* 2004). The binding of IP<sub>3</sub> increases the sensitivity of the receptor to calcium and triggers Ca<sup>2+</sup> release from the ER further stimulating the channel. However, eventually IP<sub>3</sub>R-mediated Ca<sup>2+</sup> release leads to channel inactivation as high calcium concentration inhibits the receptor (Berridge *et al.* 2003). The release of calcium from ER has also been suggested to be coupled to the activation of the two-pore channels (TPC) located on acidic organelles such as lysosomes (Patel and Brailoiu 2012). It has been proposed that TP channels respond to NAADP (nicotinic acid dinucleotide phosphate) by releasing Ca<sup>2+</sup> from acidic stores (Patel *et al.* 2011). This is thought to lead to the local increase in calcium concentration which stimulates RyR and IP<sub>3</sub>R located in close proximity triggering larger Ca<sup>2+</sup> release events (Kilpatrick *et al.* 2013).

The intracellular rise in calcium regulates a number of distinct cellular processes. The end effect of Ca<sup>2+</sup> signal is defined by its spatiotemporal characteristics and by the expression profile of proteins involved in signal processing. These proteins fulfil three functions essential for the activation of downstream processes, i.e. they bind calcium, decode the information and convey the signal to respective targets. The most prevalent calcium binding motif is composed of helix-loop-helix motif also known as EF-hand and is found in proteins such as calmodulin, troponin C, S100 and many others. Most EF-hand proteins contain an even number of EF-hands which occur in pairs as tandem repeats, however some exceptions from this rule exist such as in the recently identified penta-EF subfamily (Krebs and Michalak 2007). Moreover, some calcium sensors such as annexins do not contain the canonical EF-hand motif all together but bind calcium using unique and discontiguous calcium-coordinating residues contained within internally repeated  $\alpha$ -helical domain (Morgan *et al.* 2004).

Calcium is one of the most versatile signalling molecules involved in diverse signalling pathways. It is indispensable for every cell to fulfil its function, to react to and integrate stimuli originating from within and outside the cell, ultimately being responsible for organism survival. However, calcium has an ambivalent nature; while being essential for life in particular and extreme circumstances it might become a death signal. Moreover, even subtle alterations in calcium signalling result in pathological conditions and have been linked to some of the major diseases in humans. For example abnormal function of ryanodine receptors is associated with heart failure, cardiac myopathies and life-threatening arrhythmias (Marx *et al.* 2000; Priori *et al.* 2001; Tang *et al.* 2012).

## 1.2 Ryanodine receptor isoforms

There are three known mammalian isoforms of RyRs: RyR1, RyR2 and RyR3. The alternative nomenclature of those receptors directly corresponds to the location of their primary identification, i.e.; RyR1 is alternatively called skeletal isoform and was first detected in skeletal muscle (Takeshima *et al.* 1989), RyR2 is also known as cardiac isoform as it was initially found in the cardiac muscle (Nakai *et al.* 1990). RyR3 cDNA was primarily isolated from a brain tissue and, as expected, this isoform was named accordingly (Hakamata *et al.* 1992). An extensive analysis of ryanodine receptor expression pattern revealed that in fact the most abundant isoform in the brain is RyR2 while RyR3 was shown to be widely expressed at relatively low levels in many tissues (Giannini *et al.* 1995; Murayama and Ogawa 1996). Interestingly, different RyR isoforms were reported to be often simultaneously present in the same cell, e.g. RyR2 and RyR3 in cardiomyocytes (Gorza *et al.* 1997), RyR1 and RyR3 in neonatal mammalian skeletal muscles (Yang *et al.* 2001). A concomitant expression of all three isoforms was shown to take place in smooth muscle cells (Löhn *et al.* 2001). Those findings raised the possibility that ryanodine receptors may in fact exist as heterotetrameric channels similar to IP<sub>3</sub> receptors (Monkawa *et al.* 1995). Indeed, in a heterologous expression system, RyR2 was capable of forming functional heterotetrameric channels with RyR1 and RyR3 while RyR1 failed to interact with RyR3, in agreement with earlier observations (Murayama and Ogawa 1997; Flucher

*et al.* 1999; Xiao *et al.* 2002). However, physiological significance of those findings remains to be verified as others did not observe RyR2/RyR3 mixed tetramers in native tissues (Murayama and Ogawa 1996).

The diversity of ryanodine receptors is further extended by the fact that alternatively spliced variants of each isoform have been reported (Table 1.1) (Futatsugi *et al.* 1995; Marziali *et al.* 1996; Tunwell *et al.* 1996). Alternatively spliced RyR variants do not only exhibit tissue- and developmental stage-specific distribution but their unique expression patterns have also been linked to pathological conditions (Kimura *et al.* 2005; Bruno *et al.* 2012). Interestingly, some of the spliced variants, when recombinantly expressed, have been reported to form mixed oligomers not only with their normally-spliced counterparts but also with other isoforms and modulate their function in a dominant negative manner (Jiang *et al.* 2003; George *et al.* 2007).

Genes for the three mammalian isoforms are located on different chromosomes (19q, 1q and 15q for human RyR1, 2 and 3 respectively) and code for proteins of approximately 5000 amino acids which share an overall 65% sequence identity (Lanner *et al.* 2010). The highest degree of sequence diversity maps to three divergent regions; D1 which spans residues 4210-4562, D2: located between residues 1353 and 1397 and D3 containing residues 1852-1890 (coordinates for RyR2). Those divergent regions have been suggested to define functional differences between isoforms. Notably, the D2 region, which is almost completely absent in RyR3, has been suggested to be one of the critical determinants for excitation-contraction coupling in skeletal muscle (Perez *et al.* 2003). The highest degree of sequence homology is located in the extreme C-terminus which contains the pore and is essential for the oligomerisation into functional tetramers (Gao *et al.* 1997; Stewart *et al.* 2003; Lee and Allen 2007).

RyR isoform	Splice variant	Details	Additional information	References
RyR1	ASI (-)	deletion of 5 amino acids (AGDIQ) after residue 3480	foetal variant, exhibits lower activity, upregulated in myotonic dystrophy 1	(Futatsugi et al. 1995; Kimura et al. 2005; Kimura <i>et al.</i> 2007)
RyR1	ASII (-)	deletion of 6 amino acids (VINRQN) after residue 3864		(Futatsugi et al. 1995)
RyR2	24bp	insertion of 8 amino acids (VTGSQRSK) after residue 1479	reduced activity, anti-apoptotic properties	(Tunwell et al. 1996; George et al. 2007)
RyR2	30bp	insertion of 10 amino acids (FAIDSLCGFG) after residue 3715	reduced activity, highly expressed at embryonic stage	(Tunwell et al. 1996; George et al. 2007)
RyR3	ASI (-)	deletion of 5 amino acids (AMQVL) after residue 3335		(Marziali et al. 1996)
RyR3	ASII (-)	deletion of 6 amino acids (LIVRER) after residue 3710		(Marziali et al. 1996)
RyR3	As-8a	deletion of 29 amino acids after residue 4405	does not form functional channels, exclusively expressed in smooth muscles	(Marziali et al. 1996; Jiang et al. 2003)

**Table 1.1** Alternatively spliced variants of RyR

### 1.3 Ryanodine receptor structure

Ryanodine receptors are the largest known ion channels composed of four identical subunits with the C-terminal part comprising the transmembrane domains that form a  $\text{Ca}^{2+}$ -conducting pore. The large N-terminal portion of the protein serves as a scaffold for interaction with accessory proteins, ions and other regulatory molecules. The size of the receptor constitutes a major challenge in structural analysis. Our current knowledge of RyR structure is still limited, however due to the advances in single-particle cryo-electron microscopy (cryo-EM), the availability of crystal structures of some of the receptor domains and information derived from biochemical and spectroscopy-based studies, a more detailed picture of receptor structure is beginning to emerge.

### 1.3.1 Primary sequence motifs

The analysis of the RyR2 primary sequence with the Conserved Domain search tool available at the NCBI website (<http://www.ncbi.nlm.nih.gov/Structure/cdd/wrpsb.cgi>) reveals the presence of structural motifs present in other proteins (Figure 1.1). These domains include: two MIR domains, three SPRY domains, two copies of RIH domain, one RIH-associated domain, four repeats of RyR domain, a pair of EF hand motifs and a domain shared with a putative motility protein. With few exceptions, the functional roles of these domains remain unknown.

SPRY domains are thought to be one of the most common folds in higher eukaryotes, however their role and function is poorly understood (Perfetto *et al.* 2013). They do not possess any enzymatic activity and can be found in proteins of diverse functions. At present SPRY domains are generally believed to be implicated in protein-protein interactions and have been suggested to function as adaptor domains enabling other proteins to be brought into spatial proximity (Woo *et al.* 2006). In RyR1, the second of the three SPRY domains has been shown to bind to the II-III loop of the L-type calcium channel and to mediate inter-domain interactions within the channel itself by binding to residues located towards RyR1 C-terminus (Tae *et al.* 2009a; Tae *et al.* 2009b; Tae *et al.* 2011).

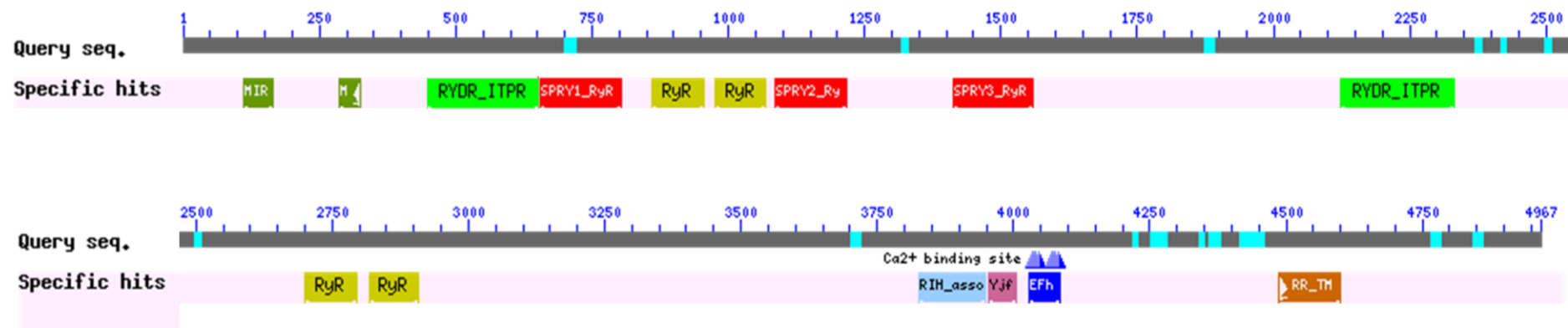


**Figure 1.1** Graphical representation of motifs identified in RyR2 primary sequence (Accession number Q92736) with the NCBI Conserved Domain search tool;

**MIR** (dark green): Domain found in O-mannosyltransferases, IP<sub>3</sub>R and RyR, unknown function

**RYDR\_ITPR or RIH** (light green): the RyR and IP<sub>3</sub>R Homology domain, unknown function

**SPRY** (red): initially identified in *Dictyostelium discoideum* kinase sp1A and RyR, found in three copies in all three RyR isoforms

**RyR** (yellow): Ryanodine receptor domain, found in four copies in all three RyR isoforms

**RIH\_associated** (light blue): RyR and IP<sub>3</sub>R Homology associated

**YjF\_motility protein** (purple): putative motility protein domain; in *Bacillus subtilis* likely to be involved in motility or flagellin production, contains two highly conserved asparagine residues

**EF-hand motif** (dark blue): EF-hand, calcium binding motif, one pair in RyR

**RR\_TM** (orange): 4-6 transmembrane domain region

Recently, two of the RyR domains located in the central portion of the protein and arranged in a tandem repeat, have been crystallised by two independent groups (Sharma *et al.* 2012; Yuchi *et al.* 2012). Consistent with a tandem arrangement, the crystal structure revealed the presence of two symmetrical subdomains connected by a long loop. Notably, a significant portion of this loop was shown to be flexible and contain two previously identified phosphorylation sites (S2808 and S2814 for RyR2) (see Section 1.5.6) thus the proposed name “phosphorylation domain”. Interestingly, incubation of this domain with PKA and CaMKII revealed additional phosphorylation sites which, with one exception, were shown to reside in the connecting loop or its direct proximity (Yuchi *et al.* 2012). Notably, this region is also targeted by eleven mutations associated with RyR1 dysfunction implying an important role of this domain in channel function (see Section 1.6.1). Several prokaryotic proteins also contain similar domains corresponding to either single or tandem repeats (Yuchi *et al.* 2012). Based on the reported crystal structure, a pseudo-atomic model of the two N-terminal RyR domains was generated (Zhu *et al.* 2013). Following FRET-based experiments and computational docking, the authors proposed that those two structurally homologous domains are involved in an inter-subunit interaction.

Marx *et al.* identified three conserved leucine/isoleucine zipper motifs (LZ) in RyR2 sequence and showed that they mediate interaction with phosphatases (PP1 and PP2A) and kinases (PKA) through their respective anchoring proteins (Marx *et al.* 2001a). Two of those motifs are also present in RyR1 (Figure 1.2).

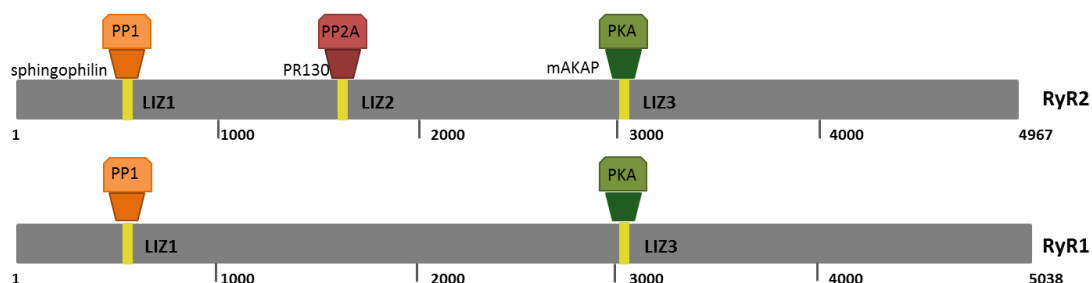


**Figure 1.2** Location of the leucine/isoleucine zipper motifs on RyR2 and RyR1 that bind to leucine zipper motifs on adaptor proteins anchoring phosphatases and kinases

### 1.3.2 Three-dimensional architecture

In the absence of the full length RyR crystal structure, single-particle cryo-EM has provided valuable insights into the architecture of RyR oligomeric assembly (Serysheva *et al.* 2005). Considerable advances in instrumentation and image processing ultimately led to RyR reconstitution maps which reached sub-nanometre resolution allowing to define structural sub-regions within each subunit and predict some of the secondary structure elements (Serysheva *et al.* 2008). Moreover, a systematic comparison of images obtained from channels in an open and closed conformation shed light on global structural changes associated with receptor gating (Samso *et al.* 2009). A combination of cryo-EM-based techniques with the insertion of GFP tags in a defined position within RyR primary sequence allowed assigning the three dimensional location to some of the particularly interesting regions including; DR1 (Liu *et al.* 2002), DR2 (Liu *et al.* 2004), DR3 (Zhang *et al.* 2003b; Jones *et al.* 2008), N-terminal and central domain mutation hot spots (Liu *et al.* 1994; Liu *et al.* 2005; Wang *et al.* 2007) and two putative PKA phosphorylation sites (Meng *et al.* 2007; Jones *et al.* 2008). However, upon emergence of atomic structures of RyR domains determined by X-ray crystallography, it became clear that the location assigned by GFP-based differential mapping should be interpreted with caution as this method was shown to be error prone. Notably, docking of the N-terminal crystal structure into the cryo-EM map of RyR1 (Tung *et al.* 2010) located its position 60Å away from the one assigned with GFP-based differential mapping. Similarly, docking of the crystal structure of the phosphorylation domain (central domain RyR motif repeat) revealed some discrepancies between locations identified by those two techniques (Sharma *et al.* 2012; Yuchi *et al.* 2012).

RyR has a mushroom-like shape with the majority of the protein located in the cytoplasm forming a large cytoplasmic assembly connected to the transmembrane region by a stalk-like structure (Hamilton and Serysheva 2009) (Figure 1.3). The cytoplasmic portion of the functional channel has dimensions of 280 x 280 x 120Å and is composed of clamped-shaped regions located at the corners of the assembly

which are connected to the central rim and to the stalk-like structures. The transmembrane region has dimensions of  $120 \times 120 \times 60\text{\AA}$ .

Docking of the recently crystallised “phosphorylation domain” into the cryo-EM map of the full length receptor placed this domain at the edge of the clamp structures while the RyR1 N-terminus (residues 1-559, rabbit RyR1) was assigned to the centre of the cytoplasmic assembly forming a vestibule around the four-fold axis (Tung et al. 2010) (Figure 1.3). Structurally, the crystallised fragment folds into three separate domains; domain A and B which form two  $\beta$ -trefoil domains and domain C composed of a bundle of five  $\alpha$ -helices (Figure 1.4). Notably, the structure of the amino-terminal region of the IP<sub>3</sub>R1 (residues 1-604, rat IP<sub>3</sub>R1) is strikingly similar to that of RyR1. This IP<sub>3</sub>R1 fragment also folds into three domains which can be individually superposed to the corresponding domains of RyR1 (Seo et al. 2012). The conservation of the N-terminal region between RyR1 and IP<sub>3</sub>R1 is further manifested in its arrangement in the corresponding full length receptor. Docking of this structure into the cryo-EM map of the full length IP<sub>3</sub>R placed this fragment also in the centre of the cytoplasmic assembly forming a vestibule around the four-fold axis. This type of arrangement strongly suggests that a physical and functional interaction between the N-termini of adjacent subunits is plausible.

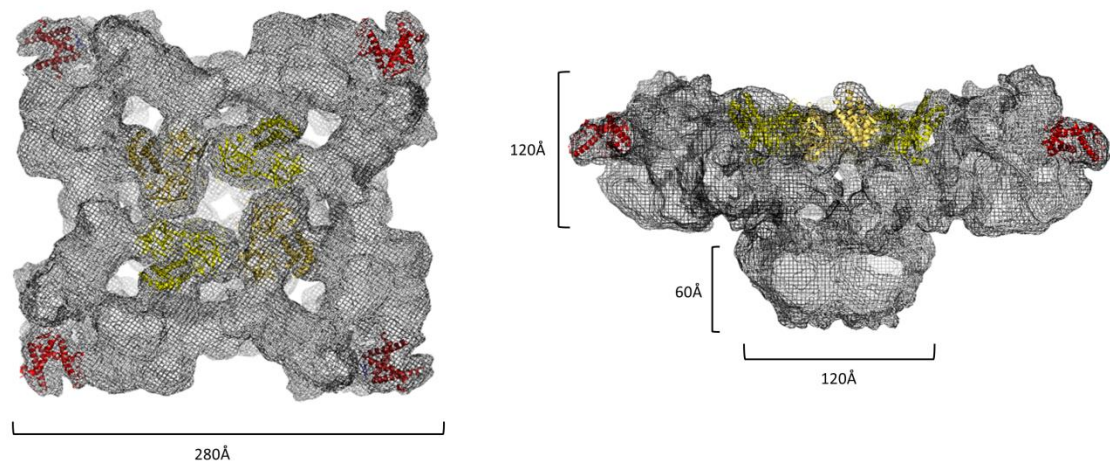


**Figure 1.3** Architecture of RyR tetrameric assembly; top view and side view on left and right panel respectively. Location of N-terminal domain and phosphorylation domain (in yellow and red respectively) obtained through docking of respective crystal structures into cryo-EM map of RyR1. Images created using The PyMOL Molecular Graphic Software (based on (Tung et al. 2010; Yuchi et al. 2012)

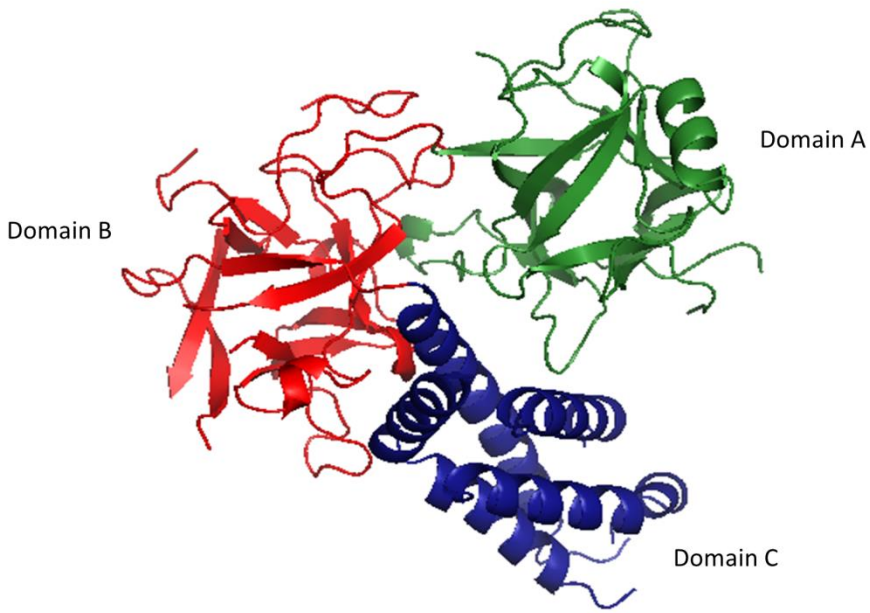


**Figure 1.4** Structure of the rabbit RyR1 N-terminus (1-559), the extreme 27 residues of the C-terminus are not visible in the structure, other fragments missing correspond to flexible parts of the connecting loops. Images created using The PyMOL Molecular Graphic Software (Tung et al. 2010)

### 1.3.3 Transmembrane domains and the pore region

The RyR channel pore is formed by the C-terminal portion of the protein. A carboxyl terminal fragment (~130kDa) containing the putative transmembrane segments was shown to form a cation-selective channel which, similarly to the native protein, was activated by calcium and modulated by ryanodine (Wang *et al.* 1996; Bhat *et al.* 1997). As both the N- and C-terminal fragments of RyR were shown to reside on the cytoplasmic site, membrane topology models propose an even number of membrane-spanning segments (Grunwald and Meissner 1995). Initial models predicted as few as four and as many as twelve transmembrane domains (Takeshima *et al.* 1989; Zorzato *et al.* 1990; Brandt *et al.* 1992). A subsequent model built on empirical evidence and proposed by Du and colleagues predicted eight transmembrane helices which, in respect to the twelve transmembrane segments suggested earlier by Zorzato and colleagues (Zorzato *et al.* 1990), included segments: M3, M4 (alternatively M4a and M4b), M5, M6, M7a, M7b, M8 and M10 (Du *et al.* 2002a). The putative M9 segment was suggested to act as a pore-forming helix which does not transverse the

membrane. Following analysis of the high resolution cryo-EM RyR map Ludtke and colleagues suggested that regions M3 and M4 (M4a/M4b) do not form transmembrane segments but a fragment of this sequence forms a helix which is oriented parallel to the plane of SR membrane (Ludtke *et al.* 2005) (Figure 1.5).

According to a homology model of the RyR pore region based on the crystal structure of the bacterial potassium channel, the last two transmembrane helices (M8 and M10) correspond to the respective outer and inner helices of the bacterial channel pore while the connecting loop (previously assigned as M9 segment) constitutes a short pore helix followed by a selectivity filter (Welch *et al.* 2004). This hypothetical model was supported by a number of observations. In an earlier report, Gao *et al.* showed that mutation of highly conserved amino acids located in the luminal loop connecting domain M8 with M10 affected channel conductance, calcium dependence and ryanodine binding (Gao *et al.* 2000). In agreement with this model, a high resolution cryo-EM map which enabled definition of some of the secondary structures showed a similar arrangement of  $\alpha$ -helices around the pore (Samso *et al.* 2009). Moreover, the comparison between an open and closed conformation of the channel, revealed that the inner helices (M10) undergo structural changes analogous to those of the bacterial potassium channel.

A combination of experimental and computational methods defined the location of critical residues determining channel selectivity and high conductance (Ramachandran *et al.* 2009). Those residues included the putative selectivity filter (GGGIG motif), two negatively charged residues located immediately after (D4894-E4900 in rabbit RyR1) and residues located in the cytosolic side of the inner helix (M10) (residues D4938 and D4945 in RyR1). A schematic model of the RyR transmembrane segments and the channel pore is presented in Figure 1.5.

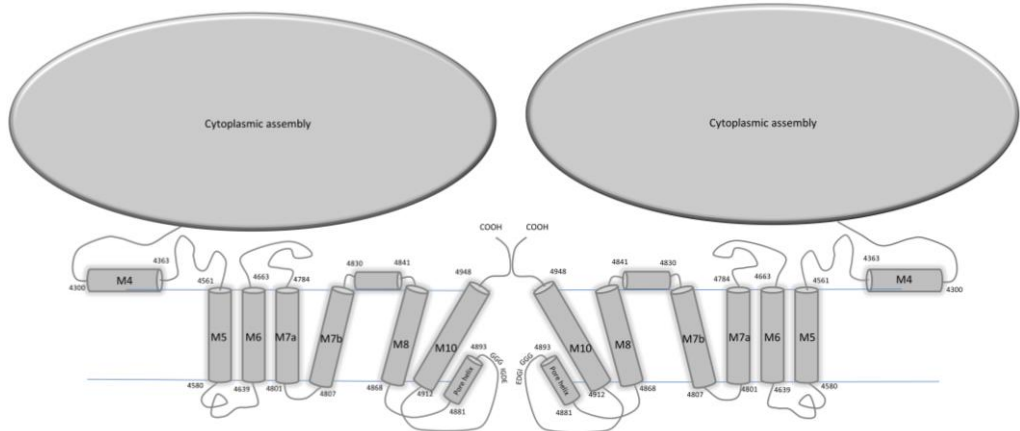


**Figure 1.5** A hypothetical model of the channel pore and transmembrane segments based on Ludtke *et al.* 2005 and Ramachandran *et al.* 2013. Helical segments assigned on the basis of the initial model predicting 10 transmembrane domains, for simplicity only two subunits shown; coordinates given for rabbit RyR1

## 1.4 RyR and excitation-contraction coupling

Ryanodine receptors are key components of excitation-contraction coupling (EC), a process which allows for an electrical signal occurring at the plasma membrane to be converted into the mechanical activation of a muscle cell. The critical event in this process involves mobilisation of calcium ions from intracellular stores which bind to myofilament protein troponin C enabling muscle contraction. RyR-mediated release of  $\text{Ca}^{2+}$  is triggered by changes in the sarcolemmal membrane potential, which activates the L-type voltage-gated calcium channels also known as dihydropyridine receptors (DHPR). Dihydropyridine receptors are composed of five subunits;  $\alpha 1$ ,  $\alpha 2$ ,  $\beta$ ,  $\gamma$  and  $\delta$  (Coronado *et al.* 2004). The DHPR  $\alpha 1$  subunit contains four internal repeats of six transmembrane domains and forms a channel pore while the  $\beta$  subunit controls calcium current. The role of the remaining subunits is not well defined. DHPRs and RyRs are located in close proximity at sites where the sarcolemmal membrane faces the junctional SR creating a central point where an electrical signal is converted into calcium release triggering muscle contraction. The molecular basis of RyR activation upon electrical stimulus ultimately depends on the muscle type. In cardiac muscle, RyR2 becomes activated upon  $\text{Ca}^{2+}$  influx through L-type channels triggered by depolarisation of the plasma membrane, a mechanism known as calcium-

induced calcium release (CICR) (Fabiato 1983). In skeletal muscle, RyR1 is physically coupled to DHPR such that a conformational transition in the latter, triggered by changes in membrane potential, is directly transmitted to the former causing it to open (Numa *et al.* 1990; Tanabe *et al.* 1990; Beam *et al.* 1992; Nakai *et al.* 1998b; Grabner *et al.* 1999). The tight association between RyR1 and DHPR underlies a unique geometrical alignment of two proteins which can be observed by electron microscopy (Protasi *et al.* 1998). In this highly ordered array, a group of four DHPR channels (tetrad) directly interacts with alternate ryanodine receptors in such a way that one subunit of an underlying RyR1 is physically linked to one DHPR within the cluster. Notably, the interaction between those two channels also involves a positive feedback response preventing DHPR inactivation (Nakai *et al.* 1996). Moreover, RyR1-mediated  $\text{Ca}^{2+}$  release positively regulates the surface expression of DHPR (Avila *et al.* 2001b).

The functional and physical coupling between RyR1 and DHPR has been extensively studied in an attempt to identify residues which are critical for this complex interaction. It has been shown that coupling between those two proteins is dictated by isoform-specific determinants located in both skeletal L-type channel and skeletal isoform of ryanodine receptor (Nakai *et al.* 1997) (Tanabe *et al.* 1990). As a result of experiments analysing the effects of expression of DHPR chimeric proteins in dysgenic myotubes (lacking the DHPR  $\alpha 1$  subunit), the putative cytoplasmic region located between transmembrane repeats II and III (loop II-III) in the DHPR  $\alpha 1s$  subunit was proposed to constitute a major determinant responsible for RyR1-DHPR interaction (Tanabe *et al.* 1990). Additional sites supporting physical/functional interaction between the two receptors are believed to lie between transmembrane repeats III and IV and within the cytoplasmic C-terminal tail of the  $\alpha 1s$  subunit (Sencer *et al.* 2001; Weiss *et al.* 2004). Further determinants were proposed to reside in the DHPR  $\beta 1a$  subunit and account for orthograde signalling (Cheng *et al.* 2005).

Expression of chimeric RyR proteins in dyspedic (RyR1-deficient) myotubes resulted in the identification of some of the putative regions within the RyR1 sequence. It was shown that a fragment between amino acids 1635-2636 containing the D3 region is able to sustain orthograde and retrograde signalling whereas residues located downstream (2636-3720) underlie retrograde signalling (Nakai *et al.* 1998a). Within those two large fragments, sites responsible for functional coupling between the two

proteins do not fully overlap with those involved in physical association linked to the formation of DHPR tetrads (Protasi *et al.* 2002). As the ability to structurally and functionally interact with the calcium L-type channel is a unique feature of the skeletal ryanodine receptors isoform, a considerable amount of attention was devoted to the regions of highest divergence. Among the three divergent regions, the D2 represents the site of the most prominent difference among the three RyR isoforms and its key role in EC coupling was reported by independent groups (Yamazawa *et al.* 1997; Perez *et al.* 2003). However, chemical crosslinking of the full length RyR1 and a short fragment of the II-III loop from DHPR, which was shown to activate the channel at low calcium levels, suggested that the interaction site is in fact located upstream of the D2 region between residues 450-1400 (Bannister and Ikemoto 2006). Subsequently, Cui *et al.* reported that the II-III loop binds to residues 1085-1208 which represent the second SPRY domain in RyR1 (Cui *et al.* 2009). This communication was in agreement with previous reports showing that a short region within the second SPRY domain (residues 1076-1112) specifically binds to the recombinant DHPR II-III loop (Leong and MacLennan 1998a). Interestingly, an overlapping site on RyR1 (residues 954-1112) was also proposed to constitute a binding determinant for the DHPR III-IV loop (Leong and MacLennan 1998b). The C-terminal tail of DHPR was shown to interact with the RyR1 calmodulin-binding site (CaM-binding site) and calmodulin-like domain (CaMLD) containing two putative EF-hand motifs (Sencer *et al.* 2001; Xiong *et al.* 2006). The binding site for the DHPR  $\beta$  subunit was proposed to reside between residues 3200-3600 and undergo modulation by a basic region located immediately downstream of alternatively spliced region I (Cheng *et al.* 2005).

In conclusion, coupling between those two proteins is dictated by multiple sites spread throughout a considerable portion of RyR1. Since physical contact between the two is essential for the functional interaction to occur, discrimination between sites fulfilling these specific roles remains challenging. Considering the size of RyR, the functional signal from DHPR is most likely transmitted through a number of allosteric interactions within RyR itself which further complicates the identification of putative regions.

## 1.5 RyR regulation

RyRs are part of a macromolecular complex composed of FKBP12/12.6, calmodulin, triadin, junctin and protein kinases and phosphatases many of which are associated with the receptor through adaptor proteins (Berridge et al. 2003; Lanner et al. 2010). Most of the modulators interact with the cytoplasmic portion of the protein at locations distant from the channel pore suggesting that RyR gating is allosterically regulated by a complex network of inter- and intra-subunit interactions. Despite a high degree of sequence identity and almost identical three dimensional architecture (cryo-EM based maps), RyRs display an isoform-specific response to some of the most important physiological regulators including calcium and magnesium ions, calmodulin, ATP and DHPR.

### 1.5.1 Calcium, magnesium and ATP

Calcium plays a central role in the physiological modulation of channel activity. RyR1 displays a bell-shaped dependence on  $\text{Ca}^{2+}$  concentration, i.e. low micromolar calcium activates the channel while millimolar levels have an inhibitory effect, a phenomenon explained by the presence and cooperation between a high-affinity calcium activating site and an inhibitory low-affinity site (Meissner *et al.* 1997). RyR2 and RyR3 on the other hand were shown to have a decreased sensitivity to calcium inhibition and displayed a more potent response to calcium activation, i.e. for the same extent of channel activity, RyR1 requires both  $\text{Ca}^{2+}$  and ATP (Lanner *et al.* 2010). It is widely accepted that cytoplasmic levels of calcium are critical for the regulation of channel activity; however some reports also suggest an equally important role for luminal calcium (Jiang *et al.* 2004; Diaz-Sylvester *et al.* 2011). Although the impact of the SR  $\text{Ca}^{2+}$  content on RyR activity has been shown by a number of investigators, a precise mechanism of this effect remains under debate. In particular, many authors support the notion that luminal calcium controls the activity of the channel indirectly, either through the so called “feed-through” mechanism, in which  $\text{Ca}^{2+}$  released from SR acts via cytoplasmic binding sites (Xu and Meissner 1998; Laver *et al.* 2008) or through the calcium-induced dissociation of the accessory

protein - calsequestrin (CSQ) from the RyR macromolecular complex (Gyorke *et al.* 2004) (see Section 1.5.4). Others however argue that luminal calcium regulates channel activity directly via binding to the sites located on the luminal portion of the channel (Ching *et al.* 2000).

Two presumed EF hand motifs are located in the C-terminal portion of the protein and two additional putative calcium binding sites identified through  $\text{Ca}^{2+}$  interaction with recombinant RyR1 fragments were proposed to reside further upstream (residues 1861-2094 and 3657-3776) (Chen and MacLennan 1994). However, other studies showed that RyR sensitivity to activation is retained upon expression of the 130kDa C-terminal portion of the protein suggesting that the putative sites are in fact located in the extreme C-terminus (Bhat *et al.* 1997). Interestingly, Fessenden *et al.* reported that mutation of critical residues within the two putative EF hand motifs (4081-4092, 4116-4127) did not change functional responses to agonists and depolarisation in intact myotubes suggesting that those regions are not essential for calcium-dependent regulation of the channel (Fessenden *et al.* 2004). However, according to Xiong *et al.*, a fragment containing both EF hand motifs (4064-4210) represents a domain which folds in a manner similar to calmodulin, binds  $\text{Ca}^{2+}$  and modulates channel function (Xiong *et al.* 2006). Based on mutation of highly conserved acidic amino acids located in the RyR C-terminus, others proposed that calcium sensitivity to activation is determined by a single residue in all three isoforms (E4032, E3987 and E3885 for RyR1, 2 and 3 respectively) (Chen *et al.* 1998; Du and MacLennan 1998; Li and Chen 2001). Hence, the emerging picture strongly suggests that determinants of calcium sensitivity are spread over a considerable stretch of residues in the primary sequence of the RyR C-terminus. It is likely that these residues are in fact located in close proximity in the three dimensional structure. However, until this structure is known, the determination of calcium binding sites remains a challenging task because the majority of currently used functional assays are not able to discriminate between residues which directly bind calcium and those involved in the conduction of calcium-triggered signals.

RyRs display an isoform-specific calcium inactivation profile, a phenomenon which naturally drew attention to regions of highest divergence between isoforms such as the D3 region. Nevertheless, the replacement of this region in RyR1 with the corresponding RyR2 sequence or deletion of this fragment did not alter calcium

dependence (Du and MacLennan 1999). On the contrary, a set of RyR1 chimeras, in which the D1 region and fragments of immediate proximity located upstream and downstream of D1 were replaced with the corresponding RyR2 sequence, displayed a substantially reduced sensitivity to  $\text{Ca}^{2+}$ -mediated inhibition (Du and MacLennan 1999). Following further experiments, the D1 region was proposed to modulate channel responsiveness to  $\text{Ca}^{2+}$  indirectly (Du *et al.* 2000).

Magnesium ( $\text{Mg}^{2+}$ ) is a potent RyR inhibitor and its role in channel regulation has been recently more recognised. Concentration of free  $\text{Mg}^{2+}$  in the cytoplasm is 1mM, which is around  $10^4$  times more than calcium concentration during diastole. Competitive binding of magnesium to calcium activation and/or inhibitory sites has been suggested to constitute the molecular mechanism of  $\text{Mg}^{2+}$  effect on channel function (Lanner *et al.* 2010). Laver *et al.* suggested that magnesium is in fact the key factor controlling RyR activity (Laver and Honen 2008). According to this model, the interplay between four distinct binding sites which display the ability to bind both cations underlies the mechanism of channel regulation. The luminal activating site does not select between calcium and magnesium and the inhibitory effect of the latter is a consequence of preventing binding of the former. The cytoplasmic activation site exhibits a substantially higher affinity for  $\text{Ca}^{2+}$  while  $\text{Mg}^{2+}$  binding promotes channel closure. Both inhibitory sites are located in the cytoplasm and have different affinities for  $\text{Ca}^{2+}$ . The lower affinity site is also able to bind magnesium. Notably, an independent group reported similar findings, however in addition to the luminal non-selective binding site,  $\text{Ca}^{2+}$  selective site on the SR lumen was also found (Diaz-Sylvester *et al.* 2011). Both studies concluded that the RyR activity is dynamically modulated by distinct sites with unique binding properties which are located in both the cytoplasmic and luminal regions of the channel.

Among adenine nucleotides, ATP is the most powerful activator of RyR. It has a potent effect on RyR1 function and a relatively modest impact on RyR2 (Lanner *et al.* 2010). Since, in the native milieu of the cell, most ATP is in complex with magnesium, it has been suggested that under physiological conditions, the observed effect of ATP constitutes a combination of two mechanisms, i.e. subtle changes in the levels of free  $\text{Mg}^{2+}$  through formation of a  $\text{Mg}^{2+}/\text{ATP}$  complex and the direct effect of this complex on RyR activity.

### 1.5.2 Calmodulin

In addition to a direct regulation by calcium, RyRs are modulated by those ions through interaction with calmodulin. CaM is a dumbbell-shaped  $\text{Ca}^{2+}$  binding protein expressed ubiquitously in all eukaryotic cells. It contains four EF hand motifs, two in each globular lobe. Calmodulin regulates RyR in an isoform specific manner, i.e. it inhibits RyR2 at all  $\text{Ca}^{2+}$  concentrations, while it has a biphasic effect of RyR1, inhibitory at micromolar calcium and activating at lower concentrations when it exists in a calcium-free form (apoCaM) (Hamilton and Serysheva 2009). Using limited tryptic digestion of RyR1, the calmodulin binding site was mapped to residues 3600-3637 (Moore *et al.* 1999). Subsequently, it was reported that the above fragment exclusively binds the C-terminal lobe of both apoCaM and  $\text{Ca}^{2+}/\text{CaM}$  while the N-terminal lobe binding sequence is located at sites distant in primary sequence from the C-lobe-binding residues (Samsó and Wagenknecht 2002; Xiong *et al.* 2002). The binding of calmodulin to RyR was shown to impede the formation of inter-subunit disulphide bonds while oxidation prevented CaM interaction with the receptor (Porter Moore *et al.* 1999; Zhang *et al.* 1999). Based on those findings calmodulin was suggested to bind across two subunits within the tetrameric channel. In agreement with this model the RyR1 N-terminal fragment identified as an additional CaM-binding site (1975-1999) is located in immediate proximity of the N-terminal sequence containing cysteine involved in the inter-subunit disulphide bond (Zhang *et al.* 2003a). Calmodulin was shown to bind to the corresponding sequence in RyR2 (residues 3583-3603) implying that the determinants of CaM isoform-specific regulation are located somewhere else in the protein (Yamaguchi *et al.* 2003). Notably, Yamaguchi *et al.* reported that when five non-conserved residues in the C-terminal flanking region of RyR2 CaM binding site were substituted with those of RyR1, the loss of the RyR2-specific inhibition at submicromolar calcium was observed (Yamaguchi *et al.* 2004).

Recently, defective binding of calmodulin to RyR2 has been implicated in heart failure, cardiac hypertrophy and channel dysfunction observed in the presence of arrhythmia-associated mutations (Yamaguchi *et al.* 2007; Ono *et al.* 2010; Xu *et al.* 2010; Gangopadhyay and Ikemoto 2011). Moreover, the addition of a recombinant form of calmodulin exhibiting higher binding affinity for RyR2 was able to restore

abnormal calcium handling in failing cardiomyocytes (Hino *et al.* 2012). In further support of CaM role in the pathogenesis of RyR-associated disorders, a recent genome-wide linkage analysis revealed that the disease phenotype can also be triggered by mutations in the calmodulin gene (Nyegaard *et al.* 2012). Notably, one of the identified mutants displayed a severely compromised interaction with the peptide corresponding to the RyR2 CaM-binding domain at sub-activating calcium levels. This would suggest that, at diastole, CaM-mediated inhibition of RyR2 is severely disturbed leading to an increase in channel open probability consistent with the phenotype observed for RyR2 mutations associated with arrhythmias.

### 1.5.3 Other EF-hand proteins: sorcin and S100A1

Sorcin is another calcium-binding protein which regulates RyR function. It is a member of the penta EF-hand motif protein family and has an isoform-specific impact on channel function. *In vitro*, sorcin exhibits an inhibitory effect on RyR2, while it stimulates RyR1 (Zissimopoulos and Lai 2007). Although the inhibition of RyR2 by sorcin is thought to be calcium-independent, the translocation of sorcin from the cytoplasm into membranous compartments prerequisite for the RyR2/sorcin interaction to occur, is triggered by an increase in  $\text{Ca}^{2+}$  level (Lokuta *et al.* 1997; Farrell *et al.* 2003). *In vivo* studies reported contradictory results implying that sorcin-mediated regulation of channel function has a high level of complexity (Meyers *et al.* 2003; Suarez *et al.* 2004; Frank *et al.* 2005) . Because sorcin binds other proteins involved in calcium signalling, the evaluation of its effects on RyR activity *in vivo* remains challenging. In addition to sorcin, other EF-hand proteins have been recognised to regulate channel function including calumenin and S100A1 (Lanner *et al.* 2010). S100A1 protein is a symmetric homodimer with each subunit having a low affinity pseudo EF-hand motif and a second high affinity canonical EF-hand calcium binding domain (Wright *et al.* 2005). It has been shown that at systolic calcium levels S100A1 competes directly with CaM for the same binding site on RyR which would explain the mechanism by which S100A1 activates RyR (Wright *et al.* 2008). According to this model, CaM displacement by S100A1 would relieve the channel from the inhibitory effect of the former. In agreement with the competition between

those two proteins; a mutation of one amino acid within the CaM binding domain, which impairs calmodulin binding, abolishes S100A1 binding as well (Yamaguchi *et al.* 2011). *In vivo*, S100A1 seems to be essential for the physiological response of cardiac muscle to acute  $\beta$ -adrenergic stimulation (Du *et al.* 2002b).

#### 1.5.4 SR proteins: calsequestrin, triadin and junctin

Calsequestrin is a low-affinity and high capacity calcium-binding protein which resides in the lumen of SR and exists as a mixture of monomers and multimers. The dynamic linear polymerisation of CSQ is thought to confer its high  $\text{Ca}^{2+}$  binding capacity (Kim *et al.* 2007) while monomers appear to be responsible for the regulatory function of the protein (Qin *et al.* 2008; Terentyev *et al.* 2008b). There are two isoforms of calsequestrin; CSQ1 which is found in skeletal muscles and CSQ2 which is expressed in cardiomyocytes and slow-twitch muscles. The two isoforms are nearly identical in their three dimensional structure; however differ in respect to their  $\text{Ca}^{2+}$  binding capacities with the skeletal isoform being able to bind more calcium ions (Park *et al.* 2004). Calsequestrin is believed to modulate RyR activity indirectly through binding to anchoring proteins; triadin and/or junctin which are embedded in the SR membrane (Lanner *et al.* 2010). The CSQ2-mediated inhibition of RyR2 function was proposed to involve binding to triadin/junctin once calcium SR concentration drops below a threshold level constituting therefore a luminal calcium sensor responsible for termination of  $\text{Ca}^{2+}$  release (Gyorke *et al.* 2004). Consistent with a critical role of calsequestrin in cardiac muscle, genetic defects in CSQ2 have been linked to stress-induced ventricular arrhythmia (see Section 1.6.2) and CSQ2 null mice exhibited CPVT-like phenotype (Knollmann *et al.* 2006). Interestingly, these animals retained functional calcium storage maintained by a compensatory increase in SR volume and, under basal conditions, displayed normal contractile function. Arrhythmia-associated mutations in the CSQ2 gene were shown to either affect protein  $\text{Ca}^{2+}$  binding capacity or impair CSQ2 ability to modulate RyR2 function (Kim *et al.* 2007; Qin *et al.* 2008; Terentyev *et al.* 2008b). The fact that CSQ2 mutations which cause distinct defects at the molecular level lead to a similar CPVT phenotype strongly suggest that  $\text{Ca}^{2+}$  buffering and CSQ2-mediated regulation

of RyR2 activity are equally important for maintaining normal calcium handling in cardiomyocytes. Notably, Qin *et al.* argued that CSQ1 has a minor effect on RyR1 function and its physiological role in skeletal muscle is in fact restricted to  $\text{Ca}^{2+}$  buffering (Qin *et al.* 2009).

Recently, triadin and calsequestrin were suggested to be involved in structural organisation of the SR. In particular, triadin ablation was shown to result in a 50% reduction in the contacts between junctional SR and T-tubules implying that triadin is indispensable for cardiac function through maintenance of calcium release units (Chopra *et al.* 2009). The inter-dependence of protein levels of triadin, junctin and calsequestrin (Knollmann 2009) suggests a strong functional cross-talk between those proteins making it very difficult to establish their physiological role independently.

### 1.5.5 FK506-Binding Proteins (FKBP)

FKBPs belong to a family of highly conserved proteins that bind immunosuppressive drugs such as FK506 and rapamycin. Those proteins are involved in a number of diverse biochemical processes including protein folding, receptor signalling and transcription (Lanner *et al.* 2010). Two isoforms; FKBP12 and FKBP12.6 (also known as calstabin 1 and 2 respectively) were shown to physically interact with ryanodine receptors and modulate their function (Marx *et al.* 1998; Ondrias *et al.* 1998; Gaburjakova *et al.* 2001). RyR2 exhibits much higher affinity for FKBP12.6 while RyR1 binds both isoforms with similar affinity, however a considerably higher expression of FKBP12 isoform in skeletal muscle results in the latter being the predominant form bound to RyR1 (Chelu *et al.* 2004). FKBP12 and 12.6 display cis-trans peptidyl-prolylisomerase activity, nonetheless experimental findings suggest that enzymatic activity does not play a role in RyR modulation (Timerman *et al.* 1995).

Binding of FKBP isoforms to their respective targets was proposed to stabilise the closed state of the channels and to promote a process of coupled gating between adjacent RyR channels (Marx *et al.* 1998; Ondrias *et al.* 1998; Marx *et al.* 2001b). Subsequently, a defective association between RyR2 and FKBP12.6 following

channel phosphorylation by PKA was proposed to underlie receptor dysfunction observed in arrhythmia-associated mutations and heart failure (Marx et al. 2000; Wehrens *et al.* 2003; Yano *et al.* 2003; Wehrens *et al.* 2005) (see Section 1.6.2.1). This hypothesis was however challenged by many independent groups which failed to observe changes in RyR2/FKBP12.6 interaction and the phosphorylation status of the channel in pathological conditions (George *et al.* 2003; Stange *et al.* 2003; Jiang *et al.* 2005; Liu *et al.* 2006; Hunt *et al.* 2007; Zissimopoulos *et al.* 2009). The role of FKBP in channel modulation was further examined by Xiao *et al.* who investigated the effect of FKBP12.6 on RyR2 function by three independent techniques, i.e. single channel recordings, ryanodine binding assays and calcium imaging (Xiao *et al.* 2007). The authors concluded that the loss of calstabin 2 does not alter channel function. More importantly, the same group also showed that FKBP12.6-null mice do not exhibit enhanced susceptibility to stress-induced arrhythmia further questioning the hypothesis of FKBP-mediated channel dysfunction. The role of FKBP12.6 in the physiologically relevant modulation of RyR2 activity remains uncertain since only 10-20% of RyR2 was shown to be bound to this protein in ventricular myocytes (Guo *et al.* 2010; Zissimopoulos *et al.* 2012).

Similar to the disputable function of calstabins in RyR regulation, there is also a considerable amount of controversy in respect to the location of the FKBP-binding site in the RyR primary sequence. Initially, the FKBP12-binding site was proposed to reside in the central portion of RyR1 and involve one critical residue (V2461) (Gaburjakova *et al.* 2001). Other groups were unable to recapitulate those results (Masumiya *et al.* 2003; Zissimopoulos and Lai 2005a). Zissimopoulos *et al.* showed that FKBP12.6 binding to RyR2 is retained upon recombinant expression of the RyR2 C-terminus (Zissimopoulos and Lai 2005b). In addition, minor binding was also detected in the N-terminal portion of the protein which was in agreement with an earlier report by Masumiya *et al.* who proposed the N-terminal domain as a main determinant for FKBP12.6 binding (Masumiya *et al.* 2003). In a very recent report it has been suggested that both N-terminal and central domains contribute to the FKBP12 biniding epitope in RyR1 (Girgenrath *et al.* 2013)

### 1.5.6 Phosphorylation

PKA-mediated phosphorylation of RyR2 was proposed to constitute a physiological mechanism by which cardiac muscle meets the demand for increased contractility and heart rate during stress or exercise. Consequently, this hypothesis was further expanded to pathological conditions, in which hyper-phosphorylation of a single residue (S2808, human RyR2) and subsequent dissociation of calstabin 2 was proposed to play a major role in RyR2 dysfunction observed during heart failure (Marx *et al.* 2000; Antos *et al.* 2001; Oda *et al.* 2005; Yano *et al.* 2005; Wehrens *et al.* 2006). Similarly, a CaMKII-specific phosphorylation site (S2814, human RyR2) was proposed to constitute a mechanism by which an increased heart rate modulates RyR2 activity to augment muscle contractility (Kushnir *et al.* 2010). A decrease in CaMKII-mediated RyR2 phosphorylation was suggested to underlie an impaired force-frequency relationship observed in heart failure (Wehrens *et al.* 2004).

The PKA phosphorylation of S2808 as a mechanism of channel modulation by  $\beta$ -adrenergic stimulation was disputed by other groups. MacDonnell *et al.* reported no difference in response to sympathetic agonist activation between wild type mice and animals carrying an alanine substitution (S2808A) at the putative RyR2 phosphorylation site (MacDonnell *et al.* 2008). In agreement with this study, recombinant expression of RyR1 and RyR2 mimicking constitutively phosphorylated (aspartate substitution) and dephosphorylated channels (alanine substitution) (S2843 and S2809 for rabbit RyR1 and RyR2 respectively), revealed no significant differences in channel function (Strange *et al.* 2003). Furthermore, George and colleagues showed that RyR2 global phosphorylation levels are indistinguishable between wild type channels and channels carrying arrhythmia-linked mutations in both stimulated and unstimulated cardiomyocytes thus undermining the major role of increased RyR2 phosphorylation in the pathogenesis of arrhythmia (George *et al.* 2003). Moreover, Xiao *et al.* showed that in fact S2030 is the major PKA phosphorylation site in RyR2 and that S2808 remains substantially phosphorylated irrespective of the activation of the sympathetic nervous system (Xiao *et al.* 2006). Similarly, the involvement of PKA-mediated hyper-phosphorylation of RyR2 in the pathogenesis of heart failure remains controversial (Jiang *et al.* 2002b). Reasons for these discrepancies are unclear. However, recent work by Huttlin *et al.* involving

large-scale analysis of the phospho-proteome of several mouse organs revealed that RyR2 is phosphorylated *in vivo* at multiple sites (available at <https://gygi.med.harvard.edu/phosphomouse/index.php>) (Hutlin et al. 2010). The emerging picture strongly suggests that phosphorylation-dependent modulation of channel function might be much more complex than initially believed. The ultimate effect of phosphorylation would then depend on the modification site and the abundance of the modified residues, constituting a possible explanation for the amount of controversy associated with the role of phosphorylation in channel function. In agreement with the above, the evaluation of the PKA and CaMKII phosphorylation sites *in vitro* within the recently crystallised phosphorylation domain revealed that multiple sites are targeted by those two kinases (Yuchi et al. 2012) (see Section 1.3.1).

### 1.5.7 Redox modifications

Redox modifications are widely accepted to constitute an important mechanism regulating the function of ryanodine receptors (Aghdasi et al. 1997b; Wu et al. 1997). Depending on the isoform, RyR contains 89-100 cysteines, of which up to fifty were proposed to be in a reduced state. A set of those residues is believed to be hyper-reactive enabling the receptor to be covalently modulated by redox compounds and to respond to subtle changes in the redox potential within the cellular milieu (Xu et al. 1998a; Eu et al. 2000; Feng et al. 2000; Sun et al. 2003). The availability of those hyper-reactive cysteines for modification, i.e. their redox potential, is in turn modulated by channel activators and inhibitors implying a complex mechanism of regulation (Xia et al. 2000; Marinov et al. 2007).

Identification of the cysteines involved in redox-dependent modification of RyR has been undertaken by a number of independent groups and those findings are summarised in Table 1.2. A number of conflicting observations has been reported, however those discrepancies are most likely associated with different experimental conditions, e.g. presence of channel regulators or oxygen tension. A high level of complexity in the redox-dependent channel regulation has been further supported by experiments performed by Petrochenko and colleagues who showed that

combinatorial mutation of the putative hyper-reactive cysteines is not sufficient to eliminate RyR1 response to changes in redox potential (Petrotchenko *et al.* 2011).

Redox modifications of RyR are believed to underlie a physiological mechanism controlling muscle performance (Lamb and Posterino 2003; Posterino *et al.* 2003; Wang *et al.* 2010; Sun *et al.* 2011; Beigi *et al.* 2012). In principle, oxidising agents activate the channel with a concomitant formation of inter- and intra-subunit disulphide bonds while alkylation inhibits the channel and blocks the formation of covalent bonds across subunits (Aghdasi *et al.* 1997b; Wu *et al.* 1997). Moreover, oxidation-induced inter-subunit crosslinking is protected by calmodulin, implying that oxidation and calmodulin regulate RyR1 activity by inducing changes at the site of an inter-subunit contact. The above mechanism was proposed to involve C3635, which is located within the CaM-binding site (Porter Moore *et al.* 1999; Zhang *et al.* 2003a). The same cysteine was shown to be targeted by S-nitrosylation resulting in channel activation, an effect exclusively observed in conditions of low physiological oxygen tension (Eu *et al.* 2000; Sun *et al.* 2001a). In addition, cysteines other than C3635 were shown to determine RyR1 sensitivity to changes in cellular redox potential implying a complex mechanism in which a set of specific residues have adapted to mediate effects of particular modifications (Sun *et al.* 2001a; Petrotchenko *et al.* 2011). It has been proposed that redox-sensing cysteines are located within highly specialised domains where a unique local microenvironment enhances their reactivity (Feng *et al.* 1999). Thiol groups of redox-sensing cysteines exhibit low pKa, which enables formation of highly reactive thiolate anions. These unique chemical properties arise from stabilising interactions between the thiolate anion and the side chains of neighbouring amino acids (Brandes *et al.* 2009).

Cysteine	RyR isoform	Endogenous	Induced	Additional information	Reference
36	RyR1 (rabbit)	oxidation	oxidation, S-GSH		(Aracena-Parks et al. 2006)
253	RyR1 (rabbit)	-	S-NO/S-GSH		(Aracena-Parks et al. 2006)
315	RyR1 (rabbit)	S-NO/S-GSH	S-NO./ S-GSH		(Aracena-Parks et al. 2006)
811	RyR1 (rabbit)	S-NO/S-GSH	S-NO/ S-GSH		(Aracena-Parks et al. 2006)
906	RyR1 (rabbit)	S-NO/S-GSH	S-NO/ S-GSH		(Aracena-Parks et al. 2006)
1040	RyR1 (rabbit)	-	S-NO/S-GSH	identified as highly reactive in conditions promoting channel closure, reactivity dependent on the GSH/GSSG ratio	(Voss <i>et al.</i> 2004; Aracena-Parks et al. 2006; Petrotchenko et al. 2011)
1303	RyR1 (rabbit)	-	S-NO	as above	(Voss et al. 2004; Aracena-Parks et al. 2006; Petrotchenko et al. 2011)
1591	RyR1 (rabbit)	S-NO/S-GSH	S-GSH		(Aracena-Parks et al. 2006)
1781	RyR1 (rabbit)	not established	not established	reactivity dependent on the GSH/GSSG ratio, involved in redox-sensing	(Petrotchenko et al. 2011)
2326	RyR1 (rabbit)	oxidation, S-NO/S-GSH	oxidation, S-GSH	reactivity dependent on the GSH/GSSG ratio	(Aracena-Parks et al. 2006; Petrotchenko <i>et al.</i> 2006; Petrotchenko et al. 2011)
2363	RyR1 (rabbit)	oxidation, S-NO/S-GSH	oxidation, S-GSH		(Aracena-Parks et al. 2006)
2436	RyR1 (rabbit)	not established	not established	identified as highly reactive in conditions promoting channel closure, involved in redox-sensing	(Voss <i>et al.</i> 2004b) (Petrotchenko et al. 2011)
2565	RyR1 (rabbit)	not established	not established	identified as highly reactive in conditions promoting channel closure	(Voss <i>et al.</i> 2004b)
2606	RyR1 (rabbit)	not established	not established	identified as highly reactive in conditions promoting channel closure, involved in redox-sensing	(Voss <i>et al.</i> 2004b) (Petrotchenko et al. 2011)
2611	RyR1 (rabbit)	not established	not established	identified as highly reactive in conditions promoting channel closure	(Voss <i>et al.</i> 2004b)
3193	RyR1 (rabbit)	S-GSH	S-GSH		(Aracena-Parks et al. 2006)

3635	RyR1 (rabbit)	oxidation and S-NO/S-GSH	oxidation, S-NO/S-GSH	identified as highly reactive in conditions promoting channel closure, involved in calmodulin-dependent modulation of channel activity, nitrosylation affected by pO <sub>2</sub>	(Porter Moore et al. 1999; Sun et al. 2001a; Sun et al. 2003; Voss et al. 2004; Aracena-Parks et al. 2006)
4958	RyR1	oxidation		proposed to maintain RyR three dimensional structure via formation of internal disulphide bond, a part of CXXC motif	(Hurne et al. 2005)
4961	RyR1	oxidation		as above	as above

**Table 1.2** List of cysteines reported to mediate redox modulation of RyR

The mechanism underlying increased sensitivity of the channel to activation in the presence of mild oxidising agents is thought to be associated with destabilisation of the closed conformation of the channel induced by a shift in the thiol redox state without full oxidation of those residues (Petrotchenko et al. 2011). Similarly, preferential labelling of hyper-reactive cysteines in the presence of agents decreasing RyR activity would be associated with increased availability of domains containing critical thiols upon conformation changes triggered by channel closure (Feng et al. 1999). However others proposed that a reduced number of residues available for chemical labelling upon channel activation is in fact associated with oxidation of hyper-reactive cysteines to disulphides driven by a drop in channel redox potential in the presence of agents increasing RyR opening probability (Xia et al. 2000). In agreement with the former, Sun and colleagues showed that the availability of C3635 for S-nitrosylation exclusively at physiological low oxygen tension is determined by the difference in the receptor conformation and not by cysteine oxidation to disulphides at ambient O<sub>2</sub> (Sun et al. 2003). Moreover, oxidation of cysteines not involved in redox sensing *per se* is associated with substantial activation of RyR1 which, upon prolonged exposure becomes irreversibly inactivated (Sun et al. 2001b). Notably, some of the cysteines which were shown to be oxidised were also identified as targets for other covalent modifications (Aracena-Parks et al. 2006). Consistent with the notion that the same cysteine undergoes different modification depending on the conditions, Aghdasi et al. showed that nitric oxide donors prevent oxidation-induced activation of the channel and block inter-subunit disulphide bond formation (Aghdasi et al. 1997a). Moreover, Hurne et al. proposed that some of disulphide bonds are indispensable for channel function via stabilisation of the RyR three-dimensional structure (Hurne et al. 2005). In this study, mutation of two cysteines within a conserved CXXC motif, which has been shown to be employed by many proteins for formation, isomerisation and reduction of disulphide bonds (Fomenko and Gladyshev 2002, 2003), resulted in a dysfunctional RyR1 unable to support EC coupling and unresponsive to activators.

Both RyR1 and RyR2 have been shown to be endogenously nitrosylated (Xu et al. 1998a; Eu et al. 2000) and alterations in this process have been proposed to underlie some of the pathological conditions associated with RyR dysfunction. Neuronal NOS-derived nitric oxide has been proposed to exert its protective effect on RyR2

function by preventing its excessive oxidation (Gonzalez *et al.* 2007; Gonzalez *et al.* 2010; Cutler *et al.* 2012). This observation is of particular interest since increased levels of RyR oxidation have been reported to accompany heart failure and other muscle-associated disorders (Yano *et al.* 2005; Terentyev *et al.* 2008a; Belevych *et al.* 2009). The protective effect of RyR nitrosylation was however questioned by other groups which showed that both RyR1 and RyR2 are excessively S-nitrosylated in pathological conditions linked to the increased activation of the channel (Chen *et al.* 1993; Bellinger *et al.* 2008; Bellinger *et al.* 2009; Fauconnier *et al.* 2010). However, those apparently conflicting findings might be explained by a mechanism in which excessive oxidative stress leads not only to the loss of normally S-nitrosylated cysteines but, through the formation of peroxynitrate, S-nitrosylates other thiol residues which in physiological conditions would remain inaccessible (Gonzalez *et al.* 2010). The above mechanism would ultimately lead to the net effect of channel hypernitrosylation, as reported by others.

In summary, a tight interplay between different redox modifications appears to determine the ultimate effect on RyR activity. The high complexity of channel response to reducing/oxidation agents is governed by multiple factors; availability of cysteines which determines the identity and quantity of residues modified, type and reactivity of the chemical compounds used and the experimental set up (e.g. physiological versus ambient oxygen tension, closed versus open channel, presence of other redox active species). The detailed physiological and pathological consequences of RyR redox modifications remain unclear.

### 1.5.8 Pharmacological modulation of RyR

Ryanodine receptors are regulated by a number of exogenous compounds. Pharmacological agents with current or prospective clinical applications for RyR1 and RyR2-associated disorders are described in Section 1.6.1 and 1.6.2.2 respectively. Other compounds that influence gating of the channel either directly or indirectly by affecting its interaction with accessory proteins include local anaesthetics and immunosuppressive agents, food ingredients, fungicides, insecticides and peptide toxins (Table 1.3).

Some of those compounds have been widely used to study RyR function with ryanodine being the most widely used agent in a laboratory setting. In respect to RyR, ryanodine is of particular importance for at least two reasons; firstly, its biological properties (i.e. selective binding to RyR) permitted the identification of the channel itself and secondly its selective binding to the receptor's open conformation makes it an indispensable tool in RyR functional studies (Sutko *et al.* 1997). Ryanodine is a natural product found in members of the genus *Ryania* and long before its current application it had been appreciated as a source of toxic compounds and later on used as an insecticide. Ryanodine has a complex effect on RyR function, i.e. binding of this compound to its high affinity site (nanomolar range) activates the channel and locks it in a reduced conductance state, while higher concentrations (micromolar) inhibit the channel (Sutko *et al.* 1997). It is generally believed that each functional RyR tetramer contains a single high affinity binding site (Lai *et al.* 1989; Tanna *et al.* 1998). The relationship between high and low affinity binding sites can be described by two different models. The first model assumes the existence of four identical (one in each subunit) but negatively cooperative binding sites, of which affinity gradually decreases as more ryanodine molecules are bound (Pessah and Zimanyi 1991). The second model proposes that high and low affinity binding sites are also functionally coupled but they are physically distinct (Wang *et al.* 1993).

The high affinity binding site for ryanodine has been proposed to reside within the RyR C-terminus. This notion is based on a number of findings, i.e. the C-terminal portion of RyR1 (~130kDa) forms a cation-selective channel which is regulated by ryanodine (Bhat *et al.* 1997) and ryanodine specifically labels a tryptic fragment corresponding to the C-terminal region (~76kDa) (Callaway *et al.* 1994; Witcher *et al.* 1994). However, the precise location of the high affinity ryanodine binding site remains controversial. Some of the features of the ryanoids interaction with RyR, i.e. the accessibility of the binding site from the cytoplasmic side upon channel opening (Tanna *et al.* 1998) and the presence of reduced channel conductance upon ryanodine association, would imply that its site is in fact located within the conduction pathway. In support of this hypothesis, single amino acid substitutions within the putative pore-forming segment reduce or abolish high affinity ryanodine binding (Zhao *et al.* 1999; Gao *et al.* 2000; Wang *et al.* 2003; Du *et al.* 2004). Chen *et al.* proposed that ryanodine binds within the central cavity of the channel pore such that its pyrole ring

interacts with the unique sites adjacent to the selectivity filter while the polar side is exposed to the pore pathway and contacts the solvent (Chen *et al.* 2002). Others suggested however that ryanodine induces an indirect effect on the channel pore and modulates RyR gating allosterically (Fessenden *et al.* 2001; Bidasee *et al.* 2003; Paolini *et al.* 2004).

Compound	Primary application	Binding site	Effects on channel gating	References
ryanodine	insecticide, toxin	binding site at the RyR C-terminus	activation followed by irreversible inactivation at $\mu\text{M}$ concentrations	(Callaway et al. 1994; Tanna et al. 1998; Zhao et al. 1999; Fessenden et al. 2001)
caffeine	stimulant, food ingredient	calcium-dependent binding site proposed to reside at the C-terminus and calcium-independent binding site in the cytoplasmic portion of RyR	activation by calcium-dependent mechanism, at higher concentrations ( $>5\text{mM}$ ) activation is calcium-independent	(Sitsapesan and Williams 1990; Treves et al. 2002)
ruthenium red	inorganic dye	multiple binding sites identified in the RyR primary sequence	inhibition	(Chen and MacLennan 1994; Xu et al. 1999)
procaine and tetracaine	local anaesthetics	not established	as above	(Xu et al. 1998b)
halothane	volatile anaesthetic	as above	calcium-dependent activation, triggers muscle contracture in MH-susceptible patients	(Bull and Marengo 1994; Glover et al. 2004; Liang et al. 2009)
4-chloro-meta-cresol	fungicide, preservative	binding site proposed to reside in the cytoplasmic portion of RyR	activation	(Zorzato et al. 1993; Herrmann-Frank et al. 1996; Treves et al. 2002)
natrin	snake venom toxin	not established	inhibition	(Zhou et al. 2008)
imperatoxin A	scorpion venom toxin	proposed to bind to the DHPR peptide A – binding site	activation	(Dulhunty et al. 2004; Lee et al. 2004)
FK506 and rapamycin	immunosuppressant	binding to FKBP12/12.6	dissociation of FKBP12/12.6 proposed to activate the channel and lead to uncoupled gating	(Ondrias et al. 1998; Gaburjakova et al. 2001; Marx et al. 2001b)
tricyclic antidepressants, phenothiazines and anthracyclines	anti-psychotic and chemotherapeutic agents	binding to CSQ	activation through the mechanism of increased free SR $\text{Ca}^{2+}$ levels due to the disruption of CSQ polymerisation process	(Park et al. 2005)

**Table 1.3** List of selected agents modulating RyR function

## 1.6 RyR-associated disorders

Calcium signals operate within a wide temporal range controlling fast and slow cellular responses. In myocytes, a rapid release of calcium from internal stores through ryanodine receptors triggers muscle contraction. This mechanism involves binding of  $\text{Ca}^{2+}$  ions to contractile proteins. Muscle responsiveness to subsequent stimuli is determined by its ability to promptly reduce calcium levels back to its resting concentration. A tight control of this process is essential for excitation-contraction coupling and a contractile response which is adequate to any given physiological trigger. Because calcium ions play also a central role in regulating slow cellular responses such as transcription and translation, any disruption in this control might have long-term consequences.

As ryanodine receptors activity is one of the key factors determining the amount, time and frequency of calcium release from the sarcoplasmic reticulum, their dysfunction has been associated with a number of muscle-associated disorders. Mutations in RyR genes have a direct causative role in skeletal and heart muscle diseases such as malignant hyperthermia (MH), central core disease (CCD) and catecholaminergic polymorphic ventricular tachycardia (CPVT). RyR-acquired defects have also been proposed to underlie other disorders such as heart failure (HF); however the direct causative role in the disease progression remains to be established as some authors reported normal RyR2 function in HF (Jiang et al. 2002b).

### 1.6.1 RyR1-associated disorders

Mutations in RyR1 are associated with two congenital skeletal muscle disorders; malignant hyperthermia and central core disease.

Malignant hyperthermia is a pharmacogenetic disease inherited in autosomal dominant fashion. Susceptible individuals develop a life-threatening generalized muscle contracture and a hypermetabolic response following the exposure to volatile anaesthetics (e.g. halothane) and depolarising muscle relaxants (e.g. succinylcholine) (Betzenhauser and Marks 2010). A related syndrome referred to as porcine stress

syndrome was identified in certain lines of domestic swine (Fujii *et al.* 1991). The first MH-associated mutation in humans was identified in the N-terminal part of the RyR1 protein and corresponded to the analogous amino acid substitution earlier identified in swine (Gillard *et al.* 1991). Until now, a number of RyR1 mutations have been linked to MH phenotype. Interestingly, disease-susceptibility has also been associated with mutations in the gene coding for the DHPR  $\alpha 1$  subunit (Monnier *et al.* 1997) and has been reported in the CSQ1 knockout mouse (Dainese *et al.* 2009). Although no CSQ1-associated skeletal myopathy has been identified so far, those findings suggest that the CSQ1 gene might be a potential candidate for linkage analysis in families where mutations in the RyR1 gene are excluded.

Malignant hyperthermia exhibits a significant clinical overlap with another disorder linked to mutations in the RyR1 gene – central core disease. The defining characteristic of CCD is the presence of cores of metabolically inactive tissue (devoid of mitochondria) in the centre of muscle fibres. The disease symptoms include motor developmental delay, a moderate muscle weakness which is mainly affecting lower limbs and sometimes MH-like symptoms (Betzenhauser and Marks 2010). The classical CCD phenotype has been linked to the RyR1 mutations which tend to cluster in the C-terminal portion of the protein and are inherited in a dominant fashion. Interestingly, another type of myopathy – multiminicore disease (MmD), which is inherited in a recessive manner, has also been linked to the RyR1 gene. At the cellular level, the disease is manifested by the presence of multiple minicores in the majority of muscle fibres while the clinical phenotype is highly variable, ranging from symptoms characteristic for CCD to a general muscle weakness accompanied by a respiratory impairment (Zhou *et al.* 2007). It has been suggested that MmD associated with recessive mutations in the RyR1 gene is in fact a pathological subtype of CCD (Ferreiro *et al.* 2002; Duarte *et al.* 2011).

Initially, RyR1 mutations were reported to exclusively reside in three defined regions of channel's primary structure, i.e. N-terminal, central and C-terminal, however later studies showed that they are in fact spread throughout the entire length of the protein (MacLennan and Zvaritch 2011). Until now, around 300 mutations have been described and most of them include missense substitutions and small in-frame deletions, which are believed to result in altered gating behaviour of the channel. Recently, quantitative defects in RyR1 expression leading to substantially reduced

protein levels and associated with severe forms of congenital myopathies have been also reported (Zhou et al. 2007; Monnier *et al.* 2008). Notably, some of these recessive mutations were shown to be heterozygous at the genomic level, however homozygous at the mRNA level due to the epigenetic silencing of the other allele.

At the cellular level, mutations in the RyR1 gene are believed to result in calcium mishandling. Early studies, which analysed the contractile response of muscle obtained from affected individuals in the presence of caffeine or halothane, established that MH/CCD mutations increase RyR1 sensitivity to activation indicating a gain-of-function mechanism (Betzenhauser and Marks 2010). Functional studies of MH and CCD mutant channels in heterologous expression systems corroborated earlier findings and showed that mutant RyR1 proteins exhibit hypersensitivity to activating agents and promote a variable degree of store depletion and an increase in intracellular resting calcium (Dirksen and Avila 2002). Expression of RyR1 carrying MH mutations in dyspedic myotubes allowed further characterisation of defects in a more physiological setting. Yang *et al.* reported that MH channels are hypersensitive to stimulation by direct activators (e.g. caffeine), exhibit increased sensitivity to plasma membrane depolarisation, decreased inhibition by magnesium and calcium and an increased activity at sub-activating  $\text{Ca}^{2+}$  levels (Yang *et al.* 2003). Similarly, MH-associated mutations in the DHPR  $\alpha 1$  subunit were shown to lead to the analogous phenotype, i.e. enhanced sensitivity of RyR1 to endogenous and exogenous activators (Weiss *et al.* 2004). Results obtained in functional studies led to the hypothesis that RyR1 mutations associated with CCD result in chronic calcium leak which is responsible for  $\text{Ca}^{2+}$ -mediated destruction of mitochondria and subsequent core formation, while in MH-associated mutations, an uncontrolled leak leading to muscle contracture is triggered by administration of volatile anaesthetics (Betzenhauser and Marks 2010).

This universal mechanism linking channel dysfunction to the observed phenotype does not however apply to all RyR1 mutations. Avila *et al.* demonstrated that CCD mutations located within the RyR1 putative pore region do not result in leaky channels but give rise to DHPR-uncoupled channels which lack depolarisation-induced calcium release (Avila *et al.* 2003). Further characterisation of those mutants in HEK293 cells revealed that calcium sensitivity and peak amplitude is severely compromised in the homozygous scenario, however, while co-expression with wild

type RyR1 rescues the former, it fails to restore normal calcium transients (Du et al. 2004). Hence, the emerging picture points towards a distinct mechanism of channel dysfunction and consequently a heterogeneous effect on cellular calcium handling and EC coupling in mutations associated with three distinct phenotypes: MH only, MH/CCD and CCD. In agreement with this notion, Dirksen and Avila showed that both MH and MH/CCD mutations exhibit voltage dependence shifted to a more negative potential and display significantly higher incidence of spontaneous  $\text{Ca}^{2+}$  oscillations, however only MH/CCD mutations lead to an increase in resting calcium levels and reduced SR content (Dirksen and Avila 2004). Similarly, Brini and colleagues showed that CCD-mutations but not MH mutations result in SR store depletion (Brini *et al.* 2005). Those studies led to the hypothesis that mutations associated solely with the MH phenotype result in moderately hypersensitive channels which cause substantial calcium leak only upon stimulation with triggering agents and without those, cellular compensatory mechanisms are sufficient enough to maintain normal calcium handling. Conversely, mutations which lead to the mixed MH/CCD phenotype exhibit a substantial increase in basal activity promoting SR store depletion, which leads to diminished calcium release during EC coupling and consequently to muscle weakness. Although the mechanism of channel dysfunction in CCD-associated mutations which exhibit functional EC-uncoupling is strikingly different, those mutations ultimately lead to the same phenotype associated with muscle weakness due to reduced depolarisation-induced calcium release (Avila and Dirksen 2001; Avila *et al.* 2003). It was further suggested that the formation of cores is determined by reduced  $\text{Ca}^{2+}$  transients (due to store depletion or EC-uncoupling) rather than an increase in resting calcium. Mice expressing one of the CCD-uncoupling mutations showed many features commonly observed in human patients; however the manifestation of the phenotype was highly variable indicating that additional factors may contribute to the clinical presentation of the disease (Zvaritch *et al.* 2009). Notably, others reported that the EC-uncoupled phenotype is accompanied by an increase in resting calcium and SR store depletion, an observation indicative of leaky channels (Lynch *et al.* 1999; Brini *et al.* 2005)

MH episodes are typically rapid and severe and, if not treated promptly, result in a very high mortality rate reaching over 80% (Betzenhauser and Marks 2010). Dantrolene, which was synthesized in 1967 as a new class of skeletal muscle relaxant,

has been successfully used to manage MH episodes following a multicentre study which proved its high efficacy (Snyder *et al.* 1967; Kolb *et al.* 1982). At the cellular level, dantrolene was found to suppress the depolarisation-induced calcium release from SR (Szentesi *et al.* 2001). The therapeutic effect of dantrolene was subsequently linked to its direct effect on RyR1, where it was shown to reduce caffeine-induced channel activation and rescue the hypersensitive phenotype associated with MH mutations (Zhao *et al.* 2001). Using photoaffinity labelling, Paul-Petzer *et al.* demonstrated that the dantrolene binding site is located on RyR1 and is composed of amino acids 590-609 (Paul-Pletzer *et al.* 2002). Currently, there is no effective therapy for treatment of symptoms associated with RyR1 mutations resulting in CCD. As some of those mutations exhibit a partially overlapping phenotype with those leading to MH only, one might speculate that in those particular cases dantrolene would have the ability to oppose muscle weakness resulting from SR store depletion by preventing channel hyperactivation. In those patients, disease management would probably require chronic dantrolene administration likely to cause a number of CNS-linked side effects (Inan and Wei 2010).

### 1.6.2 RyR2-associated disorders

Mutations in the RyR2 gene have been linked to emotional stress and exercise induced arrhythmias associated with two diseases displaying partially overlapping clinical phenotype: CPVT and arrhythmogenic right ventricular dysplasia (ARVD2). In addition, mutations in the RyR2 gene have also been linked to sudden infant death syndrome (SIDS) (Tester *et al.* 2007).

The first comprehensive clinical evaluation of CPVT patients was described by Leenhardt *et al.* and involved 21 children (Leenhardt *et al.* 1995). The initial notion considered CPVT as a disease exclusively manifesting at a very young age, however it was later shown that the first symptoms might also occur at adulthood. The disease is associated with episodes of potentially lethal arrhythmias triggered by emotional or physical stress. It displays a high mortality rate of up to 50% due to the fact that patients usually remain undiagnosed until the first arrhythmic episode occurs (Medeiros-Domingo *et al.* 2009). Late diagnosis is directly linked to the fact that in

the absence of appropriately high  $\beta$ -adrenergic stimuli, CPVT mutations do not cause any structural abnormalities in the heart and patients present normal cardiac function at rest (Priori *et al.* 2001). On the other hand, ARVD2, which also puts patients at increased risk of arrhythmia, is associated with progressive degeneration with fibrofatty replacement of the right ventricle (Tiso *et al.* 2001). Because there is significant phenotypic overlap between those two disorders and very often mild structural abnormalities of the heart are only apparent upon post mortem examination but remain undetectable with a standard echocardiography procedure, it has been suggested that the two disorders represent variable phenotypic representation of the same disease (Bauce *et al.* 2002; d'Amati *et al.* 2005). Some of the patients diagnosed with CPVT indeed display minor structural abnormalities of the right ventricle detected with echocardiography however they do not fulfil the criteria to be included in the ARVD2 group.

CPVT/ARVD2 originating from mutations in the RyR2 gene is inherited in an autosomal dominant fashion; however the disease exhibits incomplete penetrance, i.e. carriers of the same mutation present different severity of symptoms and some remain completely asymptomatic (silent carriers) indicating the involvement of other factors (Bauce *et al.* 2002; Priori *et al.* 2002; Postma *et al.* 2005). In support of additional determinants influencing the clinical phenotype, males were shown to be at a significantly higher risk of cardiac events. Notably, additional factors directly linked to RyR2 such as protein expression profile and subunit composition have been implicated in the disease severity (Milting *et al.* 2006). An autosomal recessive form of CPVT has been linked to mutations in the calsequestrin 2 gene (Lahat *et al.* 2001; di Barletta *et al.* 2006). A recessive form of CPVT accompanied by muscle weakness has also been reported in two families with mutations in triadin gene (Roux-Buisson *et al.* 2012). In those patients, triadin defects ultimately resulted in the absence of the protein (two mutations leading to premature stop codons and one missense mutation affecting protein stability). Only recently, a CPVT-like phenotype inherited in a dominant fashion and associated with mutations in the calmodulin gene has also been reported (Nyegaard *et al.* 2012). Since both CSQ2 and CaM constitute endogenous regulators of RyR2 function while triadin is believed to mediate RyR/CSQ interaction, an arrhythmogenic phenotype seems to be ultimately determined by the RyR's inability to maintain normal calcium handling.

The direct link between mutations in the RyR2 gene and CPVT/ARVD2 was shown in 2001 (Priori et al. 2001; Tiso et al. 2001). Until now, more than 140 mutations in the RyR2 gene linked to exercise and emotional stress induced arrhythmia have been reported (Table 1.4). The majority of the mutations are missense substitutions, however in-frame deletions and duplications have been also found. Interestingly, the deletion within exon 3 was shown to result in an unusual phenotype in which typical stress-induced arrhythmia is accompanied by depressed left ventricular function and dilated cardiomyopathy (Bhuiyan et al. 2007). A comprehensive analysis of patients diagnosed with RyR2-associated arrhythmias revealed that mutations exhibit higher tendency to cluster in three distinctive regions than those associated with skeletal muscle disorders (Medeiros-Domingo et al. 2009). Those regions include the three mutation hot spots described earlier for RyR1; N-terminal domain (residues 77-466), central domain (2246-2534) and C-terminal region (3778-4959). Although RyR2 was not considered a polymorphic gene, around 10% of missense variants were found in control subjects (Medeiros-Domingo et al. 2009). The three most commonly found polymorphic substitutions are: Q2958R, G1886S, and G1885E. Interestingly, the concomitant presence of the two latter substitutions (composite heterozygote) was reported in an ARVD2 patient and, at the molecular level, was associated with a hyperactive channel demonstrating that common polymorphisms may in fact lead to a clinical phenotype (Milting et al. 2006).

The electrographic pattern of ventricular tachycardia closely resembles the arrhythmia associated with calcium overload and delayed afterdepolarisation (DAD) observed during digitalis toxicity (Priori et al. 2001). By analogy, the occurrence of arrhythmia in RyR2 mutation carriers has been long suspected to involve calcium mishandling which becomes apparent during emotional or physical stress associated with  $\beta$ -adrenergic stimulation. The degeneration of the right ventricle in ARVD2 patients was suggested to be triggered by prolonged calcium overload leading to mitochondria damage and subsequent apoptosis of cardiomyocytes (d'Amati et al. 2005). Although the exact molecular mechanism of channel dysfunction remains a subject of debate, it is believed that a higher propensity of mutant RyR2 for spontaneous openings upon exposure to  $\beta$ -adrenergic stimulation underlies the mechanism of delayed afterdepolarisation and triggered arrhythmia. The spontaneous calcium release during diastole is thought to activate the sodium/calcium exchanger

in the plasma membrane which removes excess calcium at the expense of sodium ions entering the cytoplasm. This mechanism of calcium removal with concomitant sodium influx was proposed to result in plasma membrane depolarisation during diastole, i.e. delayed afterdepolarisation which, if high enough, would trigger an action potential leading to triggered arrhythmia (Priori and Chen 2011). Interestingly, a number of recent reports suggest that cardiac Purkinje cells exhibit a greater propensity to develop abnormalities in calcium handling implying their primary role in triggering arrhythmic events in CPVT patients (Herron *et al.* 2010; Kang *et al.* 2010). CPVT/ARVD2 mutations have been evaluated in mouse knock-in models and recapitulated the phenotype of susceptible patients, i.e. ventricular tachycardia developed upon exercise or injection of epinephrine. In agreement with the disease manifestation in humans, mice carrying CPVT-associated mutations did not exhibit any structural heart abnormalities while subtle right ventricular impairment was reported for the R176Q mutation associated with the ARVD2 phenotype (Cerrone *et al.* 2005; Kannankeril *et al.* 2006; Uchinoumi *et al.* 2010; Suetomi *et al.* 2011). Analysis of calcium handling in cardiac myocytes isolated from mutant mice revealed a higher incidence of spontaneous  $\text{Ca}^{2+}$  oscillations upon  $\beta$ -adrenergic stimulation in agreement with the hypothesis of an uncontrolled leak through RyR2 (Kashimura *et al.* 2010; Uchinoumi *et al.* 2010; Suetomi *et al.* 2011).

No	Mutation type	Amino acid change	Domain	Phenotype	References
1	deletion	1.1kb deletion (N57-G91)	including N-terminal hot spot	CPVT, DCM, AF, LV function depressed	(Bhuiyan et al. 2007)
2	deletion	3.6kb deletion (exon 3)	as above	CPVT	(Medeiros-Domingo et al. 2009)
3	missense	L62F	upstream of N-terminal hot spot	CPVT	(Medeiros-Domingo et al. 2009)
4	missense	A77V	N-terminal hot spot	CPVT/ARVD2	(d'Amati et al. 2005)
5	missense	M81L	as above	CPVT	(Medeiros-Domingo et al. 2009)
6	missense	P164S	as above	CPVT	(Choi et al. 2004)
7	missense	R169Q	as above	CPVT	(Hsueh et al. 2006)
8	missense	R176Q	as above	ARVD (in combination with T2504M), CPVT	(Tiso et al. 2001; Haugaa et al. 2010)
9	missense	V186M	as above	CPVT	(Tester et al. 2006)
10	missense	E189D	as above	CPVT	(Jiang et al. 2010)
11	missense	G230C	as above	CPVT	(Meli et al. 2011)
12	missense	H240R	as above	CPVT	(Medeiros-Domingo et al. 2009)
13	missense	E243K	as above	CPVT	(Medeiros-Domingo et al. 2009)
14	missense	F329L	as above	CPVT	(Medeiros-Domingo et al. 2009)
15	missense	R332W	as above	CPVT	(Medeiros-Domingo et al. 2009)
16	cSNP	V377M	as above		(Medeiros-Domingo et al. 2009)
17	missense	G357S	as above	CPVT	(Medeiros-Domingo et al. 2009)
18	missense	S406L	as above	CPVT	(Jung et al. 2012)
19	missense	R414C	as above	CPVT	(Tester et al. 2005a; Creighton et al. 2006)
20	missense	R414L	as above	SCD associated with drowning	(Choi et al. 2004)
21	missense	T415R	as above	CPVT	(Medeiros-Domingo et al. 2009)
22	missense	I419F	as above	SCD	(Choi et al. 2004)
23	missense	R420W	as above	CPVT/ARVD	(Bauce et al. 2002)
24	missense	R420Q	as above	CPVT	(Medeiros-Domingo et al. 2009)
25	missense	L433P	as above	ARVD	(Tiso et al. 2001)

26	missense	P466A	as above	syncope	(Tester <i>et al.</i> 2005b)
27	<i>cSNP</i>	<i>V507I</i>	downstream of N-terminal hot spot		(Medeiros-Domingo et al. 2009)
28	missense	A549V	as above	CPVT	(Medeiros-Domingo et al. 2009)
29	missense	S616L	as above	CPVT	(Marjamaa <i>et al.</i> 2009)
30	missense	R739H	as above	CPVT	(Medeiros-Domingo et al. 2009)
31	missense	R1013Q	as above	CPVT	(Medeiros-Domingo et al. 2009)
32	missense	R1051P	as above	CPVT	(Marjamaa <i>et al.</i> 2009)
33	<i>cSNP</i>	<i>A1136V</i>	as above		(Medeiros-Domingo et al. 2009)
34	missense	T1107M	as above	CPVT	(Medeiros-Domingo et al. 2009)
35	missense	E1724K	as above	CPVT	(Postma <i>et al.</i> 2005)
36	missense	E1837K	as above	CPVT	(Medeiros-Domingo et al. 2009)
37	<i>cSNP</i>	<i>G1885E</i>	outside hot spots, within D3 region	if expressed in composite heterologous fashion with G1886S leads to ARVD2	(Milting <i>et al.</i> 2006)
38	<i>cSNP</i>	<i>G1886S</i>	as above	if expressed in composite heterologous fashion with G1885E leads to ARVD2	(Milting <i>et al.</i> 2006)
39	missense	E2045G	upstream central domain hot spot	CPVT	(Medeiros-Domingo et al. 2009)
40	missense	V2113M	upstream central domain hot spot	CPVT	(Medeiros-Domingo et al. 2009)
41	missense	G2145R	as above	CPVT/SCD	(Marjamaa <i>et al.</i> 2011)
42	<i>cSNP</i>	<i>Y2156C</i>	as above		(Medeiros-Domingo et al. 2009)
43	missense	H2168Q	as above	CPVT	(Medeiros-Domingo et al. 2009)
44	<i>cSNP</i>	<i>E2183V</i>	as above		(Medeiros-Domingo et al. 2009)
45	missense	D2216V	as above	CPVT	(Medeiros-Domingo et al. 2009)
46	missense	S2246L	central domain hot spot	CPVT	(Priori <i>et al.</i> 2001)
47	missense	A2254V	as above	CPVT	(Postma <i>et al.</i> 2005)
48	missense	R2267H	as above	SIDS	(Tester <i>et al.</i> 2007)

49	missense	E2296Q	as above	CPVT	(Medeiros-Domingo et al. 2009)
50	missense	V2306I	as above	CPVT	(Laitinen et al. 2003)
51	missense	F2307L	as above	CPVT	(Medeiros-Domingo et al. 2009)
52	missense	E2311D	as above	CPVT	(Priori et al. 2002)
53	missense	V2321M	as above	CPVT	(Nishio et al. 2008)
54	missense	P2328S	as above	CPVT	(Laitinen et al. 2001)
55	missense	F2331S	as above	SCD	(Creighton et al. 2006)
56	missense	G2337V	as above	CPVT	(Haugaa et al. 2010)
57	missense	R2359Q	as above	SCD/CPVT	(Aizawa et al. 2007)
58	missense	N2386I	as above	CPVT/ARVD	(Tiso et al. 2001; Bauce et al. 2002)
59	missense	A2387T	as above	syncope	(Tester et al. 2005b)
60	missense	A2387P	as above	CPVT	(Bagattin et al. 2004)
61	<i>cSNP</i>	<i>M2389L</i>	as above		(Medeiros-Domingo et al. 2009)
62	missense	Y2392C	as above	ARVD	(Baucé et al. 2002)
63	missense	A2394G	as above	CPVT	(Postma et al. 2005)
64	missense	R2401H	as above	CPVT	(Aizawa et al. 2007)
65	missense	R2401L	as above	SCD	(Creighton et al. 2006)
66	missense	A2403T	as above	CPVT	(Choi et al. 2004)
67	missense	R2404T	as above	CPVT	(Beckmann et al. 2008)
68	missense	R2474S	as above	CPVT	(Priori et al. 2001)
69	missense	R2420W	as above	CPVT	(Medeiros-Domingo et al. 2009)
70	missense	V2475F	as above	CPVT	(Tester et al. 2005a)
71	<i>missense</i>	<i>L2487I</i>	as above	<i>CPVT</i>	(Tester et al. 2005b)
72	missense	T2504M	as above	ARVD	(Tiso et al. 2001)
73	missense	T2510A	as above	CPVT	<a href="http://www.fsm.it/cardmoc/">http://www.fsm.it/cardmoc/</a>
74	missense	L2534V	as above	CPVT	(Hasdemir et al. 2004)
75	<i>cSNP</i>	<i>Q2958R</i>	downstream of central domain hot spot		(Tiso et al. 2001)
76	missense	N3308S	as above	unusual phenotype, arrhythmia at rest	(Marjamaa et al. 2009)
77	missense	R3570W	as above	SCD, arrhythmia at rest	(Marjamaa et al. 2011)
78	missense	L3778F	C-terminal hot spot	CPVT	(Priori et al. 2002)
79	missense	C3800F	as above	syncope of unknown origin	(Tester et al. 2005b)

80	missense	L3879P	as above	CPVT	(Medeiros-Domingo et al. 2009)
81	missense	Q3925E	as above	CPVT	(Medeiros-Domingo et al. 2009)
82	missense	S3938R	as above	CPVT	(Tester et al. 2006)
83	missense	G3946S	as above	CPVT	(Priori et al. 2002)
84	missense	G3946A	as above	CPVT	(Medeiros-Domingo et al. 2009)
85	missense	S3959L	as above	CPVT	<a href="http://www.fsm.it/cardmoc/">http://www.fsm.it/cardmoc/</a>
86	missense	M3972I	as above	CPVT	(Medeiros-Domingo et al. 2009)
87	missense	D3973H	as above	CPVT	(Medeiros-Domingo et al. 2009)
88	missense	L3974Q	as above	CPVT	(Medeiros-Domingo et al. 2009)
89	missense	K3997E	as above	CPVT	(Medeiros-Domingo et al. 2009)
90	missense	F4020L	as above	CPVT	(Postma et al. 2005)
91	cSNP	V4010M	as above		(Tester et al. 2005b)
92	missense	E4076K	as above	CPVT	(Postma et al. 2005)
93	missense	N4097S	C-terminal hot spot, CaM-like domain	SCD	(Tester et al. 2004)
94	missense	N4104K	as above	CPVT	(Priori et al. 2001)
95	missense	N4104I	as above	CPVT	(Postma et al. 2005)
96	cSNP	L4105F	as above		(Hasdemir et al. 2008)
97	missense	H4108N	as above	CPVT	(Postma et al. 2005)
98	missense	H4108Q	as above	CPVT	(Postma et al. 2005)
99	missense	S4124G	as above	CPVT	(Medeiros-Domingo et al. 2009)
100	missense	S4124T	as above	syncope of unknown origin	(Tester et al. 2005b)
101	missense	R4144C	as above	CPVT	(Berge et al. 2008)
102	missense	E4146K	as above	SCD	(Tester et al. 2004)
103	missense	Y4149S	as above	CPVT	(Medeiros-Domingo et al. 2009)
104	missense	R4157Q	as above	CPVT	(Medeiros-Domingo et al. 2009)
105	missense	T4158P	as above	SCD	(Tester et al. 2004)
106	missense	Q4159P	as above	CPVT	(Medeiros-Domingo et al. 2009)
107	missense	N4178S	as above	CPVT	(Medeiros-Domingo et al. 2009)
108	missense	E4187Q	as above	CPVT	(Medeiros-Domingo et al. 2009)
109	missense	T4196A	as above	CPVT	(Tester et al. 2006)

110	missense	Q4201R	as above	CPVT	(Laitinen et al. 2001)
111	<i>cSNP</i>	<i>A4282V</i>	C-terminal hot spot, D1 region		(Tester et al. 2005b)
112	<i>cSNP</i>	<i>R4307C</i>	as above		(Medeiros-Domingo et al. 2009)
113	<i>cSNP</i>	<i>G4315E</i>	as above		(Medeiros-Domingo et al. 2009)
114	missense	E4431K	as above	CPVT	(Berge et al. 2008)
115	missense	R4497C	as above	CPVT, non-responsive to $\beta$ -blockers	(Priori et al. 2001; Cerrone et al. 2005)
116	missense	F4499C	as above	CPVT	(Choi et al. 2004)
117	missense	M4504I	as above	CPVT	(Bagattin et al. 2004)
118	missense	A4510T	C-terminal hot spot, putative M5 domain (Fig.1.5)	CPVT	(Choi et al. 2004)
119	missense	F4511L	as above	CPVT	<a href="http://www.fsm.it/cardmoc/">http://www.fsm.it/cardmoc/</a>
120	missense	A4556T	C-terminal hot spot	syncope of unexplained origin	(Tester et al. 2005b)
121	missense	S4565R	as above	SIDS	(Tester et al. 2007)
122	missense	V4653F	as above	CPVT	(Laitinen et al. 2001)
123	missense	A4607P	as above	CPVT	(Bagattin et al. 2004)
124	missense	E4611K	as above	CPVT	(Berge et al. 2008)
125	missense	W4645R	as above	CPVT	(Medeiros-Domingo et al. 2009)
126	missense	K4650E	as above	CPVT	(Medeiros-Domingo et al. 2009)
127	duplication	4657-4658 insertion of EY	as above	syncope of unexplained origin	(Tester et al. 2005b)
128	missense	G4662S	as above	CPVT	(Postma et al. 2005)
129	missense	G4671R	as above	CPVT	(Choi et al. 2004)
130	missense	G4671V	as above	CPVT	(Haugaa et al. 2010)
131	deletion	N4736 del	as above	CPVT	(Medeiros-Domingo et al. 2009)
132	missense	H4762P	C-terminal hot spot, M7b/M8 loop (S4-S5 linker)	CPVT	(Postma et al. 2005)
133	missense	V4771I	C-terminal hot spot	CPVT	(Priori et al. 2002)
134	missense	R4790Q	C-terminal hot spot, putative M8 domain	CPVT	(Medeiros-Domingo et al. 2009)

135	missense	K4805R	C-terminal hot spot	CPVT	(Medeiros-Domingo et al. 2009)
136	missense	R4822H	C-terminal hot spot, pore helix/selectivity filter	CPVT	(Medeiros-Domingo et al. 2009)
137	missense	I4848V	C-terminal hot spot, putative M10 domain	CPVT	(Choi et al. 2004)
138	missense	F4851C	as above	SCD/CPVT	(Aizawa et al. 2007)
139	missense	A4860G	as above	CPVT	(Priori et al. 2002)
140	missense	I4867M	as above	CPVT	(Priori et al. 2002)
141	missense	V4880A	C-terminal hot spot	CPVT	(Bagattin et al. 2004)
142	missense	N4895D	as above	CPVT	(Priori et al. 2002)
143	missense	P4902L	as above	CPVT	(Laitinen et al. 2003)
144	missense	P4902S	as above	CPVT	(Postma et al. 2005)
145	missense	G4936R	as above	CPVT	(Medeiros-Domingo et al. 2009)
146	missense	E4950K	as above	CPVT	(Priori et al. 2002)
147	missense	R4959Q	as above	CPVT	(Laitinen et al. 2003)

**Table 1.4** List of arrhythmia-linked mutations and SNP as of June 2013

### 1.6.2.1 Mechanism of channel dysfunction

The mechanism underlying RyR2 dysfunction remains under debate. The basic question of how mutations located in different domains lead to the same phenotype, i.e. increased activity of the channel in circumstances mimicking stress and exercise, have been addressed by multiple research groups but a common consensus has not been reached. The majority of experiments aiming to dissect the molecular mechanism of channel dysfunction were performed using heterologously expressed RyR2. The evaluation of the effect of arrhythmia-linked mutations on channel function was performed using calcium imaging, single channel recordings and [<sup>3</sup>H]ryanodine binding. These studies revealed that the presence of mutations induce gain-of-function changes in the RyR2 function which is reflected by an increased sensitivity to activation by calcium, caffeine and cAMP-mobilising agents (Jiang *et al.* 2002a; George *et al.* 2003; Jiang *et al.* 2004; Thomas *et al.* 2005). In agreement with the fact that the CPVT-associated phenotype becomes unmasked during stress

and exercise, most studies reported that in the native environment of a cardiomyocyte, calcium handling becomes defective only upon high frequency pacing or  $\beta$ -adrenergic stimulation (George et al. 2003; Jung et al. 2012). Those experiments established two general features of the CPVT phenotype; first, recombinantly expressed channels exhibit increased basal activity and second, in the cellular milieu of cardiac cells  $\beta$ -adrenergic stimulation or infusion with activating agent is necessary to induce the disease phenotype. Physiologically,  $\beta$ -adrenergic stimulation constitutes a major component of the “fight-or-flight response” which allows for a rapid increase in heart rate and contractility to fulfil augmented demand for blood supply in circumstances of acute stress. Activation of  $\beta$ -adrenergic receptors on cardiac myocytes stimulates the production of cAMP which is an activator of PKA. PKA phosphorylates numerous substrates involved in EC coupling including DHPR, RyR2 and phospholamban. These modifications have positive inotropic and chronotropic effect on the heart muscle (Betzenhauser and Marks 2010).

It was proposed that phosphorylation of RyR2 by PKA at a specific residue (S2808) causes dissociation of FKBP12.6 from the channel complex which results in an increased sensitivity for cytosolic  $\text{Ca}^{2+}$ -dependent activation (Marx et al. 2000; Meli et al. 2011) (see Section 1.5.6). This physiological mechanism underlying cardiomyocyte response following stress and exercise challenge was proposed to be dysfunctional in the presence of CPVT mutations. The authors showed that mutant RyR2 channels exhibit reduced affinity for FKBP12.6 and are significantly more sensitive to PKA-mediated activation (Wehrens et al. 2003). This hypothesis was further extended to explain RyR2 dysfunction in heart failure, where chronic  $\beta$ -adrenergic stimulation was proposed to lead to channel hyper-phosphorylation and subsequent depletion of FKBP12.6 (Marx et al. 2000; Yano et al. 2003; Oda et al. 2005). The central role of FKBP12.6 in channel dysfunction was reinforced by CPVT-like symptoms observed in FKBP12.6 knock-out mice (Wehrens et al. 2003). However, other groups failed to observe exercise-induced arrhythmia in the FKBP12.6 null mice and were unable to reproduce the majority of previous findings supporting the above hypothesis (Xiao et al. 2007). Notably, no difference in FKBP12.6 binding was reported between wild type RyR2 and RyR2 carrying arrhythmia-associated mutations (Liu et al. 2006; Zissimopoulos et al. 2009). George

et al. corroborated earlier findings showing reduced interaction between FKBP12.6 and RyR2 following  $\beta$ -adrenergic stimulation, however this effect was indistinguishable between mutant and wild type channels (George et al. 2003). Furthermore, the notion that PKA-mediated phosphorylation of RyR2 at a single residue (S2808) constitutes a critical component of cardiomyocyte regulation by the sympathetic nervous system was questioned since mutation of this residue did not change the contractile response to cAMP-mobilising compounds (MacDonnell et al. 2008). In agreement with the above, Xiao et al. reported that the phosphorylation level of S2808 does not substantially increase following  $\beta$ -adrenergic stimulation (Xiao et al. 2006). Furthermore, Sedej and colleagues showed that arrhythmogenic events in mouse cardiomyocytes with a human CPVT mutation can be effectively triggered by calcium overload in the absence of  $\beta$ -adrenergic stimulation suggesting a mechanism independent of RyR2 phosphorylation (Sedej et al. 2010).

An alternative mechanism by which adrenergic stimulation unmasks channel dysfunction in CPVT patients was proposed by Jiang and colleagues (Jiang et al. 2004; Jiang et al. 2005). According to this model, arrhythmia-associated mutations increase RyR2 sensitivity to luminal calcium. One of the downstream targets of sympathetic signalling is phospholamban, which inhibits SR  $\text{Ca}^{2+}$  ATPase (SERCA) pump. PKA-mediated phosphorylation of phospholamban relieves its inhibition on SERCA and thus promotes calcium uptake. The rise in the  $\text{Ca}^{2+}$  SR content ultimately allows for the increase in the strength and frequency of cardiac muscle contraction. According to this hypothesis, in the presence of arrhythmia-associated mutations, the RyR2 threshold for activation by luminal calcium is reduced. This leads to an increased propensity of the channel to open in circumstances of high SR  $\text{Ca}^{2+}$  load such as stress and exercise. This depolarisation independent mechanism of calcium discharge has been referred to as store-overload-induced calcium release (SOICR). In support of this hypothesis, the authors showed that in single channel recordings, the significant difference in channel activation between wild type and mutant RyR2 can be observed upon changes in luminal but not cytosolic calcium levels (Jiang et al. 2005). Notably, mutations in the major SR calcium buffering protein (CSQ2), which lead to an identical arrhythmogenic phenotype, were shown to significantly lower its binding capacity for  $\text{Ca}^{2+}$  (Kim et al. 2007). Those findings strongly support the role of luminal calcium in the pathogenesis of CPVT in agreement with SOICR being a

common mechanism of channel dysfunction in arrhythmia linked to CSQ2 and RyR2 mutations.

Notably, some groups reported that mutant channels are not only hypersensitive to calcium activation but they also possess an impaired sensitivity to calcium and/or magnesium-dependent inactivation (Lehnart *et al.* 2004; Thomas *et al.* 2005). Furthermore, Tang *et al.* suggested that the reduction in the sensitivity to calcium-mediated inhibition is a common defect in RyR2 mutations associated with ARVD2 and dilated cardiomyopathy (Tang *et al.* 2012). According to the authors, a decrease in channel inhibition delays termination of SR  $\text{Ca}^{2+}$  release and consequently leads to the increase in the cytoplasmic  $\text{Ca}^{2+}$  transient. Abnormal calcium transients are currently recognised as an important factor triggering cardiac remodelling thus providing possible explanation for the structural changes occurring in hearts of some patients positive for RyR2 mutations.

The hypotheses presented above propose different mechanisms by which abnormal calcium release is triggered by sympathetic stimulation; however they do not provide an explanation to how RyR2 mutations located in different parts of the protein lead to an almost identical phenotype. Because RyRs constitute one of the biggest channels with the majority of protein located in the cytoplasm at a considerable distance from the channel pore, it is reasonable to assume that the receptor must be regulated by long-distance interactions between discrete structural/functional domains. Most of the RyR modulators are believed to bind to the cytoplasmic portion of the protein (Sharma *et al.* 2006; Cornea *et al.* 2009) therefore an allosteric regulation within the receptor would enable it to promptly alter its gating properties in response to changes occurring at distant cytoplasmic sites. In support of this view, Samso and colleagues reported that multiple, large conformational changes in the receptor structure occur during channel opening (Samso *et al.* 2009). Moreover, the structural rearrangement of cytoplasmic domains is tightly coupled to the structural changes in the ion gate further supporting the notion of long-range allosteric pathways being in control of channel gating. Ikemoto and colleagues proposed that arrhythmia-associated mutations interfere with this process (Yamamoto *et al.* 2000; Uchinoumi *et al.* 2010). In their hypothesis, an aberrant interaction between critical domains destabilises the closed state of the channel rendering it more sensitive to stimuli. These stimuli could be PKA-mediated phosphorylation of RyR2 triggering dissociation of FKBP12.6

or/and increased SOICR. The common phenotype of mutations located in different hot spots is determined by the fact that N-terminal, central and C-terminal hot spots constitute critical interacting domains involved in channel gating control (Yamamoto and Ikemoto 2002a; George *et al.* 2004; Hamada *et al.* 2007; Yamamoto *et al.* 2008). A detailed description of current knowledge regarding domain-domain interactions and their role in the control of RyR activity will be covered in Section 1.7.

### 1.6.2.2 Existing therapies

Current management of arrhythmia originating from RyR2 mutations involves the use of  $\beta$ -blockers combined with exercise restriction (Leenhardt *et al.* 2012). However, the efficacy in preventing arrhythmic episodes is highly variable with some patients remaining at very high risk of SCD (Hayashi *et al.* 2009; Haugaa *et al.* 2010; Sy *et al.* 2011). Patients who do not respond to standard  $\beta$ -blocker therapy are recommended to receive implantable cardioverter-defibrillator (ICD); however given the young age of patients, the use of defibrillator in disease management remains a challenging option. It is clear, that the available therapy for CPVT treatment has substantial limitations. Current advances in the understanding of channel function have provided some guidance in the development and design of novel therapies. A combination of *in vitro* data and animal studies led to some encouraging results which suggest the efficacy of drugs other than  $\beta$ -blockers.

The efficacy of flecainide in preventing arrhythmia associated with mutations in CSQ and RyR2 has been reported in animal models (Watanabe *et al.* 2009; Liu *et al.* 2011a). Notably, the drug was also effective in two patients carrying RyR2 and CSQ2 mutations who were not responsive to a standard  $\beta$ -blocker therapy (Watanabe *et al.* 2009). Flecainide is a sodium channel blocker, however some reports suggested its direct action on RyR2 (Hilliard *et al.* 2010). Liu and colleagues proposed that anti-arrhythmic effects of flecainide are mediated by preventing sodium entry in response to RyR2-mediated calcium leak (Liu *et al.* 2011a). It is currently however not clear whether flecainide acts through sodium channels, RyR channels or both (Watanabe *et al.* 2011; Sikkel *et al.* 2013a, b).

JTV519 (K201) was reported to have a cardio-protective effect in animal models of heart failure through a direct action on RyR2 (Kohno *et al.* 2003). Its effect was proposed to involve stabilisation of RyR2/FKBP12.6 complex (Yano *et al.* 2003). Subsequently, JTV519 was shown to prevent SOICR in HEK293 cells expressing one of the arrhythmia-associated RyR2 mutants; however its anti-arrhythmic properties were proposed to be independent of FKBP12.6 (Hunt *et al.* 2007). The identification of the JTV519-binding site within the cytoplasmic portion of the RyR2 (residues 2114-2149) brought about an alternative model explaining the cardioprotective effects of this drug (Yamamoto *et al.* 2008). According to this model, JTV519 promotes stabilisation of inter-domain interactions within cytoplasmic part of the RyR channel. *In vitro*, the drug was shown to reduce diastolic leak and improve diastolic function in human cardiomyocytes in conditions of acute calcium overload (Sacherer *et al.* 2012) and to prevent the development of hypertrophy in rat neonatal cardiomyocytes (Hamada *et al.* 2009). In animal models, JTV519 was shown to block left ventricle (LV) remodelling and to preserve LV diastolic and systolic function thus preventing the development of heart failure (Yano *et al.* 2003). The fact that RyR2 dysfunction in heart failure and CPVT is believed to share the same mechanism, i.e. increased sensitivity to activation producing diastolic calcium leak, JTV519 was expected to produce a therapeutic effect in the scenario of arrhythmia-linked mutations. Accordingly, the drug prevented arrhythmic episodes in the R2474S knock-in mouse model and was also protective against the destabilising effects of an N-terminal domain peptide (Suetomi *et al.* 2011). However, in the knock-in mouse model carrying one of the C-terminal arrhythmia-associated mutations (R4496C), JTV519 failed to rescue the disease phenotype either in animals or in isolated myocytes (Liu *et al.* 2006). Moreover, JTV519 did not reduce  $\text{Ca}^{2+}$  spark frequency induced by a C-terminal domain peptide and had no effect in the S2246L knock-in mouse model (Tateishi *et al.* 2009; Suetomi *et al.* 2011). Those findings clearly indicate that the drug's cardio-protective effect is directly dependent on the RyR2 mutation site and therefore possess a limited potential in clinical setting. Alternatively, JTV519 may have limited efficacy and therefore might be unable to prevent arrhythmic events in mutations associated with more severe phenotype. Indeed, both mutations, which were resistant to JTV519 treatment were shown to result in serious defects in calcium handling, i.e. R4497C patients and knock-in animal models were reported to respond very poorly to the standard  $\beta$ -blocker therapy

(Cerrone et al. 2005), while the presence of S2246L mutation was shown to lead to unusually high  $\text{Ca}^{2+}$  spark frequency and low SR content in the absence of sympathetic stimulation (Suetomi et al. 2011).

A number of recent communications reported a protective effect of dantrolene in heart failure and CPVT. This is somewhat unexpected in the context of earlier reports showing no appreciable effect on RyR2 function (Zhao et al. 2001). *In vitro*, dantrolene was shown to prevent hypertrophy in neonatal cardiomyocytes (Hamada et al. 2009) and eliminate DAD events both in failing cardiomyocytes (Kobayashi et al. 2009) and in patient-specific stem cell model of CPVT (Jung et al. 2012). Dantrolene has also been proven to prevent arrhythmic episodes in a number of CPVT animal models (Kobayashi et al. 2010; Suetomi et al. 2011). More importantly, dantrolene was shown to prevent arrhythmogenic calcium release without compromising systolic function in heart failure (Maxwell et al. 2012). This finding is of particular importance in respect to the potential use of dantrolene in the clinical setting where CPVT susceptible patients would most likely have to be on a sustained dantrolene treatment. Dantrolene was shown to suppress RyR1-mediated depolarisation-induced calcium release from SR (Szentesi et al. 2001) and if a similar effect was to take place in case of RyR2, the drug would be expected to result in a substantial compromise of heart contractility, a particularly deleterious effect in patients with HF and ARVD2. The preservation of systolic function by dantrolene and its efficacy in preventing arrhythmic events upon  $\beta$ -adrenergic stimulation strongly supports an earlier notion suggesting a conformation sensitive mechanism of dantrolene binding to the RyR2. In this report, the authors showed that RyR2 has an intrinsic ability to bind dantrolene *in vitro*, however in the native channel this property is lost (Paul-Pletzer et al. 2005). It is plausible that dantrolene binds only to the dysfunctional channel, in which a conformation change has been triggered by arrhythmia-associated mutations. Kobayashi and colleagues proposed that the binding of dantrolene to residues 601-620 directly corrects the defective interaction between N-terminal and central domains, thus stabilising the channel in its closed conformation (Kobayashi et al. 2009). However, in light of new findings showing that in the RyR 3D structure, the dantrolene binding site is located at a considerable distance away from the central domain, the mechanism was refined and proposed to involve an allosteric effect involving a number of additional domain-domain contacts (Wang et al. 2011).

An increasing body of evidence indicates that manipulation of the CaMKII pathway may represent another therapeutic approach for the suppression of  $\text{Ca}^{2+}$ -mediated arrhythmias. According to Curran *et al.* the SR calcium leak triggered by  $\beta$ -adrenergic stimulation is directly dependent on the phosphorylation of RyR2 by CaMKII and remains independent of the PKA activation (Curran *et al.* 2007). Furthermore, Liu *et al.* showed that CaMKII inhibition prevented arrhythmia in a mouse model of CPVT which was accompanied by a decrease in the phosphorylation of RyR2 at S2814 (Liu *et al.* 2011b). In agreement with this study, overexpression of CaMKII in a mouse knock-in model of CPVT, resulted in significantly higher incidence of ventricular arrhythmia (Dybкова *et al.* 2011).

## 1.7 RyR – an allosteric protein

Ryanodine receptors constitute one of the largest ion channels. Only a small portion of the protein (~10%) forms an ion pore while the remaining part that faces the cytoplasm is believed to serve as a scaffold responsible for interaction with modulatory agents. The considerable size of the protein (~ 5000 amino acids) and substantial distance between channel pore and regulatory binding sites calls for the mechanism enabling fast signal transduction between cytoplasmic and membrane-embedded parts of the protein. The existence of dynamic cross-talk between structural/functional domains within RyR has been proposed to modulate channel activity. Until now, a number of domains critically involved in channel function together with their putative interacting partners have been identified (Figure 1.6).

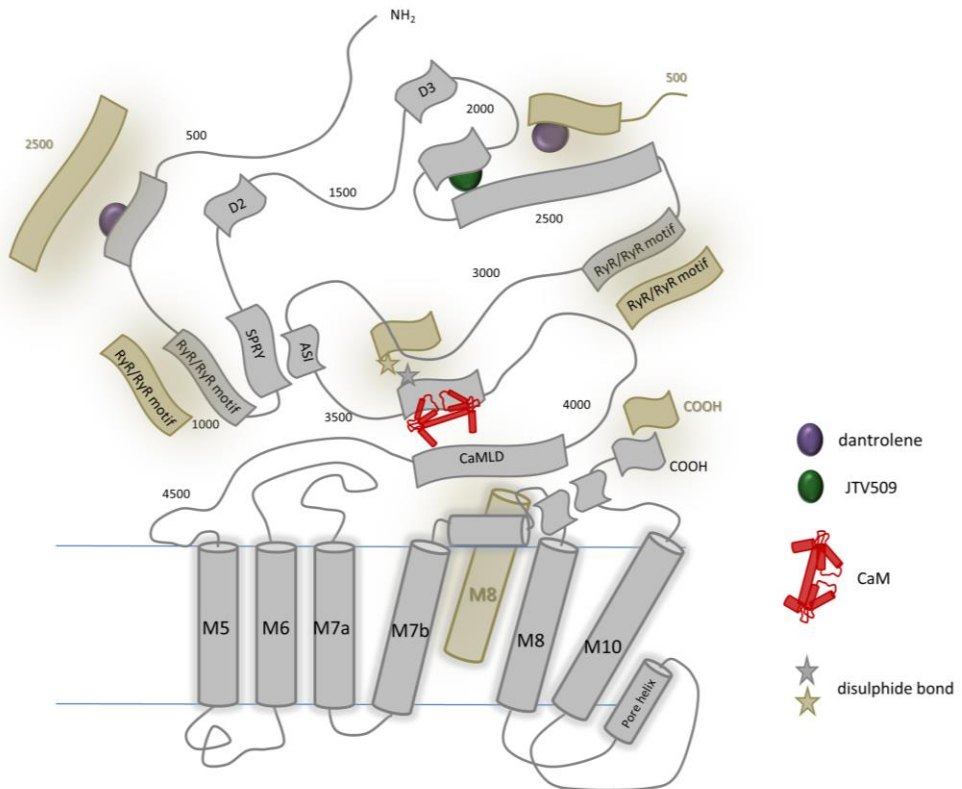


**Figure 1.6** Graphical illustration of domain-domain interactions; regions in light brown correspond to neighbouring subunits in a homotetrameric complex, for detailed description see text in Section 1.7

### 1.7.1 N-terminal – central domain interactions

Initially, the concept of the interaction between N-terminal and central domains was purely theoretical and emerged as a consequence of the fact that MH/CCD mutations were shown to cluster in those two regions and, irrespective of their location, led to the same phenotype. This hypothesis was primarily tested in experiments, where the effect of short synthetic peptides corresponding to those critical domains was evaluated on channel function in [ $^3\text{H}$ ]ryanodine binding assays (El-Hayek *et al.* 1999; Yamamoto *et al.* 2000; Yamamoto and Ikemoto 2002a). Those experiments showed that the addition of central domain peptides (residues 2474-2495 and 2442-2477 for RyR2 and RyR1 respectively) or N-terminal peptides (residues 601-620 and 590-609 for RyR2 and RyR1 respectively) activates the channel at low (diastolic)

concentrations of calcium. As a result, a more detailed hypothesis was proposed, in which a close contact between N-terminal and central domains was claimed to stabilize the closed state of the channel. This concept was further supported by subsequent experiments, in which a conformation-sensitive probe incorporated into a putative domain contact site, showed that peptide-induced channel activation coincides with an increase in the domain-domain distance (Yamamoto and Ikemoto 2002b; Oda et al. 2005). In agreement with the above hypothesis, antibodies raised against the central and N-terminal peptides produced an identical effect, i.e. activated the channel at low calcium and increased the domain-domain distance (Kobayashi *et al.* 2004).

Dynamic changes in the interaction between N-terminal and central domains were proposed to underlie the physiological activation process of EC-coupling (Yamamoto and Ikemoto 2002b; Bannister and Ikemoto 2006). The evidence that physiological regulation of RyR changes the interaction between proposed domain interfaces has led to the concept that channel dysfunction in disease might originate from defective domain-domain interactions. In support of this hypothesis, the presence of domain peptides elicited the phenotype observed in channels carrying disease-associated mutations (Lamb *et al.* 2001; Shtifman *et al.* 2002; Yang *et al.* 2006). More importantly, the introduction of MH/CCD-associated mutations into those peptides resulted in a substantial reduction of their activating properties (Yamamoto *et al.* 2000; Yamamoto and Ikemoto 2002a; Bannister *et al.* 2007). In agreement with those studies, mutated channels failed to undergo further activation in the presence of domain peptides, an observation indicative of a pre-existing defect at the domain contact site (Murayama *et al.* 2007) The increase in the N-terminal – central domain distance upon the introduction of disease-associated mutations was confirmed later in experiments monitoring changes in the spectroscopic properties of conformation-sensitive probes (Uchinoumi *et al.* 2010; Suetomi *et al.* 2011). Notably, the extent of domain “unzipping” in RyR2 was shown to be variable and depend on the mutation site, i.e. the R2474S mutation was reported to induce partial domain unzipping which became further aggravated in the presence of β-adrenergic agonists, while the S2246L mutation was shown to result in a fully unzipped state irrespective of β-adrenergic stimulation. In support of the critical involvement of N-terminal – central domain interaction in channel dysfunction, the ability of dantrolene to correct the defective

domain - domain association was shown to underlie its therapeutic activity (Kobayashi *et al.* 2005; Suetomi *et al.* 2011). An analogous mechanism of channel dysfunction was proposed to be involved in the pathogenesis of heart failure (Oda *et al.* 2005; Kobayashi *et al.* 2009). The increased leak through RyR2 has been suggested to result from the defective N-terminal – central domain interaction caused by changes in the RyR2 post-translational modifications such as oxidation and hyperphosphorylation (Oda *et al.* 2005; Yano *et al.* 2005).

The site-specific labelling of RyR1 using a central domain peptide as a carrier identified its binding partner somewhere within the first 600 amino acids (Kobayashi *et al.* 2005). A subsequent FRET-based study proposed that N-terminal – central domain interaction involves regions located across two neighbouring subunits (Liu *et al.* 2010). An additional inter-subunit domain-domain interaction was proposed to involve two structurally homologous domains containing a tandem repeat of RyR motifs located in the N-terminal and central portion of RyR (Zhu *et al.* 2013)

The N-terminal - central domain interface was shown to undergo dynamic changes in the presence of the central fragment of the DHPR II-III loop (peptide C) (Bannister and Ikemoto 2006). This interaction was proposed to facilitate domain unzipping at sub-activating calcium range underlying a mechanism of RyR1 activation in the process of EC-coupling. In this study, the peptide C binding site was identified within residues 450-1500. Subsequently, the DHPR II-III loop was shown to bind *in vitro* to the second RyR1 SPRY domain (residues 1085-1208) (Cui *et al.* 2009). Interestingly, the determinants mediating II-III loop and SPRY domain interaction were shown to be located in the N-terminal portion of the II-III loop (peptide A) which does not overlap with the region believed to be critical for EC-coupling, i.e. the central portion of the II-III loop (peptide C) (Nakai *et al.* 1998b). Consequently, the SPRY domain was proposed to be nonessential for EC coupling but to influence channel opening by means of an inter-domain interaction with residues located in the central portion of the protein and containing the developmentally regulated splice region I (ASI) (residues 3471-3500) (Tae *et al.* 2011). Alternative splicing of this region gives rise to two protein variants characterised by the presence or absence of residues 3481-3485 (ASI+ and ASI- respectively); the latter being the juvenile form which has a decreased activity (Kimura *et al.* 2005). Kimura and colleagues proposed that the interaction between the domain encompassing the ASI region and its binding partner

stabilises the closed conformation of the channel and that the degree of RyR inhibition is modulated by the presence or absence of the ASI residues (Kimura et al. 2007; Kimura *et al.* 2009).

The N-terminal – central domain interaction has been recently shown to be allosterically coupled to another central region – the calmodulin-binding domain (CaMBD; residues 3583-3603, RyR2) (Oda *et al.* 2013). In this study, the weakening of N-terminal – central domain interaction significantly reduced CaM-binding, while the presence of calmodulin stabilised the N-terminal – central domain contact. In agreement with this study, reduced binding of CaM to RyR2 has been reported to occur in pathologies such as heart failure and CPVT, where a destabilisation of the putative domain interaction was shown (Ono *et al.* 2010; Xu *et al.* 2010; Hino *et al.* 2012). Xu and colleagues reported that CaM binding becomes significantly decreased upon  $\beta$ -adrenergic stimulation only in cardiomyocytes expressing RyR2 with a CPVT-associated mutation. Notably, dantrolene, which had been earlier shown to correct the defective inter-domain interactions, restored CaM binding. Notably, the addition of high concentrations of calmodulin was also able to partially attenuate disease phenotype however, contrary to dantrolene, calmodulin did not reverse domain “unzipping” (Ono *et al.* 2010).

### 1.7.2 Interactions within central domains

The interaction between two regions located within the central part of RyR2 was determined in experiments aiming to identify the binding site of JTV519 (Yamamoto *et al.* 2008). The drug was shown to specifically bind to a short fragment encompassing residues 2114-2149. The JTV519-binding site was in turn proposed to interact with a long stretch of residues located downstream (2234-2750). The interaction between those newly identified domains was shown to be defective in failing cardiomyocytes. Moreover, changes at the interface of those two central domains were shown to be directly coupled to the previously described N-terminal – central domain interaction in a reciprocal manner, i.e. disruption of the latter induced tight association in the former. The disruption of tight association within central domains by JTV519 was proposed to restore the defective contact between N-

terminal and central domain in failing hearts. A similar scenario was suggested to explain the therapeutic efficacy of JTV519 in some of the CPVT-associated RyR2 mutants (Suetomi et al. 2011). Notably, the drug-binding fragment corresponds to the domain peptide previously demonstrated to suppress activating effects of the central domain peptide routinely used to disturb N-terminal – central domain interface in RyR1 (Yamamoto et al. 2000).

### 1.7.3 Central and C-terminal domain interface

The CaMBD (residues 3614-3643) was proposed to modulate RyR1 activity by two independent mechanisms: by binding calmodulin and by interaction with another putative RyR1 regulatory domain (Rodney et al. 2005). Zhu et al. showed that CaMBD contains two functional domains; the N-terminal portion acting as an activator and the C-terminal part which possess inhibitory properties (Zhu et al. 2004). The interaction of these two domains with their putative binding partners in RyR1 was proposed to be modulated by CaM in such a manner that binding of apoCaM to the C-terminal portion of CaMBD results in channel activation by means of masking the inhibitory domain and allowing for protein-protein interaction between the activating domain and its binding partner. On the other hand, binding of calcium to CaM displaces the  $\text{Ca}^{2+}$ /CaM complex towards the N-terminal portion of CaMBD, which in turn exposes the inhibitory domain thus changing CaM from an activator to an inhibitor of RyR1.

The putative binding partner for CaMBD was identified by Xiong and colleagues in the C-terminal portion of RyR1 (residues 4064-4210) (Xiong et al. 2006). This fragment was proposed to adopt calmodulin-like conformation and showed to possess an intrinsic ability to bind  $\text{Ca}^{2+}$  (Xiong et al. 2006). The interaction between those two domains was proposed to underlie a mechanism of calcium-dependent channel activation. In the proposed scenario, the CaMBD induces a conformation change in the central portion of the calmodulin-like domain (CaMLD) which activates the channel. Thus, it is not a tight interaction between these domains *per se* that accompany channel activation but the transmission of conformation signal between the two (Gangopadhyay and Ikemoto 2008). This hypothesis is supported by the fact

that distinct antibodies raised against either the calmodulin-binding domain or the calmodulin-like domain inhibit the channel. Earlier studies showed that synthetic peptides corresponding to each of these putative domains exert identical but very complex action on RyR1 function, i.e. moderately activate the channel at low calcium concentrations, prevent full activation and relieve channel inhibition at higher calcium levels (Xiong et al. 2006). Tateishi *et al.* on the other hand showed that in RyR2, a peptide corresponding to CaMLD potentiates channel response to activation (Tateishi et al. 2009). An earlier report proposed that the calmodulin-like domain is composed of two functional regions; one being an activating site and the other having an inhibitory role (Gangopadhyay and Ikemoto 2006).

CaMLD lies within a long stretch of residues assigned as a C-terminal mutation “hot spot”. The potential role of this region in the mutation-associated RyR1 dysfunction was suggested by Hamada and colleagues who showed that the activating properties of the CaMLD synthetic peptide become substantially reduced in the presence of MH-linked mutations (Hamada et al. 2007). The defective interaction between CaM-binding domain and CaM-like domain has been subsequently suggested to underlie channel dysfunction in heart failure and arrhythmia-linked mutations (Ono et al. 2010; Xu et al. 2010). In the model proposed by Hino and colleagues, the reduced interaction between RyR2 N-terminal and central domains occurring in heart failure or upon  $\beta$ -adrenergic stimulation in the presence of arrhythmia-linked mutations leads to an increased interaction between CaMBD and CaMLD which causes aberrant channel activation and concomitantly reduces the binding of calmodulin (Hino et al. 2012). In agreement with this model, the addition of an antibody against CaMBD or the expression of the mutant isoform of CaM with increased RyR2-binding affinity, restored normal calcium handling (Gangopadhyay and Ikemoto 2011; Hino et al. 2012). Those observations supported the proposed mechanism, in which both proteins would act as “molecular wedges” thus preventing the aberrant interaction between those domains.

#### 1.7.4 Interaction within C-terminal domains

An effective transduction of cytoplasmic signals into the channel pore underlies the ability of the channel to promptly respond to the binding of channel regulators and posttranslational modifications. George and colleagues performed experiments, in which they expressed a number of overlapping cytoplasmic fragments in combination with the predicted pore-forming segments and assessed their ability to interact and form functional receptors (George et al. 2004). Based on this study, a region located between residues 3722 and 4610 (designated as “I domain”) was suggested to be critically involved in channel regulation. The authors proposed that a number of discrete regions located in this domain dynamically interact with one another within one subunit in order to functionally integrate cytoplasmic modulatory events with the transmembrane assembly. Tateishi and colleagues showed that the I-domain is allosterically coupled to the N-terminal/central domain interface in a manner that disruption of the latter triggers changes in the former (Tateishi et al. 2009). In this functional interaction, N-terminal – central domain cross-talk seems to play a superior role, as the changes in the I-domain do not coincide with alterations at the other domain interface. Notably, channel dysfunction resulting from CPVT mutations located within this domain or from the addition of the corresponding I-domain peptide, displays some unique properties such as resistance to JTV519 (Liu et al. 2006; Tateishi et al. 2009). Moreover, George and colleagues proposed that the I-domain mutations substantially differ from central domain mutations in respect to the conformational changes that occur following channel activation (George et al. 2006).

The I-domain contains the region with CaM-like properties, which was proposed to constitute an interacting partner for the CaMBD located in the central portion of RyR (see Section 1.7.3). Further studies revealed that this region might also be involved in an interaction with other determinants located in the transmembrane region. Hamada and colleagues showed that a synthetic peptide corresponding to the M7b-M8 cytoplasmic loop of RyR1 (Figure 1.5, Section 1.3.3) binds to the I-domain fragment that contains the CaMLD (Hamada et al. 2007). Interestingly, this peptide elicited complex response at sub-threshold calcium concentrations and activated the channel at above-threshold calcium levels. The authors proposed that an interaction between M7b-M8 loop and the CaMLD has an overall inhibitory effect on channel function;

however under specific conditions some activating determinants located in the CaMLD become unmasked. This hypothesis is in agreement with the earlier suggestion that the CaMLD contains both functional determinants (Gangopadhyay and Ikemoto 2006). The role of the M7b-M8 loop in channel gating was further investigated by Murayama *et al.* who showed that the N-terminal part of this loop forms an  $\alpha$ -helix (Murayama *et al.* 2011). Mutational analysis revealed that the formation of this secondary structure is essential for the control of channel gating. According to a RyR1 structural model generated using computational and electrophysiological methods, the N-terminal part of the loop referred to in the Murayama studies, is in fact located in the preceding transmembrane domain; however residues located immediately downstream form an  $\alpha$  helix (Ramachandran *et al.* 2013). In this model, the M7b-M8 linker is critically involved in channel gating through dynamic interactions with the C-terminal region of transmembrane domain M10 within the same subunit and domain M8 from an adjacent subunit. Other studies proposed that the M7b-M8 linker interacts with the C-terminal tail governing tetramerisation of the channel (Lee and Allen 2007). Interestingly, the analogous cytoplasmic loop in the IP<sub>3</sub>R was suggested to directly interact with the extreme N-terminus from a neighbouring subunit enabling the transmission of the cytoplasmic activation signal, i.e. IP<sub>3</sub> binding, to the channel pore (Boehning and Joseph 2000; Schug and Joseph 2006).

The assembly of functional RyR complexes is believed to involve the extreme C-terminus. Gao and colleagues reported that the deletion of the final 15 amino acids gives rise to inactive channels (Gao *et al.* 1997). In support of this finding, Stewart *et al.* showed that the C-terminal tail of RyR2 (terminal 100 amino acids) is capable of self-tetramerisation and this ability is lost upon deletion of the last 15 residues (Stewart *et al.* 2003). Gu and colleagues showed that the deletion of last 15 C-terminal amino acids from the full-length RyR1 abolishes ryanodine binding and results in an inactive channel implying that the formation of a tetrameric complex is impaired (Gao *et al.* 1997).

### 1.7.5 Interaction between RyR tetrameric complexes

The first notion that multiple RyR tetramers might be physically linked to each other came with the analysis of electron microscopy pictures of junctional SR showing that RyRs form ordered chequerboard-like arrays, in which receptors associate by a partial overlap with their neighbours (Saito *et al.* 1988; Franzini-Armstrong 1999). Those arrays contained a variable number of channel units depending on the type of muscle investigated and together with DHPRs were proposed to form functional calcium release units (Franzini-Armstrong *et al.* 1998, 1999). A physical association between RyR tetramers was also observed during sucrose density gradient centrifugation suggesting an intrinsic ability of both cardiac and skeletal RyR to mediate this process (Marx *et al.* 1998; Marx *et al.* 2001b). In support of those findings, Yin and Lai showed that isolated purified RyRs associate into a large two-dimensional lattice (Yin and Lai 2000). These observations further strengthen the notion that physical interaction between tetrameric complexes underlies an important physiological mechanism regulating the performance of calcium release units. The functional coupling between ryanodine receptors was demonstrated by Marx and colleagues, who observed simultaneous gating of channels reconstituted into planar bilayers in the presence of FKBP12/12.6 (Marx *et al.* 1998; Marx *et al.* 2001b). The direct physical contact between RyRs was later confirmed by detailed analysis of crystalline arrays at 20Å resolution (Yin *et al.* 2005a; Yin *et al.* 2005b). Projection of cryo-EM-based RyR maps on a single RyR within an array suggested that the inter-tetramer molecular association is mediated by a region located at the edges of the cytoplasmic clamp structure and earlier proposed to represent the three dimensional localisation of the D2 region (Liu *et al.* 2004; Yin *et al.* 2005a). Additional determinants located between residues 2540-3207 involved in this interaction were proposed by Blayney and colleagues (Blayney *et al.* 2004). In principle, a direct conformational coupling between RyR tetramers would provide a much faster and efficient Ca<sup>2+</sup> release from the SR. This mechanism would be highly advantageous in a very fast process such as EC-coupling. In support of this hypothesis, the physical and functional interaction between RyRs appears to be highly dependent on physiologically relevant regulators of channel function such as Ca<sup>2+</sup>, Mg<sup>2+</sup> and ATP (Porta *et al.* 2012).

An allosteric interaction between RyR tetramers within an array adds another level of control ensuring an effective and concerted response to external stimuli. Since coupled RyRs exhibit substantial differences in gating behaviour compared to individual channels (Porta et al. 2012), this regulatory mechanism calls for caution in the interpretation of data obtained from single channels recordings. Notably, differences in the tetramer-tetramer interaction might in fact underlie some of the alterations in RyR function observed in pathological conditions such as heart failure and RyR-associated mutations. In agreement with this notion, Liang and colleagues reported that purified RyR1 isolated from MH-susceptible porcine skeletal muscles show a significantly lower propensity to oligomerise (Liang et al. 2009).

## 1.8 Hypothesis and Aims

The activity of ryanodine receptors is allosterically controlled by a dynamic cross-talk between structural/functional domains. In recent years a great number of such domains has been identified and their role in the regulation of channel function has been thoroughly investigated (Section 1.7). Moreover, defective domain-domain interactions have been proposed to underlie channel dysfunction observed in genetic and acquired RyR-associated disorders (Section 1.6). In spite of extensive research, our understanding of the receptor structure-function relationship remains very limited and awaits further investigation.

The central hypothesis of this thesis is based on the identification of a novel inter-subunit domain interaction involving human RyR2 N-terminus (the BT4L fragment, residues 1-906). Recombinantly expressed RyR2 N-terminus was shown to tetramerise with the concomitant formation of disulphide bonds. It has been hypothesised that N-terminus interaction might be involved in the regulation of channel activity and that defective N-terminus inter-subunit cross-talk might underlie the mechanism of channel dysfunction observed in arrhythmia-susceptible individuals carrying CPVT/ARVD2 mutations. Thus, the principal aim of this study was to characterise this novel interaction both biochemically and functionally.

The primary goal was to identify determinants mediating tetramerisation of the RyR2 N-terminus. The rationale was to design a number of BT4L truncated fragments and internal deletion mutants and to investigate their propensity for tetramerisation. As it was hypothesised that disulphide bond formation takes place across subunits, it was assumed that mutation of putative cysteines would not only expose the identity of residues involved in disulphide bridges but also reveal important inter-subunit contact sites.

Functional assays were employed to dissect the role of N-terminus self-association in the modulation of channel activity. It was speculated that if the above interaction was involved in channel regulation, disruption of endogenous N-terminus interaction within full-length RyR2, should trigger changes in its activation profile. Furthermore, the defective N-terminus self-association was hypothesized to underlie the mechanism of channel dysfunction observed in the presence of arrhythmia-associated

mutations. In this respect the objective was two-fold; first to evaluate the effect of such mutations on RyR2 N-terminus tetramerisation properties and channel function and second, to assess whether dantrolene, a drug targeting RyR1 and used to treat MH symptoms, could rescue the disease phenotype.

# Chapter 2

## Materials and Methods

## 2 Materials and Methods

### 2.1 Materials

All chemicals and reagents were of analytical grade and were obtained from Fisher Scientific or Sigma-Aldrich unless stated otherwise. All solutions were prepared in the laboratory unless an alternative source is stated. All equipment for DNA electrophoresis, DNA visualisation and image acquisition, protein electrophoresis and blotting was obtained from Bio-Rad unless stated otherwise. Antibodies were purchased from Santa Cruz Biotechnology unless indicated otherwise, the full list of antibodies is provided in Table 2.1.

#### 2.1.1 Molecular biology

TAE, 50x: 2 M Tris, 2 M acetic acid, 50 mM EDTA

EDTA, 0.5 M: prepared from 0.5 M Na<sub>2</sub>EDTA, pH 8.0

DNA loading buffer, 5x: 25% v/v glycerol, 0.25% w/v orange G

DNA molecular weight markers: 2-Log DNA Ladder obtained from New England BioLabs (NEB) and 1kb DNA Ladder Plus obtained from Invitrogen

Agarose: PeqGold Universal-Agarose obtained from Peqlab

Ethidium bromide, 1% (w/v)

Plasmid purification kits: Qiagen Plasmid Maxi Kit obtained from Qiagen and Wizard Plus SV Minipreps DNA Purification System obtained from Promega

PCR purification kit: QIAquick PCR Purification Kit and DyeEx Kit obtained from Qiagen

Gel extraction kit: QIAquick Gel Extraction Kit obtained from Qiagen

DNA sequencing kit: BigDye Terminator v3.1 Cycle Sequencing Kit obtained from Life Technologies.

Restriction endonucleases and ligases: obtained from NEB

DNA polymerases: *Pfu* DNA Polymerase and *Taq* DNA Polymerase obtained from Promega

T7 Gene 6 Exonuclease, 50 U/ $\mu$ l: obtained from Affimetrix

Mutagenesis kit: QuikChange II XL Site-Directed Mutagenesis Kit obtained from Agilent Technologies

### 2.1.2 Protein biochemistry

Tris, 0.5 M, pH 6.8

Tris, 1.5 M, pH 8.8

SDS, 10% (w/v)

Ammonium persulphate, 10% (w/v)

Protein loading buffer, 5x: 0.06 M Tris, 2% (w/v) SDS, 10% (v/v) glycerol, 5 mM EDTA, 0.25% (w/v) bromophenol blue

Reducing protein loading buffer: as above with 10%  $\beta$ -mercaptoethanol

Electrophoresis running buffer, 10x: 3% (w/v) Tris, 14.4% (w/v) glycine, 1% (w/v) SDS

Protein molecular weight markers: Kaleidoscope Prestained Standards and Precision Plus Protein WesternC Standards obtained from Bio-Rad

Dye-based protein stain: Imperial Protein Stain based on Coomassie Brilliant Blue R-250 purchased from Thermo Scientific

Carbonate transfer buffer, 10x: 0.84% (w/v) NaHCO<sub>3</sub>, 0.318% (w/v) Na<sub>2</sub>CO<sub>3</sub>

Wet transfer buffer: 20% (v/v) methanol, 1x carbonate transfer buffer, 0.02% (w/v) SDS

Semi-dry transfer buffer: 48 mM Tris, 39 mM glycine, 0.0375% (w/v) SDS with or without 20% (v/v) methanol

TBS, 10x: 200 mM Tris, 1.37 M NaCl, pH 7.4

TBS-T: 1x TBS, 0.1%, (v/v) Tween-20

TBS-T Marvel: 1x TBS, 0.1%, (v/v) Tween-20, 5% (w/v) Marvel

Glutaraldehyde, 25% (v/v)

DTT, 2 M

Homogenisation buffer: 5 mM HEPES, 0.3 M sucrose, pH 7.4

Immunoprecipitation buffer (IP buffer): 150 mM NaCl, 20 mM Tris, 1% (w/v) CHAPS, pH 7.4

Co-immunoprecipitation buffer (co-IP buffer): 150 mM NaCl, 20m M Tris, 0.5% (w/v) CHAPS, pH 7.4

nProtein A and nProtein G Sepharose 4 Fast Flow beads obtained from GE Healthcare Life Science

Protein G Dynabeads obtained from Life Technologies

Sodium azide, 5% (w/v)

Protease inhibitors: Protease Inhibitor Cocktail Tablets obtained from Roche

Acrylamide: 40% acrylamide and bis-acrylamide solution, 37.5:1 obtained from BioRad

TEMED

Protein assay kit: Pierce BCA Protein Assay Kit obtained from Thermo Scientific

ECL reagent: Pierce ECL Western Blotting Substrate obtained from Thermo Scientific

Glass beads: acid-washed, 425-600 µm (30-40 U.S. sieve) obtained from Sigma-Aldrich

### 2.1.2.1 Sucrose density gradient ultracentrifugation

Hypo-osmotic homogenisation buffer: 20 mM Tris, 1 mM EDTA, pH 7.4

CHAPS/PC solution: 10% (w/v) CHAPS, 5% (w/v) PCEGTA, 0.1 M NaCl, 5 M

Tris/HEPES solution: 1 M Tris, 2 M HEPES

CaCl<sub>2</sub>, 0.1 M

Gradient buffer: 300 mM NaCl, 25 mM Tris, 50 mM HEPES, 0.3 mM EGTA, 0.1 mM CaCl<sub>2</sub>, 0.3% (w/v) CHAPS, 0.15% PC, 2 mM DTT, pH 7.4

Sucrose solutions, 5, 25 and 45% (w/w) in gradient buffer

High salt solubilisation buffer: 1 M NaCl, 0.15 mM CaCl<sub>2</sub>, 0.1 mM EGTA, 25 mM PIPES, 0.6% CHAPS, 0.3% PC, 2 mM DTT, pH 7.4

### 2.1.2.2 [<sup>3</sup>H]ryanodine binding

Ryanodine Binding buffer: 1 M KCl, 25 mM PIPES, 1 mM EGTA, 1 mM HEDTA, 1 mM NTA, pH 7.4

Caffeine, 100 mM

CaCl<sub>2</sub>, 20 mM

Ryanodine, 1 mM

[<sup>3</sup>H]ryanodine, 1 µM, obtained from PerkinElmer (95 Ci/mmol)

### 2.1.3 Yeast culture

All glassware, growth media and other solutions used were sterilised. Sterile plastic was obtained from Greiner Bio-One, Fisher Scientific, spreaders were purchased from Microspec.

YPD medium: 2% (w/v) peptone, 1% (w/v) yeast extract, 2% (w/v) glucose, 2% (w/v) agar (for plates only)

Glucose, 20% (w/v)

DO supplements, 10x: stock solutions lacking Leucine (DO/-Leu) or Tryptophan (DO/-Trp) or both amino acids (DO/-Leu-Trp)

YNB, 10xSD minimal medium: 1x YNB and 1x DO as appropriate, supplemented with 2% (w/v), 2% agar (for plates only)

DMSO

TE, 10x: 100 mM Tris, 10 mM EDTA, pH 7.5

LiAc 10x: 1 M CH<sub>3</sub>COOLi, pH 7.5

PEG 3350, 50% (w/v)

PEG/LiAc: 40% (w/v) PEG 3350, 1x TE, 1x LiAc

TE/LiAc: 1x TE, 1x LiAc

Z buffer: 100 mM Na<sub>2</sub>HPO<sub>4</sub>, 40 mM NaH<sub>2</sub>PO<sub>4</sub>, 10 mM KCl, 1 mM MgSO<sub>4</sub>, pH 7.0

X-Gal stock solution, 2% (w/v): X-Gal in DMF

Z buffer/X-Gal solution: 0.27% (v/v) β-mercaptoethanol, 0.033% (w/v) X-Gal in Z buffer

Z buffer/β-mercaptoethanol: 0.27% (v/v) β-mercaptoethanol in Z buffer  
Z buffer/ONPG: 0.4% (w/v) OPNG in Z buffer/β-mercaptoethanol, pH 7.0

Na<sub>2</sub>CO<sub>3</sub>, 1 M

Yeast Protein Extraction buffer: 20 mM Tris, 150 mM NaCl, 1% Triton X-100, pH 7.4

#### 2.1.4 Bacterial culture

All glassware, growth media and antibiotics used were sterile. Antibiotics and bacteria broth powder (LB-Broth Lennox) were obtained from Formedium and prepared following manufacturer recommendations. Sterile plastic was obtained from Greiner Bio-One, Fisher Scientific, spreaders were purchased from Microspec.

Glucose, 20% (w/v)

SOC medium: 2% (w/v) tryptone, 0.5% (w/v) yeast extract, 0.05% (w/v) NaCl, 0.018% (w/v) KCl, 0.095% (w/v) MgCl<sub>2</sub>·6H<sub>2</sub>O, 0.4% glucose

MgCl<sub>2</sub>, 1 M

SB medium: 3.2% (w/v) tryptone, 2% (w/v) yeast extract, 0.5% (w/v) NaCl

SB-Plus medium: 4% (w/v) glucose, 10 mM MgCl<sub>2</sub> in SB medium

Glycerol

Ampicillin, 10% (w/v)

Kanamycin, 3% (w/v)

#### 2.1.5 Mammalian cell culture

Sterile plasticware was obtained from Greiner Bio-One, Fisher Scientific, Corning and Becton Dickinson. Basal cell culture media, media supplements, trypsin and FBS were purchased from Gibco. Saline and sterile water were provided by Fresenius Kabi.

L-glutamine, 100x

FBS, heat inactivated

Trypsin-EDTA, 1x: 0.05% trypsin, phenol red

DMEM basal medium: 0.45% (w/v) glucose, phenol red, sodium pyruvate, sodium bicarbonate, L-glutamine

DMEM complete medium: 10% (v/v) FBS, 1x L-glutamine in DMEM basal medium

Transfection reagent: Express-In, polymer-based transfection reagent purchased from Thermo Scientific

## 2.1.6 Oligonucleotides

Oligonucleotides were obtained from Sigma-Aldrich. For standard PCR, primers were purified by desalting, modified oligonucleotides and oligonucleotides used in mutagenesis were purified by HPLC. Depending on the application, three different working solutions were prepared; 20 µM for standard PCR, 3.5 µM for sequencing PCR and 125 ng/µl for mutagenesis. The full list of primers used in this study is provided in Table 2.2.

## 2.1.7 Plasmid Vectors

Plasmid vectors used in the yeast two-hybrid screen, provided with Clontech Matchmaker Gal4 Two-Hybrid System included;

- pACT2: cloning vector used to generate fusions of protein of interest (referred to as prey) with GAL4 AD and HA epitope tag, contains LEU2 nutritional selection gene enabling identification of positive yeast clones and ampicillin resistance gene for positive selection in *E.coli*. For a detailed vector map please refer to Figure 2.1
- pGBT7: cloning vector used to generate fusions of protein of interest (referred to as bait) with GAL4 DNA-BD and c-Myc epitope tag, contains TRP1 nutritional selection gene enabling identification of positive yeast

clones and kanamycin resistance gene for positive selection in *E.coli*. For a detailed vector map please refer to Figure 2.2

- pVA3-1: positive control used with pTD1-1; encodes a GAL4 DNA-BD/murine p53 fusion protein
- pTD1-1: positive control used with pVA3-1; encodes a GAL4 AD/SV40 large T-antigen fusion protein

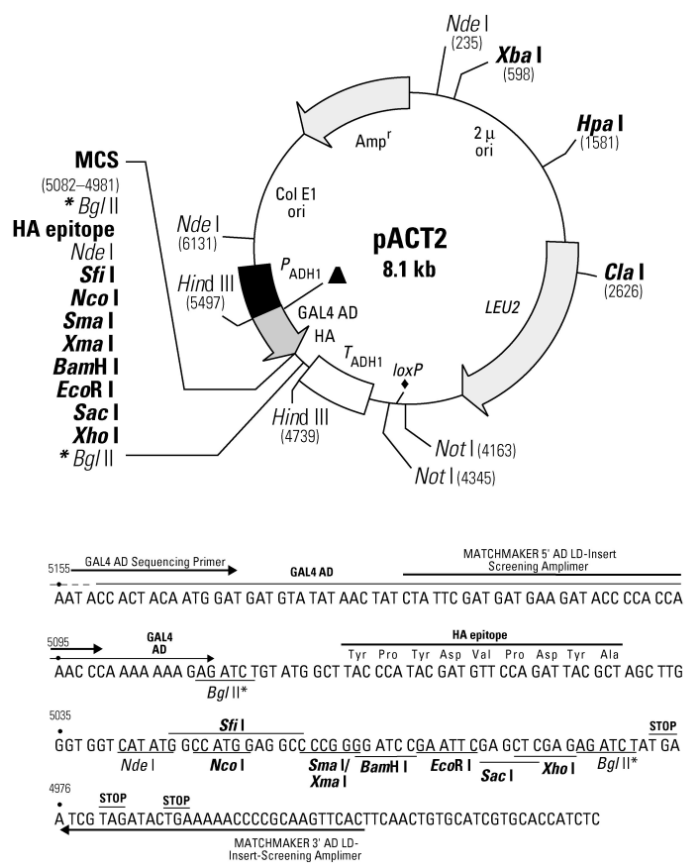


**Figure 2.1** Restriction sites and a detailed map of pACT2 multiclonin

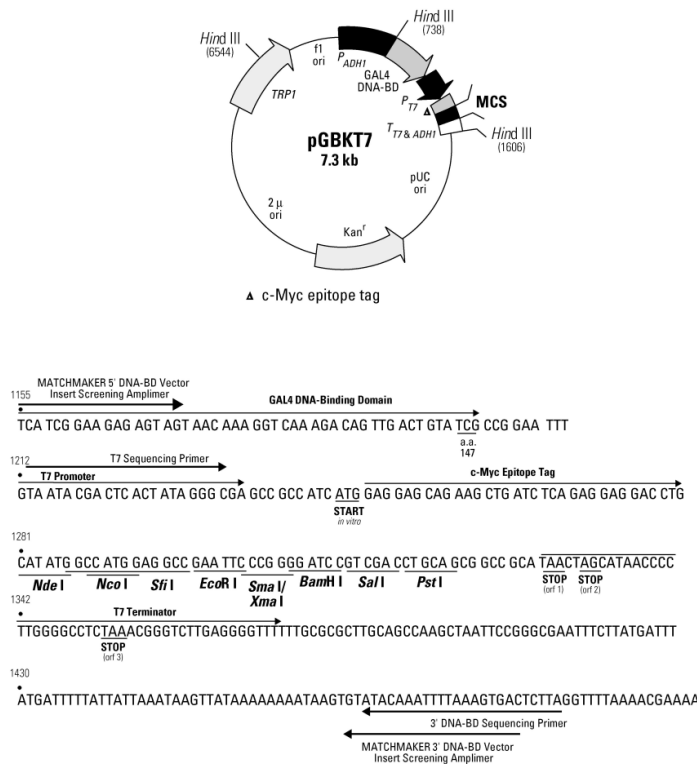


**Figure 2.2.** Restriction sites and a detailed map of pGBK7 multicloning site

The following plasmid vectors were used for a recombinant protein expression in mammalian cells:

- pcDNA3 (Invitrogen): contains ampicillin resistance gene for positive selection in *E.coli* and neomycin resistance gene allowing selection of stable transformed mammalian cells. For a detailed map of this vector please refer to Figure 2.3
- pCR3 (Invitrogen): contains ampicillin resistance gene for positive selection in *E.coli* and kanamycin/neomycin resistance gene allowing selection of stable transformed mammalian cells. For a detailed map of this vector please refer to Figure 2.4
- pCR3-c-Myc modified: derived from pCR3 vector, the original MCS has been replaced with the new MCS allowing for expression of c-Myc tagged proteins. For a detailed map of this vector please refer to Figure 2.5

- pCR3-HA modified: derived from pCR3 vector, the original MCS has been replaced with the new MCS allowing for expression of HA tagged proteins. For a detailed map of this vector please refer to Figure 2.6

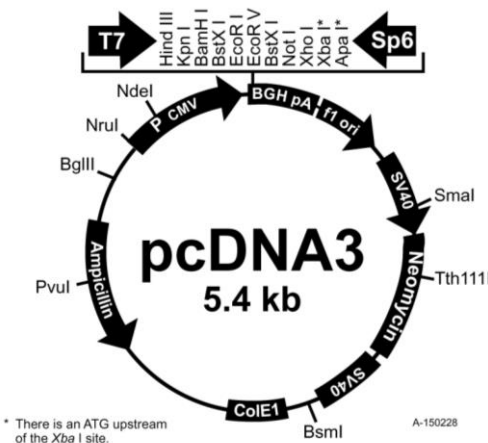


**Figure 2.3** Restriction sites and MCS of pcDNA3 vector; asterisk indicates restriction sites which are not unique to the MCS.

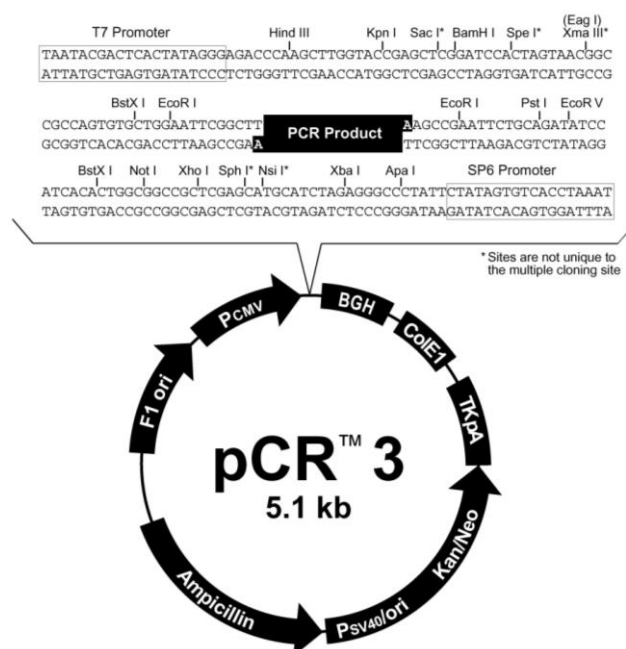


**Figure 2.4** Restriction sites and and a detailed map of pCR3 multicloning site

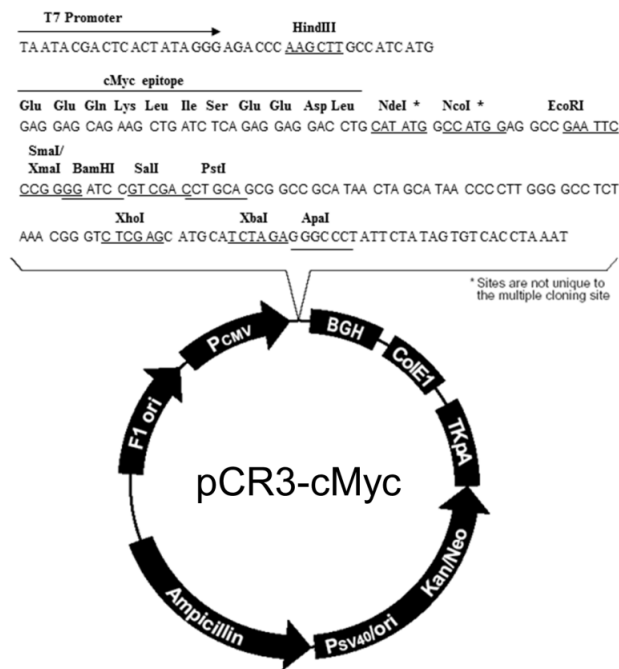


**Figure 2.5** Restriction sites and and a detailed map of pCR3-c-Myc multicloning site

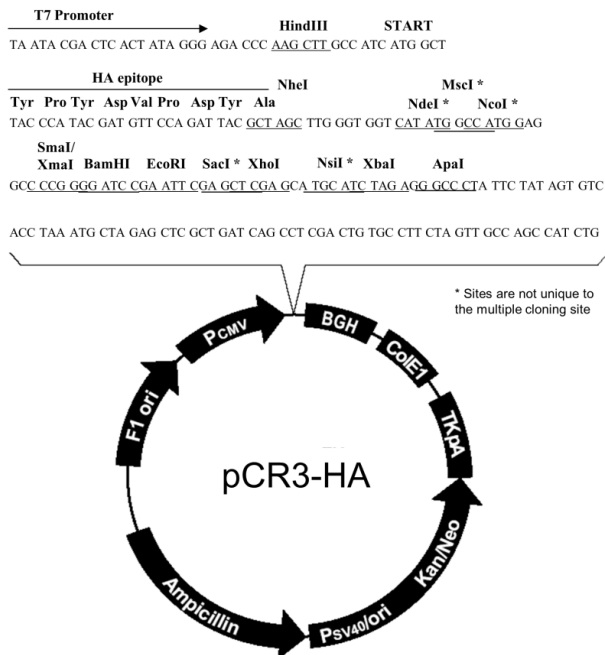


**Figure 2.5** Restriction sites and and a detailed map of pCR3-HA multicloning site

<b>Antibody (Ab)</b>	<b>Epitope/ Specificity</b>	<b>Concentration</b>	<b>Species/Ab class</b>	<b>Application</b>	<b>Working dilution</b>
c-Myc monoclonal	Residues 408-439 of c-Myc of human origin	200 µg/ml	Mouse IgG <sub>1</sub>	Western blot	1:500
1093 (antiserum)	residues 4454- 4474 of human RyR2		Rabbit serum	Western blot	1:1000
HA-probe monoclonal	internal region of the influenza hemagglutinin protein	200 µg/ml	Mouse IgG <sub>2a</sub>	Western blot	1:500
HA polyclonal	internal region of the influenza hemagglutinin protein	200 µg/ml	Rabbit IgG	co-IP, IP	1:20, 1:10
Normal IgG	N/A	400 µg/ml	Rabbit	co-IP	1:40
Anti-rabbit polyclonal HRP conjugated (Sigma- Aldrich)	N/A		Goat IgG	WB	1:10000
Anti-mouse HRP conjugated	N/A	400 µg/ml	Goat IgG	WB	1:5000

**Table 2.1** List of antibodies

Primer name	Sequence (5' – 3')	Length	Tm (°C)	GC (%)	Additional information	Application
SPREV.2343-62 (R)	AACCGTCGACATGTTGGTTGGTGA GCTTA	30	76.3	46.6	<i>Sa</i> I, 10b mismatch	Generation of BT4 <sup>A12</sup> construct
V8.1531-48 (F)	GAAGAACATCACGCACAGCC	18	62.6	55.6		Generation of BT4 <sup>A12</sup> construct, BT4L <sup>L433P</sup> mutant, sequencing
RyR2C244S.FOR	GGACACATGGACGAGAGTCTCACTG TCCCTTC	32	78.0	56.2	T→A substitution	Generation of BT4L <sup>C244S</sup> mutant
RyR2C244S.REV	GAAGGGACAGTGAGACTCTCGTCCA TGTGTCC	32	78.0	56.2	A→T substitution	Generation of BT4L <sup>C244S</sup> mutant
RyR2C615/618/620SFOR	GGTTCTGGATGTCTTGTCTCCTCACTCT CTGTTTCCCACGGGGTTGCAGTCG	52	90.3	56.8	G→C, G→C, G→C substitution	Generation of BT4L <sup>C615/618/620S</sup> mutant
RyR2C615/618/620SREV	CGGACTGCAACCCCGTGGGAAACA GAGAGTGAGGACAAGACATCCAGAAC	52	90.3	56.8	C→G, C→G, C→G substitution	Generation of BT4L <sup>C615/618/620S</sup> mutant
RyR2C577SFOR	GGCATTCTGGAAGTTTACACTCTG TTTAGTAGAAAGTCCAGAAGC	47	77.4	40.4	G→C substitution	Generation of BT4L <sup>C577S</sup> mutant
RyR2C577SREV	GCTCTGGACTTCTACTAAAACAG AGTGTAAAACCTCCAGAATGCC	47	77.4	40.4	C→G substitution	Generation of BT4L <sup>C577S</sup> mutant
RyR2C548SFOR	GGAAATCGAAAAACTCTGCTCAATT TTCTGGCTCCC	37	77.7	43.2	G→C substitution	Generation of BT4L <sup>C548S</sup> mutant
RyR2C548SREV	GGGAGCCAGAAAATTGAGCAGAGT TTTACGATTCC	37	77.7	43.2	C→G substitution	Generation of BT4L <sup>C548S</sup> mutant

RyR2C633SFOR	CCAGCATCTCATCT <u>C</u> TGACAATCTC CTACCAGG	33	76.4	51.5	G→C substitution	Generation of BT4L <sup>C633S</sup> mutant
RyR2C633SREV	CCTGGTAGGAGATTGTC <u>A</u> GAGATGA GATGCTGG	33	76.4	51.5	C→G substitution	Generation of BT4L <sup>C633S</sup> mutant
RyR2C361S.FOR	TACGGTGACTCAGTAT <u>C</u> CTATATAC AACATGTAGACAC	38	69.7	39.5	G→C substitution	Generation of BT4L <sup>C361/615/618/620S</sup> mutant
RyR2C361S.REV	GTGTCTACATGTTGTATAG <u>G</u> ATA CTGAGTCACCGTA	38	69.7	39.5	C→G substitution	Generation of BT4L <sup>C361/615/618/620S</sup> mutant
RyR2R176QFOR	GAAGGGAGAAAAAGTACA <u>A</u> GTTGGA GATGACCT	32	70.1	40.6	G→A substitution	Generation of BT4L <sup>R176Q</sup> mutant
RyR2R176QREV	AGGTCATCTCCA <u>A</u> CT <u>T</u> GTA <u>T</u> TTTC TCCTTC	32	70.1	40.6	C→T substitution	Generation of BT4L <sup>R176Q</sup> mutant
JWREV.2821-40 (R)	<u>TT</u> GGATCCGGACCATACTGCCAGCC A	26	79.3	57.7	<i>Bam</i> HI, 6 base mismatch	Generation of BT4L <sup>L433P</sup> mutant
RevB8-9loop	GTCATCAGAGGC*A*G*G*GTGTATG GT	24	58.0	54.1	4 phosphorothioate linkages	Generation of BT4L <sup>β8-β9loop</sup> deletion mutant
ForB8-9loop	GCCTCTGATGAC*C*T*C*ATCTTAGT T	24	53.7	45.8	4 phosphorothioate linkages	Generation of BT4L <sup>β8-β9loop</sup> deletion mutant
Rev377-385loop	TATAGATTCAC*G*T*C*CACAGAC TG	24	45.9	41.6	4 phosphorothioate linkages	Generation of BT4L <sup>β22-β23loop</sup> deletion mutant
For377-385loop	GTGAAATCTATA*C*A*A*CGTAAGG CT	24	47.7	37.5	4 phosphorothioate linkages	Generation of BT4L <sup>β22-β23loop</sup> deletion mutant

Rev B20-21loop	TACTGAGGAAGA*C*C*G*GAAGGT AAATGCTGTTGATTACATCAGC	45	74.7	42.2	4 phosphorothioate linkages	Generation of BT4L <sup><math>\beta</math>20-<math>\beta</math>21loop</sup> deletion mutant
For B20-21loop	TCTCCTCAGTA*T*G*C*TATATACA ACATGTAGACACAGGCCTATGG	45	74.3	42.2	4 phosphorothioate linkages	Generation of BT4L <sup><math>\beta</math>20-<math>\beta</math>21loop</sup> deletion mutant
Rev delta12	GACATCATGTTG*G*T*T*TGGTGAG CTTACAGTACGAGCAATACAACC	45	77.8	44.4	4 phosphorothioate linkages	Generation of BT4L <sup>SPRY<math>\beta</math>5-<math>\beta</math>6loop</sup> deletion mutant
For delta12	CAACATGATGTC*A*T*C*AGTTGCT GTTTAGATCTGAGTGCCCCAAGC	45	81.5	46.6	4 phosphorothioate linkages	Generation of BT4L <sup>SPRY<math>\beta</math>5-<math>\beta</math>6loop</sup> deletion mutant
V2(+) (F)	GATGAAGACTGCTCAAGGTGG	21	64.2	52.4		Sequencing
V1(+) (F)	CTGTGTCTGTTCATGCAC	18	56.5	50.0		Sequencing
V1(-) (R)	CACGTACTTGTCTGTGTC	18	56.5	50.0		Sequencing
V6.1999-2016 (F)	GCTTCTTCAGGCATTCTG	18	59.2	50.0		Sequencing
SPFOR.2153-2170 (F)	ATGGTGGACCACACAGAG	18	60.1	55.6		Sequencing
V1.2519-2536 (F)	CTGTAAGCTCACCAAACC	18	56.2	50.0		Sequencing

**Table 2.2** Full list of primers; restriction site underlined, mutated/mismatch residue shaded, asterisk indicates the location of a phosphorothioate-containing bond, (F) and For: forward primer, (R) and Rev: reverse primer

## 2.2 Methods

General molecular biology and biochemistry techniques were performed according to protocols covered in Molecular Cloning (Sambrook *et al.* 1989) and optimised procedures established by other members of staff within the laboratory. When applicable, some techniques were performed according to manufacturer's recommendations. All procedures were carried out in agreement with local guidelines covered in the WHRI Health and Safety handbooks.

### 2.2.1 Molecular biology methods

#### 2.2.1.1 Standard PCR

PCR reaction was carried out following the recommendations provided by the manufacturer of DNA polymerase. For high fidelity PCR products *Pfu* DNA polymerase was used, *Taq* DNA polymerase was used for diagnostic purposes. Annealing temperature of a PCR reaction was set at approximately 5-10 °C below primer melting temperature. Extension time depended on the length of the expected PCR product and was calculated assuming 2 min for every 1 kb to be amplified. Typical PCR reaction mixture and cycling conditions are presented in Tables 2.3 and 2.4 respectively.

Components	Volume (µl)	Final concentration
10x buffer with MgSO <sub>4</sub>	5	1x
dNTP (20 mM)	0.5	0.2 mM
Forward primer (20 µM)	1	0.4 µM
Reverse primer (20 µM)	1	0.4 µM
DNA template	Variable	<0.5 µg/50 µl
DNA polymerase	Variable	1 U/50 µl
Nuclease-free water	to a final volume of 50 µl	

**Table 2.3** Typical components of a standard PCR reaction

Step	Temperature (°C)	Time (minutes)	Number of cycles
Initial denaturation	95	2	1
Denaturation	95	1	
Annealing	50-65	1	30
Extension	72	variable	
Final extension	72	10	1
Incubation	4	indefinite	1

**Table 2.4** Typical cycling conditions of a standard PCR reaction

### 2.2.1.2 DNA sequencing

Sequencing PCR was carried out according to instructions provided with BigDye Terminator v3.1 Cycle Sequencing Kit. Briefly, a PCR reaction was set up in 10 µl and contained typically 200-500 ng of plasmid DNA and 3.5 pmol of a relevant sequencing primer. Cycling conditions are presented in Table 2.5.

Step	Temperature (°C)	Time	Number of cycles
Initial denaturation	96	2 min	1
Denaturation	96	30 sec	
Annealing	50	15 sec	25
Extension	60	4 min	
Incubation	4	indefinite	1

**Table 2.5** Cycling conditions of a sequencing PCR reaction

PCR products were purified with DyeEx Kit. Sequencing was performed at the Cardiff University CBS DNA sequencing facility. NCBI Basic Local Alignment Tool available online at <http://blast.ncbi.nlm.nih.gov/> was used for sequence alignment and analysis.

#### 2.2.1.3 DNA digestion with restriction endonucleases

DNA was digested with appropriate restriction enzymes according to manufacturer's instructions. Typically, a reaction was set in 20 µl and contained 0.5-2 µg of DNA depending on the subsequent downstream application. For a double digest performed in one step, buffer compatibility was evaluated using NEB Double Digest Finder online tool (<https://www.neb.com/tools-and-resources/interactive-tools/double-digest-finder>). For a two-step reaction, the second digest was preceded by DNA purification using QIAquick PCR Purification Kit. Reactions were incubated at 37 °C for 2 h unless otherwise stated. DNA was analysed by agarose gel electrophoresis. For DNA cloning, the appropriate fragment was excised from the gel and purified with QIAquick Gel Extraction Kit following manufacturer's recommendations.

#### 2.2.1.4 DNA ligation

DNA ligation was conducted according to manufacturer's instructions. Typically, a reaction was set up in 20 µl and contained 20-200 ng of total DNA with 3:1 molar ration of insert:vector. Reaction was incubated for 2 h at room temperature. Typically, 8 µl of ligation reaction was used to transform electrocompetent *E.coli* DH5 $\alpha$  strain (please refer to Section 2.2.1.8 for a detailed description of the transformation procedure).

### 2.2.1.5 Agarose gel electrophoresis

Agarose gel electrophoresis was used to analyse and separate DNA fragments following PCR or restriction digest. Agarose was dissolved in 1x TAE by boiling at the appropriate concentration depending on the size of DNA fragments to be separated (0.9 – 1.2%). Once lukewarm, the agarose solution was supplemented with ethidium bromide at 0.01% (w/v) final concentration. DNA samples were loaded in 1x DNA loading buffer alongside DNA molecular weight markers. Electrophoresis was run under constant voltage (typically 80 V) until desirable DNA fragment separation was obtained. Gels were visualised under UV illumination using gel documentation system (Gel Doc).

### 2.2.1.6 Mutagenesis

Mutagenesis was performed following manufacturer's recommendations. Briefly, 10–100 ng of plasmid DNA was subjected to a PCR reaction in the presence of complementary primers containing the desired nucleotide substitution. PCR mixture components and cycling conditions are presented in Tables 2.6 and 2.7 respectively.

Components	Volume (µl)	Final concentration
10x buffer with	5	1x
dNTP mix*	1	n/a
Forward primer (125 ng/µl)	1	125 ng/50 µl
Reverse primer (125 ng/µl)	1	125 ng/50 µl
DNA template	Variable	≤100 ng/50 µl
QuickSolution reagent*	3	unknown
<i>PfuUltra</i> DNA polymerase	1	2.5 U/50 µl
Nuclease-free water	to a final volume of 50 µl	n/a

**Table 2.6** Components of a mutagenic PCR reaction; asterisk indicate proprietary composition

Step	Temperature (°C)	Time	Number of cycles
Initial denaturation	95	1 min	1
Denaturation	95	50 sec	18
Annealing	60	50 sec	
Extension	68	8 min (1 min/1kb)	
Final extension	68	7 min	1
Incubation	4	indefinite	1

**Table 2.7** Cycling conditions of a mutagenic PCR reaction

Primers were designed according to the Primer Design Guideline provided with the mutagenesis kit. In summary, both forward and reverse primers contained the desired mutation and annealed to the same sequence on the opposite strands of the plasmid DNA. Oligonucleotides were at least 32 nucleotide bases in length and had a relatively high melting temperature (Table 2.2).

Following PCR, reactions were incubated for 1 h at 37 °C in the presence of 10 U of *DpnI* restriction enzyme, which specifically digests methylated DNA (i.e. parental plasmid DNA). *DpnI*-treated reaction was used to transform 45 µl of XL-Gold Ultracompetent *E.coli* cells provided with the kit. Transformation protocol was performed following manufacturer's guidelines. Briefly, bacteria were incubated in a 14 ml polypropylene tube in the presence of 2 µl of β-mercaptoethanol (provided with the kit) on ice for 10 min with gentle agitation every 2 min. Subsequently, 2 µl of *DpnI*-treated DNA was added to the cells. After 30 min incubation on ice, the bacteria were subjected to a 42 °C heat pulse for 30 sec. This was followed by 2min incubation on ice. Following addition of 0.5 ml SOC medium, cells were incubated at 37 °C for an hour with shaking at 225 rpm. Bacterial suspension was plated on two LB-agar plates (250 µl each) containing the appropriate antibiotic and incubated overnight at 37 °C.

### 2.2.1.7 Introducing deletions into plasmid DNA

Deletions were introduced into plasmid DNA following a slightly modified method described earlier (Stoynova *et al.* 2004). Briefly, primers were designed to contain four consecutive phosphorothioate residues located 12 nucleotides from the 5'end of

each oligonucleotide allowing a controlled digestion with T7 Gene 6 Exonuclease. This step converts a blunt PCR product into 12 nucleotide 3' overhangs located at both ends of the amplified fragment. In addition, the 6 outermost nucleotides of each primer are complementary to the 6 nucleotides of the opposite strand primer located immediately before the phosphorothioate residues. This feature ensures self-circularisation of a PCR product immediately after exonuclease treatment. Graphical representation of this process describing generation of the BT4L<sup>β8-β9loop</sup> deletion mutant as an example is shown in Figure 2.7.

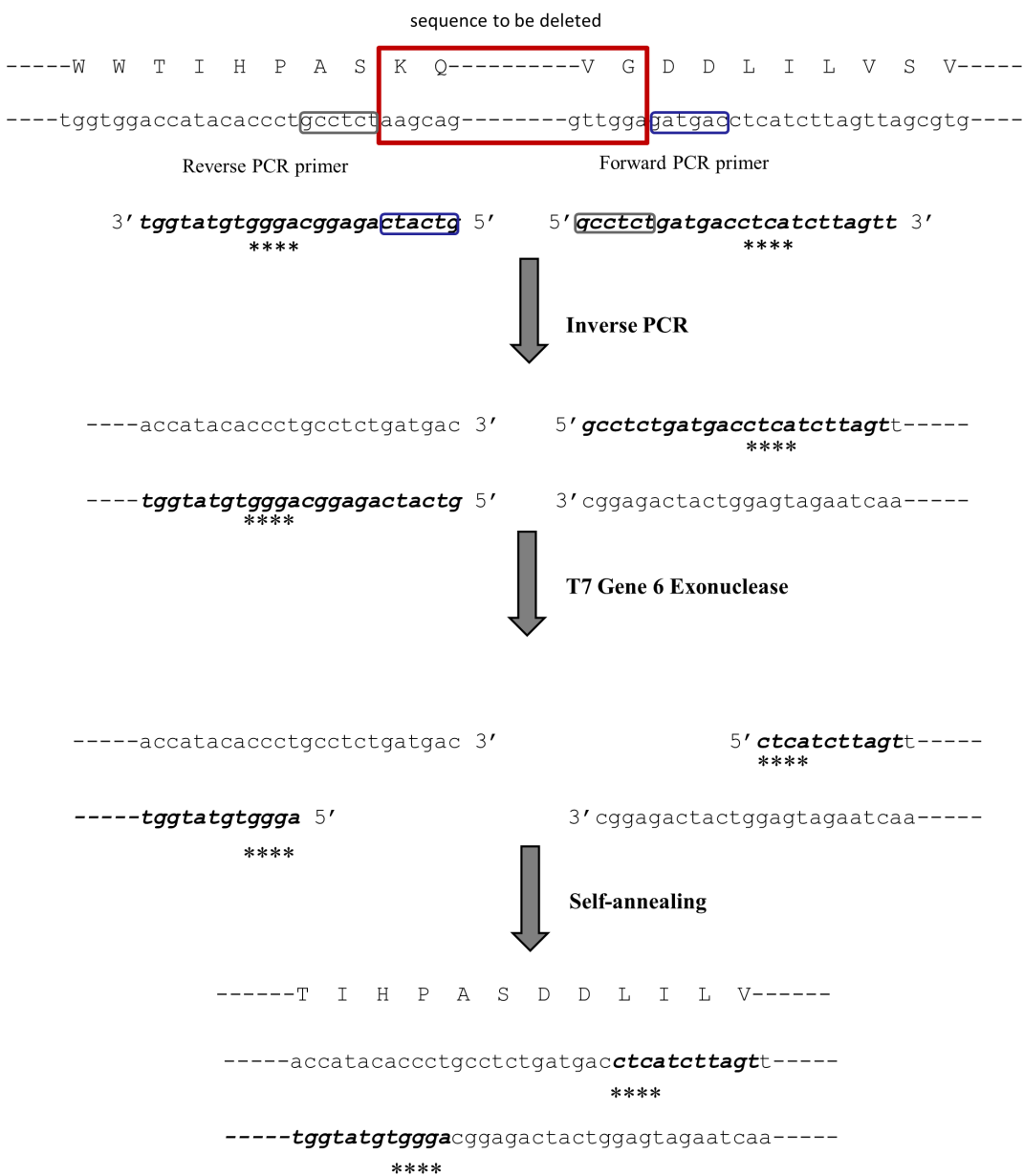


**Figure 2.7** Schematic summary of the procedure leading to the generation of the BT4L<sup>B8-B9loop</sup> deletion mutant; asterisk indicates the location of modified nucleotides

PCR reactions were conducted using reagents provided with the mutagenesis kit (for PCR mixture components please refer to Table 2.6). PCR cycling conditions followed a modified protocol described in section 2.2.1.6 and are shown in Table 2.8.

Step	Temperature (°C)	Time	Number of cycles
Initial denaturation	95	2 min	1
Denaturation	95	1 min	20
Annealing	52-60	50 sec	
Extension	68	16 min	
Final extension	68	7 min	1
Incubation	4	Indefinite	1

**Table 2.8** Typical cycling conditions of a deletion-introducing PCR

Following amplification, samples were treated with 20 U of *DpnI* enzyme at 37 °C for an hour. Digestion with 100 U of T7 Gene 6 Exonuclease was carried out at 37 °C for 10min followed by enzyme inactivation at 80 °C for 10 min. Bacteria transformation was performed according to the protocol described in section 2.2.1.6.

### 2.2.1.8 Electroporation of bacteria

Bacteria electroporation was carried out with BioRad Genepulser set as follows: 25µF, 200 Ω and 2.5 kV. Prior to transformation, electrocompetent cells (*E.coli*, DH5α strain) were transferred into an electroporation cuvette and incubated on ice with 8 µl of a ligation mixture for 5 min. Following an electrical pulse, cells were suspended in 800 µl of SOC medium and transferred into a sterile 14 ml polypropylene tube which was incubated at 37 °C for an hour with shaking at 225 rpm. Transformation reaction (1/10<sup>th</sup> and 9/10<sup>th</sup>) was plated on two LB-agar plates containing the appropriate antibiotic and incubated overnight at 37 °C.

### 2.2.1.9 Chemical transformation of bacteria

Transformation with large plasmids (i.e. the full length RyR2) was performed using chemically competent bacteria as follows; 25 µl of XL-Gold Ultracompetent *E.coli* cells (Agilent Technologies) were incubated in the presence of 1 µl of β-mercaptoethanol (provided with the kit) on ice for 10 min with gentle agitation every 2 min. Subsequently, cells were incubated on ice for 30 min in the presence of 1 ng of plasmid DNA. The bacteria were then subjected to 42 °C heat pulse for 30 sec followed by 2 min incubation on ice. Bacteria were incubated in 1 ml of SOC medium at 30 °C for 90 min with shaking at 225 rpm. Transformation reaction (1/10<sup>th</sup> and 9/10<sup>th</sup>) was plated on two LB-agar plates containing ampicillin and incubated at 30 °C for around 18 h.

### 2.2.1.10 Colony screen and plasmid isolation

Following bacteria transformation, a number of colonies were screened for the presence of the recombinant plasmid of interest. Whenever possible, the correct orientation and size of the DNA insert was confirmed by restriction mapping and further verified by sequencing. For identification of positive clones, plasmids were isolated from an overnight mini culture (3 ml), which was inoculated with a single colony, using Wizard Plus SV Minipreps DNA Purification System. Briefly, 1.5 ml of saturated culture was harvested by centrifugation (14 000x g for 1 min) and processed for plasmid isolation following the manufacturer's recommendations. The process involved consecutive steps of cell lysis, centrifugation and DNA binding to the kit columns followed by two ethanol-based washing steps. Plasmid DNA was eluted with 30 µl of water and typically 2-4 µl (8 µl for low copy number plasmids) and 1-2 µl was used for restriction mapping and DNA sequencing respectively.

Verified clones were grown in large volumes (typically 200 ml) overnight and processed with Qiagen Plasmid Maxi Kit which uses bacterial alkaline lysis followed by binding of plasmid DNA to an anion-exchange resin. Briefly, bacteria were harvested by centrifugation at 10 000 xg for 5 min and subjected to cell lysis followed by lysate filtration, DNA column binding and washing. Plasmid DNA was eluted

from the column and underwent two consecutive steps of precipitation (isopropanol followed by 70% ethanol). Air-dried DNA pellet was dissolved in 500 µl of sterile deionised water. DNA concentration (absorbance at 260 nm) and quality (ratio of absorbance at 260/280 nm) was assessed using a spectrophotometer. Plasmid DNA was stored at -20 °C.

Large plasmids (the full length RyR2 constructs) were isolated from cultures grown at 30°C until OD<sub>600</sub> of 1 was reached. Typically eight 400ml flasks were processed for plasmid isolation. This was performed using Qiagen Plasmid Maxi Kit with a modified protocol. Briefly, following cell lysis and prior to lysate filtration, bacterial lysate was cleared by centrifugation at 14 000 xg for 10 min. In total, 3.2 litres of culture was processed using four filters and two DNA-binding columns provided with the kit. DNA pellet was dissolved in 500 µl of sterile deionised water and stored at -80 °C in small aliquots.

## 2.2.2 Protein Biochemistry Methods

### 2.2.2.1 Mammalian cell homogenisation

Cell pellets of HEK293 cells expressing the protein of interest harvested from one 100 mm Petri dish were re-suspended in ice-cold homogenisation buffer (typically 500-800 µl) supplemented with protease inhibitors. Cells were homogenised on ice by 20 passages through a needle (0.6x30 mm) in the presence of approximately 200 µl of glass beads (pre-washed in the homogenisation buffer). Cell homogenates were subjected to 10min centrifugation at 1500 xg, followed by 10 min centrifugation at 18 000 xg and the supernatant was saved.

For cell pellets obtained from 6-well plates, the protocol described above was scaled down accordingly. Briefly, cell pellets were re-suspended in 200 µl of ice-cold homogenisation buffer supplemented with protease inhibitors. Cell homogenisation was performed by three rounds (30 sec each) of vigorous vortexing in the presence of glass beads. The remaining steps of cell lysate preparation were as described in the previous paragraph.

#### 2.2.2.2 Determination of protein concentration

Protein concentration was evaluated using the BCA colorimetric assay according to the manufacturer's guidelines. Briefly, duplicates of two dilutions of the original sample (typically 1/10 and 1/20) as well as serial dilutions of BSA protein (1000-62.5 µg/ml) were mixed with the BCA kit reagents and incubated at 37 °C for 30 min. Samples' absorbance was measured at 560nm using a Multiscan EX (Labsystems) spectrophotometer and protein concentration was calculated using a standard curve produced by known concentrations of BSA.

#### 2.2.2.3 Chemical crosslinking

Chemical crosslinking was performed using glutaraldehyde at a final concentration of 0.0025% (v/v). Prior to chemical crosslinking, cell lysates were divided into two aliquots and one aliquot was treated with DTT (10 mM, 1 h, 4 °C). Subsequently, both DTT-treated and untreated samples were divided into 8 aliquots each (typically 20-50 µg of total protein as assessed by the BCA assay) and subjected to crosslinking in the following time points: 0 min, 2 min, 5 min, 10 min, 15 min, 20 min, 30 min and 1 h. The reaction was stopped with the addition of hydrazine (2% final concentration). Samples were stored at -20 °C following the addition of protein loading buffer.

#### 2.2.2.4 Polyacrylamide gel electrophoresis

Depending on the size of proteins to be separated 4% to 12% SDS polyacrylamide mini gels (8x10 cm, 0.75 cm thick) were prepared a day before electrophoresis. Gel composition details are presented in Table 2.9.

Reagents	Volume for 2mini gels (μl)					
	Separating gel					Stacking gel
	4%	6%	8%	10%	12%	4%
Acrylamide/Bis (37.5:1) 40%	1000	1500	2000	2500	3000	500
Water	6345	5845	5345	4845	4345	3170
Tris-HCl 1.5 M, pH 8.8	2500	2500	2500	2500	2500	-
Tris-HCl 0.5 M, pH 6.8	-	-	-	-	-	1250
SDS 10%	100	100	100	100	100	50
Ammonium Persulphate 10%	50	50	50	50	50	25
TEMED	5	5	5	5	5	2.5

**Table 2.9** Polyacrylamide gel composition

Briefly, the separating gel solution was poured into the assembled gel cassette up to approximately 1 cm below the comb teeth. The solution was overlaid with 70% ethanol and allowed to polymerise for at least an hour. Subsequently, ethanol was removed and the top of separating gel was dried with paper. Stacking gel mixture was poured to the top, the comb was inserted and left to polymerise for at least 2 hours.

4% polyacrylamide gels were strengthened with 0.5% agarose as follows: 5 ml of warm 1% (w/v) solution of agarose was added to a 4% SDS-PAGE gel mixture containing 1345 μl instead of 6345 μl of water. The solution was mixed and poured into an assembled cold gel cassette up to the top and the comb was inserted. Freshly poured gel was placed in an ice-cold bath for 5min for the agarose to solidify and allowed to polymerise for 2 hours at room temperature.

Prior to loading, samples containing 1x protein loading buffer were heated at 85°C for 5 min followed by 3 min centrifugation at 12 000 xg. Samples were loaded alongside protein molecular weight markers. Electrophoresis was run in 1x electrophoresis running buffer under constant current (typically 40 mA for a cell tank containing 4 gels) until desirable protein separation was obtained. Following electrophoresis gels were either processed for blotting or stained with a dye-based protein stain.

### 2.2.2.5 Western blotting

Proteins separated by electrophoresis were transferred onto PVDF membranes (Immobilon-P obtained from Merck Millipore) using either semi-dry or wet electroblotting system. Semi-dry transfer was used to blot the full length RyR2 and was performed following manufacturer's instructions. Briefly, following electrophoresis gels were washed in deionised water and incubated in the semi-dry transfer buffer together with blotting paper and methanol-activated PVDF membranes. The blotting sandwich was then assembled and a semi-dry transfer was conducted at constant voltage (24 V) for four hours in the cold room. For wet blotting, gels were assembled into a sandwich using blotting paper and methanol-activated PVDF membranes soaked in the cold wet transfer buffer. Transfers were conducted either overnight at 45 V or for two hours at 80 V in the presence of ice packs with constant stirring in the cold room.

Following transfer, PVDF membranes were washed in deionised water and blocked for 1 h in the TBS-T Marvel buffer. Blots were then incubated in the presence of primary antibody either overnight at 4 °C or for 2 h at room temperature followed by two washing steps in the TBS-T Marvel buffer (10 min each). The incubation with the secondary antibody conjugated to horseradish peroxidase was conducted for at least an hour in room temperature and was followed by two washes in the TBS-T buffer (10 min each). Signal detection was performed using ECL reagents. X-ray films were developed using an automatic X-ray film processor (X-Ograph Compact X4 obtained from Xograph Healthcare). Film exposure depended on the signal strength but usually did not exceed 10 min.

### 2.2.2.6 Sub-cellular fractionation

HEK293 cells expressing one or more proteins of interest were harvested and homogenised as described in Section 2.2.2.1. Cell homogenates were centrifuged at 1500 xg for 10 min in order to remove unbroken cells and nuclei. Microsomal and cytosolic fractions were obtained in the subsequent centrifugation step at 100 000 xg for 1 h. Obtained pellets representing crude microsomal fraction were resuspended in

homogenisation buffer. Alternatively, following the initial 1500 xg spin, an additional intermediate centrifugation step at 10 000 xg for 10 min was included to remove mitochondria. Protein distribution was evaluated by Western blotting.

#### 2.2.2.7 Co-immunoprecipitation

Cell pellets of HEK293 cells expressing two putatively interacting fragments of interest harvested from one 100 mm Petri dish were resuspended in ice-cold co-immunoprecipitation buffer without CHAPS (typically 800 µl) supplemented with protease inhibitors and 10 mM DTT. Cells were homogenised as described in Section 2.2.2.1, subjected to 1500 xg spin and the supernatant was incubated overnight at 4 °C in the presence of 0.5% CHAPS under rotary agitation. At the same time, Protein A beads (pre-washed with the co-IP buffer) were incubated with the relevant antibody (typically 30 µl of beads with 2 µg of Ab in 200 µl of co-IP buffer). As a negative control, another set of beads was incubated with normal (non-immune) IgG of the same species as the IP antibody. Following overnight solubilisation, cell lysates were centrifuged at 18 000 xg for 10 min to remove insoluble material and incubated at 4 °C for six hours with Ab-bound beads under rotary agitation. Subsequently, beads were washed two times with the co-IP buffer for 10 min at 4 °C and collected by centrifugation at 1500 xg for 2 min. Proteins were eluted using 20 µl of 2x reducing protein loading buffer and processed for Western blotting.

#### 2.2.2.8 Sucrose density gradient ultracentrifugation

Cell pellets of HEK293 cells expressing the full length RyR2 harvested typically from 8-10 100 mm Petri dishes were subjected to sucrose density gradient ultracentrifugation. Briefly, pellets were re-suspended in hypo-osmotic homogenisation buffer supplemented with protease inhibitors at an approximate concentration of 10<sup>6</sup> cells/ml. This typically corresponded to 7.5 ml/Petri dish. Cells were homogenised on ice using a custom made cell homogeniser allowing for 25 passages through a needle (0.6x30 mm). Unbroken cells and nuclei were removed by

10 min centrifugation at 1500 xg, supernatants were divided into aliquots and subjected to centrifugation at 100 000 xg for an hour in order to obtain microsomal fractions. Following the spin, one aliquot of pellets was resuspended in a standard homogenisation buffer and protein concentration was assessed using BCA assay. This allowed for the remaining aliquots to be resuspended at a defined protein concentration (2.5 mg/ml) in the high-salt solubilisation buffer supplemented with protease inhibitors. The solubilisation process was performed in glass vials at 4 °C for an hour with constant stirring. Insoluble material was removed by centrifugation at 16 000 xg for 10 min and the obtained supernatant was layered onto the sucrose density gradient prepared earlier. Briefly, three solutions of sucrose in the gradient buffer were prepared: 5%, 25% and 40% (v/v) and allowed to mix by rotary agitation for an hour at 4 °C. The gradient was created by peristaltic pump (Masterflex L/S obtained from Cole-Parmer) equipped with two interconnected chambers allowing for a gradual dilution of the 25% sucrose with the 5% solution. This was slowly poured into centrifugation tubes (Polyallomer tubes obtained from Beckmann-Coulter) containing 5 ml of 40% sucrose cushion. Gradient centrifugation was performed at 100 000 xg for 16 h at 4 °C without active braking.

Fractions (typically 800-1000 µl) were collected and sucrose concentration was measured with a refractometer. Protein distribution was analysed by Western blotting.

#### 2.2.2.9 [<sup>3</sup>H]ryanodine binding

[<sup>3</sup>H]ryanodine binding assay was performed either on microsomal fractions (prepared as described in Section 2.2.2.6) or on cell homogenates (following centrifugation at 1500 xg for 10 min) obtained from HEK293 cells expressing the full length RyR2 with or without the BT4L fragment. Prior to the assay, the level of protein expression was assessed by Western blotting and the amount of sample subjected to [<sup>3</sup>H]ryanodine binding was adjusted accordingly. This allowed to compensate for the differences in the RyR2 expression levels between samples. Typically 300-500 µg of total protein was incubated at 37 °C for 2 h in the presence of 8 nM [<sup>3</sup>H]ryanodine in the ryanodine binding buffer containing the desired amount of free Ca<sup>2+</sup>. Free Ca<sup>2+</sup> was calculated using MaxChelator software (<http://maxchelator.stanford.edu/>) and the

following concentrations were used: 50 nM, 100 nM, 250 nM, 1  $\mu$ M, 5  $\mu$ M. For estimation of non-specific binding, samples were supplemented with 10  $\mu$ M of unlabelled ryanodine. Analysis was performed in three technical replicates for specific and two for non-specific binding. For maximum channel activation, [ $^3$ H]ryanodine binding was performed in 100  $\mu$ M free  $\text{Ca}^{2+}$  and 10 mM caffeine. Samples were filtered (GF/F glass microfiber filters obtained from Whatman), washed with the ryanodine binding buffer and incubated overnight in the scintillation liquid (Ultima Gold from Perkin Elmer) followed by the measurement of decays per minute over a period of 2 min using a scintillation counter (Tri-Carb 2100 TR obtained from Packard BioScience).

### 2.2.3 Yeast two-hybrid system

#### 2.2.3.1 Yeast Culture

*Saccharomyces cerevisiae* Y190 yeast strain supplied with Matchmaker Two-Hybrid System was revived from a frozen stock (stored at -80 °C in the YPD medium supplied with 50% glycerol). Briefly, a small portion of yeast stock was streaked on YPD agar plate and incubated at 30°C for up to 5 days until distinct colonies appeared. This plate was stored for up to one month at 4°C and constituted a viable yeast source for downstream applications.

#### 2.2.3.2 Yeast transformation

Yeast transformation was performed following the protocol provided with Matchmaker Two-Hybrid System. Briefly, 50 ml of YPD medium was inoculated with a single fresh colony and was incubated overnight at 30 °C with shaking at 250 rpm. The overnight culture was then used to refresh 200 ml of culture at OD<sub>600</sub> around 0.2-0.3 and was further incubated until OD<sub>600</sub> of around 0.5 was reached. At this point, cells were collected by centrifugation (1500 xg for 5 min), washed in

sterile deionised water and again recovered by centrifugation. The cell pellet was re-suspended in 1.6 ml of TE/LiAc solution and used for transformation as follows: 100 µl of TE/LiAc suspended yeast cells were mixed with 800 ng of each plasmid construct (pACT2 and pGBKT7) and 100 µg of herring testes carrier DNA. Subsequently, 600 µl of PEG/LiAc solution was added and following vigorous mixing, the solution was incubated for 30 min at 30 °C with shaking at 250 rpm. Cells were subjected to a heat shock (15 min at 42 °C) in the presence of 10% DMSO, followed by 2 min incubation on ice. Cells were collected by centrifugation (10 sec at 14 000 xg), resuspended in 200 µl of 1x TE buffer and plated on two appropriate SD agar plates. Plates were incubated at 30 °C for up to 5 days until distinct colonies appeared.

#### 2.2.3.3 β-galactosidase colony-lift filter assay

β-galactosidase colony-lift filter assay was performed following the protocol provided with Matchmaker Two-Hybrid System. Briefly, fresh colonies transformed with plasmids coding for two proteins to be tested for interaction were transferred from SD agar plates onto dry sterile filter paper (Whatman) which was subsequently submerged in liquid nitrogen in order to permeabilise the cells. The filter was then placed on a second filter paper pre-soaked with Z buffer/X-Gal solution prepared earlier. The filters were incubated at 30 °C and systematically inspected for the appearance of blue colonies. Cells transformed with pVA3-1 and pTD1-1 were used as positive controls.

#### 2.2.3.4 Quantitative liquid β-galactosidase assay

Quantitative β-galactosidase assay was performed according to the protocol provided with the system. Briefly, an overnight culture, which was inoculated with a single transformed colony, was used to obtain 10 ml of culture at OD<sub>600</sub> around 0.2-0.3, which was further incubated until OD<sub>600</sub> of around 0.5 was reached. The exact OD<sub>600</sub> was recorded and 500 µl of culture was centrifuged at 14 000 xg for 2 min. Cell

pellets were re-suspended in 100 µl of Z buffer and underwent repeated freeze/thaw cycles (1 min in liquid nitrogen followed by 3 min at 37 °C) in order to brake the cells open. Subsequently, 700 µl of Z buffer/β-mercaptoethanol was added to each of the reaction tubes and to the blank tube containing Z buffer only. Tubes were placed in the 30 °C incubator following the addition of 160 µl of Z buffer/ONPG and the time necessary for a yellow colour to develop was recorded. The tubes in which yellow colour was observed were mixed with 400 µl of 1 M Na<sub>2</sub>CO<sub>3</sub> and centrifuged at 14 000 xg for 5 min to remove cell debris. The supernatant's absorbance was measured at 420 nm against the blank tube. Units of β-galactosidase defined as the amount which hydrolyses 1 µmol of ONPG per minute per cell were calculated using the following formula:

$$\beta\text{-galactosidase units} = 1000 \times A_{420}/t \times 0.1 \text{ ml} \times 5 \times OD_{600}$$

where t refers to the incubation time in minutes necessary for the colour change to occur

Five colonies from each transformation were analysed.

#### 2.2.3.5 Cell homogenisation and protein extraction

For analysis of protein expression, yeast transformed (as described in Section 2.2.3.2) with the construct of interest was grown in SD minimal media. An overnight culture, which was inoculated with a single transformed colony, was used to obtain 100 ml of culture at OD<sub>600</sub> around 0.2-0.3 which was further incubated until OD<sub>600</sub> of around 0.5 was reached. At this point, cells were collected by centrifugation (1500 xg for 5 min at 4 °C), washed in ice-cold deionised water and again recovered by centrifugation. The cell pellet was resuspended in 500 µl of ice-cold protein extraction buffer supplemented with protease inhibitors. Cells were homogenised by three rounds (1 min each) of vigorous vortexing in the presence of glass beads, which were earlier washed three times in the protein extraction buffer. Cell debris was removed by centrifugation at 14 000 xg for 5 min. Protein concentration was evaluated as described in Section 2.2.2.2. Protein extracts were stored at -80 °C and subsequently analysed for protein expression by Western blotting.

## 2.2.4 Bacterial Culture

### 2.2.4.1 Culture maintenance

Untransformed *E.coli* DH5 $\alpha$  cells were stored at -80 °C in LB medium containing 50% glycerol. Transformed bacterial cells were stored in LB containing 50% glycerol and the appropriate antibiotic. Bacteria were recovered from a frozen stock by streaking a small portion of glycerol stock on LB agar plate followed by an overnight incubation at 37 °C. This plate was stored for up to one month at 4 °C.

### 2.2.4.2 Liquid cultures for plasmid isolation

For liquid overnight cultures, 1 ml of LB medium containing the appropriate antibiotic was inoculated with a single colony of transformed bacteria and incubated at 37 °C for around 8 hours with shaking at 225 rpm. Subsequently, 1 ml of growing culture was transferred into 200 ml of medium (100 ml for high copy number plasmids) and incubated overnight at 37 °C with shaking at 225 rpm. This yielded a saturated bacterial culture which was centrifuged at 10 000 xg for 10 min the following day. Cell pellets were either processed directly for plasmid isolation or stored at -80 °C.

Bacteria transformed with the full length RyR2 plasmids were cultured differently. LB medium (4 ml) supplemented with the appropriate antibiotic was inoculated with a single colony and incubated overnight at 30 °C with shaking at 225 rpm. The following day, 1 ml of the unsaturated culture was transferred into 16 ml of fresh antibiotic-containing LB medium and propagated for another 8 hours. The resulting culture was used to inoculate (2 ml) eight 400 ml flasks and allowed to grow overnight until the OD<sub>600</sub> of 1 was reached. Cell pellets were recovered by centrifugation at 10 000 xg for 10 min.

#### 2.2.4.3 Generation of electrocompetent cells

A single colony of untransformed *E.coli* DH5 $\alpha$  strain was used to inoculate 5ml of SB medium and incubated overnight at 37 °C with shaking at 225 rpm. The following day, 2 ml of this culture was used to inoculate 200 ml of SB-Plus medium and allowed to grow until an OD<sub>600</sub> of 0.7-0.8 was reached. At this point bacteria were divided into four aliquots and were placed on ice for 30 min. Subsequently, cells were collected by centrifugation (5000 xg for 5 min), washed in 10 ml of 10% glycerol and again recovered by centrifugation. This step was then repeated. Collected bacterial pellets were resuspended in 1 ml of 10% glycerol, divided into 100  $\mu$ l aliquots and immediately frozen down in isopropanol/dry ice bath. Electrocompetent cells were stored at -80 °C.

### 2.2.5 Mammalian Cell Culture

#### 2.2.5.1 HEK293 cell maintenance

In order to revive HEK293 cells, a frozen aliquot of cells was promptly warmed up in the 37 °C water bath and resuspended in complete DMEM medium. Cells were recovered by centrifugation at 1000 xg for 3 min, the pellet was resuspended in 5 ml of medium and cells were seeded in a T25 flask. The flask was placed in the 37 °C incubator with 5% CO<sub>2</sub> and cells were allowed to grow until confluence of around 90% was reached. At this point, the cells were washed with saline and were detached enzymatically (1 ml of trypsin-EDTA solution). Trypsin was inactivated by the addition of 5 ml of complete DMEM medium and cells were recovered by centrifugation (1000 xg for 3 min). The pellet was resuspended in 10 ml of medium and cells were seeded in a T75 flask.

HEK293 culture was maintained by passaging the cells whenever confluence of around 90% was reached. The split ratio depended on the downstream application and varied from 1:5 to 1:30.

### 2.2.5.2 Transfection

A day before transfection approximately  $5 \times 10^6$  or  $0.6 \times 10^6$  cells were seeded in the one 100mm Petri dish or in one well of a six-well plate respectively. Routinely this was achieved by allowing cells to grow until 90% confluence on the respective dishes and splitting them at 1:5 ratio a day before transfection. The following day cells were subjected to transfection using commercially available transfection reagent Express-In following the manufacturer's recommendations. Briefly, for a 100 mm Petri dish, 12 µg of total plasmid DNA was diluted in 1200 µl of serum-free DMEM. This solution was mixed rapidly with 60 µl of Express-In diluted in 1200 µl of serum-free DMEM. Following 20 min incubation, 3.6 ml of serum-free DMEM was added to the mixture. The old medium was replaced with DNA/Express-In mixture and the cells were allowed to incubate for around four hours after which the medium was supplemented with 6 ml of 20% FCS-containing DMEM.

For transfection of cells in a 6-well plate the above protocol was scaled down as follows: 2 µg of total DNA and 10 µl of Express-In was diluted in 200 µl of serum-free DMEM. Following complex formation 600 µl of medium was added to the mixture which was used to transfect the cells. After four hours the medium was supplemented with 1 ml of 20% FCS-containing DMEM.

24 h post-transfection cells were washed with 10 ml or 2 ml (for 100 mm Petri dish and 6-well plate respectively) saline and enzymatically dethatched (2 ml and 0.5 ml of trypsin-EDTA respectively). Trypsin was inactivated by the addition of complete DMEM medium and cells were recovered by centrifugation (1500 xg for 3 min). Pellets were re-suspended in saline, centrifuged and allowed to dry. Cell pellets were stored at -80 °C.

### 2.2.5.3 Long term storage

For long term storage, 90% confluent HEK293 cells were harvested from T75 flasks. Collected pellets were washed in saline, recovered by centrifugation and resuspended in FCS supplemented with 10% DMSO (3 ml per T75 flask). Cells, divided into 1ml

aliquots, were slowly frozen down at -80 °C and subsequently transferred to liquid nitrogen.

# Chapter 3

Identification of cysteines  
involved in the tetramerisation of  
the RyR2 N-terminus

### 3 Identification of cysteines involved in the tetramerisation of the RyR2 N-terminus

#### 3.1 Introduction

It has been generally accepted that the structural determinants required for RyR2 tetramer formation lie within the RyR2 C-terminus (Gao et al. 1997; Stewart et al. 2003). Likewise, the determinants for tetramer assembly in the structurally and functionally similar IP<sub>3</sub>R were also mapped to the C-terminal part of the protein (Galvan *et al.* 1999). However, unpublished findings from our laboratory imply that the oligomerisation determinants might not be restricted to the RyR2 C-terminus but are also present at the N-terminus. This hypothesis is based on data originating from analysis of oligomerisation ability of truncated fragments of the human RyR2 N-terminus. It has been shown by chemical crosslinking that the N-terminal part of the receptor, when expressed in HEK293 cells, possesses an intrinsic ability to tetramerise. Moreover, this process was found to involve the formation of disulphide bonds, i.e. the tetramer formed by the N-terminus is retained upon non-reducing (without DTT) SDS-PAGE in the absence of chemical crosslinking. Notably, upon chemical crosslinking, the RyR2 N-terminus also forms tetramers in reducing conditions implying that the formation of disulphide-bonds does not constitute a prerequisite step for oligomerisation. The summary of unpublished findings is presented in Table 3.1 and in Figure 3.1.

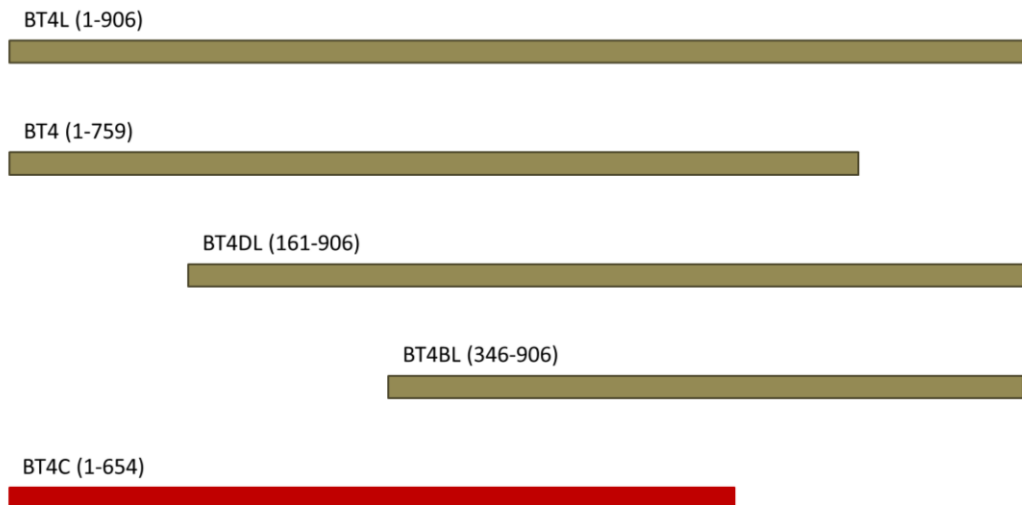


**Figure 3.1** Schematic representation of RyR2 N-terminal fragments; fragments in dark green form disulphide-mediated tetramers, BT4C (in red) exclusively forms disulphide-mediated dimers

			Oligomers observed in chemical crosslinking (MW in kDa)				DTT-sensitive oligomers
Construct	Coordinates in RyR2	No of residues	Monomer	Dimer	Trimer	Tetramer	
<b>BT4L</b>	1-906	906	101	202	303	<b>404</b>	tetramer
<b>BT4</b>	1-759	759	85	170	255	<b>340</b>	tetramer
<b>BT4C</b>	1-654	654	73	<b>146</b>	<b>219</b>	<b>292</b>	dimer
<b>BT4BL</b>	346-906	560	63	126	189	<b>252</b>	tetramer
<b>BT4DL</b>	161-906	745	82	164	246	<b>328</b>	tetramer

**Table 3.1** Summary of oligomerisation pattern of truncated N-terminal fragments of RyR2 expressed in HEK293 cells. The dominant type of oligomer formed by chemical crosslinking is shown in bold. Oligomers retained upon non-reducing SDS-PAGE (in the absence of chemical crosslinking) indicative of the existence of disulphide bonds are shown in the last column

Based on the above findings a working hypothesis of the N-terminus self-interaction within the RyR2 tetramer was created. The model assumes the existence of at least two distinct interfaces within each subunit involved in the oligomerisation. This type

of arrangement would enable the formation of a tetramer around the fourfold symmetry axis, and with each subunit potentially providing two independent cysteine residues involved in inter-subunit disulphide bond formation. The graphical illustration of the model is presented in Figure 3.2. In agreement with the working hypothesis, docking of the crystal structure of the N-terminal part of rabbit RyR1 (residues 1-559) into the cryo-EM map of native RyR1 revealed that this type of inter-subunit interaction is indeed plausible (Tung et al. 2010).

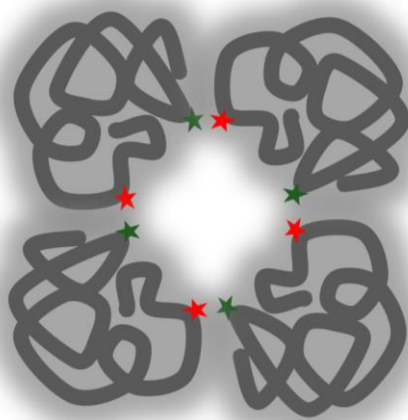


**Figure 3.2** Graphical illustration of the RyR2 N-terminus inter-subunit interaction; cysteine residues involved in disulphide bond formation are represented by stars

The model implies that in the absence of one of the cysteines the RyR2 N-terminus becomes unable to form any type of oligomers by disulphide bonds. Therefore, the ability of the BT4C (residues 1-654) fragment to create by disulphide bonds dimers and not tetramers (Table 3.1) undermines this hypothesis. If indeed one of the cysteines present in the BT4L fragment (residues 1-906) and absent in the shorter BT4C fragment was involved in the covalent bond formation between subunits, the fragment should not form any disulphide-linked oligomers but remain a monomer. However, this apparently discrepant result may have another plausible explanation. The shorter BT4C fragment has a substantially reduced self-interaction ability which is evident in a chemical crosslinking assay where it forms predominantly dimers with

only minor contribution of trimers and tetramers appearing towards longer crosslinking time-points. Thus it is speculated that the severely decreased stability of higher oligomers may prevent the formation of subsequent disulphide bonds that are necessary to hold the tetramer together.

Having established a hypothetical model of N-terminus self-interaction, the aim was to establish the identity of the cysteine residues participating in the inter-subunit association. It was presumed that the replacement of a putative cysteine residue within the BT4L fragment would deprive it of its ability to form disulphide-linked tetramers; however the ability to form oligomers following chemical crosslinking would be retained. On the other hand, if the replaced cysteine was not involved in the formation of inter-subunit covalent bonds, the fragment would retain its ability to form disulphide bond-mediated tetramers which would be present following separation with non-reducing SDS-PAGE.

Amino acid replacement by site-directed mutagenesis constitutes a valuable and widely accepted investigative tool used to study the relationship between protein structure and function such as the involvement of specific amino acids in enzymatic activity or exploring key residues which mediate protein-protein interactions. In our experimental setting, this technique was used with the intention to determine the identity of cysteines involved in the inter-subunit covalent bonds. In circumstances when the amino acid role is investigated in respect to its function (in our case the ability to mediate the formation of disulphide bonds), the substitution should be restricted to an amino acid of similar size and physical properties. This approach aims to assure that the phenotype of the mutant can be correlated to the loss/gain of function rather than to the disruption of local/global structure of the protein under investigation. For this reason, in our experiments, cysteines were replaced with serines (Figure 3.3).

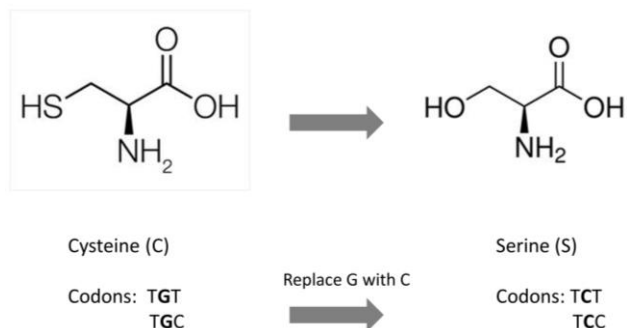


**Figure 3.3** The chemical structure of cysteine and serine. The replacement of G with C at the second position of two cysteine codons alters the DNA sequence to code for serine

The BT4L fragment contains 20 cysteines (Figure 3.4) which, according to the proposed concept, would require to be tested as single mutants. However, in order to increase experimental throughput, cysteines located in close proximity of one another such as C615/618/620 and C757/758 were tested together as triple and double mutants respectively. In addition, some of the cysteines were excluded from the analysis. This decision was based on the results of previous experiments showing that all truncated versions of the BT4L fragment are able to form DTT-sensitive oligomers (Table 3.1, Figure 3.1). It was speculated that cysteines in the extreme part of the N-terminus encompassing residues 1-345 (C24, C36, C47, C65, C131/2, C158, and C244) and C-terminus within residues 760-906 (C822) were most likely not involved in the disulphide bond formation as fragments lacking those residues retained the ability to form DTT-sensitive oligomers (BT4BL and BT4). For this reason two of those residues were used as negative controls (C36 and C244).



**Figure 3.4** Graphical representation of the cysteine location within the BT4L fragment

In summary, five new cysteine BT4L mutants ( $\text{BT4L}^{\text{C}244\text{S}}$ ,  $\text{BT4L}^{\text{C}548\text{S}}$ ,  $\text{BT4L}^{\text{C}577\text{S}}$ ,  $\text{BT4L}^{\text{C}615/618/620\text{S}}$  and  $\text{BT4L}^{\text{C}633\text{S}}$ ) were created and tested together with five previously prepared ( $\text{BT4L}^{\text{C}36\text{S}}$ ,  $\text{BT4L}^{\text{C}361\text{S}}$ ,  $\text{BT4L}^{\text{C}501\text{S}}$ ,  $\text{BT4L}^{\text{C}736\text{S}}$  and  $\text{BT4L}^{\text{C}757/758\text{S}}$ ). HEK293 cells were used to express all recombinant fragments, as those cells do not endogenously express RyR2. Furthermore, in the course of this investigation and as a result of difficulties in data interpretation, additional mutants containing a combination of multiple cysteine substitutions were generated and analysed ( $\text{BT4L}^{\text{C}361/501\text{S}}$ ,  $\text{BT4L}^{\text{C}361/615/618/620\text{S}}$  and  $\text{BT4L}^{\text{C}501/615/618/620\text{S}}$ ).

Concomitantly, a second independent experimental approach to address the identity of cysteines involved in the tetramerisation of the BT4L fragment was undertaken, i.e. mass spectrometry. The fundamental concept of this procedure was based on consecutive steps of chemical reactions allowing for selective labeling of putative cysteines followed by protein immunoprecipitation and mass spectrometry-based analysis (Aracena-Parks et al. 2006; Petrotchenko et al. 2006). For a detailed description of the experimental rationale please refer to Figure 3.5.

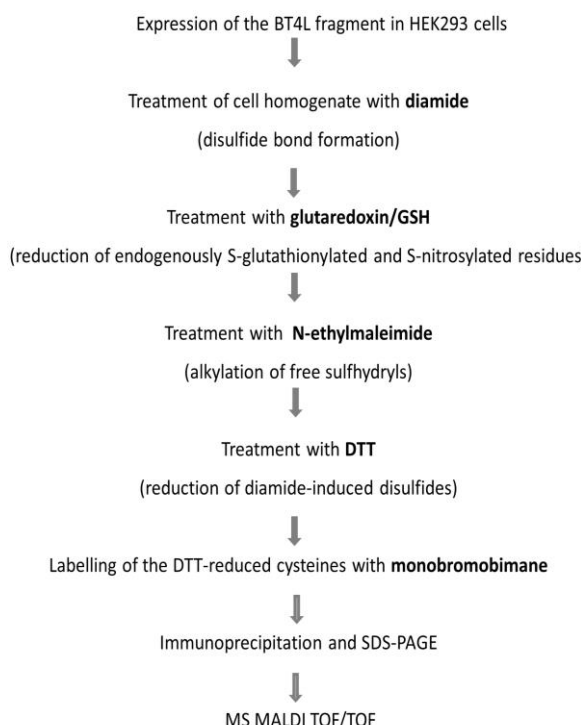


**Figure 3.5** Scheme describing site-specific labelling of sulphhydryl residues with monobromobimane for mass spectrometry-based identification of cysteines involved in disulphide bond formation

Current advances in mass spectrometry such as the development of soft ionisation techniques allowing for ionisation of macromolecules without their fragmentation, design of sophisticated mass analysers and construction of complex multistage instruments has put this field in the centre of protein research. In principle, commonly used mass spectrometry instruments are able to analyse a complex mixture of biomolecules and provide a researcher with information concerning the identity, quantity and post-translational modification of a given protein. However, in practice this type of analysis is extremely complicated and quite often not possible to perform. In respect to the experimental goal, it was pivotal to ascertain that the obtained peptide spectrum contains fragments with cysteines of interest. In addition there were concerns about the ultimate amount of monobromobimane-labelled residues as it was expected it to be relatively low. The reasoning was based on three factors; firstly, it was expected that a limited amount of diamide-induced disulphides would be formed, which in turn would affect the number of residues labelled with monobromobimane. Secondly, there were concerns about the efficiency of the labelling reaction and thirdly some portion of the monobromobimane moiety was anticipated to be cleaved under ionisation conditions as reported earlier (Petrotchenko et al. 2006). In the context of the above, the prerequisite step for this experimental approach to work was to obtain a sufficient quantity of the pure BT4L fragment. This task was addressed by means of immunoprecipitation of the BT4L fragment expressed in HEK293 cells.

Thus, the aim of the study presented in this Chapter was to identify cysteine residues involved in disulphide-mediated oligomerisation of the RyR2 N-terminus by two independent techniques: mutagenesis and mass spectrometry.

## 3.2 Methods

### 3.2.1 Site-directed mutagenesis approach

Site-directed mutagenesis of the BT4L construct (pCR3-c-Myc vector containing the BT4L coding sequence) was performed as described in Section 2.2.1.6. Following

sequence verification of mutagenesis-obtained constructs, DNA fragments containing the desired mutation were subcloned into the wild type BT4L plasmid in order to reduce the risk of spontaneous mutations introduced in a random location within the plasmid during mutagenic PCR. This was performed as follows; the verified mutant plasmid and the destination plasmid were digested with appropriate restriction endonucleases, separated by agarose gel electrophoresis and subjected to DNA ligation using the gel extracted DNA fragments of interest (described in detail in Section 2.2.1.3, 2.2.1.4 and 2.2.1.5). For restriction enzymes used in subcloning of DNA fragments for each BT4L cysteine mutant please refer to Table 3.2. Subsequently, the ligation reaction product was used to transform bacteria by means of electroporation (Section 2.2.1.8). Obtained colonies were screened as described in Section 2.2.1.10. The positive clones were sequenced further to cover the length of the whole subcloned DNA fragment and once the sequence was verified, large volume overnight bacterial cultures were set up for plasmid isolation as described in Section 2.2.1.10.

Construct	Mutagenic PCR template plasmid	Restriction endonucleases	Double (D) or sequential (S) digest	Coordinates of the subcloned fragment (bp)
BT4L <sup>C244S</sup>	BT4L	<i>Pml</i> II, <i>Bsp</i> EI	S	727 – 1377
BT4L <sup>C548S</sup>	BT4L	<i>Bsp</i> EI, <i>Sal</i> I	D	1377 - downstream of the last residue of the BT4L fragment (2839)
BT4L <sup>C577S</sup>	BT4L	<i>Bsp</i> EI, <i>Sal</i> I	D	as above
BT4L <sup>C615/618/620S</sup>	BT4L	<i>Bsp</i> EI, <i>Sal</i> I	D	as above
BT4L <sup>C633S</sup>	BT4L	<i>Bsp</i> EI, <i>Sal</i> I	D	as above
BT4L <sup>C361/615/618/620S</sup>	BT4L <sup>C615/618/620S</sup>	<i>Pml</i> II, <i>Sal</i> I	S	727- downstream 2893
BT4L <sup>C501/615/618/620S</sup>	BT4L <sup>C501S</sup>	<i>Bsp</i> EI, <i>Sal</i> I	D	1377 – downstream 2893

**Table 3.2** List of restriction endonucleases used in subcloning. Coordinates correspond to the human RyR2 mRNA, accession number: X98330

Obtained plasmids were used to transfect HEK293 cells growing on six-well plates as described in Section 2.2.5.2. Each experiment involving cysteine mutants was performed with concomitant transfection of cells with the wild-type BT4L. Cell pellets obtained 24 hours after transfection were homogenised (Section 2.2.2.1) and half of the sample was treated with DTT (4 °C, 1 h, 10 mM). Total protein concentration was evaluated using BCA colorimetric assay and, depending on the experiment, 20-50 µg of total protein from DTT-treated and untreated samples were subjected to SDS-PAGE and Western blotting (for details please refer to Section 2.2.2.3.and 2.2.2.4). The BT4L fragment expressed from a pCR3-c-Myc vector contains an N-terminal c-Myc epitope. This allows for the protein to be detected by a c-Myc antibody (Table 2.1). The secondary anti-mouse HRP-conjugated Ab was used for protein visualisation using ECL-based detection kit.

### 3.2.1.1 Chemical crosslinking

HEK293 cells growing on 100 mm Petri dishes were transfected with the BT4L<sup>C361S</sup> construct as described in Section 2.2.5.2. Each experiment was performed with a concomitant transfection of cells with the wild-type BT4L plasmid serving as a positive control. Cell pellets obtained 24 hours after transfection were homogenised (Section 2.2.2.1) and one aliquot was treated with DTT (4 °C, 1 h, 10 mM). Total protein concentration was evaluated using BCA colorimetric assay and depending on the experiment 20-50 µg of total protein was subjected to glutaraldehyde crosslinking in a time-dependent manner (Section 2.2.2.2). Proteins were separated by SDS-PAGE and subsequently blotted onto PVDF membranes (for details please refer to Section 2.2.2.3.and 2.2.2.4). The c-Myc antibody and anti-mouse HRP-conjugated Ab were used to detect protein presence (Table 2.1). Tetramer to monomer ratio was determined by performing densitometry analysis using BioRad Quantity One software. Percentage of tetramer was calculated as follows %T=OD<sub>T</sub>/(OD<sub>T</sub>+OD<sub>M</sub>)x100 where OD<sub>T</sub> and OD<sub>M</sub> corresponds to optical density obtained within one time point for tetramer and monomer bands respectively. Statistical analysis was carried out using paired, 2-tailed Student's *t* test to test mean

of difference in tetramer formation between BT4L<sup>C361S</sup> and wild-type BT4L within each time-point studied.

### 3.2.2 Mass spectrometry approach

#### 3.2.2.1 Immunoprecipitation

The immunoprecipitation of the RyR2 N-terminus (residues 1-906) expressed in HEK293 cells was performed using a diverse set of experimental conditions aiming to optimise the final result. For details of each experimental setting please refer to Table 3.3. The optimised version was performed as follows: HEK293 cell pellets obtained from five 100mm Petri dishes transfected with AD4L construct (the pCR3 vector encoding RyR2 residues 1-906 with N-terminal HA epitope) were homogenised in 4ml of immunoprecipitation buffer without CHAPS but supplemented with protease inhibitors. Cells were homogenised as described in Section 2.2.3.5 and subjected to 1500 xg spin followed by overnight incubation of the supernatant at 4 °C in the presence of 1% CHAPS under rotary agitation. Following overnight solubilisation, cell lysates were centrifuged at 18 000 xg and the supernatant was incubated at 4 °C for six hours with Protein A beads (100 µl of pre-washed beads was used for 1 ml of cell lysate). This step aimed to pre-clear the cell lysate in order to decrease the non-specific binding and was repeated overnight and again for six hours the following day. Concurrently, two 25 µl aliquots of pre-washed Protein A beads were incubated with 4 µg of HA polyclonal antibody (Table 2.1) in 200 µl of the IP buffer. Following the three rounds of pre-clearing, cell lysate was incubated with HA Ab-bound beads (1 ml of lysate with 25 µl of beads) at 4 °C for six hours. Subsequently beads were recovered by centrifugation and incubated with the remaining volume of the cell lysate overnight. The following day, beads were washed with the IP buffer three times for 10 min at 4 °C and collected by centrifugation at 1500 xg for 2 min. Proteins were eluted using 20 µl of 2x reducing protein loading buffer, two samples were combined and loaded into one well of 12% SDS-polyacrylamide gel. Following the electrophoresis, the gel was washed in

deionised water, placed in 1% acetic acid and immediately transported to the Cardiff University CBS Mass Spectrometry Facility for further processing.

<b>Exp.</b>	<b>Matrix</b>	<b>Protein fragment</b>	<b>IP buffer</b>	<b>Pre-clearing steps</b>	<b>Antibody</b>	<b>Final washing step</b>
<b>I</b>	Protein G Dynabeads (20-40 µl)	BT4L	homogenisation buffer with 0.4% CHAPS	no	1-2 µg of c-Myc Ab	2x10 min at 4 °C
<b>II</b>	As above	As above	homogenisation buffer with 1% CHAPS	O/N with 40 µl of beads (1x)	As above	As above
<b>III</b>	100 µl of Protein G Dynabeads	As above	As above	O/N with 100 µl of beads (1x)	2 µg of cMyc	As above
<b>IV</b>	100 µl of Protein A Sepharose beads	AD4L	As above	As above	2 µg of HA polyclonal Ab	As above
<b>V</b>	50 µl of Protein G Sepharose beads	BT4L	As above	As above	4 µg of c-Myc Ab	3x10 min at 4 °C
<b>VI</b>	100 µl of Protein A Sepharose beads	AD4L	homogenisation buffer with 1% CHAPS and BSA at 200 µg/ml	As above	2 µg of HA polyclonal Ab	As above
<b>VII</b>	25 µl of Protein A Sepharose beads	As above	IP buffer	6 h with 100 µl of beads (3x)	As above	As above
<b>VIII</b>	2 aliquots of 25 µl of Protein A Sepharose beads	AD4L (4 Petri dishes transfected)	As above	6 h with 100 µl of beads per Petri dish (3x)	2 aliquots of 4 µg of HA polyclonal Ab	As above

**Table 3.3** A summary of experimental conditions undertaken in the immunoprecipitation process

### 3.2.2.2 Sample preparation for mass spectrometry

All techniques used at the Mass Spectrometry Unit were conducted following local standard operating procedures. Briefly, upon arrival the gel was stained with Coomassie using the Colloidal Coomassie Blue Staining Kit (Invitrogen) following manufacturer's recommendations. The following day, three plugs corresponding to the immunoprecipitated protein were removed from the stained band and placed on a 96-well plate. Additionally, a plug from a band equivalent to the antibody heavy chain or one of the protein markers ( $\beta$ -galactosidase or BSA) was taken. This served as a positive control and allowed for assessment of quality of downstream procedures including protease digestion and equipment performance. Obtained plugs were dehydrated using a solution of acetonitrile (50% in 0.1% trifluoroacetic acid) and destained with 50% acetonitrile in 25 mM ammonium bicarbonate. Subsequently, plugs were washed in 25 mM ammonium bicarbonate until Coomassie stain was removed completely, dehydrated with acetonitrile solution and dried in the oven. Following reduction and alkylation, samples were dehydrated as described above and subjected to protease digestion. Depending on the experiment, different enzymes alone or in combination were used. For details of proteases and digestion conditions please refer to Table 3.4.

Experiment	Protease	Conditions (per gel plug)
I	trypsin (Promega)	62.5 ng trypsin in 25 mM ammonium bicarbonate, 37 °C for 4 h
II	chymotrypsin (Promega)	62.5 ng chymotrypsin in 100mM Tris buffer, pH 8, room temperature for 3h, sample was cleaned up and concentrated using ZipTip resin
III	trypsin/chymotrypsin	Sequential procedure using optimal conditions for trypsin and chymotrypsin respectively
IV	V8 protease (ProteaBio Europe SAS)	62.5 ng of V8 protease in 25 mM ammonium bicarbonate, 37 °C for 4 h
V	V8 protease/trypsin	62.5 ng of each 25 mM ammonium bicarbonate, 37 °C for 4 h

**Table 3.4** Summary of proteases and digestion conditions used prior to mass spectrometry analysis

Following digestion, plugs were placed in an ultrasonic water bath to facilitate peptide extraction from gel plugs. The buffer surrounding the plug was transferred to a clean plate, dried in the oven and subsequently stored at -20 °C. On the day of the analysis, dried peptides were dissolved in the acetonitrile solution and around 10% of the initial sample was loaded onto a 384 well MALDI target plate and mixed with the appropriate matrix. If necessary, additional 20% of sample was loaded into the well and the remaining amount was kept at -20 °C should further analysis be needed. Samples were run on the ABI 4800 MALDI TOF/TOF Analyser.

### 3.3 Results

#### 3.3.1 Site-directed mutagenesis

All plasmid DNA constructs designed to express BT4L containing the desired cysteine to serine substitution were successfully generated and their DNA sequence was confirmed. A typical set of results representing intermediate steps of the mutagenesis process is shown in Figure 3.6.

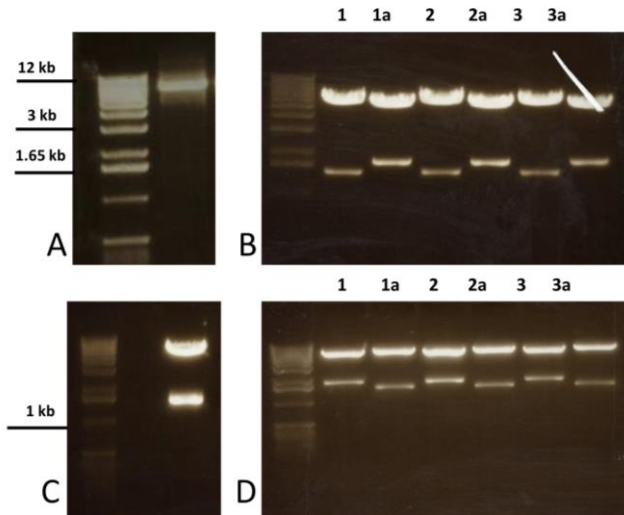


**Figure 3.6** Intermediate steps of the experimental procedure generating the BT4L<sup>C577S</sup> construct; A: DNA gel showing the amplification product obtained in the mutagenic PCR, B: indicative digest of clones following bacteria transformation with the mutagenesis product (1-3: plasmid DNA obtained from three clones and cut with *Bsp*EI/*Sal*I, 1a-3a cut with *Hind*III), C: restriction digest (*Bsp*EI/*Sal*I) of the positive clone verified by sequencing, the lower band (~1.5 kb) corresponding to the fragment containing cysteine 577 substitution was cut out of the gel and subcloned into the native BT4L fragment, D: indicative digest of three clones obtained in the subcloning step (1-3: plasmid DNA obtained from three clones and cut with *Hind*III, 1a-3a cut with *Bsp*EI/*Sal*I)

### 3.3.1.1 Cysteines: 36, 244, 548, 577, 633, 736, 757 and 758 are not involved in disulphide bond formation

Wild-type BT4L (RyR2 residues 1-906) expressed in mammalian HEK293 cells produces a protein band of ~100 kDa representing BT4L monomers (Figure 3.7). In non-reducing conditions, an additional high molecular weight band corresponding to an oligomeric form is also observed. This band is no longer present when samples are treated with the reducing agent DTT suggesting that BT4L oligomerisation involves formation of disulphide bonds between cysteine residues. Based on the molecular weight of a BT4L monomer, a tetramer is predicted to appear as a ~400 kDa band. However, as evident in Figure 3.7 the high molecular weight band exhibits somewhat smaller size. This apparent reduced molecular weight is consistent with a compact arrangement of a tetrameric assembly which would be expected to experience less gel retardation than a corresponding linear form. Thus the high molecular weight band

evident in Figure 3.7 corresponds to the DTT-sensitive oligomer composed of four BT4L monomers.

In concert with the results previously obtained (Table 3.1), the substitution of cysteines 36 and 244 did not affect disulphide bond-mediated tetramerisation of the BT4L fragment (Figure 3.7; A and B). Similarly, the ability to form DTT-sensitive tetramers was retained by two other mutants BT4L<sup>C736S</sup> and BT4L<sup>C757/578S</sup> (Figure 3.7; F). These findings are in agreement with the previously proposed explanation of the BT4C fragment's inability to form DTT-sensitive tetramers as discussed in Section 3.1. Likewise, disulphide bond-mediated oligomers were formed by cysteine mutants BT4L<sup>C548S</sup>, BT4L<sup>C577S</sup> and BT4L<sup>C633S</sup> (Figure 3.7, E and G).

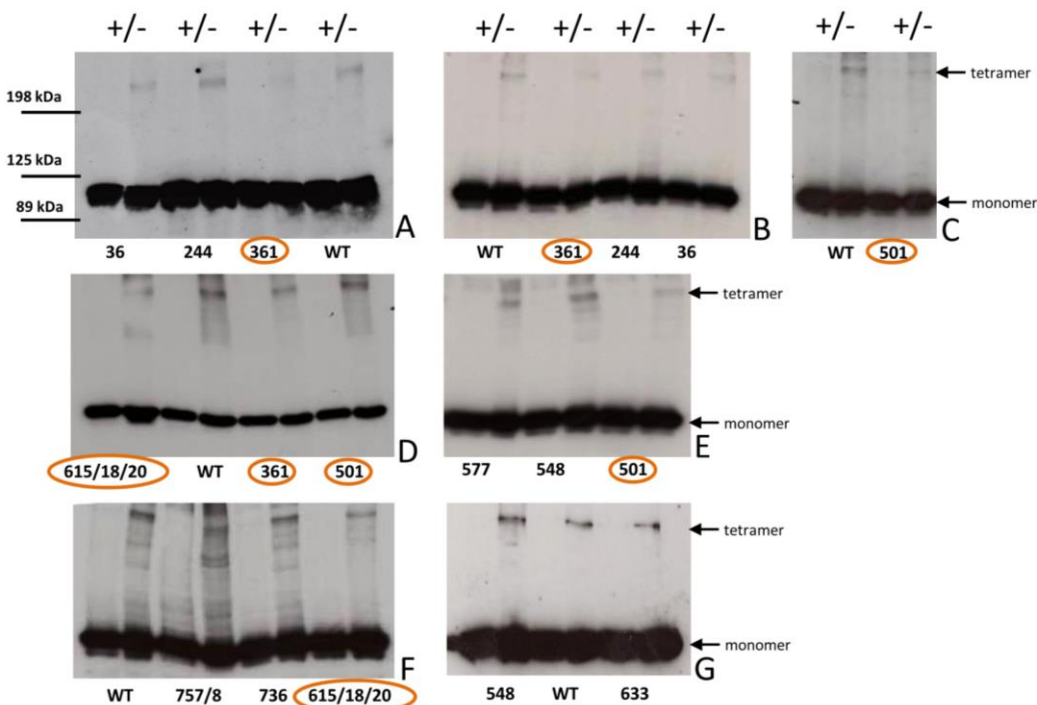


**Figure 3.7** Representative blots of cysteine mutants; +/- DTT-treated and untreated samples respectively. Each mutant was tested concomitantly with the wild-type BT4L fragment in at least five independent experiments. Putative candidates in circles. Monomer and tetramer indicated by arrows

### 3.3.1.2 Cysteines mutants BT4L<sup>C361S</sup>, BT4L<sup>C501S</sup> and BT4L<sup>C615/618/620S</sup> display variable behaviour

In contrast to the mutants discussed in the preceding section, which were consistently indistinguishable from the wild-type BT4L fragment, the substitution of cysteines 361, 501 and 615/618/620 led to ambiguous results. All three mutants, i.e. two single and one triple substitution, displayed either severely reduced cysteine-mediated tetramer formation or a complete absence of oligomers in DTT-free samples (Figure 3.7; A-F, indicated by orange circles). However, the extent to which tetramers were reduced or absent was not reproducible; varied between mutants and between experiments. Those results were not readily interpretable in respect to the proposed model which assumed an “all or nothing” scenario. It should be emphasised that, in theory, the removal one of the two cysteines involved in the disulphide bond, should result in complete ablation of disulphide bond-mediated tetramers. Hence, it was speculated that the partial, non-reproducible ability of mutants BT4L<sup>C361S</sup> BT4L<sup>C501S</sup> and BT4L<sup>C615/618/620S</sup> to form DTT-sensitive tetramers may arise from the formation of alternative disulphide bonds, in which the missing residue is compensated for by other cysteine located in spatial proximity, a phenomenon which was observed by others (Zha *et al.* 2009) . In the context of the above, it was speculated that the generation of additional mutants containing a combination of the aforementioned cysteine substitutions would help to resolve this issue.

### 3.3.1.3 The combined mutants suggest an important role of cysteine 361 in the formation of disulphide bond-mediated tetramers

Contrary to expectations, the generation and testing of BT4L constructs containing multiple cysteine substitutions did not produce a definitive conclusion in respect to the identity of residues involved in disulphide bond formation. All three BT4L mutants; BT4L<sup>C361/501S</sup>, BT4L<sup>C361/615/618/620S</sup> and BT4L<sup>C501/615/618/620S</sup>, displayed either severely reduced cysteine-mediated tetramer formation or complete absence of oligomers in DTT-free samples (Figure 3.8). This partial ability of tetramerisation was in disagreement with the assumptions of the model. Furthermore, experiment to

experiment variability remained an unresolved issue. However, some important observations were made; the ability to form DTT-sensitive tetramers decreased in the following order:  $\text{BT4L}^{\text{C501/615/618/620S}} > \text{BT4L}^{\text{C361/615/618/620S}} > \text{BT4L}^{\text{C361/501S}}$  clearly indicating an additive effect of cysteine mutations. In particular the propensity to create cysteine-mediated oligomers was critically reduced in mutants lacking cysteine 361 and almost completely abolished in the double mutant  $\text{BT4L}^{\text{361/501}}$ . However, mutation of cysteine 501 alone or in combination with residues 615/618/620 had a rather moderate effect on disulphide-mediated oligomerisation.

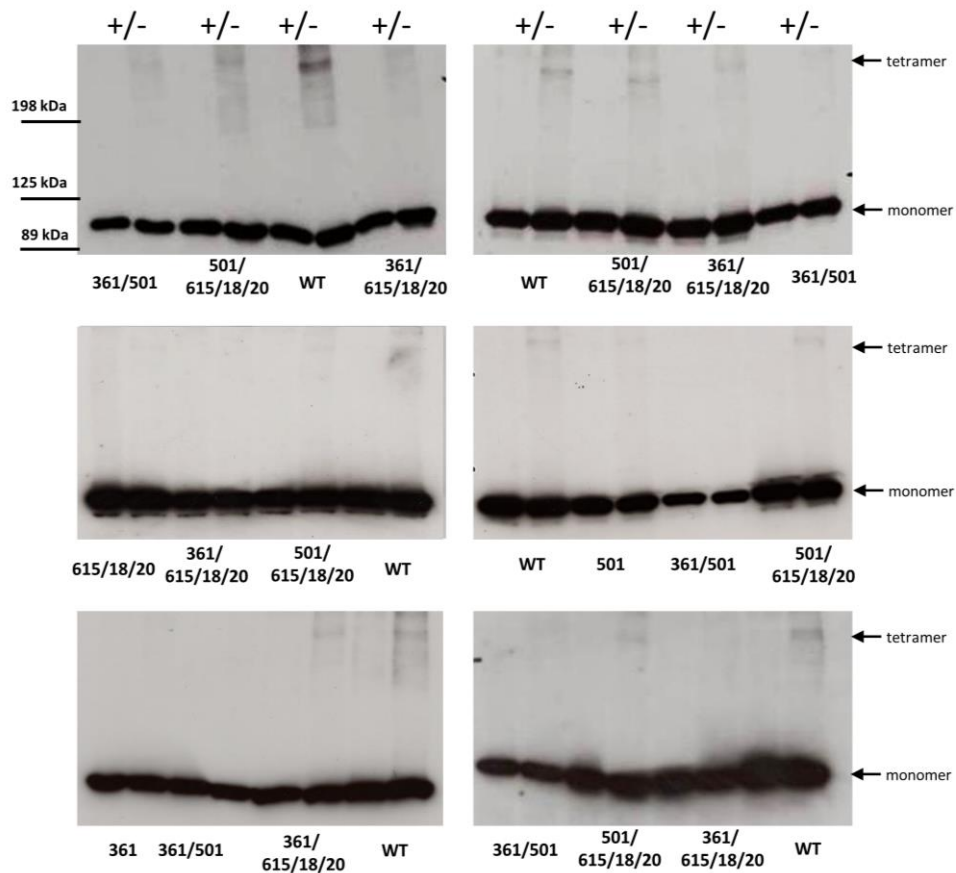


**Figure 3.8** Representative blots of combined cysteine mutants; +/- DTT-treated and untreated samples respectively. Each mutant was tested concomitantly with the wild-type BT4L fragment in at least seven independent experiments. Monomer and tetramer indicated by arrows

### 3.3.1.4 Chemical crosslinking of BT4L<sup>C361S</sup> suggests additional disulphide-independent role of cysteine 361 in tetramer formation

The involvement of cysteine 361 in the oligomerisation of the RyR2 N-terminus was investigated further. The principal aim was to determine whether the severely reduced ability of this mutant to tetramerise in a DTT-sensitive manner is solely dependent on the fact that cysteine 361 is involved in disulphide bond formation or whether this residue is also taking part in a non-covalent type of inter-subunit interaction. The above task was performed using time-dependent chemical crosslinking, a chemical reaction that creates covalent bonds between interacting molecules and therefore enables preservation of the oligomeric status of the interacting protein partners during SDS-PAGE. It was anticipated that comparison of the oligomerisation propensity between wild-type BT4L and BT4L<sup>C361S</sup> in DTT-treated samples (where there are no disulphide-mediated interactions) would help to clarify the role of cysteine 361.

Glutaraldehyde crosslinking of BT4L<sup>C361S</sup> was performed with the concomitant crosslinking of the wild type fragment transfected on the same day as the mutant. Since our experimental set up involved a multistep procedure with many factors affecting the final outcome including transfection efficiency, protein expression, crosslinking conditions and protein transfer, the inclusion of BT4L<sup>WT</sup> enabled us to evaluate the tetramerisation propensity of the BT4L<sup>C361S</sup> relative to its wild-type counterpart within each experiment. With this approach the effect of experimental variability in our analysis was substantially reduced.

Representative blots showing chemical crosslinking of BT4L<sup>WT</sup> and BT4L<sup>C361S</sup> are presented in Figure 3.9. Time-dependent tetramer formation is reflected by the presence of ~400 kDa band which becomes more pronounced as the duration of chemical crosslinking increases. At ambient conditions (in the absence of DTT), there is a clear reduction in tetramer levels formed by the BT4L<sup>C361S</sup> mutant compared to its wild-type counterpart. (Figure 3.9; left panel). Cumulative data (n=9) following densitometry analysis are presented in the left panel in Graph 3.1. In the presence of the C361S mutation, the amount of tetramers observed prior to glutaraldehyde addition (0 time-point) and indicative of disulphide bond-mediated oligomers, is reduced by 60%. The difference in the oligomerisation propensity between the mutant

and the wild-type fragment decreases towards longer crosslinking time-points. The effect is statistically significant in every time point studied.

Qualitatively, the crosslinking performed in the presence of DTT did not reveal major alterations in the BT4L tetramerisation propensity induced by cysteine 361 substitution (Figure 3.9; right panel). However, quantitative analysis ( $n=7$ ) following densitometry measurements revealed that the  $\text{BT4L}^{\text{C361S}}$  fragment displays a reduced ability to tetramerise compared to the wild-type fragment in reducing conditions as well (Graph 3.1; right panel). The presence of the C361S reduced oligomerisation on average by 70%, however the effect was statistically significant only for some of the time-points studied. The fact that the above mutant exhibited reduced oligomerisation under conditions where disulphide bonds are absent (DTT addition), implies that cysteine 361 is also involved in non-covalent protein-protein interactions mediating RyR2 N-terminus tetramerisation. However, additional effects originating from the substitution of cysteine with more polar serine residue cannot be excluded.

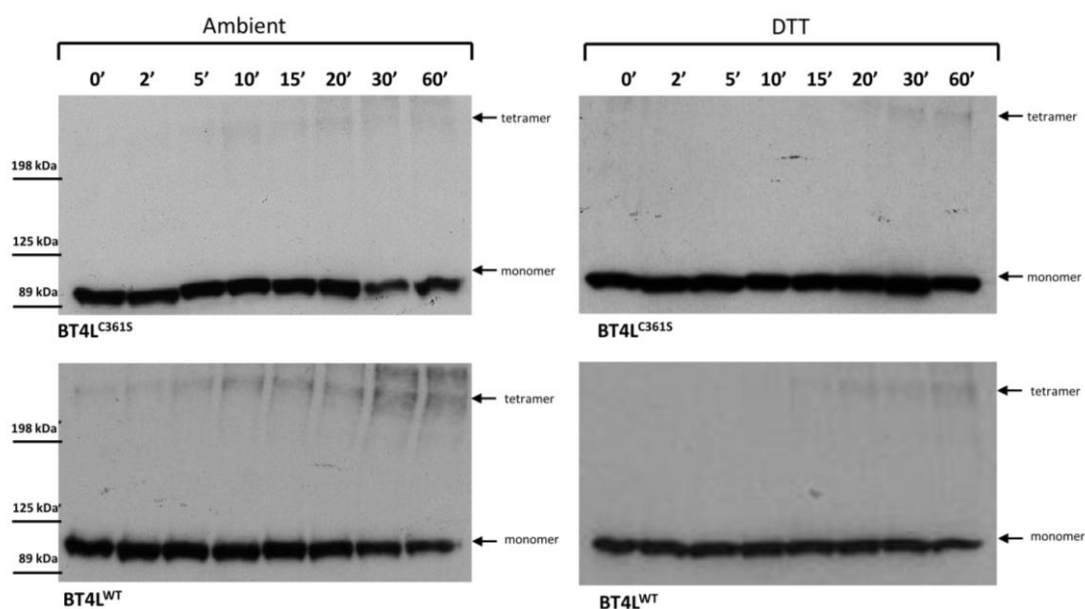
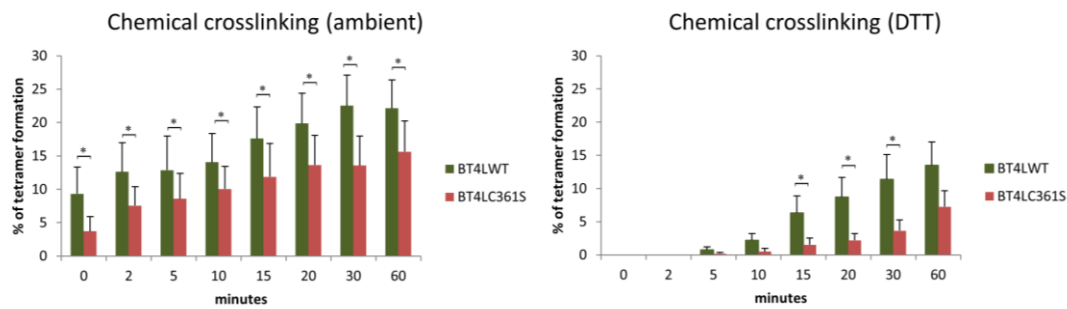


**Figure 3.9** Representative blots of chemical crosslinking experiments illustrating time-dependent tetramer formation of  $\text{BT4L}^{\text{C361S}}$  and  $\text{BT4L}^{\text{WT}}$  fragments in the presence and absence of DTT (right and left panel respectively). Time-points in minutes as indicated. Tetramer and monomer indicated by arrows



**Graph 3.1** Densitometry analysis of BT4L<sup>WT</sup> and BT4L<sup>C361S</sup> tetramer formation in chemical crosslinking assay at ambient and reducing conditions. Percentage of tetramer calculated as described in Section 3.2.1.1. Data are shown as mean +/-SEM, n=9 and n=7 for ambient and reducing conditions respectively; \* statistical significance at p<0.05 calculated using paired, 2-tailed Student's *t* test

### 3.3.2 Mass spectrometry

#### 3.3.2.1 Immunoprecipitation

The task of obtaining sufficient quantities of the pure N-terminal fragment by immunoprecipitation proved to be very difficult. The initial approach using Protein G Dynabeads with c-Myc Ab failed to precipitate the BT4L protein and showed relatively high levels of non-specific binding (Table 3.3; experiments I-II). Western blot analysis revealed that the level of captured protein is hardly detectable. In a subsequent experiment the performance of Protein G Dynabeads with Protein A Sepharose beads was compared (Table 3.3; experiment III-IV). As Protein A exhibits very low affinity for mouse IgG<sub>1</sub> (which is mouse monoclonal c-Myc Ab isotype), for this particular experiment cells were transfected with the AD4L construct (HA-tagged RyR2 residues 1-906). This enabled the use of Protein A compatible antibody, i.e. rabbit HA Ab. While the AD4L fragment was immunoprecipitated with Protein A Sepharose beads, the use of Protein G Dynabeads proved again to be unsuccessful (Figure 3.10). Western blot analysis revealed that with moderate levels of c-Myc Ab bound to the beads, the amount of immunoprecipitated BT4L protein remained hardly detectable. Thus the failure of this particular approach was determined by two factors:

low binding affinity of c-Myc Ab for Protein G Dyanbeads and the inability of the c-Myc Ab to bind to its epitope on the BT4L fragment. However, since the non-specific binding of Protein A beads was considerable and the level of immunoprecipitated protein was very low, an additional experiment using c-Myc Ab in combination with new Protein G Sepharose beads was performed (Table 3.3; experiment V). Those beads however exhibited extremely high non-specific binding and at this point this experimental approach was not pursued any further (Figure 3.11). Instead the focus was shifted back to Protein A Sepharose beads and the HA-tagged AD4L construct.

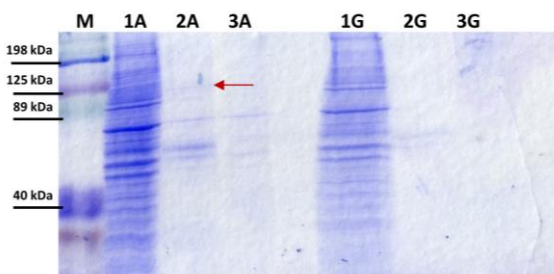


**Figure 3.10** Coomassie stained gel of the RyR2 N-terminus precipitation with Protein A Sepharose beads and Protein G Dynabeads in lanes 1A-3A and 1G-3G respectively. Lanes: M; molecular weight markers, 1; material eluted from beads used in pre-clearing step, 2; material eluted from beads incubated with the relevant antibody (HA for Protein A and c-Myc for Protein G beads), 3; material eluted from beads without Ab. Red arrow indicates the immunoprecipitated AD4L fragment.

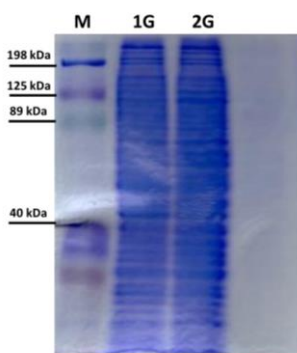


**Figure 3.11** Coomassie stained gel of the immunoprecipitation of the BT4L fragment with Protein G Sepharose beads. Lanes: M; molecular weight marker, 1G; material eluted from beads incubated with c-Myc Ab, 2G; material eluted from beads used in pre-clearing step.

Protein A Sepharose beads were used in the subsequent experiment where AD4L immunoprecipitation was performed in the presence of BSA (Table 3.3; experiment VI) however non-specific binding remained high. In the following experiment, this issue was addressed by two modifications: switching to salt containing buffer (150 mM NaCl); i.e. the previously used homogenisation buffer was substituted with the IP-buffer (for composition details please refer to Section 2.1.2) and increasing the number of pre-clearing steps. This modification allowed for a successful immunoprecipitation of the AD4L fragment with minimal amount of non-specific material (Table 3.3; experiment VII). The identity and quality of the protein was confirmed by mass spectrometry. However, at this point there were still concerns about the relatively low amount of purified protein which would constitute a considerable difficulty in pursuing the experimental approach as discussed earlier in Section 3.1. In order to address this issue, in the subsequent experiment (Table 3.3; experiment VIII) four times as much cell material as before was processed and increased amount of HA Ab was used (Table 3.3; experiment VIII). This modification allowed for a satisfactory level of the AD4L fragment to be obtained (Figure 3.12).

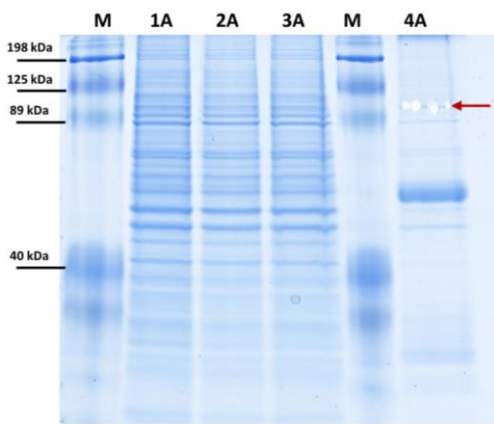


**Figure 3.12** Coomassie stained gel of the RyR2 N-terminus precipitation with Protein A Sepharose beads. Lanes: M; molecular weight markers, 1A-3A; material eluted from the beads used in three consecutive pre-clearing steps, 4A material eluted from beads incubated with the HA Ab. Red arrow indicates immunoprecipitated AD4L fragment with gel plugs removed for a downstream mass spectrometry analysis.

### 3.3.2.2 Spectral analysis

The peptide spectrum obtained from purified AD4L protein samples, which underwent a standard trypsin digestion, was analysed in respect to the presence of particular peptides. This was performed by comparison of the peaks present in the sample spectrum with peptide masses obtained following *in silico* trypsin digestion of the RyR2 sequence encompassing residues 1-906 (Table 3.5).

Position in the fragment	Mass	Cysteine residues	Peptide sequence	Presence in the spectrum
16-30	1729.8425	C24	TDDEVVLQCTATIHK	No
35-45	1207.5888	C36	LCLAAEGFGNR	Yes
46-56	1285.6093	C47	LCFLESTSNSK	Yes
57-76	2274.1798	C65	NVPPDLSICTFVLEQSLSVR	No
123-137	1821.7717	C131/132	HSYSGMYLCCLSTSR	No
143-167	2832.3297	C158	LAFDVGLQEDTTGEACWWTIHPASK	No
236-257	2531.1401	C244	LLHGHMDECLTVPSGEHGEEQR	No
356-380	2946.3978	C361	YGDSVCYIQHVDTGLWLTYQSVDVK	No
486-504	2321.1264	C501	QNLFQEEMINLVLECIDR	No
547-561	1753.8326	C548	NCAQFSGSLDWLISR	No
565-590	2833.5379	C577	LEASSGILEVLHCVLVESPEALNIK	No
610-626	1956.9816	C615/18/20	VLDVLCSLCVCHGVAVR	No
627-640	1636.8224	C633	SNQHLICDNLLPGR	Yes
695-739	4780.1109	C736	VGWASTEGYSPYPGGGEWG GNGVGDDLFSYGFDGLHLWSGCIAR	No
751-769	2155.9998	C757/8	TDDVISCCLDLAPSISFR	Yes
813-829	1918.9771	C822	FLPPPGYAPCYEAVLPK	No

**Table 3.5** A summary of the spectral analysis of trypsin-digested sample with mass acquisition set between 700-3000 MW. *In silico* digest was performed using online PeptideMass tool available at <http://web.expasy.org>.

Unfortunately, most of the cysteine-containing peptides failed to appear in the spectrum. At this point this result was attributed to the fact that most of those fragments were of high molecular weight. This problem was addressed in the subsequent set of experiments where the purified AD4L protein was subjected to digestion using a combination of proteases (Table 3.4; experiment III and V). While a combined digestion with trypsin and chymotrypsin did not produce any valid data, the combination of trypsin and V8 protease resulted in a good quality spectrum (Table 3.6). However, this modification failed to significantly enrich the spectrum in cysteine-containing peptides.

Position in the fragment	Mass	Cysteine residue	Peptide sequence	Presence in the spectrum
20-30	1269.6983	C24	VVLQCTATIHK	Yes
35-40	676.3334	C36	LCLAAE	Yes
46-50	681.3276	C47	LCFLE	No
57-70	1603.8036	C65	NVPPDLSICTFVLE	No
123-137	1821.7717	C131/132	HSYSGMYLCLLSTS	No
157-167	1356.6517	C158	ACWWTIHPASK	No
244-251	862.3975	C244	CLTVPSGE	No
356-380	2946.3978	C361	YGDSVCYIQHVDTGLWLTYQSV DVK	No
501-504	563.2606	C501	CIDR	No
547-561	1753.8326	C548	NCAQFSGSLDWLISR	No
574-580	968.5233	C577	VLHCVLVE	Yes
610-626	1956.9816	C615/18/20	VLDVLCSLCVCHGVAVR	No
627-640	1636.8224	C633	SNQHLICDNLLPGR	Yes
713-739	2956.3471	C736	WGNGNGVGDDLFSYGF DGLHLWS GCIAR	No
751-769	2155.9998	C757/8	TDDVIS CCLDL SAPSISFR	Yes
813-824	1410.6398	C822	FLPPPGYAPCYE	No

**Table 3.6** Summary of the spectral analysis of trypsin/V8 protease-digested sample with mass acquisition not restricted. *In silico* digest was performed using online PeptideMass tool available at <http://web.expasy.org>.

Due to this inability to produce a relevant set of spectral data, the mass spectrometry-based approach to identify cysteines participating in RyR2 N-terminus disulphide bond formation was not pursued further.

## 3.4 Discussion

The principal aim of the study presented in this Chapter was to identify cysteines involved in RyR2 N-terminus disulphide bond formation. Two independent techniques were used; amino acid mutagenesis and mass spectrometry-based approach. The latter was not pursued beyond the optimisation phase as the fundamental condition for this approach to work, i.e. detection of peptides containing candidate cysteine residues, was not accomplished. The failure to produce experimentally relevant peptide spectrum might be influenced by many factors. It is well established that the nature of peptide spectra depends highly on the length of peptide fragments generated and their amino acid composition (Medzihradzky *et al.* 2000). The use of different digestion conditions enables to manipulate the type of fragments generated, however, the identity of fragments appearing in the spectrum depends on a number of factors and remains very hard to predict. The low probability of some peptide fragments to be ionised combined with the relatively low quantity of protein (obtained from an eukaryotic expression system and purified by immunoprecipitation) are likely to be the main factors accounting for the inability to perform cysteine identification by means of mass spectrometry.

### 3.4.1 Cysteines involved in disulphide bond formation do not reside in the BT4L N- and C-terminus

The design of cysteine mutants was primarily based on the results of previous experiments involving truncated BT4L fragments (Table 3.1) which suggested that disulphide-mediated oligomerisation of the RyR2 N-terminus involves cysteines located in the centre of the BT4L fragment i.e. within residues 346-759. This reasoning was based on the fact that constructs lacking the first 345 and the last 147 residues (BT4BL and BT4 respectively) retained the ability to tetramerise in a DTT-sensitive manner. In agreement with this hypothesis, both mutants  $\text{BT4L}^{\text{C36S}}$  and  $\text{BT4L}^{\text{C244S}}$  serving as negative controls, were indistinguishable from the wild-type fragment, i.e. oligomerised into tetramers unless treated with DTT (Figure 3.6). Similarly both constructs with substitutions of cysteines present in the BT4 fragment

and absent in the BT4C fragment (BT4L<sup>C736S</sup> and BT4L<sup>C757/758S</sup>) retained the ability to form DTT-sensitive tetramers (Figure 3.6). This finding is in agreement with the earlier proposed interpretation of the BT4C fragment (residues 1-654) forming disulphide-mediated dimers rather than tetramers. Assuming that the hypothetical model of interaction is correct, if one of the above three cysteines (present in the BT4 fragment forming disulphide-mediated tetramers) was involved in disulphide bond formation, there should be no oligomers formed. Since mutation of those three cysteines in the BT4L fragment did not affect the ability to form DTT-sensitive tetramers, the formation of disulphide-mediated dimers by BT4C results from its severely compromised oligomerisation ability.

### 3.4.2 The elusive role of cysteine 361 in the oligomerisation process

Further investigation of cysteines within residues encompassed by the coordinates of BT4C and BT4BL fragments (346-654) did not provide a definite answer to the query. Firstly, the possibility that cysteines 548, 577 and 633 might be involved in the formation of disulphide bonds was excluded as all three mutants retained the ability to tetramerise in DTT-free samples (Figure 3.7). In contrast to the above, the data obtained from constructs containing substitutions of the remaining cysteines 361, 501, 615/618/620 was not conclusive (Figure 3.7). Generation of mutants containing a combination of serine substitution for the above cysteine residues did not resolve this issue completely. However, those results indicated that mutation of cysteine 361 has the most profound effect on the formation of DTT-sensitive tetramers (Figure 3.8).

If cysteine 361 is involved in the formation of disulphide bonds what is the identity of its partner and why did the mutants retain the ability to form tetramers? Tetramer formation, although severely compromised, is difficult to interpret in the context of our model which predicts “all or nothing” scenario. Assuming that the proposed hypothesis is correct, one possible explanation is that none of those five cysteines (i.e. 361, 501 and 615/618/620) mediates formation of disulphide bonds. Instead they participate in non-covalent inter-subunit protein-protein association either directly or

indirectly via allosteric effects. Indeed, chemical crosslinking experiments revealed that cysteine 361 affects tetramer formation even in the presence of the reducing agent DTT, which implies its role in the disulphide-independent interaction (Figure 3.9, Graph 3.1).

### 3.4.3 DTT-sensitive tetramers – alternative models of interaction

If cysteine 361 mediates self-association of the BT4L fragment into tetramers in a manner independent of disulphide bonds, then which cysteines participate in disulphide bond formation? As all the putative residues within the BT4L fragment were mutated, the list of possible other candidates is empty. This then brings another question; if one assumes that none of the cysteines within the BT4L fragment is involved in the disulphide-mediated N-terminus association, why are the oligomers sensitive to DTT-treatment? In principle, following SDS-PAGE all non-covalent interactions should be destroyed and in the absence of inter-subunit disulphide bonds one would expect the BT4L fragment to be solely in a monomeric form, which is clearly not the case. Thus, one should consider the possibility of formation of SDS-resistant oligomers, a phenomenon well documented in the literature (Rotem *et al.* 2010) and also encountered in this study on some occasions. Notably, resistance of protein oligomers to a combination of denaturants such as SDS and urea was reported by others (Bai *et al.* 2010). Nevertheless, if the retention of an oligomeric form is indeed due to SDS-resistance, one should not observe any difference between samples treated or not treated with DTT. The dependence of BT4L tetramer formation on the presence of a reducing agent clearly points out towards the involvement of disulphide bonds. One possible explanation to account for the effect of DTT is the presence of intra-subunit disulphide bonds (between cysteine residues located within the same subunit) that confers SDS-resistance by means of structural changes within the fragment allowing it to interact much more effectively within a tetramer. In fact, major alterations in protein structure as well as changes in the resistance of protein oligomers to chemical and physical protein denaturants upon formation of intra-molecular disulphide bonds have been reported by others (Grande

*et al.* 2002; Brandes et al. 2009). Moreover, in RyR1, allosteric effects of covalent modifications of N-terminal cysteines were described by Wu and colleagues (Wu et al. 1997). In this study, the authors showed that the alkylation of sulphhydryls located within the RyR1 N-terminus prevents the formation of inter-subunit disulphide bonds involving residues located in distant fragments of the protein. Thus the experimental variability observed for some of the cysteine mutants investigated in the course of this work i.e. their remaining ability to form DTT-sensitive oligomers might originate from partial SDS-resistance conferred by the presence of multiple intra-subunit disulphide bonds.

There is also an alternative scenario. Assuming a more complex model of N-terminus association, where the inter-subunit covalent interaction is mediated by multiple disulphide bonds, i.e. involving more than two cysteines per subunit, identification of putative candidates by mutagenesis becomes clearly unfeasible. This above possibility would also explain why the ability to tetramerise is retained even in mutants containing multiple cysteine substitutions.

Finally, one should consider a prominent flexibility of biological systems to compensate for missing components. In respect to this study, it would mean formation of alternative disulphide bonds between the remaining cysteine and other cysteines located close enough to replace the mutated residue. Notably, this phenomenon has been observed by others using equivalent experimental approach, i.e. mutagenesis (Zha et al. 2009). Formation of disulphide bonds is strictly dependent on the reactivity of a given cysteine and the distance between its putative partners. Most cytoplasmic thiols have  $pK_a$  values greater than 8 which make them largely non-reactive. The lower  $pK_a$  values of cysteines involved in covalent modifications are defined by their surrounding microenvironment. Thus in order for one cysteine to compensate for the other, two conditions must be fulfilled: the residue should be close enough and it should also possess unique chemical properties rendered by neighboring amino acids. Although challenging, this type of compensation has been well documented. In a study aiming to characterize a single-cysteine thioredoxin A mutant, the authors showed that substitution of a so called “attacking” cysteine with unique chemical properties resulted in its role being undertaken by a neighboring residue normally lacking those properties in the wild-type protein (Kouwen *et al.* 2008). More importantly, the new role is fulfilled by substantial conformational

changes within the protein structure. Therefore, the potential ability of other cysteines to compensate for the missing residue further complicates data interpretation obtained by mutagenesis.

### 3.4.4 Location of putative cysteine residues – feasibility of disulphide bond formation

In the course of this study, the crystal structure of the rabbit RyR1 N-terminus (residues 1-559) was published (Tung et al. 2010). This enabled to visualize the tertiary arrangement of cysteine residues conserved between RyR1 and RyR2 and assess their location in the broad context of disulphide bond formation. More importantly, the docking of the above structure into the full length of RyR1 cryo-EM map revealed potential sites of inter-subunit interaction which were of our primary interest.

RyR1 cysteine 346 which is equivalent to residue 361 in RyR2 is located at the boundary of  $\beta$ 20-21 loop and  $\beta$ -strand 21. This loop lies near an inter-subunit contact site and was suggested to be involved in the inter-subunit salt bridge. Notably, based on the docking of the crystal structure obtained for a highly similar IP<sub>3</sub>R N-terminus into the cryo-EM map of the full length channel, the  $\beta$ 20- $\beta$ 21 loop together with the  $\beta$ 8- $\beta$ 9 loop constitutes the major contact point between adjacent subunits (Seo et al. 2012).

However according to the docking, cysteine 361, which substitution appears to have the most profound effect on the formation of DTT-sensitive tetramers, is relatively far away from the suggested inter-subunit interface and is also buried by part of the  $\beta$ 20-21 loop (Figure 3.13). The above would suggest that this residue is unlikely to be accessible for any type of disulphide bond formation (intra- or inter-subunit). However three points should be noted. Firstly, according to the crystal structure, a different residue - cysteine 36 is also buried; nevertheless in the full length RyR1, it was shown to undergo oxidation to disulphides (Aracena-Parks et al. 2006). Secondly, the RyR1 N-terminal fragment whose structure was determined represents only 60% of the size of the BT4L construct. It is plausible that the presence of the

remaining residues affects conformation of the shorter fragment. This point is further supported by the fact that while the BT4L fragment exhibits ability to tetramerise, no oligomerisation was detected in case of the crystallised, shorter RyR1 fragment (Tung et al. 2010). Thirdly, since the RyR1 N-terminus shares only 71% sequence identity within the first 906 amino acids with human RyR2, one might expect isoform-specific, local differences in the tertiary arrangement. This difference is further reinforced by the fact that the corresponding RyR1 fragment contains 26 cysteines while there are only 20 cysteines in RyR2. Moreover, out of four cysteines reported to undergo redox modifications within this region in RyR1 (cysteine 36, 253, 315 and 811), only two are present in RyR2 (cysteine 36 and 811) (Aracena-Parks et al. 2006). Despite a high degree of sequence homology between cardiac and skeletal isoforms, the two substantially differ in their response to some of the physiological and pharmacological modulators. The subtle local differences in the protein structure are for example speculated to account for the inability of RyR2 to bind a skeletal muscle relaxant dantrolene in spite of its putative binding site (residues 601-620) being present in RyR2 (Paul-Pletzer et al. 2005).

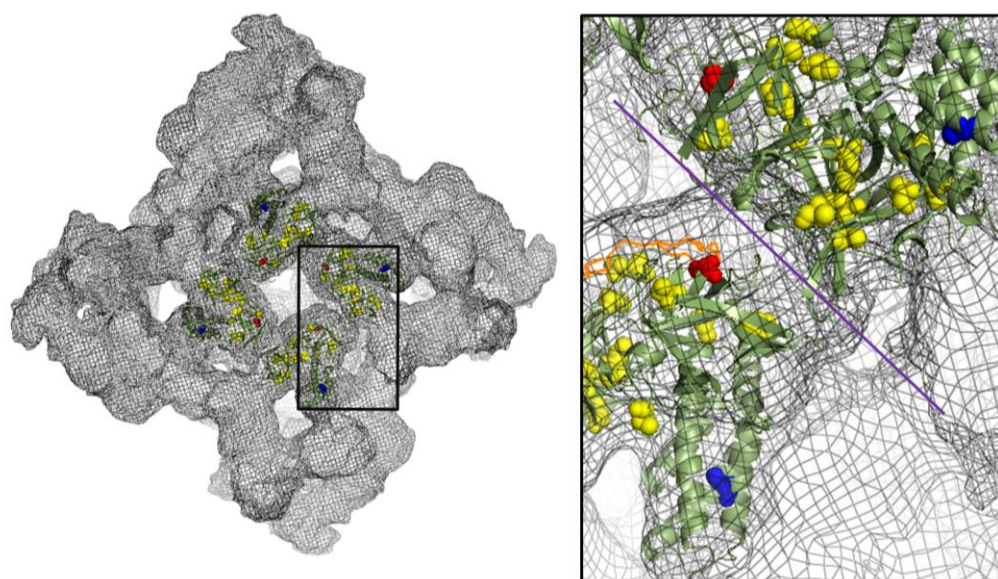


**Figure 3.13** Docking of the RyR1 N-terminus (1-559) into cryo-EM map of the full length RyR1 (Tung et al. 2010). All cysteines located in the fragment shown as yellow spheres, residues corresponding to cysteine 501 and 361 in the RyR2 in blue and red respectively, β20-21 loop in orange. Predicted subunit boundary indicated with purple line. Images created using The PyMOL Molecular Graphic Software

The publication of the N-terminus crystal structure also allowed us to visualize the location of another candidate residue – cysteine 501. As seen in Figure 3.13 cysteine 501 lies not only far away from the predicted inter-subunit boundary but is also located within an  $\alpha$ -helix which constitutes part of a five  $\alpha$ -helix bundle domain. Based on its location, cysteine 501 seems rather unlikely to be involved in the formation of disulphide bonds. The observed reduced ability of C501 mutants to form disulphide-mediated tetramers might originate from a local disturbance of the helix bundle induced by the more polar serine residue rather than its direct participation in disulphide bonds.

The location of cysteines substituted in the third mutant under investigation, i.e. BT4L<sup>C615/618/620S</sup> could not be visualized as the published crystal structure did not include those residues. The possibility of these cysteines to be involved in disulphide bond formation would be very intriguing in respect to the fact that they lie within the putative dantrolene binding site. Dantrolene has been used to treat symptoms of malignant hyperthermia, a life-threatening disorder caused by mutations in RyR1. As mentioned earlier, in spite of the presence of the dantrolene-binding sequence in RyR2, the full-length RyR2 was shown to be a very weak target for this drug. However, a growing number of reports suggest a therapeutic effect of dantrolene in cardiac disorders associated with RyR2 dysfunction such as CPVT (Kobayashi et al. 2010; Jung et al. 2012) and heart failure (Kobayashi et al. 2009; Maxwell et al. 2012). Since RyR2 defective activity is thought to be correlated with substantially increased levels of oxidative stress in heart failure, it would be intriguing to speculate that the therapeutic effect of dantrolene lies upon its ability to modulate covalent modifications of those putative cysteines. This scenario however remains to be verified. Interestingly, cysteines 615 and 618 constitute the CXXC motif, which was shown to be employed by a number of redox-sensitive proteins for formation, isomerization and reduction of disulphide bonds (Fomenko and Gladyshev 2003). The CXXC motif gives rise to a number of CxxC-derived motifs where one of the cysteines is replaced by serine or threonine (TXXC, SXXC, CXXT and CXXS). Notably, C618 is the only conserved cysteine between RyR2, RyR1, RyR3 and all three isoforms of IP<sub>3</sub>R within residues encompassing the BT4L fragment (Figure 3.14). Moreover, C615 which is conserved between ryanodine receptors is replaced

by serine in inositol trisphosphate receptors thus retaining the arrangement characteristic for CXXC-derived motifs.

RyR2	589	IKEGH <span style="color:red">HIKSIISLLDKHGRNHKVLDVILSLCVCHGVAVRSNQHLICDNLL--PGRDLLLQTRLVNHVSSMRPNIFLGVSEG</span>	666
RyR1	577	I <span style="color:red">QENHIKSIISLLDKHGRNHKVLDVILSLCVCNGVAVRSNQDLITENLL--PGRELLLQTNLINVYTSIRPNIFVGRAEG</span>	654
RyR3	576	IAE <span style="color:red">GH<span style="color:red">HIKSIISLLDKHGRNHKVLDIILCSLCCLCNGVAVRANQNLI<span style="color:red">CDNLL--PRRNLLLQTRLINDVTSIRPNIFLGVAEG</span></span></span>	653
IP3R1	610	ITAAE <span style="color:red">IDTFVSLVRKN-REPRFLDYLS<span style="color:red">DLCVSMNKSIPTQELICKAVLNPTNA<span style="color:red">DILIETKLVL<span style="color:red">SRFEF-----</span></span></span></span>	677
IP3R2	595	ITAAE <span style="color:red">IDTFVSLVRKN-REPRFLDYLS<span style="color:red">DLCVSMNKSIPTQELICKAVLNPTNA<span style="color:red">DILIETKLVL<span style="color:red">SRFEF-----</span></span></span></span>	662
IP3R3	610	IT <span style="color:red">KTEVETFVSLVRKN-REPRFLDYLS<span style="color:red">DLCVSNHIAIPVTQELICKCVLDPKNSDI<span style="color:red">LIRTEL<span style="color:red">RPVK-----</span></span></span></span>	674

**Figure 3.14** Sequence alignments of human RyR and IP<sub>3</sub>R isoforms. Multiple alignments were performed with NCBI Constraint-based Multiple Alignment Tool available online at <http://www.ncbi.nlm.nih.gov/tools/cobalt>.

### 3.4.5 Disulphide bond formation – experimental artifact?

In order to eliminate the possibility that disulphide-mediated tetramers constitute an artifact of the experimental approach undertaken in this study, additional experiments were performed using NEM (a compound which alkylates sulphhydryl groups). Cell suspension was treated with this agent prior to cell lysis to alkylate free sulphhydryl groups. Since DTT-sensitive oligomers were also observed in samples treated with NEM (Figure 3.15), the observed disulphide-linked tetramers are unlikely to result from air oxidation during sample processing.

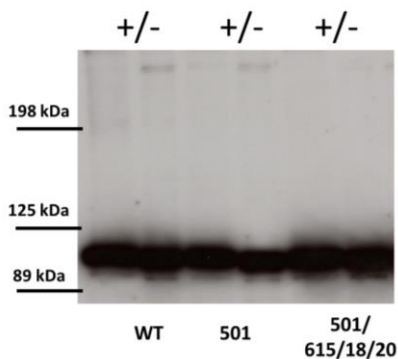


**Figure 3.15** Representative blots of cysteine mutants. Cell pellets were suspended in the homogenisation buffer containing 50 mM NEM and processed as described earlier; +/- DTT-treated and untreated samples respectively

In addition, the above experiment revealed one exceptionally relevant detail, i.e. there was an apparent difference in the electrophoretic mobility of bands corresponding to monomers between samples treated and not treated with DTT with the latter migrating faster (Figure 3.16). Cysteine alkylation of the BT4L fragment with NEM would be expected to increase the electrophoretic mobility of the fragment of around 0.12 kDa per bound molecule; assuming alkylation of all cysteines that would give a difference of around 2.4 kDa, an effect on the border of detection on a 6% gel. As DTT was added after NEM treatment, it not only reduced disulphide bonds but also reacted with NEM, minimizing the possibility of NEM being able to alkylate freshly DTT-reduced thiols. Thus, the increased mobility of a non-reduced monomer would originate solely from the intra-monomer disulphide bond or bonds which make protein conformation more compact and allow it to migrate faster. However if this was the case, the difference in the mobility between DTT treated and non-treated samples would be detectable without treatment with NEM. Since this is not the case, one might speculate that DTT treatment reduces internal disulphide bonds which are further alkylated by NEM. This is possible because NEM is present in substantial molar excess (50 mM versus 10 mM DTT). In the above scenario, the reduction of disulphide bonds would lead to changes in the protein structure making previously buried thiols exposed and therefore able to react with NEM, further increasing an apparent molecular weight of the BT4L fragment in reducing conditions. Thus, the observed increased mobility of a non-reduced monomer would originate from two additive factors; the intra-monomer disulphide bond or bonds which make protein conformation more compact and the labeling of a limited number of cysteines which are accessible in a non-reduced conformation. Notably, dramatic changes in the reactivity of protein thiols with NEM associated with alterations in protein structure has been reported by others (Bednar 1990). The explanation presented above would support the notion that there is at least one internal disulphide bond within the BT4L fragment. However, in order to confirm this hypothesis further experiment involving high-resolution SDS-PAGE and thiol-specific labeling using compounds of higher molecular weight than NEM would be required.

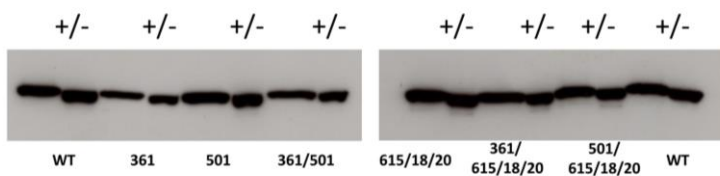


**Figure 3.16** Representative blots of cysteine mutants showing differences in the electrophoretic mobility of NEM-alkylated monomers revealed upon treatment with DTT; +/- DTT-treated and untreated samples respectively

### 3.4.6 Concluding remarks

While the identity of cysteines involved in the formation of DTT-sensitive tetramers was not conclusively determined, the results obtained in this study strongly suggest that disulphide bond formation within the RyR2 N-terminus is a physiologically relevant phenomenon. The fact that the BT4L fragment retains the ability to oligomerise upon DTT-treatment suggests that those bonds are not essential for N-terminus self-interaction. Consequently, this implies that oxidation to disulphides might constitute a regulatory mechanism. Indeed, covalent modifications of cysteines have been reported to control not only physiological aspects of muscle performance (Wang et al. 2010; Sun et al. 2011) but have been also implicated in the pathogenesis of RyR-associated disorders (Terentyev et al. 2008a; Belevych et al. 2009; Cutler et al. 2012).

The cumulative data obtained in this study call for the proposed model of interaction to be reconsidered. It is rather unlikely that DTT-sensitive oligomers originate from a single disulphide bond across subunits. The amended model of N-terminus association proposes the involvement of multiple cysteines in the formation of intra and/or inter-subunit disulphide bonds.

# Chapter 4

## Determinants of RyR2 N-terminus tetramerisation

## 4 Determinants of RyR2 N-terminus tetramerisation

### 4.1 Introduction

Based on the tetramerisation pattern of truncated BT4L fragments (unpublished findings, Table 4.1.) the core of the N-terminus association was proposed to lie in the centre of the fragment with both N-terminal and C-terminal residues contributing to the overall oligomer stability. Those studies provided general insights into N-terminus self-association process; however detailed information regarding the location of residues essential for tetramerisation was missing. Moreover, further truncation of the BT4L fragment led to the complete loss of the oligomerisation ability (Table 4.1) suggesting that fragments containing less than 50% of the original BT4L sequence are most likely inappropriately folded. Thus the principal goal of this study was to identify sites of the inter-subunit contact using an alternative approach.

Construct	Coordinates in RyR2	No of residues	Oligomer formation
BT4L	1-906	906	tetramer (strong)
BT4	1-759	759	tetramer (moderate)
BT4C	1-654	654	dimer/trimer/tetramers (minor species)
BT4BL	346-906	560	tetramer (moderate/weak)
BT4DL	161-906	745	tetramer (moderate/strong)
BT4A2	1-418	418	no
BT4B	346-759	413	no
BT4EL	565-906	341	no

**Table 4.1** Summary of chemical crosslinking of truncated BT4L fragments expressed in HEK293 cells.

The experimental design undertaken in this study aimed to focus on relatively short stretches of residues exhibiting the potential to be involved in protein-protein

interactions. Computational methods used for identification of such interfaces have evolved rapidly in recent years. Those approaches are mostly structure-dependent and therefore rely heavily on the existence of protein tertiary information. The structure-independent methods which are based on factors such as conservation of gene context and phylogenetic tree analysis are used to discover novel interactions between different gene products and therefore are not applicable to the experimental goal of this study (Szilágyi *et al.* 2005). The concept that a protein primary sequence alone can be used to predict protein-protein interaction interfaces remains somewhat controversial. A primary sequence is however sufficient to predict a local secondary structure which was shown to exhibit unique distribution at sites of protein-protein association. The detailed structural analysis of protein interfaces involved in homo-versus hetero-oligomerisation revealed for example that regular secondary structures as opposed to non-regular structures prevail in the former (Guharoy and Chakrabarti 2007). Nevertheless, application of those findings to the experimental approach undertaken in this study would in fact require the knowledge of the N-terminus tertiary structure to establish which of the putative secondary elements are located on the protein surface and thus remain physically accessible for the interaction to take place.

In the absence of such information at that time, the experiments were rationalised on the findings of the formerly conducted crosslinking experiments. As a result, the attention was drawn to the region located between residues 654 and 759. The substantial difference in the oligomerisation patterns between fragments BT4 and BT4C (Table 4.1) implied that at least some part of the sequence absent in the BT4C construct (residues 655-759) must be involved in the oligomerisation process. While the BT4 fragment (1-759) displays a slightly reduced ability to form tetramers when compared to the BT4L fragment, chemical crosslinking of the BT4C (1-654) fragment resulted in all types of oligomers including dimers, trimers and tetramers. Structure-based sequence analysis with the NCBI Conserved Domain Search Tool (<http://www.ncbi.nlm.nih.gov/Structure/cdd/>) revealed that this RyR2 sequence contains a SPRY domain which aligns with the human pyrin SPRY domain (Figure 4.1).

		β-strand 1	β-strand 2		β-strand 3	β-strand 4	
pyrin	65	. [2]. RRYNQYVVGDKTA	WILGACKTSI. [ 3]. GNMTLSP	EN	GKVVVIM[1,1]NEIQSS	118	
BT4L	670	. [2]. KWYYELMVDHTEP. [8]. LRVGWASTEG. [ 2]. PYPGGGE. [8]. DD. [1]. FSYGFDSL			HLWSGCI	737	
		β-strand 5	β-strand 6	β-strand 7	β-strand 8	β-strand 9	
pyrin	119	. [1]. PPRLLIK	E. [1]. PKRQGIFVFDY. [3]. RISTNVTAR. [ 5]. TASCASF. [2]. PGPITFP. [6]. K	180			
BT4L	738	. [1]. RTVSSPNQ. [4]. T	DDVISCCLDL. [3]. SISFRINGQP. [ 4]. FENFNI. [2]. LFFPVVSF. [2]. G	797			
		β-strand 10					
pyrin	181	NTAP[ TICCPVG 191					
BT4L	798	IKVRFLLGGRH 808					

**Figure 4.1** Structure-based sequence alignment of the human pyrin SPRY domain with the BT4L sequence using the Conserved Domain Tool; red font indicates high degree of conservation, blue indicates less conserved residues, unaligned residues in grey, β-strands highlighted in grey (based on (Weinert *et al.* 2009)).

SPRY domains generally function as protein-protein interaction motifs (Perfetto *et al.* 2013). In ryanodine receptors SPRY domains are present in three copies; however their exact role remains unknown. Structurally they are composed of two antiparallel β-sheets with β-strands connected by unstructured or α-helical linkers. In the case of pyrin the SPRY domain contains two five-stranded β-sheets in a sandwich like arrangement (Weinert *et al.* 2009) (Figure 4.2).



		β-strand 5	β-strand 6	β-strand 7	β-strand 8	β-strand 9	
pyrin	119	. [1]. PPRLLIK	E. [1]. PKRQGIFVFDY. [3]. RISTNVTAR. [ 5]. TASCASF. [2]. PGPITFP. [6]. K	180			
BT4L	738	. [1]. RTVSSPNQ. [4]. T	DDVISCCLDL. [3]. SISFRINGQP. [ 4]. FENFNI. [2]. LFFPVVSF. [2]. G	797			
BT4	738	[1]. RTVSSPNQ. [4]. T	DDVISCCCL				

**Figure 4.2** Crystal structure of pyrin SPRY domain (PDB ID: 2WL1\_A); Residues corresponding to the amino acids present in the BT4L but absent in the BT4 fragment in light grey (upper panel, image created using The PyMOL Molecular Graphic Software). Sequence alignment of BT4L and BT4 fragments with the part of the human pyrin SPRY domain (lower panel); dark grey boxes indicate β-strands

The BT4C fragment, which forms dimers, trimers and tetramers, lacks the whole SPRY domain. However, the absence of this domain *per se* cannot fully account for the observed BT4C behavior as the BT4 fragment also lacks a substantial part of SPRY domain; i.e. three full  $\beta$ -strands from one  $\beta$ -sheet and one strand from another  $\beta$ -sheet (Figure 4.2), while its tetramerisation ability is only slightly compromised as compared to the BT4L fragment. The extent of missing residues in the above fragment would be predicted to cause a serious misfolding of the domain as a whole. Hence, it was speculated that the presence of an intact SPRY domain is not essential for the process of oligomerisation; however some parts of this domain are likely to mediate N-terminus self-association. In order to identify those determinants,  $\beta$ -strand 6 and part of the preceding loop were removed. The above approach resulted in the generation of the BT4 $\Delta$ 12 construct, which lacks 12 amino acids from the BT4 C-terminus (Figure 4.3). The BT4 $\Delta$ 12 fragment was expressed in HEK293 cells, which lack endogenous RyR2 expression, and its ability to oligomerise was assessed by chemical crosslinking. The obtained results prompted us to investigate the role of the SPRY  $\beta$ 5- $\beta$ 6 loop in the context of the larger BT4L fragment. This approach was undertaken by generating an internal deletion mutant BT4L<sup>SPRY $\beta$ 5- $\beta$ 6loop</sup> which lacks 5 residues within the  $\beta$ 5- $\beta$ 6 loop of the SPRY domain (Figure 4.3)

	$\beta$ -strand 5	$\beta$ -strand 6
<b>Pyrin</b>	120 PPTRLLIK	E (P) PKRVGIFV 137
<b>BT4</b>	739 RTVSSPNQ (HLLR) T	DDVISCCCL 759
<b>BT4<math>\Delta</math>12</b>	739 RTVSSPNQ (H) 747	
<b>BT4L<sup>SPRY<math>\beta</math>5-<math>\beta</math>6loop</sup></b>	739 RTVSSPNQ (H---) -	-DVISCCCLSAP.....906

**Figure 4.3** Coordinates of the BT4 $\Delta$ 12 and BT4L<sup>SPRY $\beta$ 5- $\beta$ 6loop</sup> constructs in respect to the pyrin sequence. Grey boxes indicate  $\beta$ -strands 5 and 6, dashed lines indicate deleted residues.

In the course of our experiments, the crystal structure of the RyR1 N-terminus was published (Tung et al. 2010). This was followed by a deposition of the IP<sub>3</sub>R1 N-terminus structure, which revealed that both N-termini display nearly identical conformation, i.e. the three structural domains of IP<sub>3</sub>R1 can be individually superimposed on the corresponding domains in the RyR1. Those domains were also

shown to exhibit nearly identical relative orientation with similar domain interfaces (Seo et al. 2012). More importantly, docking of both structures into the cryo-EM maps of the corresponding full length proteins revealed a comparable arrangement of N-termini around the four-fold symmetry axis and exposed the putative sites of inter-subunit interactions. For the RyR1, those sites included flexible loops connecting  $\beta$ -strand 13 and 14,  $\beta$ -strand 22 and 23 and a part of loop connecting  $\beta$ -strand 8 and 9. In addition, the docking showed the putative inter-subunit pairing of two oppositely charged residues located within the loop connecting  $\beta$ -strand 20 and 21 (Figure 4.4). Interestingly, the docking of the IP<sub>3</sub>R1 N-terminus in the cryo-EM map of the full length receptor revealed only two prospective sites of the inter-subunit contact; loop  $\beta$ 8- $\beta$ 9 and  $\beta$ 20- $\beta$ 21.

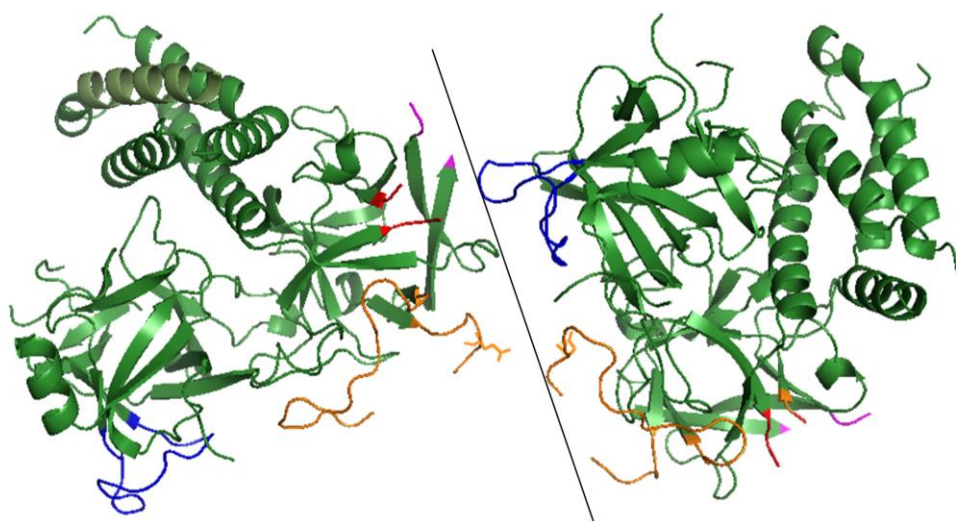


**Figure 4.4** Relative orientation of the RyR1 N-terminus docked into two subunits of the cryo-EM map of the full length receptor; line indicates predicted subunit boundary, loop  $\beta$ 8- $\beta$ 9 in blue, loop  $\beta$ 20- $\beta$ 21 in orange with two putative residues involved in a salt bridge shown as orange lines, beginning and the end of the loop  $\beta$ 13- $\beta$ 14 and  $\beta$ 22- $\beta$ 23 in red and pink respectively, large parts of both loops missing indicating high flexibility of those fragments

In order to explore the contribution of these putative loops in the process of N-terminus self-association, a series of internal BT4L deletion mutants was generated. Constructs were expressed in HEK293 cells and tested for their oligomerisation properties by chemical crosslinking. The size of the deletion in each loop was

dictated by the relative distance of the preceding and the following  $\beta$ -strands. The preservation of the three dimensional structure was imperative to evaluate the direct role of each loop in the inter-subunit interaction. Hence, only a subset of amino acids was removed from each loop assuring that a sufficient number of residues was available to bridge the gap between the two  $\beta$ -strands without imposing any structural constraints. Due to the above, it was not feasible to introduce a significant deletion in the loop  $\beta$ 13-14 which is only four residues long. The list of the generated deletion mutants with detailed information concerning the sequence and coordinates of the removed residues is presented in Table 4.2. The location of secondary structure elements and loops in the primary sequence of RyR2 is presented in Figure 4.5. A summary diagram showing positions of all deletions tested is presented in Figure 4.6.

Deletion mutant	Removed sequence	Deletion coordinates	Predicted MW (kDa) for a monomer
BT4L $^{\beta 8-\beta 9}$ loop	KQRSEGEKVRVG	167-178	100
BT4L $^{\beta 20-\beta 21}$ loop	KEKLDVGVRKEVDGGMGTSEIKYGD	335-358	99
BT4L $^{\beta 22-\beta 23}$ loop	SVRMG	381-385	101
BT4L $^{SPRY\beta 5-\beta 6}$ loop	LLRTD	748-752	101

**Table 4.2** List of generated deletion mutants showing the coordinates and primary sequence of removed fragments



**Figure 4.5** Location of secondary structure elements in the primary sequence of RyR2;  $\beta$ -strands in grey,  $\alpha$ -helices in red (based on the RyR1 N-terminus crystal structure (Tung et al. 2010) and shown for residues encompassing strands  $\beta$ 1- $\beta$ 23)

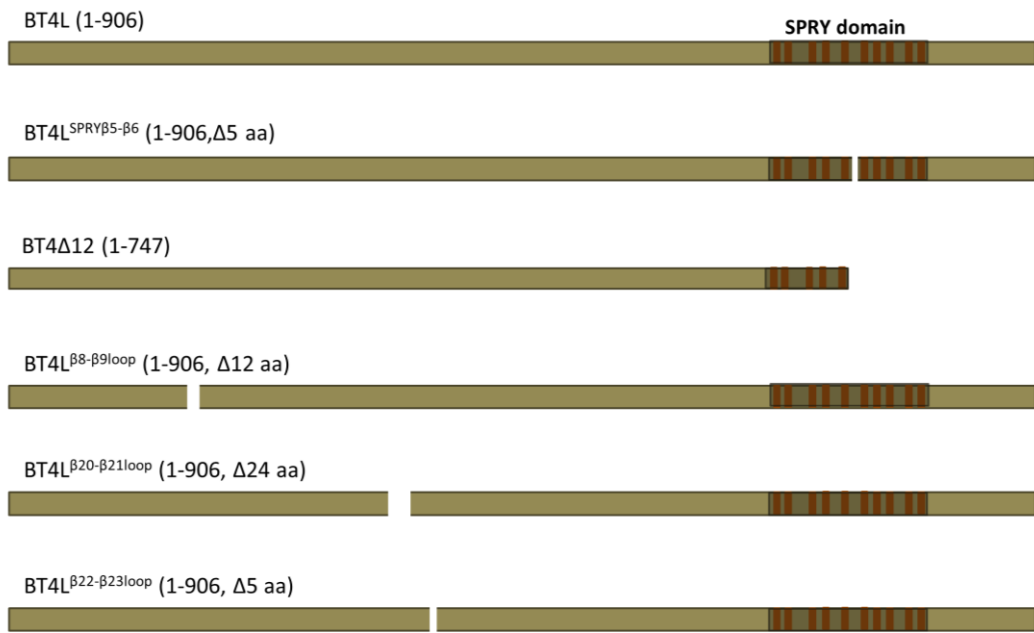


**Figure 4.6** Graphical summary of the BT4L deletion fragments tested

## 4.2 Methods

### 4.2.1 Generation of the truncated BT4Δ12 construct

The BT4Δ12 construct was generated by cloning a specific DNA fragment obtained in a standard PCR reaction (Section 2.2.1.1) into the BT4L plasmid. The PCR reaction was performed in the presence of forward and reverse primers (V8.1531-48 and SPREV.2343-62 respectively; Table 2.2) and the BT4L plasmid as a template. The PCR product (1 kb) contained a new *Sal*I restriction site at the 3' end introduced by the reverse primer. The new DNA fragment (PCR product) and the destination plasmid were digested with *Bsp*EI and *Sal*I restriction enzymes, separated by agarose gel electrophoresis and subjected to ligation following gel extraction of the fragments of interest (described in detail in Section 2.2.1.3, 2.2.1.4 and 2.2.1.5). Subsequently, the ligation reaction was used to transform bacteria by means of electroporation (Section 2.2.1.8). Obtained colonies were screened as described in Section 2.2.1.10.

The positive clone was sequenced further to cover the length of the whole subcloned DNA fragment and once the sequence was verified, large volume overnight bacterial culture was set up for plasmid isolation as described in Section 2.2.1.10.

#### 4.2.2 Generation of internal deletion mutants

Deletions were introduced into the BT4L construct as described in Section 2.2.1.7. The removal of relevant residues was verified by DNA sequencing. DNA fragments containing the desired deletions were subcloned into the wild type BT4L construct following the approach described for cysteine mutants in Section 3.2.1. Detailed information concerning restriction enzymes used in the subcloning of DNA fragments can be found in Table 4.3.

Construct	Restriction endonucleases	Double (D) or sequential (S) digest	Coordinates of the subcloned fragment (bp)
BT4L <sup>β8-β9loop</sup>	<i>Hin</i> DIII	n/a	Upstream of the start codon - 1818
BT4L <sup>β20-β21loop</sup>	<i>Pml</i> II, <i>Bsp</i> EI	S	727 - 1377
BT4L <sup>β22-β23loop</sup>	<i>Pml</i> II, <i>Sal</i> II	S	727 – downstream of the last residue of the BT4L fragment (2839)
BT4L <sup>SPRYβ5-β6</sup>	<i>Bsp</i> EI, <i>Sal</i> II	D	1377- downstream 2839

**Table 4.3** List of restriction endonucleases used in subcloning. Coordinates correspond to the human RyR2 mRNA, accession number: X98330

#### 4.2.3 Chemical crosslinking

Obtained plasmids were used to transfect HEK293 cells growing on 100 mm Petri dishes as described in Section 2.2.5.2. Each experiment was performed with a concomitant transfection of cells with the wild-type BT4L plasmid serving as a positive control. Cell pellets obtained 24 hours after transfection were homogenised (Section 2.2.2.1) and one aliquot was treated with DTT (4 °C, 1 h, 10 mM). Total

protein concentration was evaluated using BCA colorimetric assay and depending on the experiment 20-50 µg of total protein was subjected to glutaraldehyde crosslinking in a time-dependent manner (Section 2.2.2.2). Proteins were separated by SDS-PAGE and subsequently blotted onto PVDF membranes (for details please refer to Section 2.2.2.3.and 2.2.2.4). The c-Myc antibody and anti-mouse HRP-conjugated Ab were used to detect protein presence (Table 2.1). Tetramer to monomer ratio was determined by performing densitometry analysis using BioRad Quantity One software. Percentage of tetramer was calculated as follows %T=OD<sub>T</sub>/(OD<sub>T</sub>+OD<sub>M</sub>)x100 where OD<sub>T</sub> and OD<sub>M</sub> corresponds to optical density obtained within one time point for tetramer and monomer bands respectively. Statistical analysis was carried out using paired, 2-tailed Student's *t* test to test mean of difference in tetramer formation between fragments containing internal deletion and wild-type BT4L within each time-point studied.

#### 4.2.4 Co-immunoprecipitation

Co-immunoprecipitation assays were performed to confirm our findings from chemical crosslinking experiments. To assess the interaction between the wild-type BT4L and the fragment containing the β8-β9 loop deletion HEK293 cells were co-transfected with two constructs: the BT4L<sup>β8-β9loop</sup> (c-Myc-tagged) and the AD4L construct (HA-tagged BT4L fragment). In parallel experiments, AD4L was co-expressed with the wild-type BT4L which served as positive control. Co-immunoprecipitation was performed as described in Section 2.2.2.6. Polyclonal HA antibody (Table 2.1) and protein A Sepharose beads were used to immunoprecipitate the AD4L fragment. The c-Myc Ab was used in Western blot to detect the presence of co-precipitated BT4L proteins.

The level of co-precipitated BT4L proteins was determined by densitometry. In order to correct for the differences in the expression level between BT4L<sup>WT</sup> and BT4L<sup>β8-β9loop</sup> (protein input), the optical density values obtained for the co-immunoprecipitated, specifically bound protein were normalised against the amount of the input protein in the lysate. The average amount of protein in the lysate was calculated as follows: (OD<sub>1</sub>\*50 + OD<sub>2</sub>\*200)/2, where OD<sub>1</sub> and OD<sub>2</sub> represent optical

density obtained for bands corresponding to the 1/50<sup>th</sup> and 1/200<sup>th</sup> of the lysate volume processed in the co-immunoprecipitation respectively. In cases where some extent of non-specific binding occurred, the values obtained for specific binding were corrected accordingly. Statistical analysis was carried out using paired, 2-tailed Student's *t* test to test mean of difference in the amount of co-precipitated protein between BT4L<sup>WT</sup> and BT4L <sup>$\beta$ 8- $\beta$ 9loop</sup>.

### 4.3 Results

All deletion constructs (i.e. BT4L<sup>SPRY $\beta$ 5- $\beta$ 6loop</sup>, BT4L <sup>$\beta$ 8- $\beta$ 9loop</sup>, BT4L <sup>$\beta$ 20- $\beta$ 21loop</sup>, BT4L <sup>$\beta$ 22- $\beta$ 23loop</sup>) and the truncated version of the BT4 fragment (i.e. BT4Δ12) were successfully generated and their DNA sequence was confirmed. A typical set of results representing intermediate steps of construct generation are shown in Figure 4.7.

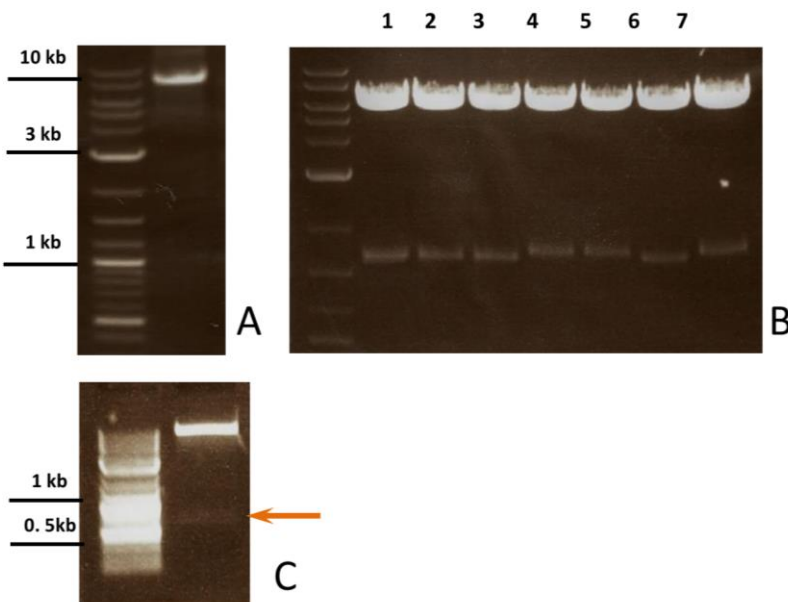


**Figure 4.7** Intermediate steps of the experimental procedure generating the BT4L <sup>$\beta$ 20- $\beta$ 21loop</sup> construct; A: DNA agarose gel showing the amplification product obtained in the PCR with deletion-introducing primers, B: indicative digest of clones following bacteria transformation with the PCR product treated with T7 Gene 6 Exonuclease (1-7: plasmid DNA obtained from seven clones and cut with *Hind*III); faster mobility of some of the lower bands indicates putative clones containing the deletion, C: restriction digest (*Pml*I/*Bsp*EI) of the positive clone verified by sequencing, the lower band (~0.6 kb, indicated by an orange arrow) corresponding to the fragment containing the 72 bp deletion was cut out of the gel and subcloned into the full length BT4L

#### 4.3.1 The BT4Δ12 displays a unique oligomerisation pattern

Chemical crosslinking of the BT4Δ12 construct (residues 1-747) revealed a distinctively different oligomerisation pattern as compared to the BT4L and the BT4 fragments. While the BT4L fragment associates into tetramers in a time dependent manner with minimal amount of dimers appearing only towards longer crosslinking time-points (analogous behaviour is exhibited by BT4, however the amount of tetramer formed is slightly lower), the BT4Δ12 construct created mostly dimers and tetramers with a minor contribution of trimers (Figure 4.8). In the absence of DTT, the predominant oligomeric species present at the beginning of chemical crosslinking was a dimer as reflected by the presence of ~164 kDa band. As the reaction proceeded in time, the amount of dimer gradually decreased with the concomitant increase in tetramer formation (~330 kDa) which became a major oligomeric form present at the 60 min time-point. In some instances a faint band corresponding to a trimer was also evident (~246 kDa). Interestingly, in reducing conditions (10 mM DTT) BT4Δ12 formed mostly trimers and tetramers. Due to the presence of intermediate oligomeric species (i.e. dimers and trimers), densitometry-based analysis of tetramer to monomer ratio was not performed.

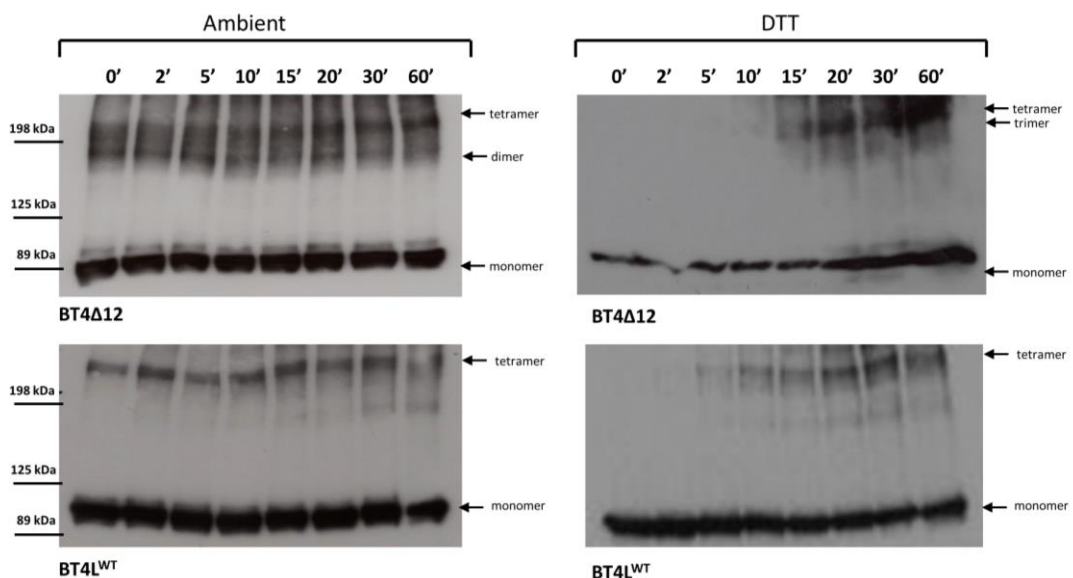


**Figure 4.8** Representative blots of chemical crosslinking experiments illustrating time-dependent oligomer formation of BT4Δ12 and BT4L<sup>WT</sup> fragments in the presence and absence of DTT (right and left panel respectively). Time-points in minutes as indicated. Oligomeric species depicted by arrows

#### 4.3.2 Deletion of the SPRY $\beta$ 5- $\beta$ 6 loop has no effect on the tetramerisation process

The BT4 $\Delta$ 12 construct (1-747) oligomerised in a manner highly similar to the considerably shorter BT4C fragment (residues 1-654). It also behaved substantially different from the BT4 fragment (1-759) which is only 12 residues longer. These findings triggered further investigation into the role of the residues missing in the BT4 $\Delta$ 12 construct. Based on the alignment with the human pyrin SPRY domain, this short stretch of residues contains the  $\beta$ -strand 6 and part of the loop connecting  $\beta$ -strands 5 and 6. It has been suggested that SPRY domains bind to their targets through a canonical interface formed by variable loops (James *et al.* 2007). Consequently, in order to evaluate the role of the  $\beta$ 5- $\beta$ 6 loop in BT4L oligomerisation process, a new construct, i.e. BT4L<sup>SPRY $\beta$ 5- $\beta$ 6loop</sup> was generated. Chemical crosslinking of BT4L<sup>SPRY $\beta$ 5- $\beta$ 6loop</sup> did not however reveal any major differences in its oligomerisation properties as compared to the full length construct (Figure 4.9). Similarly to BT4L<sup>WT</sup>, BT4L<sup>SPRY $\beta$ 5- $\beta$ 6loop</sup> formed tetramers in both reducing and non-reducing conditions.

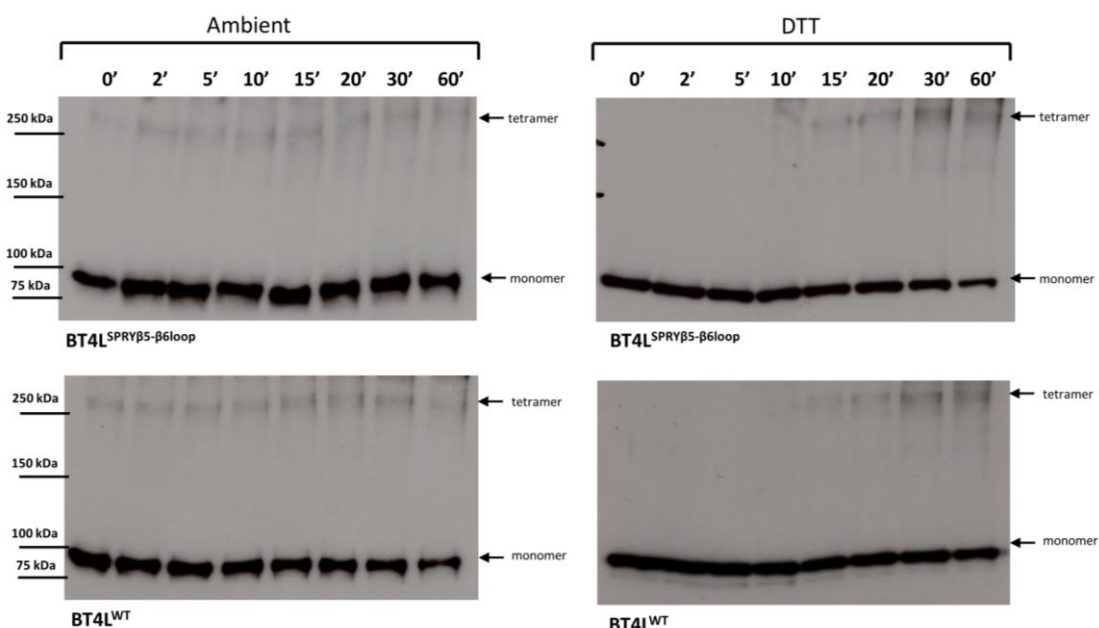
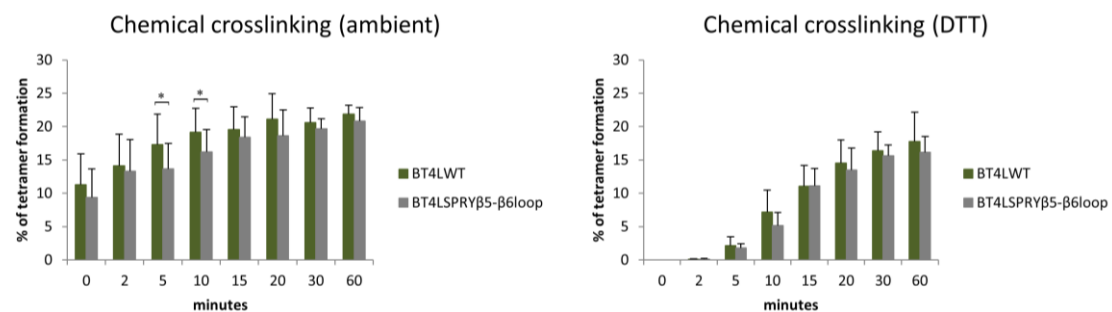


**Figure 4.9** Representative blots of chemical crosslinking experiments illustrating time-dependent tetramer formation of BT4L<sup>SPRY $\beta$ 5- $\beta$ 6loop</sup> and BT4L<sup>WT</sup> fragments in the presence and absence of DTT (right and left panel respectively). Time-points in minutes as indicated. Tetramer and monomer depicted by arrows

$\text{BT4L}^{\text{SPRY}\beta 5\text{-}\beta 6\text{loop}}$  tetramerisation propensity was determined by densitometry. As chemical crosslinking was carried out concomitantly on the  $\text{BT4L}^{\text{WT}}$  fragment,  $\text{BT4L}^{\text{SPRY}\beta 5\text{-}\beta 6\text{loop}}$  tetramer formation was assessed relative to its full-length counterpart, i.e. we tested the mean of difference between the levels of tetramer formed by both fragments for every time-point studied. Cumulative data are presented in Graph 4.1. In ambient conditions, the  $\text{BT4L}^{\text{SPRY}\beta 5\text{-}\beta 6\text{loop}}$  deletion mutant displays slightly reduced tetramerisation ability with statistically significant results obtained for only two time-points. Similarly, in reducing conditions the new construct exhibits a minor and statistically insignificant reduction in the propensity to form tetramers.



**Graph 4.1** Densitometry analysis of  $\text{BT4L}^{\text{WT}}$  and  $\text{BT4L}^{\text{SPRY}\beta 5\text{-}\beta 6\text{loop}}$  tetramer formation in chemical crosslinking assay at ambient and reducing conditions. Percentage of tetramer calculated as described in Section 4.2.3. Data are shown as mean +/-SEM, n=6; \* statistical significance at  $p<0.05$  calculated using paired, 2-tailed Student's  $t$  test

#### 4.3.3 Deletion of the $\beta 22\text{-}\beta 23$ loop has no effect on the tetramerisation process

The partial deletion of the  $\beta 22\text{-}\beta 23$  loop did not change  $\text{BT4L}$  oligomerisation pattern, i.e. the  $\text{BT4L}^{\beta 22\text{-}\beta 23\text{loop}}$  deletion mutant formed tetramers similar to the full-length construct as evident by the presence of ~400 kDa band in Figure 4.10. Those observations were confirmed by densitometry analysis of cumulative data (Graph 4.2).

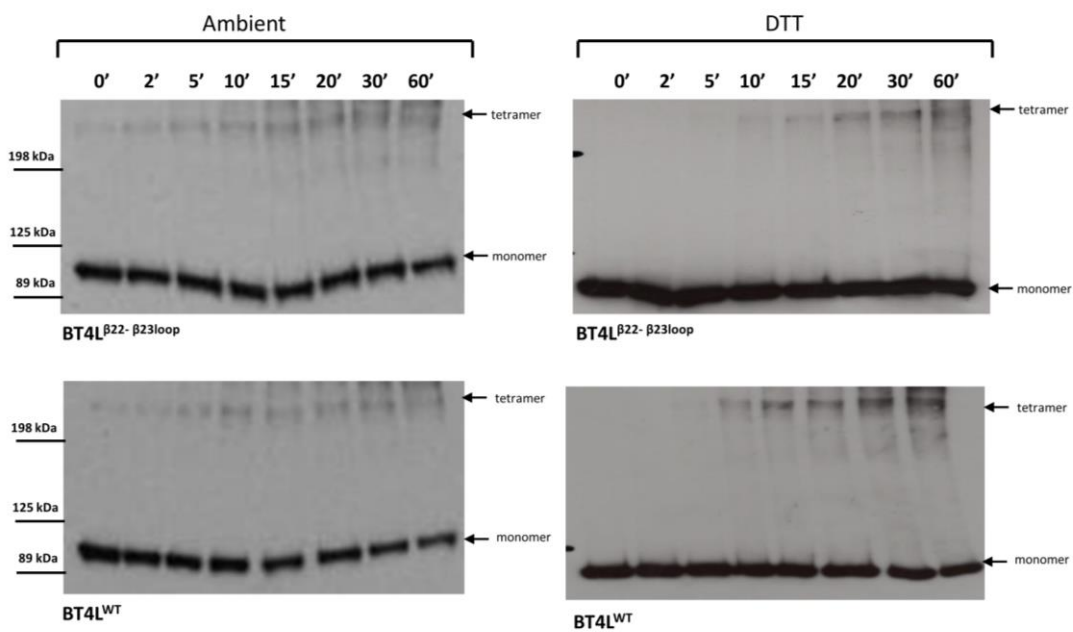
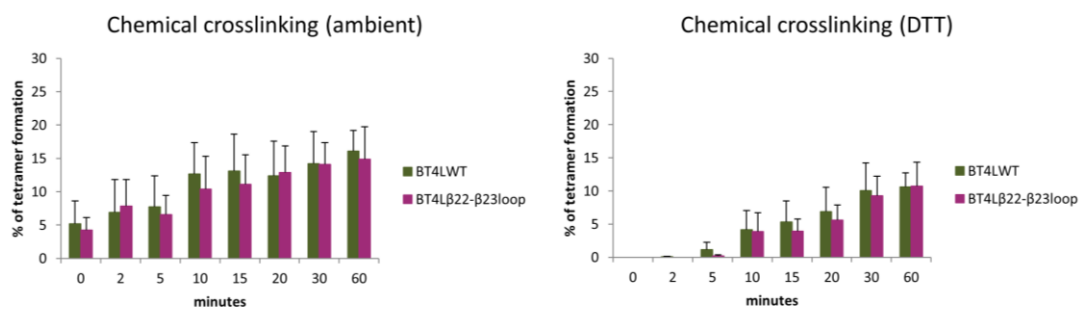


**Figure 4.10** Representative blots of chemical crosslinking experiments illustrating time-dependent tetramer formation of  $\text{BT4L}^{\beta 22-\beta 23\text{loop}}$  and  $\text{BT4L}^{\text{WT}}$  fragments in the presence and absence of DTT (right and left panel respectively). Time-points in minutes as indicated. Tetramer and monomer depicted by arrows



**Graph 4.2** Densitometry analysis of  $\text{BT4L}^{\text{WT}}$  and  $\text{BT4L}^{\beta 22-\beta 23\text{loop}}$  tetramer formation in chemical crosslinking assay at ambient and reducing conditions. Percentage of tetramer calculated as described in Section 4.2.3. Data are shown as mean +/- SEM, n=5 and n=8 for ambient and reducing conditions respectively

#### 4.3.4 Deletion of the $\beta$ 8- $\beta$ 9 loop impairs oligomerisation

The partial removal of the  $\beta$ 8- $\beta$ 9 loop in the BT4L fragment severely impaired its ability to self-associate into tetramers both in ambient and reducing conditions as assessed by chemical crosslinking (Figure 4.11).

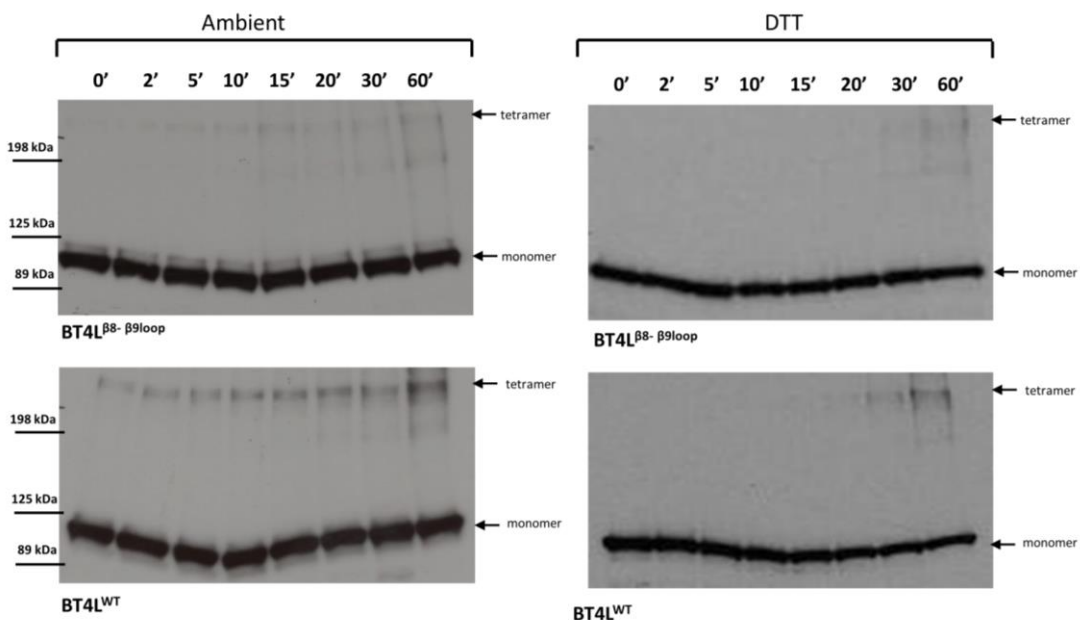
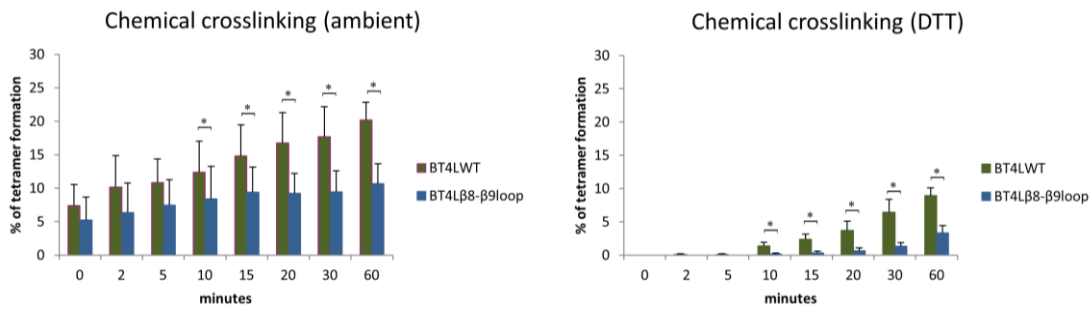


**Figure 4.11** Representative blots of chemical crosslinking experiments illustrating time-dependent tetramer formation of BT4L<sup>β8-β9loop</sup> and BT4L<sup>WT</sup> fragments in the presence and absence of DTT (right and left panel respectively). Time-points in minutes as indicated. Tetramer and monomer depicted by arrows

The results of densitometry analysis are presented in Graph 4.3. In ambient conditions, the amount of tetramer formed by the BT4L<sup>β8-β9loop</sup> deletion mutants compared to the BT4L<sup>WT</sup> fragment was reduced by 30% prior to glutaraldehyde addition (0 time-point). The difference in the ability to tetramerise significantly increased as crosslinking progressed in time. The reduced tetramer formation of BT4L<sup>β8-β9loop</sup> was even more evident in reducing conditions.



**Graph 4.3** Densitometry analysis of  $\text{BT4L}^{\text{WT}}$  and  $\text{BT4L}^{\beta 8\text{-}\beta 9\text{loop}}$  tetramer formation in chemical crosslinking assay at ambient and reducing conditions. Percentage of tetramer calculated as described in Section 4.2.3. Data are shown as mean +/- SEM, n=7 and n=6 for ambient and reducing conditions respectively; \* indicates statistical significance at  $p<0.05$  calculated using paired, 2-tailed Student's *t* test

As assessed by chemical crosslinking,  $\text{BT4L}^{\beta 8\text{-}\beta 9\text{loop}}$  exhibited severely compromised ability to self-associate into tetramers. The effect of the  $\beta 8\text{-}\beta 9$  deletion was further investigated in the co-immunoprecipitation assay. The aim was to determine whether the deletion of the  $\beta 8\text{-}\beta 9$  loop impairs the formation of mixed oligomers, i.e. composed of both fragments:  $\text{BT4L}^{\beta 8\text{-}\beta 9\text{loop}}$  and  $\text{BT4L}^{\text{WT}}$ . As described in Section 4.2.4, the AD4L fragment (HA-tagged BT4L) co-expressed with either  $\text{BT4L}^{\beta 8\text{-}\beta 9\text{loop}}$  or  $\text{BT4L}^{\text{WT}}$  was immunoprecipitated using HA Ab and the presence of co-precipitated BT4L proteins was analysed by immunoblotting with c-Myc Ab. As seen in Figure 4.12, the amount of recovered protein is substantially lower for the  $\text{BT4L}^{\beta 8\text{-}\beta 9\text{loop}}$  fragment than for its full-length counterpart while the expression of two constructs is at comparable levels (lane 1 and 2 depicted as lysate in Figure 4.12). Cumulative results were further quantitatively evaluated by densitometry as described in Section 4.2.4. This analysis revealed that the deletion of the  $\beta 8\text{-}\beta 9$  loop results in 45% reduction in the formation of mixed oligomers, i.e. in the interaction between  $\text{BT4L}^{\beta 8\text{-}\beta 9\text{loop}}$  and  $\text{BT4L}^{\text{WT}}$  (Graph 4.4).

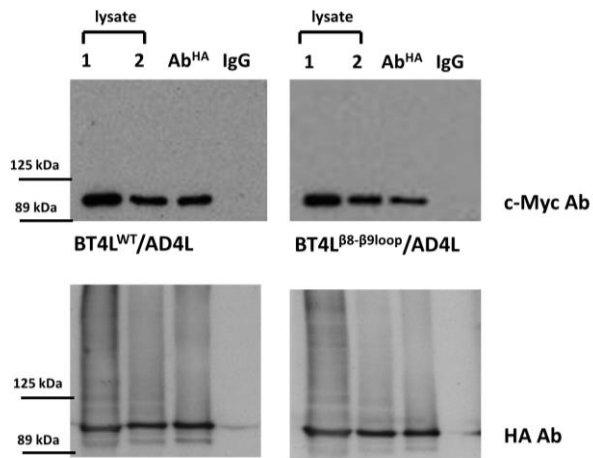
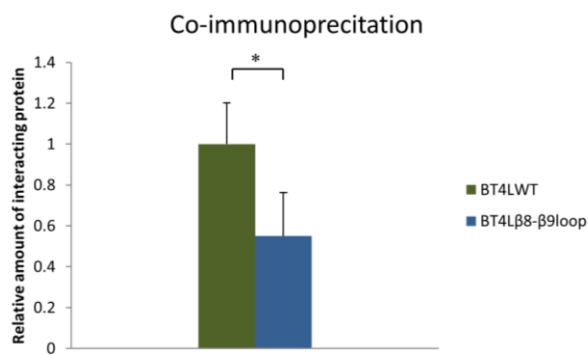


**Figure 4.12** Co-immunoprecipitation of the RyR2 N-terminus (AD4L) with BT4L<sup>β8-β9loop</sup> or BT4L<sup>WT</sup> following co-expression in mammalian HEK293 cells. Blots in the upper panel were probed with cMyc Ab; lane 1 and 2: 1/50<sup>th</sup> and 1/200<sup>th</sup> of cell lysate respectively, lane Ab<sup>HA</sup> and IgG: specific and non-specific binding respectively. Blots in lower panel were probed with HA Ab; lane 1 and 2: 1/10<sup>th</sup> and 1/50<sup>th</sup> of cell lysate, lane Ab<sup>HA</sup> and IgG: specific and non-specific binding respectively



**Graph 4.4** Cumulative co-IP data following densitometry analysis showing the effect of the β8-β9 loop deletion on the interaction with the full-length fragment. Results corrected for the difference in expression levels and non-specific binding are presented relative to protein recovered for the wild-type BT4L. Data given as mean values +/-SEM, n=4 \* statistical significance at p<0.05 using paired, 2-tailed Student's t test

#### 4.3.5 Deletion of the $\beta$ 20- $\beta$ 21 loop changes oligomerisation pattern

The deletion of the  $\beta$ 20- $\beta$ 21 loop in the BT4L fragment triggered substantial changes in the oligomerisation pattern of the N-terminal fragment (Figure 4.13). Chemical crosslinking of the BT4L $^{\beta 20-\beta 21loop}$  in ambient conditions revealed the presence of dimers, tetramers and higher oligomers. This fragment was also more prone to form non-specific aggregates, which size prevented them from entering the separating gel. In addition, these higher oligomers and aggregates displayed unusual resistance to SDS as they were occasionally observed even in samples treated with DTT and not subjected to chemical crosslinking (data not shown). This would suggest that the BT4L $^{\beta 20-\beta 21loop}$  deletion mutant has a somewhat perturbed conformation leading to aggregation of this protein. Moreover, on many occasions oligomers formed by the BT4L $^{\beta 20-\beta 21loop}$  fragment were not easily resolved by SDS-PAGE, i.e. migrated as a smear with no distinctive bands observed. In reducing conditions, mostly trimers and tetramers were formed, also some higher oligomers were also observed. The substantial difference in the BT4L $^{\beta 20-\beta 21loop}$  oligomerisation pattern prevented quantitative densitometry analysis and comparison with the BT4L fragment.

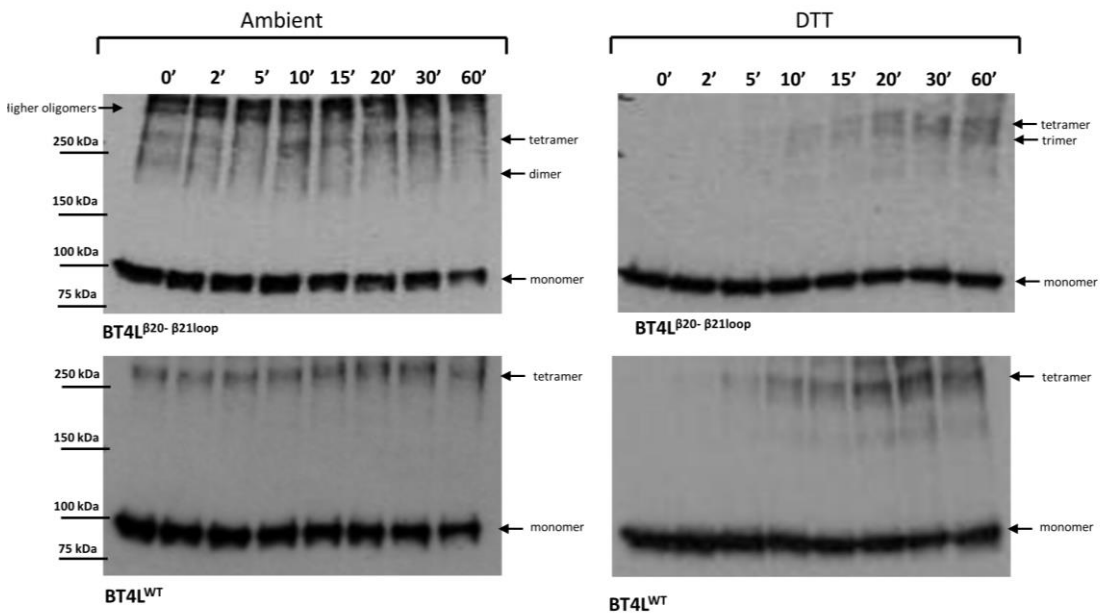


**Figure 4.13** Representative blots of chemical crosslinking experiments illustrating time-dependent tetramer formation of  $\text{BT4L}^{\beta 20-\beta 21\text{loop}}$  and  $\text{BT4L}^{\text{WT}}$  fragments in the presence and absence of DTT (right and left panel respectively). Time-points in minutes as indicated. Oligomeric forms depicted by arrows

## 4.4 Discussion

The goal of this work was to identify the sites mediating self-tetramerisation of the RyR2 N-terminus. Based on the recently published crystal structure of the RyR1 N-terminus and computational docking into the cryo-EM map of the full length protein (Tung et al. 2010), three deletion mutants lacking loops located at the putative inter-subunit contact site were generated ( $\text{BT4L}^{\beta 8-\beta 9\text{loop}}$ ,  $\text{BT4L}^{\beta 20-\beta 21\text{loop}}$ ,  $\text{BT4L}^{\beta 22-\beta 23\text{loop}}$ ). Two additional constructs, i.e.  $\text{BT4L}^{\Delta 12}$  and  $\text{BT4L}^{\text{SPRY}\beta 5-\beta 6\text{loop}}$ , were generated in order to test the contribution of SPRY domain in the inter-subunit interaction which was based on previous findings (Table 4.1). Constructs were expressed in HEK293 cells and tested for their oligomerisation properties by chemical crosslinking.

#### 4.4.1 The elusive role of SPRY domain in the inter-subunit interaction

The BT4 $\Delta$ 12 construct (residues 1-747) was generated on the basis of the following observation: the BT4 fragment (residues 1-759) which lacks part of the SPRY domain (the four C-terminal  $\beta$  strands), forms tetramers with very little dimer formation, thus has properties similar to the longer BT4L fragment while the BT4C (residues 1-654) which lacks the whole SPRY domain, forms predominantly dimers (previous findings, Table 4.1). Chemical crosslinking of the new BT4 $\Delta$ 12 construct revealed that further removal of the last 12 residues which contain part of the SPRY  $\beta$ 5- $\beta$ 6 loop and  $\beta$ -strand 6, has a profound effect on the oligomerisation pattern as observed in Figure 4.8. Unlike BT4L and BT4, BT4 $\Delta$ 12 showed preferential formation of dimers, at least in the early stages of the crosslinking reaction; similar to the BT4C construct (graphical summary of these findings is presented in Figure 4.14). Since BT4 and BT4L fragments exhibit similar oligomerisation properties and BT4 $\Delta$ 12 behaves strikingly different, it seems that residues 748-759, are involved in the tetramerisation process. However, the removal of residues 748-752 in the context of the BT4L construct (BT4L<sup>SPRY $\beta$ 5- $\beta$ 6loop</sup>) containing SPRY  $\beta$ 5- $\beta$ 6 loop resulted in a surprisingly minor effect (Figure 4.9, Graph 4.1). These findings suggest that the SPRY  $\beta$ 5- $\beta$ 6 loop is not a major tetramerisation determinant, contrary to the indication obtained from the BT4 $\Delta$ 12 construct.

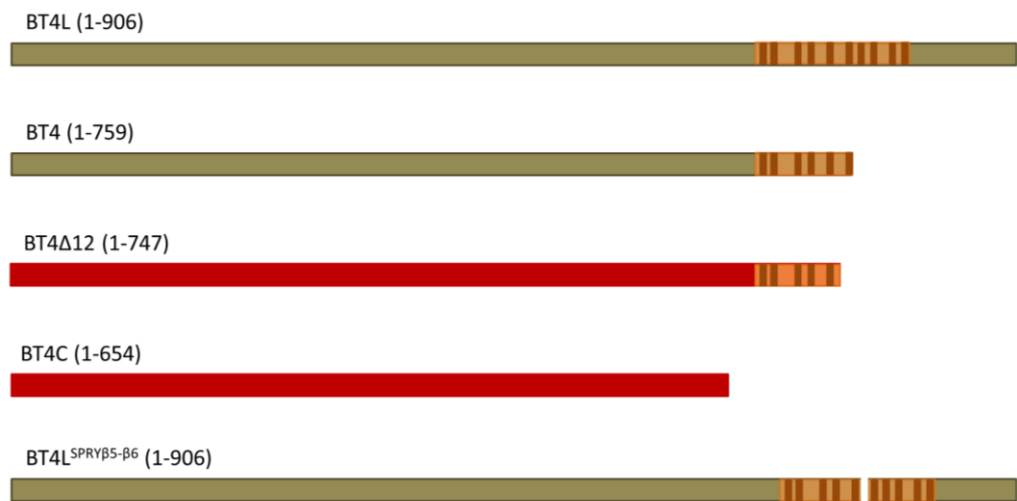


**Figure 4.14** Graphical summary of RyR2 N-terminal fragments; SPRY domain indicated in orange with brown boxes representing  $\beta$ -strands. Fragments forming predominantly tetramers in dark green, fragments forming predominantly dimers in red

It has been suggested that SPRY domains are involved in protein-protein interactions (Perfetto et al. 2013). Analysis of conserved residues among twenty SPRY domains of diverse proteins showed that they are mainly buried between two  $\beta$ -sheets and therefore they are most likely implicated in the maintenance of the tertiary structure rather than interaction with binding partners (Woo et al. 2006). The crystal structure of a SPRY domain in complex with its binding partner revealed that the binding surface is mainly composed of highly diverse loops rather than conserved  $\beta$ -strands (James et al. 2007). It was proposed that the diversification of those loops is responsible for the functional variability of proteins containing SPRY domains. Interestingly, the proposed protein-protein contact sites, i.e.  $\beta$ 2- $\beta$ 3,  $\beta$ 3- $\beta$ 4,  $\beta$ 4- $\beta$ 5 and  $\beta$ 5- $\beta$ 6 loops are all present in the BT4 fragment which tetramerise in a similar manner to the BT4L. A half of loop  $\beta$ 5- $\beta$ 6 is absent in BT4L<sup>SPRY $\beta$ 5- $\beta$ 6loop</sup> and a part of this loop is also missing in BT4Δ12; however the latter lacks also the remaining part of SPRY domain, i.e.  $\beta$ -strands 6-10 (Figure 4.14). Thus, there are two equally possible explanations for the observed discrepancy in the oligomerisation properties between BT4L<sup>SPRY $\beta$ 5- $\beta$ 6loop</sup> and BT4Δ12. Assuming that N-terminus self-association is mediated by multiple sites located throughout BT4L, the removal of the SPRY  $\beta$ 5- $\beta$ 6 loop in the context of the full fragment might not be sufficient to cause an effect due to the presence of remaining interaction determinants. Alternatively, if multiple sites within SPRY domain participate in the oligomerisation process, the spatial

arrangement of those determinants would be critical. Therefore, it is likely the removal of the SPRY  $\beta$ 5- $\beta$ 6 loop and strand  $\beta$ 6 in BT4 $\Delta$ 12 has a detrimental effect on the structure of the whole SPRY domain, and therefore affect tetramerisation indirectly without being an actual inter-subunit contact site. However, in order to conclusively confirm any of the mechanism mentioned above, further experiments are needed.

#### 4.4.2 Oligomerisation intermediates

Since the functional ryanodine receptor is composed of four subunits, a tetramer would be expected to be the physiologically relevant oligomeric form of the RyR2 N-terminus. The fact that BT4 $\Delta$ 12 preferentially forms dimers while tetramers become only more apparent towards longer crosslinking times implies that intermediate steps of the oligomerisation process are affected. In general, there could be two different pathways of tetrameric assembly; either a formation of dimers which then assemble further to form tetramers or a sequential addition of monomers through dimers and trimers. Based on the observations obtained in this work, the latter pathway is favoured. While there are predominantly dimers and tetramers in non-reducing conditions, trimers become apparent when BT4 $\Delta$ 12 is pre-treated with DTT (Figure 4.8). The fact that the longer BT4L fragment almost exclusively gives rise to tetramers indicates that their formation is an extremely fast process in which intermediates are not captured with the crosslinking technique used in this study. It is well established that reaction intermediates only accumulate to a significant extent if they precede a slow or rate-determining step in the overall reaction. The fact that BT4 $\Delta$ 12 predominantly gives dimers in ambient conditions strongly argues that the formation of oligomers higher than dimers becomes more difficult. The stability of protein complexes is determined by two components; the rate of association and the rate of dissociation. It has been suggested that the reduction in the stability of protein complexes observed upon mutation of critical residues usually reflect an increase in complex dissociation rate (Castro and Anderson 1996). However, some mutations have been shown to perturb a particular step along the association pathway (Spoerner *et al.* 2001) as we observe for the BT4 $\Delta$ 12 fragment, i.e. formation of dimers over

tetramers. Interestingly, in reducing conditions BT4Δ12 does not form dimers but instead gives mostly trimers and tetramers. This obvious difference in the oligomerisation pattern in reducing versus non-reducing conditions strongly suggests the involvement of disulphide bond formation in the process of RyR2 N-terminus tetramerisation.

#### 4.4.3 The role of the loops located at the putative inter-subunit interface

Expression of the BT4L<sup>β20-β21loop</sup> deletion mutant in HEK293 cells resulted in SDS-resistant higher oligomers and aggregates evident mostly in ambient conditions (Figure 4.13) suggesting that this mutant may have perturbed conformation leading to non-specific aggregation. While, physiologically relevant oligomers such as dimers, trimers and tetramers were observed, they were very often difficult to resolve as they tend to migrate as a smear upon SDS-PAGE. For those reasons the involvement of the β20-β21 loop in RyR2 N-terminus self-association could not be unambiguously established, however this loop appears to be critical for maintaining the tertiary structure of the RyR2 N-terminus.

According to the docking of the RyR1 N-terminus crystal structure into the pseudo-atomic map of the full length protein, the β20-β21 loop is involved in a salt bridge between two adjacent subunits. In addition, there are two arrhythmia-associated mutations within this loop R332W and G357S. The extreme C-terminal end of this loop also contains cysteine 361 which was earlier shown (Chapter 3) to affect tetramer formation in reducing conditions implying an additional disulphide-independent role of this site in the inter-subunit interaction. The β20-β21 loop was also suggested to be one of the two inter-subunit contact sites for N-terminus association in IP<sub>3</sub>R (Seo et al. 2012). In light of the cumulative data presented in Chapter 3 and 4, residues within the β20-β21 loop are likely to constitute important determinants of oligomerisation.

Deletion of the β8-β9 loop had a pronounced impact on N-terminus oligomerisation. In chemical crosslinking, BT4L<sup>β8-β9loop</sup> formed significantly fewer tetramers than the

full-length BT4L fragment in both ambient and reducing conditions indicating a substantial decline in the stability of the oligomerisation products (Figure 4.11, Graph 4.3). Moreover, BT4L <sup>$\beta$ 8- $\beta$ 9loop</sup> displayed significantly diminished association with the full length BT4L fragment as assessed by co-immunoprecipitation assay (Figure 4.12, Graph 4.4) suggesting that deletion of the  $\beta$ 8- $\beta$ 9 loop also disrupts formation of mixed oligomers. The  $\beta$ 8- $\beta$ 9 loop contains three arrhythmia associated mutations (P164S, R169Q and R176Q) implying the functional importance of residues contained within this loop. Interestingly, it was reported that none of these mutations altered thermal stability of the N-terminal domain (Lobo and Van Petegem 2009). Further to this, it was proposed that these mutations affect the association between subunits allowing the channel to be more prone to open (Kimlicka *et al.* 2013). In agreement with the functional role of this loop, a short peptide encompassing the  $\beta$ 8- $\beta$ 9 loop (residues 165-195) was capable of inducing SR Ca<sup>2+</sup> leak and increased the frequency of Ca<sup>2+</sup> sparks in cardiomyocytes (Tateishi *et al.* 2009). Further evidence for the functional importance of the  $\beta$ 8- $\beta$ 9 loop comes from studies of IP<sub>3</sub>R. The strong structural and functional evolutionary relationship between the two receptors is supported by the fact that the extreme N-terminal domain of the IP<sub>3</sub>R1, i.e. a suppressor domain, can be functionally substituted by the homologous RyR domain (Seo *et al.* 2012). Comparison of the crystal structures of the IP<sub>3</sub>R1 N-terminus with and without its ligand bound revealed that the  $\beta$ 8- $\beta$ 9 loop moves substantially upon InsP<sub>3</sub> binding further implying its role in channel gating (Seo *et al.* 2012). Although there are no disease-associated mutations in IP<sub>3</sub>R1, the substitution of a single residue (Y167) is sufficient to abolish channel activity (Yamazaki *et al.* 2010). In light of the results obtained in this study, the  $\beta$ 8- $\beta$ 9 loop is proposed to constitute a critical determinant of N-terminus self-association contributing towards tetramer stability.

The  $\beta$ 22- $\beta$ 23 loop was previously suggested to constitute one of the major inter-subunit contact points between adjacent RyR1 N-termini (Tung *et al.* 2010). The findings obtained in this study however suggest that it has a minimal, if any, effect on N-terminus self-association as there was no significant difference in the oligomerisation propensity between the BT4L <sup>$\beta$ 22- $\beta$ 23loop</sup> deletion mutant and the full-length BT4L fragment (Figure 4.10, Graph 4.2). Since only a part of this loop was removed in this study, it is plausible that the remaining residues are sufficient to mediate the association with the neighbouring subunit in a manner undistinguishable

from that of the full length loop. Alternatively, isoform-specific, local structural differences between RyR1 and RyR2 might account for the discrepant results. Nevertheless, an important point should be made. The concept of the  $\beta$ 22- $\beta$ 23 loop involvement in the inter-subunit interaction is solely inferred from computational analysis, whereas the observed lack of effect on tetramer formation by the  $\beta$ 22- $\beta$ 23 loop is based on empirical evidence, and it might in fact reflect an authentic phenomenon.

#### 4.4.4 Final remarks

In conclusion, two types of domains important for N-terminus association were identified in this study. Both regions reside in loops suggested earlier to be located at the N-terminal inter-subunit interface. Based on the findings, the  $\beta$ 8- $\beta$ 9 loop is essential to maintain the stability of the RyR2 N-terminus tetrameric assembly. The removal of  $\beta$ 20- $\beta$ 21 loop resulted in the formation of oligomers higher than tetramers and protein aggregates implying the role of this loop in the maintenance of the N-terminus tertiary structure. However, in light of findings presented in Chapter 3, i.e. mutation of a single residue (C361) within this loop compromises tetramer formation, the  $\beta$ 20- $\beta$ 21 loop is proposed to constitute another important determinant of N-terminus self-association. Since the absence of those two loops does not completely abolish N-terminus tetramer formation, additional, secondary inter-subunit contact sites must exist. Thus, N-terminus self-association appears to be governed by multiple sites which act in a synergistic manner to promote tetramer formation. One such site might be located in the N-terminal part of the SPRY domain.

The BT4L fragment forms oligomers; however monomers represent a predominant form of the RyR2 N-terminus with tetramers remaining a minor species even at the 60 min crosslinking time-point (below 25%). The failure to convert all BT4L proteins into tetramers by chemical crosslinking might indicate that BT4L oligomers undergo dynamic dissociation and association. Notably, this phenomenon was observed for other oligomeric proteins (Gu *et al.* 2002; Abulimiti *et al.* 2003). A dynamic association/dissociation between N-termini across subunits would potentially enable

this interaction to regulate RyR2 function. The role of N-terminus self-association in RyR2 function is tested in Chapter 5.

# Chapter 5

## Dissecting the role of N-terminus in RyR2 function

## 5 Dissecting the role of N-terminus in RyR2 function

### 5.1 Introduction

It is believed that RyR activity is controlled by a complex network of inter- and intra-subunit interactions which constitute a critical link between changes induced by modulators binding to its large N-terminal cytoplasmic part and the opening of the channel pore located at the C-terminus. It has been proposed that interaction between critical functional domains is pivotal for the channel to perform its function in a physiological manner (Yamamoto *et al.* 2000; Shtifman *et al.* 2002; Murayama *et al.* 2005). The disruption of domain cross-talk has been implied in RyR dysfunction observed in skeletal muscle and heart disorders (Oda *et al.* 2005; Murayama *et al.* 2007; Yamamoto *et al.* 2008; Hamada *et al.* 2009). A considerable number of functional and biochemical evidence suggested that the inter-subunit interaction between RyR N-terminal and central domain is critically involved in the regulation of channel function (Yamamoto and Ikemoto 2002a; Yang *et al.* 2006; Liu *et al.* 2010). Similarly it has been reported that the interaction within central domains involving calmodulin binding domain and calmodulin-like domain controls channel gating (Gangopadhyay and Ikemoto 2006; Xiong *et al.* 2006). Other regions suggested to transmit cytoplasmic changes to the channel pore included so called “Interacting” domain encompassing the CaMLD and residues predicted to constitute the first two transmembrane domains (Du *et al.* 2002a; George *et al.* 2004). Moreover, the CaMLD was also proposed to interact with the loop connecting transmembrane domains 4 and 5 (Hamada *et al.* 2007). For a comprehensive description of domain-domain interactions within RyR please refer to Section 1.6.

Biochemical evidence showing a novel inter-subunit interaction involving RyR2 N-terminus was presented in previous chapters. It was speculated that BT4L oligomerisation might be involved in the modulation of RyR2 activity. Thus, the principal goal of this study was to test the hypothesis that N-terminus inter-subunit interaction is involved in channel regulation.

In order to gain insights into the role of N-terminus self-association in RyR2 function, [<sup>3</sup>H]ryanodine binding assays were performed. The experimental approach involved comparison of RyR2 activation in the presence and absence of the BT4L fragment in a wide range of calcium concentrations. The reasoning behind this approach was that the exogenous BT4L fragment could compete for N-terminus binding sites presumed to exist in the native RyR2 tetramer and disrupt endogenous N-terminal inter-subunit interactions. Thus, if N-terminus oligomerisation was involved in the regulation of RyR2 activity, co-expression of the BT4L fragment with the full length channel should alter its function. Because ryanodine preferentially binds to the open channel, the use of this compound would enable to detect any alterations in channel activity. In order to rationalise the functional assay it was essential to first assess whether the BT4L fragment is able to physically interact with the full length RyR2. RyR2 constitutes an integral protein of sarcoplasmic/endoplasmic reticulum. However in the absence of transmembrane domains, the truncated protein is exclusively found in the cytoplasm (George et al. 2004). Thus, upon expression in HEK293 cells, the BT4L fragment should be located in the cytoplasm, while RyR2 should be restricted to the microsomal fraction. However, if the two proteins physically interact, the sub-cellular distribution of the BT4L fragment should change upon co-expression with RyR2. This possibility was tested by sub-cellular fractionation.

## 5.2 Methods

### 5.2.1 Sub-cellular fractionation

HEK293 cells were transfected with the BT4L construct either in combination with the empty pcDNA3 vector or with pcDNA3 containing the cDNA for the full length RyR2. Transfection was performed on cells growing on 100 mm Petri dishes as described in Section 2.2.5.2. The sub-cellular fractionation involved two sequential centrifugation steps at 1500 xg and 100 000 xg (Section 2.2.2.5). Protein content in the homogenate, microsomal and cytoplasmic fractions (1500 xg supernatant, 100 000 xg pellet and supernatant respectively) was evaluated using the BCA assay.

Typically 20-50 µg of total protein was subjected to Western blotting and probed with c-Myc Ab to assess sub-cellular BT4L distribution. Simultaneously, fractions were run on a separate 4% SDS-PAGE, agarose-containing gel, separated proteins were transferred using a semi-dry transfer system and probed with the 1093 antiserum (Table 2.1) to detect the expression of RyR2. For detailed description of Western blotting procedure please refer to Section 2.2.24.

### 5.2.2 [<sup>3</sup>H]ryanodine binding assay

For a typical [<sup>3</sup>H]ryanodine binding assay, ten 100 mm Petri dishes were transfected with the full length RyR2 alone or in combination with the BT4L fragment. 24 hour post-transfection, cells were homogenised on ice using a custom-made cell homogeniser allowing for 25 passages through a needle (0.6x30 mm). Microsomal fractions were obtained as described previously and total protein content was measured with the BCA assay. BT4L expression was confirmed by Western blots. RyR2 expression was evaluated on two levels; initially by densitometry-based analysis of Western blotted fractions and subsequently by [<sup>3</sup>H]ryanodine binding assay performed in conditions promoting maximum channel activation (and therefore leading to measurement of total RyR2 content). In order to have an equal amount of RyR2 protein in samples expressing RyR2 alone versus RyR2 plus BT4L, the amount of microsomes used was adjusted accordingly. Microsomes from untransfected HEK293 cells were used to equate total protein levels between RyR2 alone versus RyR2 plus BT4L samples. Dose-response curves were fitted with GraphPad Prism using four-parameter logistic model with bottom and top constrained to 0 and 1 respectively. Curves were compared statistically using the extra-sum of squares F test (GraphPad Prism).

## 5.3 Results

### 5.3.1 The BT4L fragment interacts with the full length RyR2

BT4L expressed on its own can be found almost exclusively in the cytoplasm (Figure 5.1, right panel). RyR2 is present in the microsomal but absent in the cytoplasmic fraction (Figure 5.1, lower panel). Upon co-expression with the full length RyR2, a considerable proportion of the BT4L fragment translocates to the microsomal fraction (Figure 5.1, left panel). This finding indirectly suggests that the physical interaction between the exogenous RyR2 N-terminus represented by BT4L and the full length channel takes place.

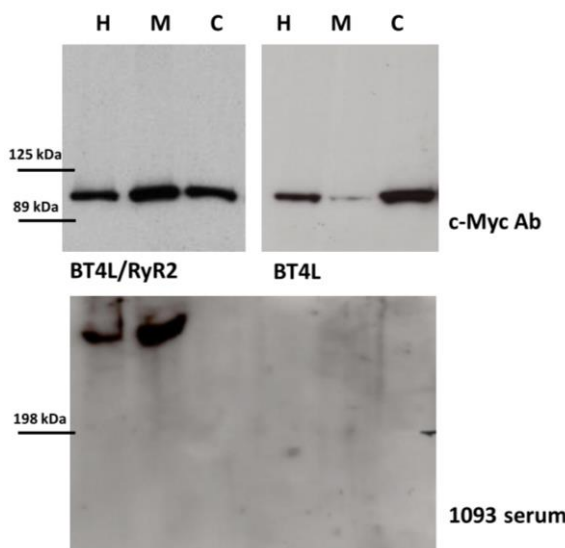
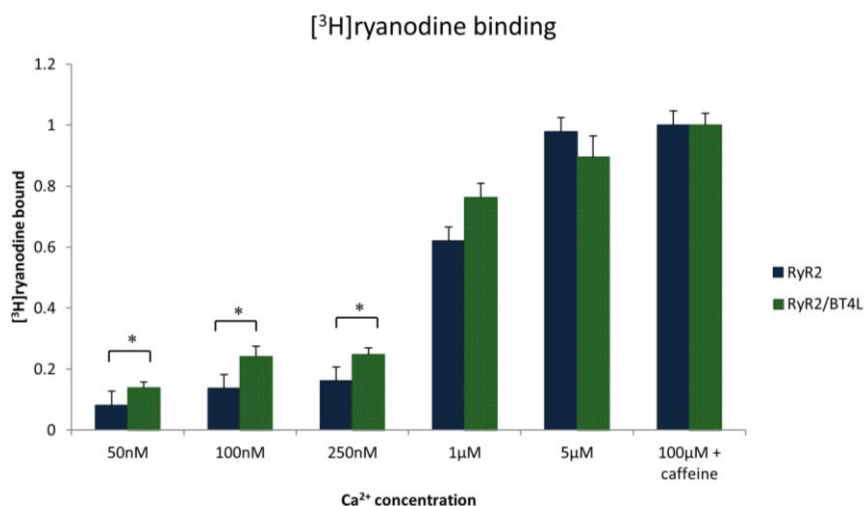


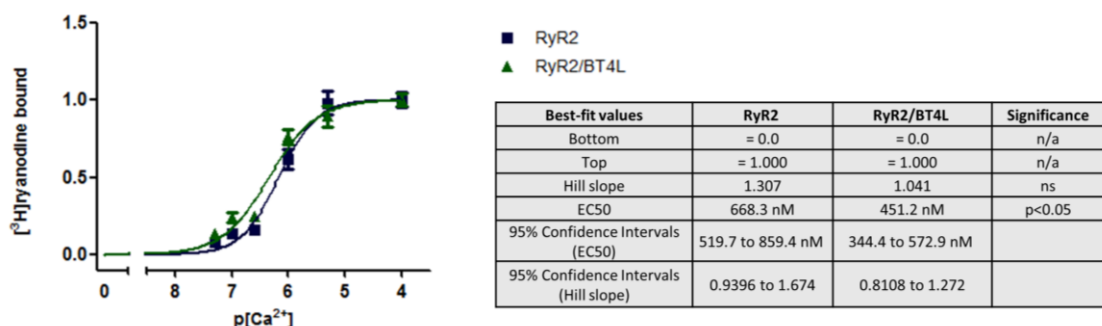
**Figure 5.1** Sub-cellular fractions obtained from cells expressing the BT4L fragment with and without the full length RyR2 (left and right panel respectively). Blots in upper panel were probed with c-Myc Ab and represent BT4L distribution over the following fractions; H: homogenate, M: microsomes, C: cytosol. Blots in lower panel were probed with 1093 serum and represent RyR2 distribution

### 5.3.2 The BT4L fragment activates RyR2 at diastolic $\text{Ca}^{2+}$

The presence of co-expressed BT4L did not affect [ $^3\text{H}$ ]ryanodine binding at  $\text{Ca}^{2+} \geq 1 \mu\text{M}$  (Graph 5.1). In contrast, at low calcium concentrations BT4L promoted on average 40% increase in RyR2 activity, which was statistically significant (Graph 5.1) implying that BT4L-triggered channel activation occurs exclusively at diastolic levels of  $\text{Ca}^{2+}$ . Comparison of the dose response curves fitted with GraphPad showed that the BT4L presence results in a statistically significantly shifts of the  $\text{Ca}^{2+}$  activation curve to the left ( $\text{EC}_{50}$  668 nM [ $\text{Ca}^{2+}$ ] for RyR2 alone versus 451 nM for RyR2/BT4L,  $p=0.026$ ) as presented in Graph 5.2.



**Graph 5.1** Graph summarising the effect of the BT4L fragment on RyR2 function as assessed in [ $^3\text{H}$ ] ryanodine binding assay in three separate experiments each performed at least in duplicate. Data are normalised to the value measured under maximum binding conditions and shown as mean +/-SEM, \* statistical significance at  $p<0.05$  calculated using unpaired, 2-tailed Student's  $t$  test



**Graph 5.2** Dose-response curve of RyR2 and RYR2/BT4L fitted with GraphPad Prism using four-parameter logistic model with bottom and top constrained to 0 and 1 respectively. Best-fit values shown in the table; n/a (non-applicable), ns (not significant)

## 5.4 Discussion

The principal goal of this study was to investigate the role of the RyR2 N-terminus self-association in the regulation of channel activity by using exogenous BT4L to disrupt N-terminal inter-subunit interaction within the RyR2 tetrameric assembly. This experimental approach was based on numerous literature reports which described the use short peptides to disrupt putative domain-domain interactions within RyR. Peptide-induced effects on channel activity were evaluated in [<sup>3</sup>H]ryanodine binding assays (Yamamoto et al. 2000; Yamamoto and Ikemoto 2002a) or by performing calcium imaging in cells (Yang et al. 2006). The BT4L fragment used in this study is much longer compared to peptides used by other groups and, as shown previously (Chapter 3 and 4), displays strong self-association properties. However, it was assumed that its interaction with the full-length RyR2 would be still possible upon simultaneous expression in HEK293 cells. This was based on two important observations; the BT4L self-association appears to be a dynamic process (Chapter 4) and based on the docking of the RyR1 N-terminus in the pseudo-atomic model of the full-length receptor, it is readily accessible (Tung et al. 2010). Indeed, as assessed by subcellular fractionation, BT4L translocates from the cytoplasmic into predominantly microsomal fraction exclusively upon co-expression with the full length RyR2 (Figure 5.1) suggestive of physical interaction between BT4L and the full-length protein.

[<sup>3</sup>H]ryanodine binding revealed that exogenous BT4L changes the RyR2 sensitivity towards calcium, i.e. promotes channel activation at sub-threshold Ca<sup>2+</sup>. It was speculated that the observed effect is a consequence of the BT4L fragment disrupting N-terminus interactions occurring between subunits in the channel as explained in Section 5.1. Thus, the tight inter-subunit association of the N-terminal part of RyR2 seems to play an important role in channel gating most likely serving to stabilise the closed conformation. However, at this stage it is not possible to discriminate whether N-terminus dissociation constitutes a primary step triggering a set of structural changes promoting channel opening or whether it remains one of many downstream allosteric events prompted by physiological agonists. In the course of experiments undertaken in this study, an extensive investigation into the structural changes triggered by arrhythmia-associated mutations in RyR1 N-terminus, led the authors to suggest analogous hypothesis, according to which a direct N-terminal inter-subunit contact undergoes a drastic disruption or alteration upon channel opening (Kimlicka et al. 2013). Further to the above, this interaction was proposed to impose an energetic barrier that needs to be overcome to allow RyR to open. A similar scenario was proposed for the IP<sub>3</sub>R, where IP<sub>3</sub> binding induces N-terminus rearrangement at the inter-subunit contact again implying that this type of association plays a pivotal role in channel opening (Seo et al. 2012).

Interestingly, the sensitisation effect produced by the BT4L fragment resembles the phenotype observed for recombinantly expressed RyR2 containing arrhythmia-associated mutations (Jiang et al. 2002a; Jiang et al. 2004). Since many of those mutations map to the N-terminus inter-subunit interface, it seems plausible that their presence might result in the disruption of this inter-subunit contact in a similar way to the effect produced by the BT4L fragment. Thus, arrhythmia-linked mutations are proposed to disrupt RyR2 N-terminus self-association. The reduced inter-subunit contact would lower the barrier for channel opening, thereby leading to sensitisation towards calcium activation. Notably, Tang and colleagues reported that the deletion of the RyR2 N-terminus (the first 305 amino acids) results in channels which are more sensitive to calcium activation and exhibit a marked reduction in the termination threshold of calcium release (Tang et al. 2012). Moreover, the authors showed that analogous changes in channel activity occur in the presence of N-terminal arrhythmia-associated mutations suggesting that this region might be

involved in the regulation of channel gating. The hypothesis of disrupted RyR2 N-terminus self-association in the presence of arrhythmia-linked mutations is tested in Chapter 6.

# Chapter 6

The effect of arrhythmia-linked mutations on N-terminus self-association

# 6 The effect of arrhythmia-linked mutations on RyR2 N-terminus self-association

## 6.1 Introduction

The work described in Chapter 4 provided evidence that the effective self-association of the RyR2 N-terminus is highly dependent on residues contained within loops predicted to occupy the inter-subunit boundary. Notably, some of those loops are also targeted by arrhythmia-linked mutations. In addition, the evidence supporting the role of N-terminus self-interaction in channel regulation was presented in Chapter 5. It was shown that in the presence of exogenous BT4L, RyR2 becomes hypersensitive to diastolic concentration of calcium. This phenomenon was proposed to be a direct consequence of the disruption of N-termini interaction across subunits. Interestingly, RyR2 hypersensitivity observed in the presence of the BT4L fragment recapitulates some of the hallmarks of RyR2 dysfunction observed in mutations leading to life-threatening arrhythmias. Hence, the aim of this study was to investigate whether the presence of a particular mutation, identified in arrhythmia-susceptible patients is able to affect the RyR2 N-terminus self-association. Moreover, to gain further insights into RyR2 structure-function relationship, the effect of arrhythmia-linked mutations was also evaluated in respect to their ability to influence N-terminus domain interaction with the full length channel.

Until now, more than 140 mutations in the RyR2 gene have been associated with episodes of stress- and exercise- induced cardiac arrhythmia (Table 1.4). Those mutations represent mostly single amino-acid substitutions and only in rare cases involve deletions or sequence duplication. Mutations in the N-terminal “hot spot” (residues 77-466) account for less than 20% of all cases reported (Priori and Chen 2011). Since this mutation cluster has been extensively studied it seems unlikely that this relatively low frequency of N-terminal mutations can be attributed to a sequencing bias. In theory, a low number of arrhythmia-associated mutations in the RyR2 N-terminus might indicate that mutations within this domain are tolerated and do not result in the arrhythmogenic phenotype thus remain undetected. On the other

hand, a low number of reported cases could also be explained by a high mortality rate. This in turn would suggest that the preservation of structural and functional attributes within the N-terminus remains essential for the channel to perform its physiological role.

There are 27 missense mutations located in the first 1000 residues of RyR2 (<http://www.fsm.it/cardmoc/> as of April 2013) and two of those (R176Q and L433P) were investigated in this study. These two amino acid substitutions were identified in Italian families, where symptoms of right ventricle partial degeneration, electrical instability and cases of sudden death were reported (Tiso et al. 2001). Notably, in those patients, the genetic picture was more complicated, i.e. R176Q co-segregated with a central domain mutation (T2504M) and L433P was accompanied by the presence of a common SNP (G1885E). However, the R176Q mutation was later reported to result in the CPVT phenotype in two patients negative for T2504M (Haugaa et al. 2010). Moreover, the T2504M substitution, when independently identified in another family, was shown to result in a considerably milder disease phenotype in the absence of R176Q implying that the latter has a prevailing role in the clinical outcome (Baucé et al. 2002) (Table 6.1). A direct link between stress-induced arrhythmia and R176Q was also confirmed in animal models (Kannankeril et al. 2006; Mathur et al. 2009).

<b>Family</b>	<b>Mutation</b>	<b>SCD episodes</b>	<b>Carriers with arrhythmic symptoms</b>	<b>Carriers with kinetic alterations in right ventricle</b>
115	R176Q/T2504M	3	100%	2/3
129	T2504M	1	29%	0
122	L433P	1	80%	1/5
X	R176Q	not reported	not reported	0

**Table 6.1** Table summarising clinical symptoms in patients carrying RyR2 mutations (Baucé et al. 2002; Haugaa et al. 2010)

Heterologously expressed RyR2<sup>R176Q</sup> displays hyper-sensitised caffeine activation (Thomas *et al.* 2004) and enhanced sensitivity to calcium (Jiang *et al.* 2005), prevalent features of arrhythmia-linked RyR2 dysfunction. However, the phenotype associated with the L433P mutation remains under debate. Jang and colleagues showed that recombinant expression of RyR2<sup>L433P</sup> leads to the effects undistinguishable from other arrhythmia-associated mutations (Jiang *et al.* 2005) while others reported that the L433P substitution leads to a substantially desensitised response (Thomas *et al.* 2004). Those findings are intriguing as both mutations lead to a similar clinical phenotype while having seemingly opposite effects on RyR2 activity. The principal goal of this study was to evaluate whether those two particular mutations alter N-terminus oligomerisation. In light of apparently different mechanisms of channel dysfunction associated with L433P and R176Q it was of particular interest to test whether the presence of those mutations exerts comparable effects on N-terminus self-interaction.

The effect of arrhythmia-linked mutations on the RyR2 N-terminus oligomerisation was evaluated by three different experimental techniques. Tetramerisation of the BT4L fragment carrying arrhythmia-linked mutations was investigated in a chemical crosslinking assay following expression in HEK293 cells. The propensity to form mixed oligomers, i.e. composed of mutation-containing fragments and BT4L<sup>WT</sup> was evaluated by co-immunoprecipitation. Those techniques assessed the effect of R176Q and L433P mutations on the N-terminus oligomerisation *in vitro*, i.e. outside the cellular environment. For the above reason, a complementary approach capable of detecting protein interactions *in situ*, was undertaken (yeast two-hybrid system).

The yeast two-hybrid technique was designed and developed in 1989 and it is one of the most widely used in protein-protein interaction studies (Fields and Song 1989). The system takes advantage of the fact that the yeast transcription factor GAL4 is composed of two physically separable and functionally independent domains, i.e. the DNA-binding domain (DNA-BD) and the activating domain (AD). Those domains, if physically separated, lose their ability to activate the GAL4 responsive genes. However if the two GAL4 domains are fused to two interacting proteins they are brought together in close physical contact regaining their capacity for transcription activation. Restoration of GAL4 transcription factor activity controls the expression of the *LacZ* reporter gene which codes for the β-galactosidase enzyme. The use of a

substrate, which upon  $\beta$ -galactosidase enzymatic activity is turned into a product of intense colour, allows for visualisation of GAL4 transcriptional activity. The colour intensity directly reflects the strength of the association between the two interacting proteins (Figure 6.1).

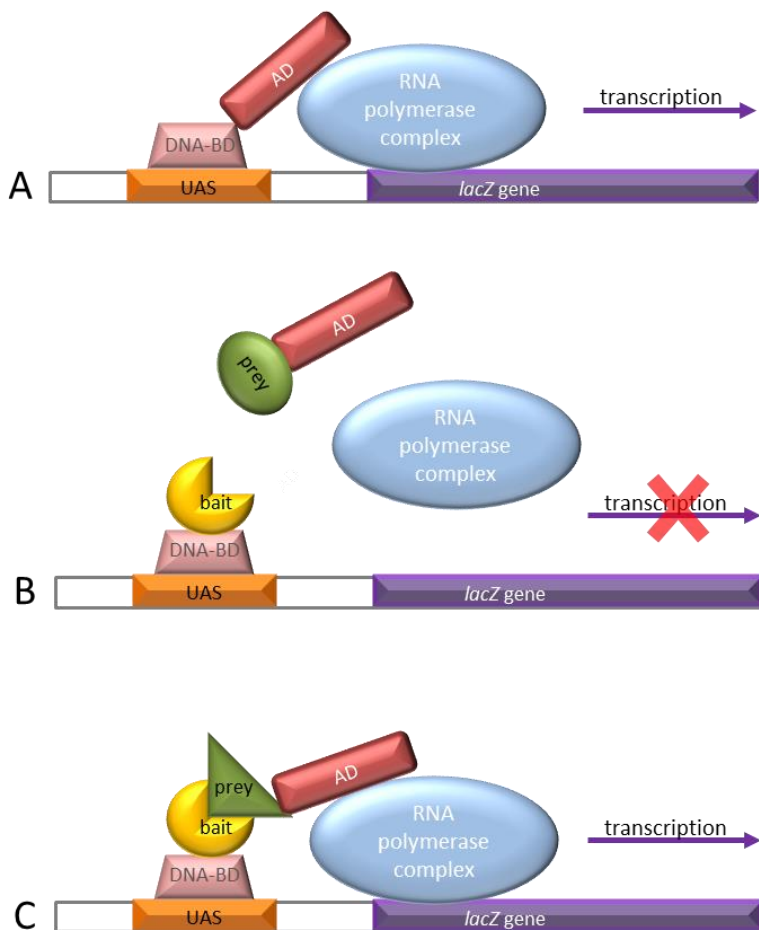


**Figure 6.1** Schematic overview of yeast two-hybrid assay; A: regular GAL4-dependent transcription of a reporter gene, B: GAL4 DNA-binding domain and activating domain are physically separated and fused to two proteins called bait and prey respectively, the two proteins do not interact and transcription of the report gene does not proceed, C: the interaction between bait and prey proteins brings the DNA-BD and AD in close contact activating the transcription of a reporter gene

Earlier, in the course of this study (Chapter 5), it was shown that sub-cellular fractionation is a valuable tool to gain insights whether two proteins located in two different cellular compartments (cytoplasm and ER for the BT4L and RyR2

respectively), have the potential to interact. Hence, the same approach was undertaken to investigate whether the presence of arrhythmia-linked mutations in the full length RyR2 alters the sub-cellular distribution of the BT4L fragment (implying altered RyR2/BT4L interaction).

The second aim of this study was to explore whether mutation-associated changes in the oligomerisation of the RyR2 N-terminus can be reversed. In light of accumulating evidence showing that dantrolene – a skeletal muscle relaxant, has the ability to rescue the RyR2 mutation-associated phenotype (Kobayashi et al. 2009; Suetomi et al. 2011; Jung et al. 2012) and the fact that the drug’s binding site is located in the N-terminal portion of the protein (residues 601-620) (Paul-Pletzer et al. 2005), dantrolene’s capability to modify mutation-induced changes in the BT4L oligomerisation was investigated.

## 6.2 Methods

### 6.2.1 Generation of the BT4L<sup>R176Q</sup> and the BT4L<sup>L433P</sup>

The BT4L<sup>R176Q</sup> mutant was generated by site-directed mutagenesis of the BT4L construct (please refer to Section 2.2.1.6. and Table 2.2 for detailed description of the mutagenesis process and primers used respectively). The DNA fragments containing the desired mutation, which presence was verified by sequencing, was subcloned into the wild type BT4L. This was performed as follows; both plasmids were digested with *Hind*III, separated by agarose gel electrophoresis and subjected to ligation following gel extraction of the fragments of interests (described in detail in Section 2.2.1.3, 2.2.1.4 and 2.2.1.5). The ligation reaction was used to transform bacteria (Section 2.2.1.8). The orientation of subcloned fragments was assessed by indicative digest with *Bsp*EI and *Sal*I and a positive clone was sequenced further to cover the whole length of the subcloned DNA fragment. Once verified, large volume overnight bacteria cultures were set up for plasmid isolation as described in Section 2.2.1.10.

The BT4L<sup>L433P</sup> construct was generated by cloning a specific DNA fragment obtained in a standard PCR reaction (Section 2.2.1.1) into the BT4L plasmid. The reaction was performed in the presence of forward and reverse primers (V8.1531-48 and JWREV.2821-40 respectively; Table 2.2) and using the full length RyR2 plasmid containing the L433P as a template. The PCR product (~1.5 kb) and the destination plasmid were digested with a combination of *Bgl*II and *Bsp*EI restriction enzymes, separated by agarose gel electrophoresis and subjected to ligation following gel extraction of the fragments of interests (described in detail in Section 2.2.1.3, 2.2.1.4 and 2.2.1.5). Subsequently, the ligation reaction was used to transform bacteria by means of electroporation (Section 2.2.1.8). Obtained colonies were screened as described in Section 2.2.1.10. A positive clone was sequenced further to cover the length of the whole subcloned DNA fragment and once the sequence was verified, large volume overnight bacteria culture was set up for plasmid isolation as described in Section 2.2.1.10.

## 6.2.2 Chemical crosslinking

Obtained plasmids were used to transfect HEK293 cells growing on 100 mm Petri dishes as described in Section 2.2.5.2. Each experiment was performed with a concomitant transfection of cells with the wild-type BT4L plasmid serving as a positive control. Cell pellets obtained 24 hours after transfection were homogenised (Section 2.2.2.1) and one aliquot was treated with DTT (4 °C, 1 h, 10 mM). Total protein concentration was evaluated using the BCA colorimetric assay and depending on the experiment 20-50 µg of total protein was subjected to glutaraldehyde crosslinking in a time-dependent manner (Section 2.2.2.2). Proteins were separated by SDS-PAGE and subsequently blotted onto PVDF membranes (for details please refer to Section 2.2.2.3 and 2.2.2.4). The c-Myc Ab and anti-mouse HRP-conjugated Ab were used to detect the BT4L protein presence (Table 2.1). Tetramer to monomer ratio was determined by performing a densitometry analysis using BioRad Quantity One software as described in Section 4.2.3

For the evaluation of the dantrolene effect on the oligomerisation properties of the mutants, cell homogenates were incubated with 1  $\mu$ M dantrolene for 1 h at 37 °C prior to glutaraldehyde crosslinking.

### 6.2.3 Co-immunoprecipitation

The interaction between mutation-containing fragments and the wild-type RyR2 N-terminus was evaluated in co-immunoprecipitation assays. HEK293 cells were co-transfected with the following combinations of constructs: BT4L<sup>R176Q</sup> and the AD4L construct (HA-tagged BT4L fragment), BT4L<sup>L433P</sup> and AD4L as well as BT4L<sup>WT</sup> and AD4L which served as positive control. Co-immunoprecipitation was performed as described in Section 2.2.2.6. Polyclonal HA antibody (Table 2.1) and protein A Sepharose beads were used to immunoprecipitate the wild type HA-tagged N-terminal fragment (AD4L) and the c-Myc Ab was used to detect co-precipitating BT4L proteins. The level of co-precipitated proteins was determined by densitometry as described in Section 4.2.4.

### 6.2.4 Yeast two-hybrid system

The effect of R176Q and L433P mutations on RyR2 N-terminus interactions *in vivo* was assessed using the yeast two-hybrid system. The bait plasmid (BD-BT4L<sup>WT</sup>) containing the BT4L fragment (RyR2, residues 1-906) fused to the GAL4 DNA-BD and c-Myc epitope (in pGK7 vector), and the prey plasmid (AD-BT4L<sup>WT</sup>) containing the same N-terminal RyR2 fragment expressed as fusion protein with GAL4 AD and HA epitope (in pACT2 vector) were generated earlier. For BD-BT4L<sup>L433P</sup> and BD-BT4L<sup>R176Q</sup>, the cDNA coding for RyR2 N-terminus (residues 1-906) was sub-cloned from the previously made plasmids for mammalian expression (section 6.2.1). The ~2.7 kb DNA fragments obtained following digestion with *Bam*HI and *Nde*I restriction enzymes were separated by agarose gel electrophoresis, purified and ligated (Section 2.2.1.3, 2.2.1.4 and 2.2.1.5) with the empty pGK7 vector previously digested with the same combination of restriction enzymes. The

ligation reaction was used to transform bacteria (Section 2.2.1.8). Colonies were screened as described in Section 2.2.1.0.

For AD-BT4L<sup>L433P</sup> and AD-BT4L<sup>R176Q</sup>, the RyR2 cDNA was sub-cloned into the empty pACT2 vector from the previously made plasmids for mammalian expression (section 6.2.1) using a combination of *Bam*HI and *Nco*I restriction enzymes. Subsequent steps of the subcloning procedure were performed as described earlier for bait plasmids.

$\beta$ -galactosidase colony-lift filter assay and quantitative liquid  $\beta$ -galactosidase assay were performed as described in Section 2.2.3.3 and 2.2.3.4 respectively. Mutation effect on the interaction was tested in the following combinations: BD-BT4L<sup>L433P</sup> with AD-BT4L<sup>L433P</sup>, BD-BT4L<sup>L433P</sup> with AD-BT4L<sup>WT</sup> and BD-BT4L<sup>WT</sup> with AD-BT4L<sup>L433P</sup> (R176Q mutation was tested analogously). The interaction between pVA3-1 coding for a DNA-BD/murine p53 fusion protein and pTD1-1 coding for an AD/SV40 large T-antigen fusion protein was used as assay quality positive control. Data obtained for the mutants were expressed relative to the interaction between the wild-type fragments, i.e. BD-BT4L<sup>WT</sup> with AD-BT4L<sup>WT</sup>.

## 6.2.5 Sub-cellular fractionation

HEK293 cells were transfected with the BT4L fragment in combination with RyR2<sup>WT</sup>, RyR2<sup>L433P</sup> or RyR2<sup>R176Q</sup>. Subsequent steps were undertaken as described earlier for the sub-cellular fractionation of the BT4L fragment expressed with or without RyR2 (Section 5.2.1). Quantitative distribution of the BT4L fragment in the microsomal versus cytosolic fraction was determined following densitometry analysis.

### 6.3 Results

Two mammalian expression constructs ( $\text{BT4L}^{\text{R176Q}}$  and  $\text{BT4L}^{\text{L433P}}$ ) and four yeast plasmids (BD-BT4L $^{\text{L433P}}$ , AD-BT4L $^{\text{L433P}}$ , BD-BT4L $^{\text{R176Q}}$ , AD-BT4L $^{\text{R176Q}}$ ) were successfully generated (Figure 6.2 and 6.3).

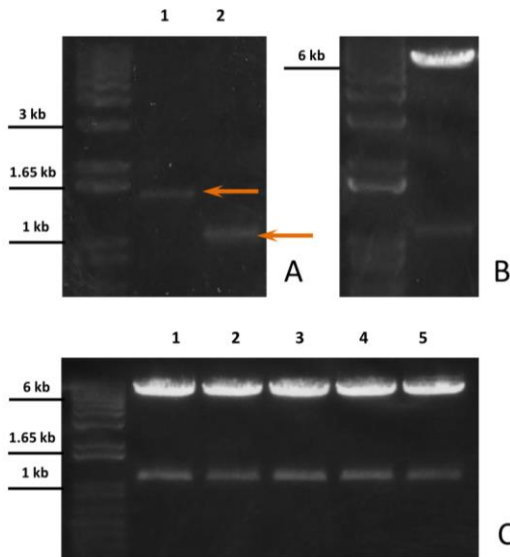


**Figure 6.2** Intermediate steps of the experimental procedure generating the  $\text{BT4L}^{\text{L433P}}$  construct; A, lane 1: DNA gel showing the amplification product (~1.5 kb) obtained in a standard PCR performed on the  $\text{RyR2}^{\text{L433P}}$ , lane 2: PCR product digested with  $\text{BgII}$  and  $\text{BspEI}$  restriction enzymes, B: restriction digest of the  $\text{BT4L}^{\text{WT}}$  plasmid ( $\text{BgII/BspEI}$ ), the upper band was purified from the gel and ligated with the purified PCR product from lane 2 in panel A, C, lanes 1-5: indicative digest ( $\text{BgII/BspEI}$ ) of clones obtained after bacteria transformation following the subcloning procedure

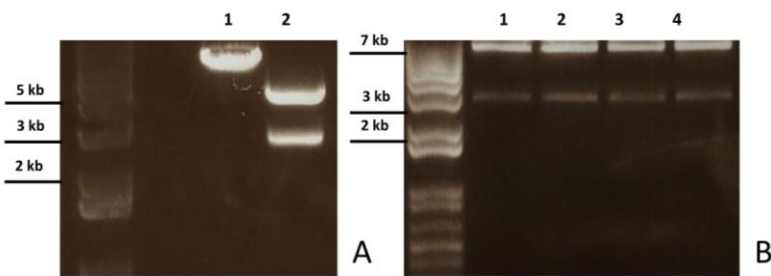


**Figure 6.3** Intermediate steps of the experimental procedure generating one of the yeast expression vectors – BD-BT4L $^{\text{R176Q}}$ ; A, lane 1: empty pGBK7 digested with  $\text{NdeI}$  and  $\text{BamHI}$  restriction enzymes, lane 2: restriction digest of  $\text{BT4L}^{\text{R176Q}}$  ( $\text{NdeI/BamHI}$ ) generating ~2.8kb fragment which was purified from the gel and cloned into purified pGBK7 from lane 1, B, lanes 1-4: indicative digest ( $\text{NdeI/BamHI}$ ) of clones obtained after bacteria transformation following the subcloning procedure

### 6.3.1 Arrhythmia-linked mutations reduce N-terminus self-association

In chemical crosslinking, BT4L<sup>R176QR</sup> and BT4L<sup>L433P</sup> retained the ability to form tetramers as reflected by the presence of ~400 kDa band (Figure 6.4 and 6.5). However, compared to the BT4L<sup>WT</sup> fragment, both mutants displayed severely compromised oligomerisation both in ambient and reducing conditions.

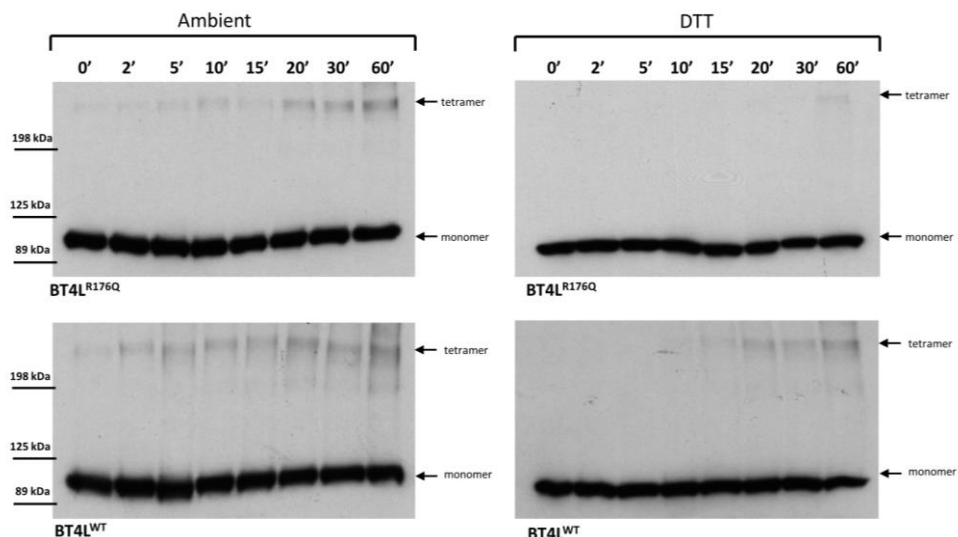


**Figure 6.4** Chemical crosslinking experiments illustrating time-dependent tetramer formation of BT4L<sup>R176Q</sup> and BT4L<sup>WT</sup> fragments in the presence and absence of DTT (right and left panel respectively). Time-points in minutes as indicated. Tetramer and monomer depicted by arrows

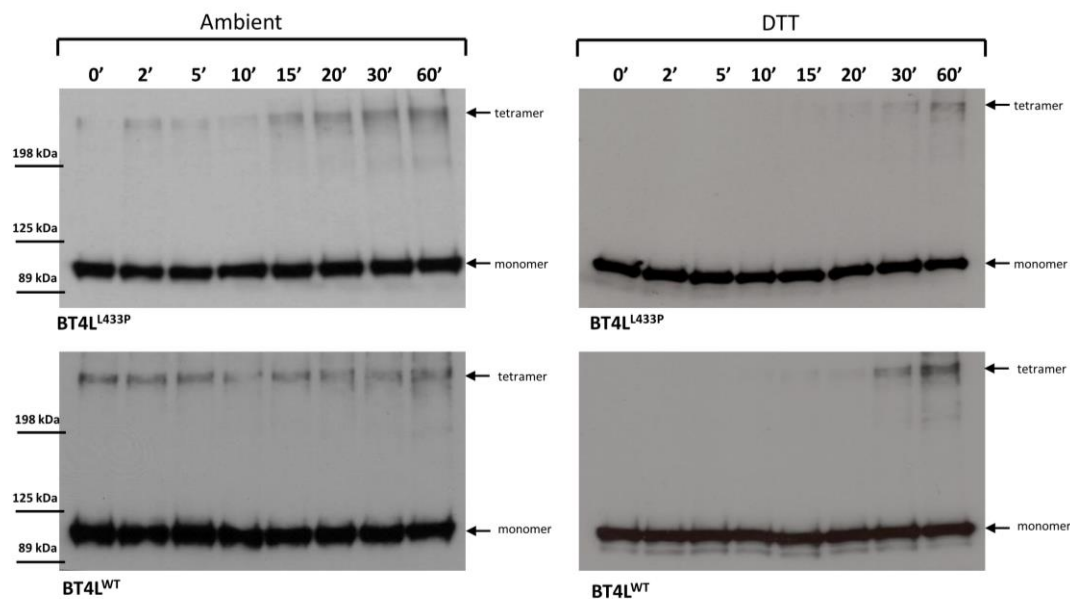
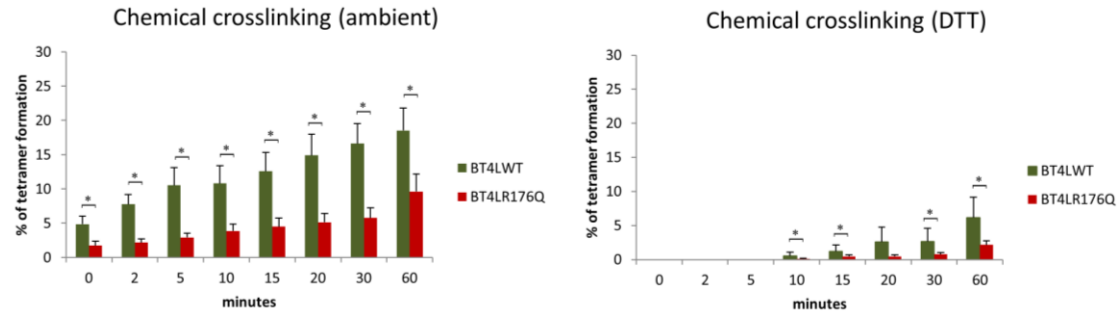
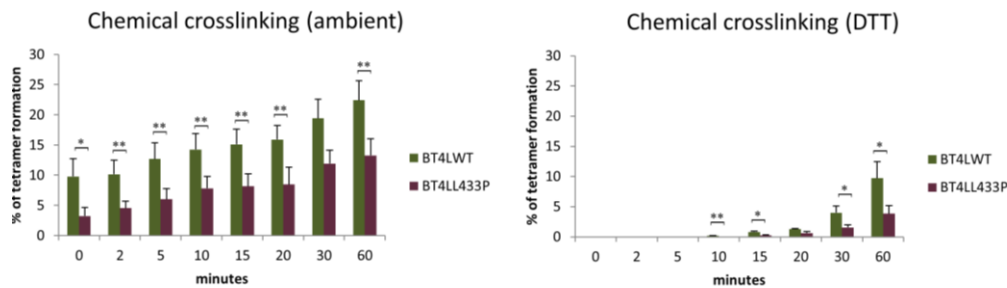


**Figure 6.5** Chemical crosslinking illustrating time-dependent tetramer formation of BT4L<sup>L433P</sup> and BT4L<sup>WT</sup> fragments in the presence and absence of DTT (right and left panel respectively). Time-points in minutes as indicated. Tetramer and monomer depicted by arrows

Cumulative data following densitometry analysis are presented in Graph 6.1 and 6.2 for BT4L<sup>R176Q</sup> and BT4L<sup>L433P</sup> respectively. In ambient conditions, the introduction of the R176Q substitution in the BT4L fragment resulted in on average 60% reduction in tetramer formation and the effect was a statistically significant for all time points studied (Graph 6.1, left panel). In reducing conditions, BT4L<sup>R176Q</sup> ability to self-associate was compromised by on average 70% with statistically significant effect for the majority of time points (Graph 6.1, right panel). The presence of the L433P mutation on average reduced BT4L oligomerisation propensity by 40% at ambient conditions and 60% in reducing conditions (Graph 6.2). The effect was statistically significant for the majority of time-points studied.



**Graph 6.1** Densitometry analysis of  $\text{BT4L}^{\text{WT}}$  and  $\text{BT4L}^{\text{R176Q}}$  tetramer formation in chemical crosslinking assay at ambient and reducing conditions. Percentage of tetramer calculated as described earlier (Section 4.2.3). Data are shown as mean +/- SEM, n=7 and n=6 for ambient and reducing conditions respectively; \* statistical significance at  $p<0.05$  calculated using paired, 2-tailed Student's *t* test



**Graph 6.2** Densitometry analysis of  $\text{BT4L}^{\text{WT}}$  and  $\text{BT4L}^{\text{L433P}}$  tetramer formation in chemical crosslinking assay at ambient and reducing conditions. Percentage of tetramer calculated as described earlier (Section 4.2.3). Data are shown as mean +/- SEM, n=7 and n=8 for ambient and reducing conditions respectively; \* and \*\* statistical significance at  $p<0.05$  and  $p<0.01$  respectively calculated using paired, 2-tailed Student's *t* test

### 6.3.2 The formation of mixed oligomers is severely compromised in the presence of the L433P mutation

The impact of both mutations on the formation of mixed oligomers was investigated by co-immunoprecipitation. HA-tagged RyR2 N-terminus (AD4L) was immunoprecipitated from HEK293 cell lysates co-expressing this protein together with (cMyc-tagged) BT4L<sup>R176Q</sup> or BT4L<sup>L433P</sup>, and the presence of co-precipitated mutant proteins was analysed by Western blotting using Ab cMyc. The R176Q substitution resulted in a minor reduction of association with the wild-type fragment, while the effect of L433P mutation was unexpectedly remarkable (Figure 6.6 and 6.7).

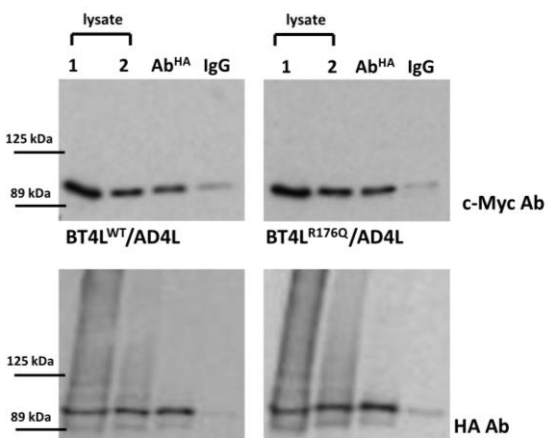


**Figure 6.6** Co-immunoprecipitation of the RyR2 N-terminus (AD4L) with BT4L<sup>R176Q</sup> or BT4L<sup>WT</sup> following co-expression in mammalian HEK293 cells. Blots in the upper panel were probed with cMyc Ab; lane 1 and 2: 1/50<sup>th</sup> and 1/200<sup>th</sup> of cell lysate respectively, lane Ab<sup>HA</sup> and IgG: specific and non-specific binding respectively. Blots in lower panel were probed with HA Ab; lane 1 and 2: 1/10<sup>th</sup> and 1/50<sup>th</sup> of cell lysate, lane Ab<sup>HA</sup> and IgG: specific and non-specific binding respectively

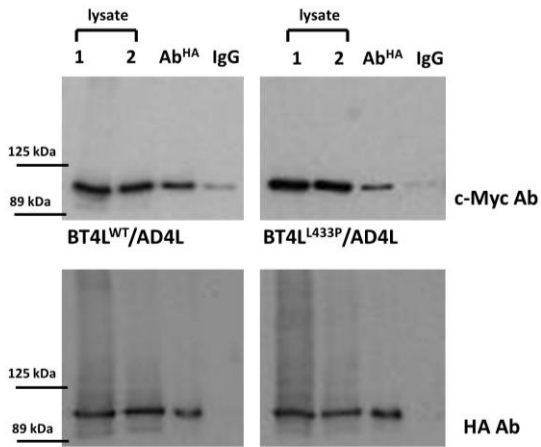
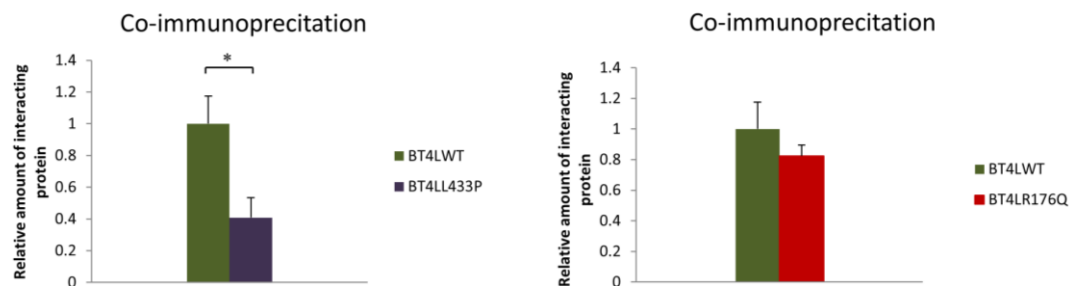


**Figure 6.7** Co-immunoprecipitation of the RyR2 N-terminus (AD4L) with BT4L<sup>L433P</sup> or BT4L<sup>WT</sup> following co-expression in mammalian HEK293 cells. Blots in the upper panel were probed with cMyc Ab; lane 1 and 2: 1/50<sup>th</sup> and 1/100<sup>th</sup> of cell lysate respectively, lane Ab<sup>HA</sup> and IgG: specific and non-specific binding respectively. Blots in lower panel were probed with HA Ab; lane 1 and 2: 1/10<sup>th</sup> and 1/50<sup>th</sup> of cell lysate, lane Ab<sup>HA</sup> and IgG: specific and non-specific binding respectively

Densitometry-based analysis was performed as described in Section 4.2.4 to quantitatively evaluate the impact of each mutation on the amount of recovered co-precipitated mutant (Graph 6.3). The presence of R176Q mutation produced a small (18%), but not statistically significant, decline in the interaction propensities between the mutant and the wild-type fragment (Graph 6.3, left panel). On the other hand, the L433P substitution resulted in 59% ( $p < 0.05$ ) reduction in the amount of mutant protein recovered after co-immunoprecipitation relative to wild-type (Graph 6.3, right panel).



**Graph 6.3** Bar chart summarising co-immunoprecipitation results for BT4L<sup>R176Q</sup> and BT4L<sup>L433P</sup> determined following densitometry analysis (left and right panel respectively). Results for co-precipitated mutant proteins are presented relative to the wild-type fragment. Data shown as mean +/- SEM, n=4 and n=5 for BT4L<sup>R176Q</sup> and BT4L<sup>L433P</sup> respectively; \* statistical significance at p<0.05 using paired, 2-tailed Student's t test

### 6.3.3 The L433P mutation perturbs RyR2 N-terminus oligomerisation *in situ* (yeast two-hybrid system)

The findings described in the previous sections, indicated that arrhythmia-linked mutations disrupt N-terminus self-association. Those experiments tested RyR2 N-terminus oligomerisation in cell lysates, an environment which substantially differs from the tightly controlled and intact cellular milieu. The yeast two-hybrid system, where detection of protein-protein interactions takes place in living yeast, was employed to evaluate whether the *in situ* observed effects can be reproduced in *in vivo* conditions. For this purpose, BT4L<sup>R176Q</sup> and the BT4L<sup>L433P</sup> were co-expressed in yeast with the wild-type fragment as recombinant proteins fused to GAL4 AD or DNA-BD (bait and prey respectively). The interaction of two mutants with themselves was investigated by expressing both bait and prey proteins as mutation-containing fragments. The expression of all six constructs used in this study (BD-BT4L<sup>WT</sup>, BD-BT4L<sup>R176Q</sup>, BD-BT4L<sup>L433P</sup>, and AD-BT4L<sup>WT</sup>, AD-BT4L<sup>R176Q</sup>, AD-BT4L<sup>L433P</sup>) was investigated as substantial differences in protein levels would affect the outcome of the assay. As shown in Figure 6.8, all recombinant proteins were expressed at comparable levels.

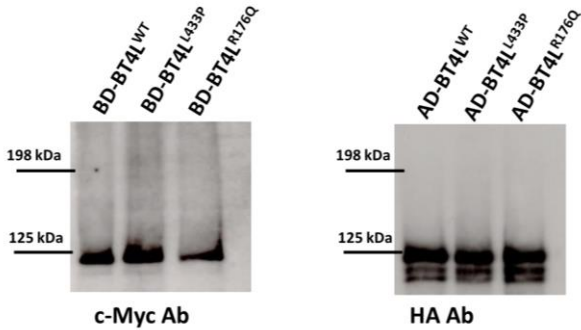


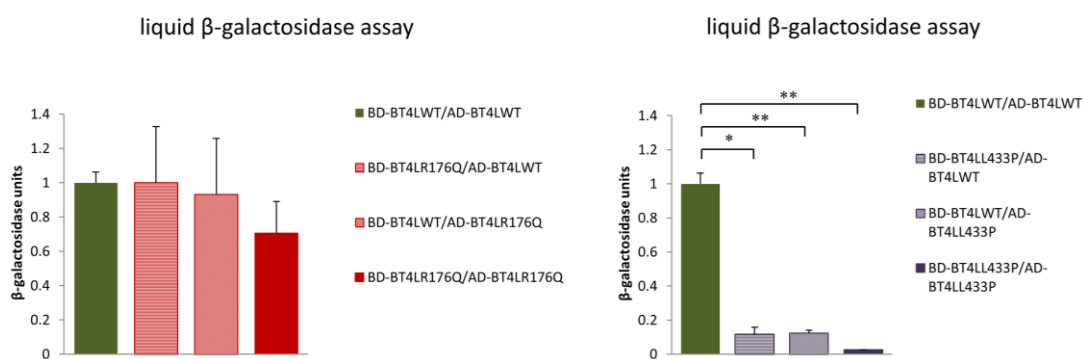
**Figure 6.8** Western blotting showing expression levels of recombinant proteins tested in yeast two-hybrid system; left pane: recombinant proteins fused with DNA-BD and tagged with c-Myc epitope, right panel: recombinant proteins fused with GAL4 AD and tagged with HA epitope

$\beta$ -galactosidase colony-lift filter assay confirmed that the RyR2 N-terminus self-association ( $\text{AD-BT4L}^{\text{WT}}/\text{BD-BT4L}^{\text{WT}}$ ) indeed takes place *in vivo* (Table 6.2). The wild-type interaction with itself is very strong, comparable to the interaction between the p53 protein (pVA3) and large T antigen (pTD1), which is a positive control commonly used in the yeast two-hybrid system. This rather qualitative assay allowed for some preliminary conclusions concerning the effect of L433P and R176Q mutations to be drawn (Table 6.2).

Bait construct	Prey construct	Expression of $\beta$ -galactosidase (conversion of X-gal into a blue product)
pVA3	pTD1	strong
$\text{BD-BT4L}^{\text{WT}}$	$\text{AD-BT4L}^{\text{WT}}$	strong
$\text{BD-BT4L}^{\text{WT}}$	$\text{AD-BT4L}^{\text{R176Q}}$	strong
$\text{BD-BT4L}^{\text{R176Q}}$	$\text{AD-BT4L}^{\text{WT}}$	strong/moderate
$\text{BD-BT4L}^{\text{R176Q}}$	$\text{AD-BT4L}^{\text{R176Q}}$	moderate
$\text{BD-BT4L}^{\text{WT}}$	$\text{AD-BT4L}^{\text{L433P}}$	moderate/weak
$\text{BD-BT4L}^{\text{L433P}}$	$\text{AD-BT4L}^{\text{WT}}$	weak
$\text{BD-BT4L}^{\text{L433P}}$	$\text{AD-BT4L}^{\text{L433P}}$	no colour change

**Table 6.2** Summary of  $\beta$ -galactosidase colony lift assay; strong, moderate and weak reflect the relative strength of colour change in time

Quantitative data was obtained using  $\beta$ -galactosidase liquid assay are presented in Graph 6.4. In agreement with the co-immunoprecipitation results, the R176Q mutation did not substantially affect the interaction with the wild-type fragment (BD-BT4L<sup>R176Q</sup>/AD-BT4L<sup>WT</sup> and (BD-BT4L<sup>WT</sup>/AD-BT4L<sup>R176Q</sup>) (Graph 6.4, left panel). As expected from the chemical crosslinking experiments, a compromised self-association was observed; however the effect was statistically insignificant (BD-BT4L<sup>R176Q</sup>/AD-BT4L<sup>R176Q</sup>). The impact of the L433P substitution *in situ* recapitulated all our previous *in vitro* findings (Graph 6.4, right panel). The presence of the L433P mutation in one of the interacting partners (mixed oligomers; BD-BT4L<sup>L433P</sup>/AD-BT4L<sup>WT</sup> or BD-BT4L<sup>WT</sup>/AD-BT4L<sup>L433P</sup>) compromised the association by over 85% relative to the interaction between the wild-type fragments (BD-BT4L<sup>WT</sup>/AD-BT4L<sup>WT</sup>). Notably, the effect of this mutation was synergistic; i.e. when the L433P substitution was present in both bait and prey proteins, the interaction was further reduced by 80%.



**Graph 6.4** Bar chart summarising the results of liquid  $\beta$ -galactosidase assay evaluating the effect of the R176Q and the L433P mutation on the N-terminus oligomerisation *in vivo* (left and right panel respectively). Results presented relative to the value obtained for self-association of the wild-type fragment (BD-BT4L<sup>WT</sup>/AD-BT4L<sup>WT</sup>). Data shown as mean +/- SEM, n=5; \* and \*\*asterisks indicate statistical significance at p<0.05 and p<0.01 respectively calculated using unpaired, 2-tailed Student's *t* test

### 6.3.4 Dantrolene partially reverses the effects of the L433P mutation

The evidently reduced tetramerisation ability of the BT4L fragments containing arrhythmia-linked mutations observed in chemical crosslinking (Section 6.3.1) was investigated in the presence of dantrolene ( $1\mu\text{M}$ ). The principal goal was to establish whether dantrolene can rescue the disease phenotype. Initially, it was investigated whether dantrolene treatment prior to chemical crosslinking is able to influence tetramerisation of the wild-type BT4L fragment. In agreement with the literature reporting no effects of the drug on RyR2, in the absence of the arrhythmia-linked mutations, dantrolene did not produce any appreciable changes on the tetramerisation propensity of the wild-type N-terminus (Figure 6.9, Graph 6.5).

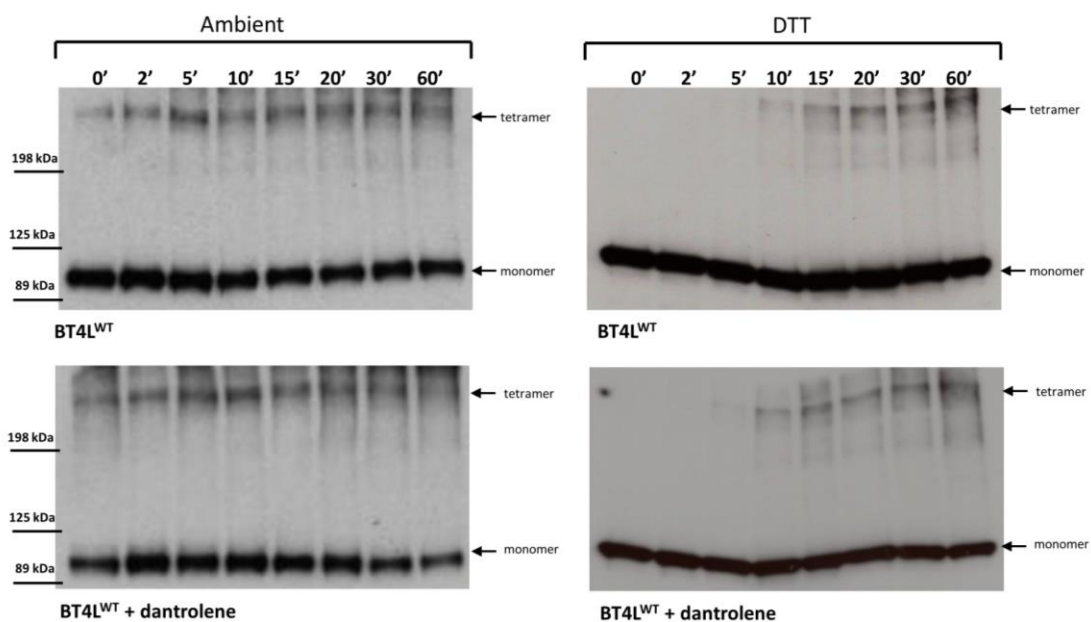
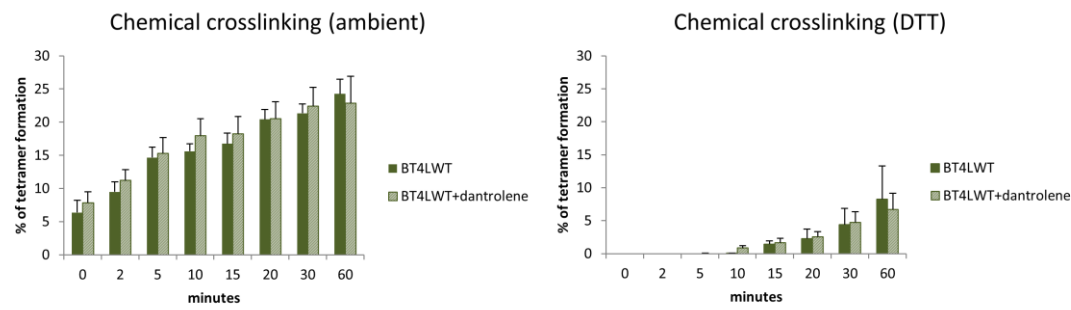


**Figure 6.9** Chemical crosslinking illustrating time-dependent tetramer formation of the BT4L<sup>WT</sup> fragment in the presence and absence of dantrolene ( $1\mu\text{M}$ ) at ambient and reducing conditions (left and right panel respectively). Time-points in minutes as indicated. Tetramer and monomer depicted by arrows



**Graph 6.5** Densitometry analysis of  $\text{BT4L}^{\text{WT}}$  tetramer formation in chemical crosslinking assay in the presence and absence of dantrolene ( $1\mu\text{M}$ ) at ambient and reducing conditions. Percentage of tetramer calculated as described earlier (Section 4.2.3). Data are shown as mean  $\pm$  SEM,  $n=7$  and  $n=6$  for ambient and reducing conditions respectively

Subsequently, chemical crosslinking of  $\text{BT4L}^{\text{R176Q}}$  and  $\text{BT4L}^{\text{L433P}}$  following pre-treatment with  $1\mu\text{M}$  dantrolene was performed. Dantrolene produced an apparent increase in the tetramer formation for  $\text{BT4L}^{\text{R176Q}}$ ; however the effect was statistically significant only for two time-points at ambient conditions (Figure 6.10, Graph 6.6). Remarkably, dantrolene substantially increased tetramer formation of the  $\text{BT4L}^{\text{L433P}}$  fragment (Figure 6.12). Analysis of cumulative data by densitometry revealed that under ambient conditions the drug promoted on average 35% increase in tetramer formation and this effect was statistically significant for the majority of time-points studied (Graph 6.7, left panel). In reducing conditions, the effect of the drug was also evident; however, it was statistically significant only at 60 min time-point (Graph 6.7, right panel).

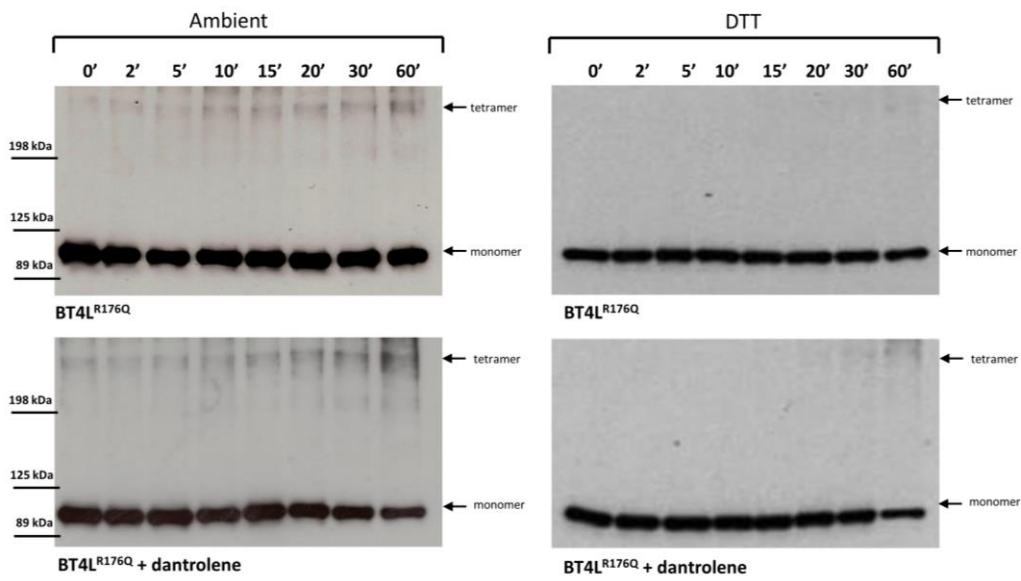
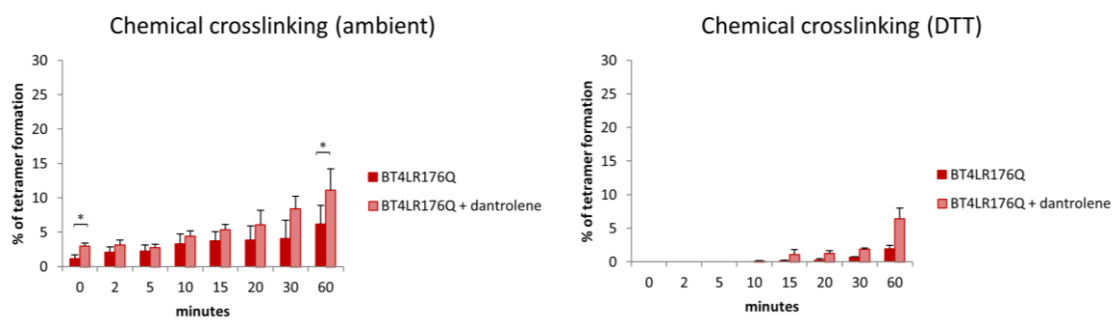


**Figure 6.10** Chemical crosslinking illustrating time-dependent tetramer formation of the BT4L<sup>R176Q</sup> fragment in the presence and absence of dantrolene (1μM) at ambient and reducing conditions (left and right panel respectively). Time-points in minutes as indicated. Tetramer and monomer depicted by arrows



**Graph 6.6** Densitometry analysis of BT4L<sup>R176Q</sup> tetramer formation in chemical crosslinking assay in the presence and absence of dantrolene (1μM) at ambient and reducing conditions. Percentage of tetramer calculated as described earlier (Section 4.2.3). Data are shown as mean +/-SEM, n=5 and n=3 for ambient and reducing conditions respectively, \* statistical significance at p<0.05 calculated using paired, 2-tailed Student's t test

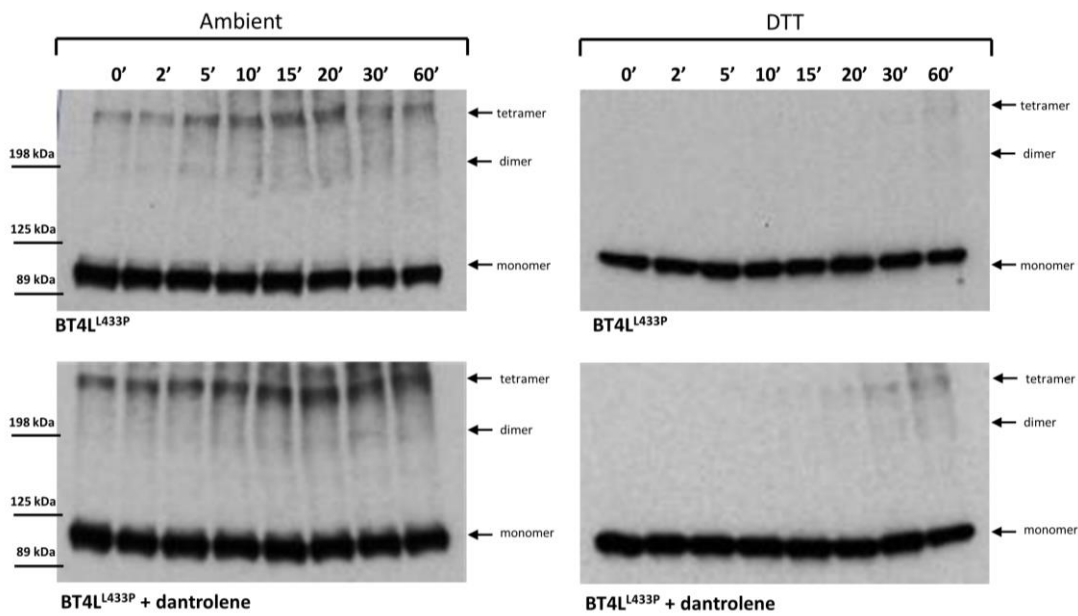
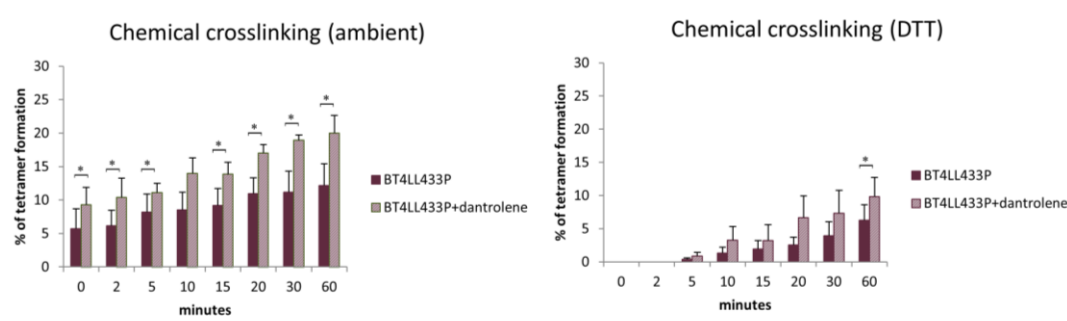


**Figure 6.11** Chemical crosslinking illustrating time-dependent tetramer formation of the BT4L<sup>L433P</sup> fragment in the presence and absence of dantrolene (1 $\mu$ M) at ambient and reducing conditions (left and right panel respectively). Time-points in minutes as indicated. Tetramer and monomer depicted by arrows



**Graph 6.7** Densitometry analysis of BT4L<sup>L433P</sup> tetramer formation in chemical crosslinking assay in the presence and absence of dantrolene (1 $\mu$ M) at ambient and reducing conditions. Percentage of tetramer calculated as described earlier (Section 4.2.3). Data are shown as mean +/-SEM, n=6 and n=7 for ambient and reducing conditions respectively, \* statistical significance at  $p < 0.05$  calculated using paired, 2-tailed Student's  $t$  test

### 6.3.5 Arrhythmia-linked mutations affect BT4L interaction with the full length channel

The co-expression of the BT4L fragment with the full-length RyR2 in HEK293 cells results in the translocation of the former from the cytoplasmic into the microsomal fraction (Chapter 5, Section 3.5.1). The same technique was used to analyse whether the presence of R176Q or L433P mutation in the full length channel alters BT4L sub-cellular distribution, i.e. whether the interaction between the BT4L fragment and the mutant channel is disrupted. Indeed, both mutations reduced the amount of the BT4L fragment in the microsomal versus cytosolic fraction as compared to the level observed upon co-expression with the wild-type RyR2 (Figure 6.12 and 6.13, upper panels). This effect was not due to the differences in the expression level between mutant and wild-type RyR2 as the amount of protein was comparable (Figure 6.12 and 6.13, lower panels).

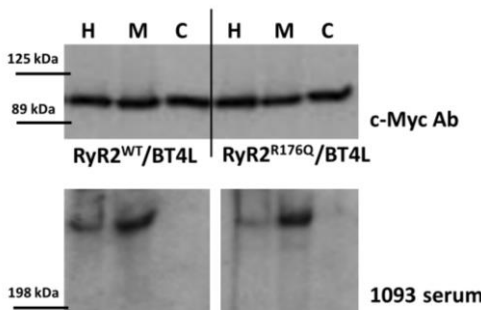


**Figure 6.12** Sub-cellular fractions obtained from cells expressing the BT4L fragment with and without the wild-type full length RyR2 or with RyR2<sup>R176Q</sup> (left and right panel respectively). Blots in the upper panel were probed with c-Myc Ab and represent BT4L distribution over the following fractions; H: homogenate, M: microsomes, C: cytosol. Blots in the lower panel were probed with 1093 serum and represent RyR2 distribution

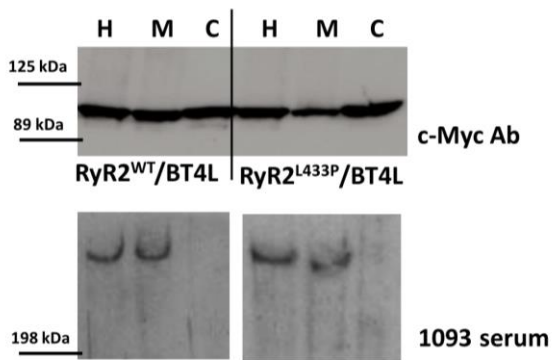
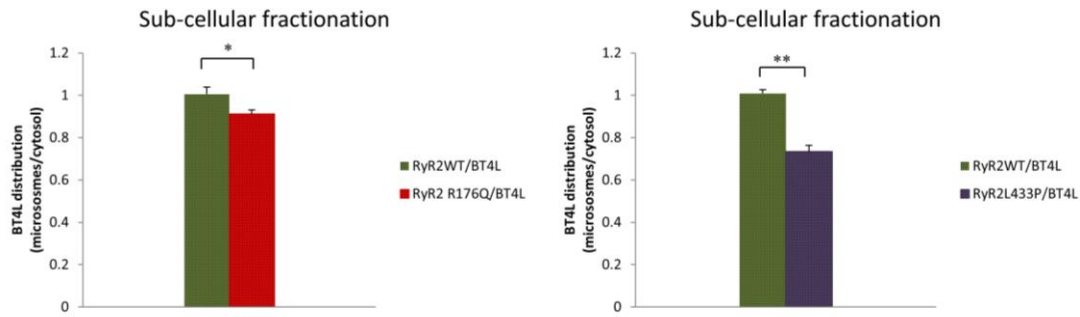


**Figure 6.13** Sub-cellular fractions obtained from cells expressing the BT4L fragment with and without the wild-type full length RyR2 or with RyR2<sup>L433P</sup> (left and right panel respectively). Blots in the upper panel were probed with c-Myc Ab and represent BT4L distribution over the following fractions; H: homogenate, M: microsomes, C: cytosol. Blots in the lower panel were probed with 1093 serum and represent RyR2 distribution

The distribution of the BT4L fragment in the microsomal versus cytosolic fraction upon co-expression with full-length RyR2 containing arrhythmia-associated mutations was quantitatively analysed by densitometry and expressed relative to the distribution observed for RyR2<sup>WT</sup>/BT4L (Graph 6.8). This analysis confirmed the initial observations; indeed both mutations resulted in statistically significant decline in the amount of BT4L in microsomal fraction implying that the presence of R176Q and L433P mutations perturbs the physical association of the BT4L fragment with the full length channel. While the introduction of the R176Q mutation induced a relatively small drop in the amount of the BT4L fragment being translocated into microsomes (Graph 6.8, left panel), the effect of L433P mutation was considerably more pronounced (27% reduction) (Graph 6.8, right panel).



**Graph 6.8** Sub-cellular distribution of the BT4L fragment upon co-expression with RyR2<sup>R176Q</sup> and RyR2<sup>L433P</sup> relative to the distribution of BT4L co-expressed with RyR2<sup>WT</sup> (left and right panel respectively). Results presented as microsomes/cytosol ratio calculated using densitometry. Data shown as mean +/- SEM, n=6 and n=4 for RyR2<sup>R176Q</sup> and RyR2<sup>L433P</sup> respectively, \* and \*\* statistical significance at p<0.05 and at p<0.01 respectively calculated using paired, 2-tailed Student's t test

## 6.4 Discussion

The goal of the study presented in this Chapter was to evaluate the effect of two N-terminal arrhythmia-linked mutations on RyR2 N-terminus oligomerisation. This task was performed using three independent techniques; chemical crosslinking, co-immunoprecipitation and yeast two-hybrid system. Moreover, tetramerisation of BT4L<sup>WT</sup> and the two mutants (BT4L<sup>R176Q</sup> and BT4L<sup>L433P</sup>) was investigated in the presence of dantrolene. In addition, the effect of arrhythmia-linked mutations on the interaction between the full length RyR2 and the BT4L fragment was assessed.

RyR2 mutations are associated with episodes of life-threatening arrhythmias. A disease phenotype becomes apparent upon  $\beta$ -adrenergic stimulation and on a cellular level is considered to result from abnormal calcium handling during diastole (Betzenhauser and Marks 2010). While elevated calcium levels are clearly a consequence of RyR2 dysfunction, the molecular mechanism behind abnormal channel gating remains elusive and controversial. Currently proposed theories for RyR2 dysfunction have been mainly based on data obtained in experiments performed on heterologously expressed channels and evaluation of animal models. At present there are a few working hypotheses including abnormal RyR2 binding of FKBP12.6 (Wehrens et al. 2003), reduced threshold for store-overload-induced

calcium release (Jiang et al. 2005) and RyR2 N-terminal – central domain unzipping (Uchinoumi et al. 2010). The involvement of the N-terminus inter-subunit interaction in RyR1 function and its putative disruption by MH/CCD-associated mutations has been very recently proposed (Kimlicka et al. 2013). Based on the docking of the RyR1 N-terminus structure into the cryo-EM map of the full-length RyR1 in an open versus closed conformation, it was suggested that the N-terminus inter-subunit contact is disrupted upon channel opening. The authors also solved crystal structures of several disease mutants and proposed that MH-associated mutations weaken interactions at the N-termini inter-subunit contact site rendering the channel more prone to activation (Kimlicka et al. 2013). However, their model of N-terminus self-association was based on *in silico* data.

#### 6.4.1 Oligomerisation of RyR2 N-terminus is affected by arrhythmia-linked mutations

The biochemical data presented in this Chapter clearly indicate that RyR2 N-terminus self-association is reduced in the presence of arrhythmia-linked mutations. The two mutations investigated in this study R176Q and L433P, were initially identified in patients diagnosed with ARVD2, a condition, which in addition to stress-induced life-threatening arrhythmia, is characterised by a progressive degeneration of the right ventricle (Tiso et al. 2001). However, they were later found in individuals with a typical CPVT phenotype (Tester et al. 2005b; Haugaa et al. 2010). In chemical crosslinking, both mutations severely compromised the ability of the BT4L fragment to tetramerise (Figure 6.4 and 6.5, Graph 6.1. and 6.2). According to the docking of the RyR1 N-terminus into the cryo-EM map of the full-length channel (Tung et al. 2010), R176Q is located at the proposed inter-subunit interface (Figure 6.14). Moreover, this residue is located in the  $\beta$ 8- $\beta$ 9 loop previously suggested to be involved in the gating of IP<sub>3</sub>R (Seo et al. 2012). Notably, the reduced ability of R176Q to form tetramers corroborated earlier findings presented in Chapter 4, i.e. the severely impaired oligomerisation of the BT4L <sup>$\beta$ 8- $\beta$ 9loop</sup> deletion mutant, in which residues 167-178 are missing. The L433P mutation, which also compromised BT4L oligomerisation, does not reside at the inter-subunit boundary (Figure 6.14).

However, the L433P constitutes part of an  $\alpha$ -helix which would be expected to be severely disrupted upon mutation to a rigid proline. This could in turn trigger long-distance alterations at the inter-subunit contact site, in agreement with the model proposed by Kimlicka and colleagues, in which MH-associated mutations that do not directly map to the inter-subunit interface have the ability to exert allosteric changes which eventually affect this interface in RyR1 (Kimlicka et al. 2013).

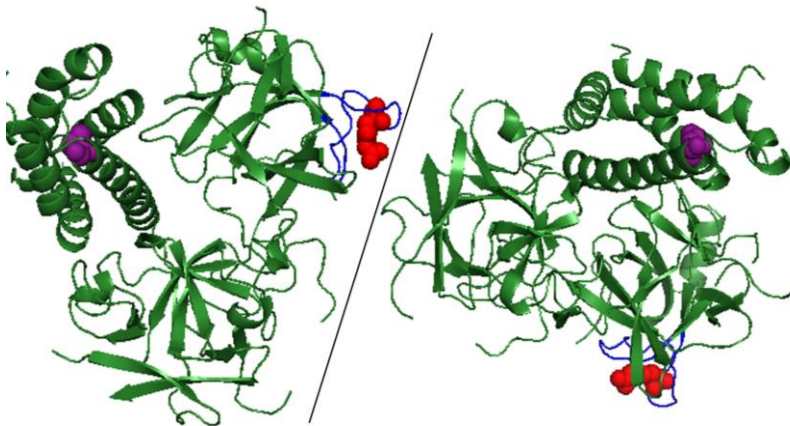


**Figure 6.14** Image showing the location of two arrhythmia-associated mutations (R176Q and L433P in red and purple respectively) relative to the predicted inter-subunit interface (depicted by a line); loop  $\beta$ 8-  $\beta$ 9 in blue

Mutations in RyR2 associated with life-threatening ventricular arrhythmia have been shown to have a dominant phenotype. Hence, the observations obtained in chemical crosslinking experiments do not directly reflect the situation in patients where both wild-type and mutated forms of RyR2 are expected to be present. To imitate the heterozygous scenario, a co-immunoprecipitation assay between the wild-type RyR2 N-terminus (AD4L) and mutation-containing BT4L fragments ( $BT4L^{R176Q}$  and  $BT4L^{L433P}$ ) was performed. Interestingly, in this assay  $BT4L^{R176Q}$  did not exhibit a significantly reduced ability to interact with its wild-type counterpart while the L433P substitution still had a profound effect (Figure 6.6 and 6.7, Graph 6.3). In agreement with the above findings, yeast two-hybrid system analysis yielded similar results; the R176Q mutant interaction with the BT4L fragment was negligibly affected, while the self-association process was impaired (Graph 6.4, left panel). Although in the latter

case, the reduction did not reach statistical significance, in combination with the crosslinking data, this outcome suggests a biologically significant phenomenon.

Although the yeast two-hybrid system has an invaluable advantage over biochemical assays in respect to its ability to evaluate protein-protein interactions *in vivo* an additional note should be made. An unquestionable drawback of this method is the rate of false-positives and false-negatives, which in most cases is believed to originate from the fact that the proteins under investigation are fused to yeast proteins (GAL4 DNA-BD and AD). This has the potential to introduce conformational changes in both, i.e. proteins of interest and yeast proteins resulting in altered propensity for protein-protein interaction and the ability to activate transcription, respectively. Secondly, physiologically relevant species formed by the BT4L fragment are tetramers, while the interaction in yeast is evaluated at the level of a dimer. Nevertheless, the *in vivo* data are consistent with earlier observations from biochemical experiments, i.e. the R176Q mutation reduces N-terminus oligomerisation in a homozygous scenario, however its effect seems to be insignificant in the heterozygote case, at least in yeast.

In agreement with the results obtained in co-immunoprecipitation, the presence of the L433P mutation profoundly impaired the formation of mixed oligomers in the yeast two-hybrid system (Graph 6.4, right panel). Notably, in *in vivo* conditions, the effect of this mutation was much more pronounced than in the biochemical assay, i.e. the association between BT4L<sup>L433P</sup> and the wild-type fragment was reduced by 87% while the interaction with itself was reduced to 2.6% of the wild-type self-association.

The biochemical and *in vivo* data obtained in this study strongly imply that N-terminus association becomes impaired upon introduction of mutations linked to ventricular arrhythmia in patients. Thus, defective N-terminus oligomerisation might underlie the molecular mechanism leading to abnormal RyR2 channel function. Moreover, the severity of the disease phenotype, i.e. the weakening of the RyR2 N-termini inter-subunit interaction, depends on the mutation site as seen with R176Q and L433P investigated here. A substantial functional heterogeneity between R176Q and L433P mutations was shown upon heterologous expression in HEK293 cells (Thomas et al. 2004). The presence of the R176Q substitution resulted in enhanced sensitivity to caffeine activation and augmented peak calcium release, a phenomenon

well documented for RyR2 mutations associated with cardiac arrhythmias. Unexpectedly, the L433P mutant channel exhibited significantly desensitised caffeine-activation profile with concomitant increase in the calcium release rate and transient duration. Since the decreased activation sensitivity of this particular mutant was counterbalanced by an increase in the calcium release rate and duration it is not surprising that on a global level both mutations resulted in a similar phenotype. However, other groups reported that the L433P substitution leads to effects indistinguishable from other arrhythmia-linked mutations, i.e. increased sensitivity to luminal calcium and to caffeine activation (Jiang et al. 2005). The reason for these conflicting findings is not clear as both groups used the HEK293 cell system to study the functional effects of this mutation. Thus the results obtained in this study confirm substantial heterogeneity of arrhythmia-associated mutations despite nearly identical clinical symptoms. A clear difference in the precise mechanism behind RyR2 pathology, which at the cellular level ultimately results in elevated diastolic calcium, is further supported by an inconsistency observed in the response to drug treatments, e.g. JTV519 was shown to be effective only in selective cases of genetic or acquired defects in RyR2 (Yano et al. 2003; Liu et al. 2006; Hunt et al. 2007; Hamada et al. 2009; Suetomi et al. 2011; Sacherer et al. 2012).

#### 6.4.2 Dantrolene

Having established that arrhythmia-linked mutations disrupt N-terminus self-association, it was investigated whether defective RyR2 N-terminal inter-subunit interactions can be restored by dantrolene. This compound was used as its putative binding site is located in the RyR2 N-terminus (residues 601-620) (Paul-Pletzer et al. 2005). Dantrolene was synthesised in 1967 as a new class of skeletal muscle relaxant and since 1977 has been widely used to treat MH, a pharmacogenetic disorder associated with RyR1 mutations (Inan and Wei 2010). Although RyR1 and RyR2 share a consensus sequence for its binding, the latter showed to be unaffected by dantrolene both in native cardiomyocytes and when heterologously expressed in HEK293 cells (Zhao et al. 2001). In agreement with these findings, tetramerisation of

the wild-type BT4L fragment in the presence of this drug remained unchanged (Figure 6.9, Graph 6.5).

It was later suggested that the dantrolene-binding site is conformation-sensitive becoming accessible in dysfunctional RyR2. This hypothesis was supported by a number of reports showing a therapeutic effect of this drug in RyR2-associated disorders (Uchinoumi et al. 2010; Xu et al. 2010). So far the therapeutic effect of dantrolene was investigated in animal models for mutations located in the central portion of the protein (Kobayashi et al. 2010) and RyR2 dysfunction associated with heart failure (Kobayashi et al. 2009; Maxwell et al. 2012). A relatively recent report presented convincing evidence for dantrolene's ability to rescue the arrhythmic phenotype in cardiomyocytes derived from patient-specific, induced pluripotent stem cells carrying a RyR2 N-terminal mutation (S406L) (Jung et al. 2012).

The molecular mechanism underlying the dantrolene effect on RyR2 has been suggested to involve stabilisation of N-terminal – central domain interactions across subunits (Kobayashi et al. 2010; Uchinoumi et al. 2010; Suetomi et al. 2011). However, a more recent FRET-based study proposed that dantrolene does not bind at the N-terminal – central domain interface but it stabilises it via allosteric effects involving a number of additional domain-domain contacts (Wang et al. 2011).

The present study sheds new light on the dantrolene mechanism of action. In chemical crosslinking dantrolene promoted tetramer formation of RyR2 N-terminus carrying the L433P mutation (Figure 6.11 and Graph 6.7). Similar observations were made for the R176Q mutation, although data did not reach statistical significance (Figure 6.10 and Graph 6.6). As the dantrolene effect on oligomerisation of the RyR2 N-terminus is evident in the absence of other putative domains, dantrolene's primary mode of action might involve stabilisation of mutation-induced, defective N-terminus self-interaction across subunits. This effect appears to be mutation-dependent as there is a significant rescue of aberrant N-terminus self-association in the case of L433P mutant but a less pronounced effect for R176Q. Notably, the R176Q mutation corresponds to the RyR1 MH-associated mutation (R163C), which symptoms were shown to be attenuated by dantrolene (Cherednichenko *et al.* 2008). Thus, the reduced ability of dantrolene to increase tetramer formation in the presence of R176Q in a biochemical assay does not preclude the possibility that this effect is sufficient to

be of biological significance. Interestingly, dantrolene efficacy was mostly statistically insignificant in reducing conditions, indicating that disulphide bonds might have a role in maintaining this type of inter-subunit interaction.

### 6.4.3 Compromised association between exogenous N-terminus and RyR2 containing arrhythmia-linked mutations

The presence of arrhythmia-linked mutations in the full length channel, reduce its interaction with the BT4L fragment (Figure 6.12 and 6.13, Graph 6.8). Again, this reduction in association is mutation dependent with L433P having a more pronounced effect. The reduced interaction of the exogenous wild-type N-terminal fragment (BT4L) with the mutant RyR2 channel might be interpreted as BT4L having a higher affinity for self-interaction rather than forming weaker, “mixed” interactions with the mutant N-terminus domain of full-length channels. Further to the above, it would also imply that the presence of the R176Q mutation has the ability to compromise N-terminus interaction in a heterozygote scenario, an effect that was beyond detection in the yeast two-hybrid system. Thus, these findings further support the proposed hypothesis that disruption of the N-terminal inter-subunit interface by arrhythmia-associated mutations might underlie the molecular mechanism of channel dysfunction that directly links to the disease phenotype.

### 6.4.4 Final remarks

The study presented in this Chapter provided evidence that the presence of arrhythmia-linked mutations disrupts N-terminus self-association and that mutation-induced defective tetramerisation can be restored by dantrolene. In Chapter 5, it was shown that the exogenous BT4L fragment activates RyR2 at diastolic calcium concentrations imitating the effects produced by arrhythmia-linked mutations. It was speculated that this phenomenon is a consequence of the BT4L fragment disrupting N-terminus interactions occurring between subunits in the full-length channel. Thus,

these observations suggest that mutation-induced defective N-terminus interactions might constitute a direct link to RyR2 increased activity at diastolic calcium levels.

# Chapter 7

Further insights into the L433P  
mutation

## 7 Further insights into the L443P mutation

### 7.1 Introduction

The findings presented in the previous Chapter indicate that the L433P mutation severely disrupts N-terminus self-association. This effect was consistently observed in experiments based on three independent techniques including chemical crosslinking, co-immunoprecipitation and *in vivo* assay using the yeast two-hybrid system. Notably, a significant rescue of the mutation-induced phenotype was observed in the presence of dantrolene, which has pronounced implications for the potential use of this drug in the treatment of RyR2 dysfunction. In order to further validate those findings, a detailed study into the oligomerisation properties of this mutation in the context of the full length RyR2 was undertaken. For this purpose, microsomal fractions obtained from HEK293 cells expressing RyR2<sup>L433P</sup> and RyR2<sup>WT</sup> were subjected to sucrose density gradient centrifugation. This method separates molecules primarily on the basis of their size under non-denaturing conditions therefore allowing for non-covalent interactions to be retained. Functional characterisation of RyR2<sup>L433P</sup> was performed using [<sup>3</sup>H]ryanodine binding assay to underpin the mechanism of channel dysfunction. Moreover, the hypothesis of the mutation-induced disruption of the N-terminus inter-subunit interactions in the full length channel was tested. For this purpose, [<sup>3</sup>H]ryanodine binding was employed to evaluate whether the presence of the exogenous BT4L fragment is able to alter channel properties in a manner similar to the one observed for wild-type RyR2. The reasoning behind this experimental approach was that if the N-terminus interaction was already defective in RyR2<sup>L433P</sup> leading to the hypersensitive phenotype, BT4L should not promote channel activation. RyR2<sup>L433P</sup> oligomerisation and function were further tested in the presence of dantrolene.

## 7.2 Methods

### 7.2.1 [ $^3\text{H}$ ]ryanodine binding assay – RyR2<sup>WT</sup> versus RyR2<sup>L433P</sup>

[ $^3\text{H}$ ]ryanodine binding was performed on cell homogenates instead of microsomes. The rationale behind the use of cell homogenates as opposed to microsomes was based on the fact that in subsequent assays we aimed to test whether the co-expression of the BT4L fragment with full length RyR2<sup>L433P</sup> affects channel activity. Since it was earlier showed that the majority of the BT4L fragment remains in the cytosol when co-expressed with RyR2<sup>L433P</sup> (Chapter 6), there was a possibility that the reduced BT4L levels (compared to when BT4L is co-expressed with RyR2<sup>WT</sup>) in the microsomal fraction might be too low to mediate any functional effects. Briefly, for a typical [ $^3\text{H}$ ]ryanodine binding assay ten 100mm Petri dishes were transfected with either RyR2<sup>WT</sup> or RyR2<sup>L433P</sup>. 24 hour post-transfection, cells were homogenised on ice using a custom-made cell homogeniser allowing for 25 passages through a needle (0.6x30 mm). Assays were performed on cell homogenates obtained following a 1500 xg centrifugation step. Total protein content was evaluated using the BCA assay. RyR2<sup>WT</sup> and RyR2<sup>L433P</sup> expression was evaluated on two levels; initially by densitometry-based analysis of Western blotted fractions and subsequently by [ $^3\text{H}$ ]ryanodine binding assay performed in conditions promoting maximum channel activation and therefore leading to the measurement of total RyR2 content. Cell homogenates obtained from untransfected HEK293 cells were used to ascertain equal total protein content between samples. [ $^3\text{H}$ ]ryanodine binding was performed as described in Section 2.2.2.8. Dose response curves were fitted with GraphPad Prism using four-parameter sigmoidal model. Statistical analysis was performed using the extra-sum of squares F test (GraphPad Prism).

## 7.2.2 [<sup>3</sup>H]ryanodine binding assay – evaluating the effect of the BT4L fragment

[<sup>3</sup>H]ryanodine binding was performed on cell homogenates obtained from HEK 293 cells transfected with the full length RyR2<sup>L433P</sup> or RyR2<sup>WT</sup> alone or in combination with the BT4L fragment. The procedure was carried out as described in Section 7.2.1.

## 7.2.3 Sucrose density gradient ultracentrifugation

For sucrose density gradient ultracentrifugation cell pellets of HEK293 cells expressing RyR2<sup>WT</sup> or RyR2<sup>L433P</sup> were typically harvested from 8-10 100 mm Petri dishes and processed as described in Section 2.2.2.7. Dantrolene effect was evaluated in separate experiments. Briefly, homogenised cells were centrifuged at 1500 xg for 10 min to remove unbroken cells and nuclei. Supernatants, divided into three aliquots and treated with or without dantrolene (1 µM), were subjected to centrifugation at 100 000 xg for an hour in order to obtain microsomal fractions. One of the microsomal pellet aliquots was used to evaluate protein concentration by the BCA assay. The remaining two pellets (one of them dantrolene-treated) were re-suspended at a protein concentration of 2.5 mg/ml in the high-salt solubilisation buffer and the dantrolene-treated sample was additionally supplemented with dantrolene to 1 µM final concentration. Following solubilisation and subsequent centrifugation to remove the insoluble material, the supernatant was layered onto the sucrose density gradient prepared as described in section 2.2.2.7. For dantrolene-containing samples separate sucrose gradients were prepared which were supplemented with dantrolene (1 µM). RyR2 distribution was evaluated by Western blotting. Quantitative analysis was performed using densitometry.

#### 7.2.4 [<sup>3</sup>H]ryanodine binding assay - dantrolene effect

Microsomal fractions obtained from HEK293 cells expressing RyR2<sup>L433P</sup> were subsequently subjected to [<sup>3</sup>H]ryanodine binding assays for the evaluation of dantrolene effect. Prior to the actual assay, 115-125 µg of microsomes were incubated with or without dantrolene for an hour at room temperature in the ryanodine binding buffer with free Ca<sup>2+</sup> concentrations adjusted to 100 nM, 1 µM and 100 µM. [<sup>3</sup>H]ryanodine binding was performed as described before.

### 7.3 Results

#### 7.3.1 RyR2<sup>L433P</sup> displays unique calcium dependence of [<sup>3</sup>H]ryanodine binding

As described in Methods (Section 7.2.1), it was assured that equal amounts RyR2<sup>WT</sup> and RyR2<sup>L433P</sup> were subjected to [<sup>3</sup>H]ryanodine binding. The expression level of the two proteins, assessed by Western blotting was found to be comparable (Figure 7.1). Protein expression was further quantified by densitometry and the amount of cell homogenate was adjusted accordingly and subjected to [<sup>3</sup>H]ryanodine binding in conditions promoting maximum channel activation (100 µM Ca<sup>2+</sup>, 10 mM caffeine). Typically, this step enables to evaluate the capacity of cell preparations for maximum [<sup>3</sup>H]ryanodine binding which reflects the total amount of functional RyR2 protein expressed. This is necessary to normalise the data for comparison between samples of different origin.

It has been shown that arrhythmia-linked mutations enhance the basal level of [<sup>3</sup>H] ryanodine binding, i.e. the differences between native and mutated channels can be primarily observed at sub-activating Ca<sup>2+</sup> levels (Jiang et al. 2004). This observation implies that in conditions promoting maximum activation of RyR2, mutation-associated differences in channel behaviour are eliminated. Therefore, evaluation of

maximum binding is considered an appropriate and valuable tool to obtain information concerning total amount of receptors present in the sample. However, there was no substantial [<sup>3</sup>H]ryanodine binding observed for RyR2<sup>L433P</sup> at any of the activating calcium concentration tested (Graph 7.1). Maximum [<sup>3</sup>H]ryanodine binding levels did not reach those observed for wild-type RyR2, even when we used twice as much material as the protein expression levels would imply.

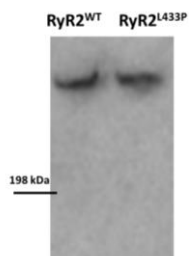
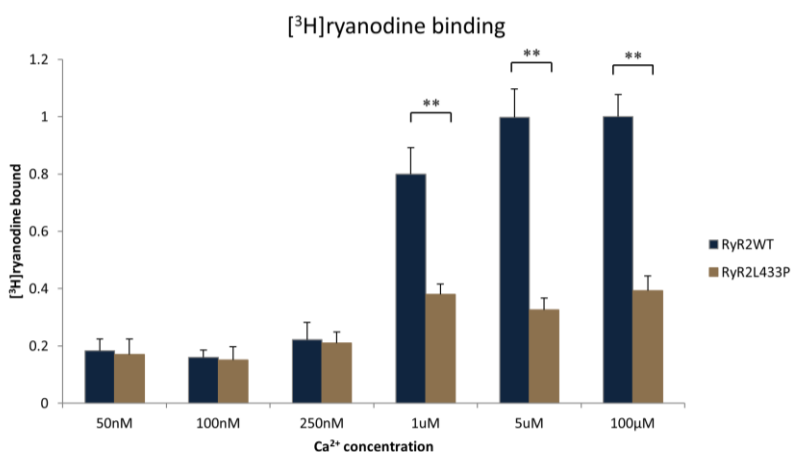
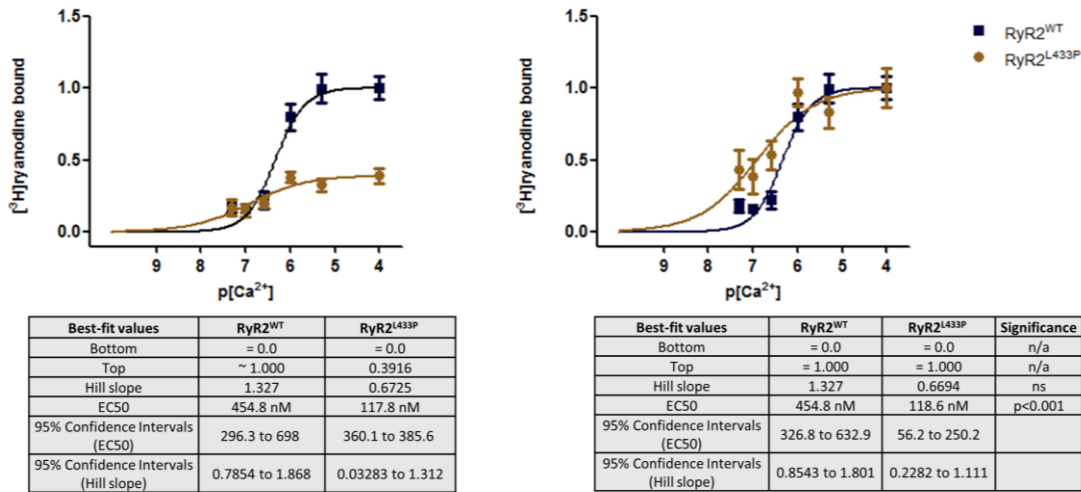


**Figure 7.1** Western blotting showing protein levels of RyR2<sup>WT</sup> and RyR2<sup>L433P</sup> upon heterologous expression in HEK293 cells.



**Graph 7.1** [<sup>3</sup>H]ryanodine binding assays of HEK293 cell homogenates expressing RyR2<sup>WT</sup> and RyR2<sup>L433P</sup> over a range of free Ca<sup>2+</sup> concentrations. Data presented relative to maximum binding obtained for the wild-type RyR2 at 100 μmol/l Ca<sup>2+</sup>. Data shown as mean +/-SEM, n=5 for 50-250 nM and n=3 for 1-100 μM Ca<sup>2+</sup> each performed at least in duplicate, \*\* statistical significance at p<0.01 calculated using unpaired, 2-tailed Student's t test

The results presented in Graph 7.1 summarise the data obtained for calcium dependence of [<sup>3</sup>H]ryanodine binding for RyR2<sup>L433P</sup> relative to RyR2<sup>WT</sup>. Dose-response curves of the above results are presented in the left panel in Graph 7.2. As shown in Graph 7.1, RyR2<sup>L433P</sup> activation is significantly diminished relative to RyR2<sup>WT</sup> (below 40 % of wild-type RyR2 at 100 μM Ca<sup>2+</sup>). As the equal amount of recombinant proteins was used, the reduced [<sup>3</sup>H]ryanodine binding in conditions promoting channel activation, implies that either RyR2<sup>L433P</sup> is unresponsive to Ca<sup>2+</sup> or exhibits reduced binding affinity for ryanodine. As high-affinity ryanodine-binding requires RyR2 tetramer (Lai et al. 1989; Tanna et al. 1998), the latter explanation would suggest that in the presence of the L433P mutation tetramer arrangement might be compromised. Moreover, contrary to the well accepted hypersensitisation to diastolic calcium exhibited by RyR2 in the presence of arrhythmia-linked mutations (Jiang et al. 2002a; Jiang et al. 2004; Fernández-Velasco *et al.* 2009), the RyR2<sup>L433P</sup> channel did not exhibit increased basal activity, i.e. no enhanced [<sup>3</sup>H]ryanodine binding at low Ca<sup>2+</sup> concentrations was observed (Graph 7.1). However, this apparent disagreement with the gain-of-function phenotype observed for other CPVT/ARVD2-associated mutations, might in fact originate from the manner in which data are normalised. In the left panel in Graph 7.2 the data for both RyR2<sup>WT</sup> and RyR2<sup>L433P</sup> are presented relative to the maximum value obtained for the wild-type channel at 100 μM Ca<sup>2+</sup>. However, when the RyR2<sup>L433P</sup> data are normalised to its own [<sup>3</sup>H]ryanodine maximum binding as presented in the right panel of Graph 7.2, it becomes clear that RyR2<sup>L433P</sup> is in fact hypersensitive to calcium-mediated activation with a significantly lower EC<sub>50</sub> (RyR2<sup>L433P</sup> EC<sub>50</sub>=118.6 nM Ca<sup>2+</sup> versus 454.8 nM Ca<sup>2+</sup> for RyR2<sup>WT</sup>, p=0.003). Nevertheless, it is important to point out that the direct comparison of EC<sub>50</sub> between RyR2<sup>L433P</sup> and RyR2<sup>WT</sup> masks important aspects of the functional impairment of this mutant. In addition, the presence of L433P substitution resulted in a slight inhibition of the channel at 5μM calcium, a phenomenon that was consistently observed throughout the experiments.

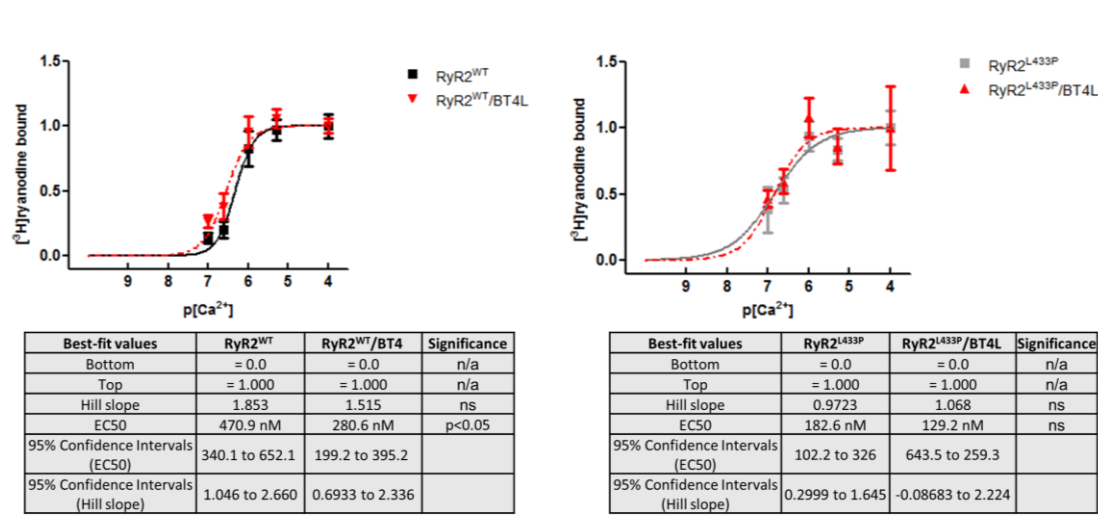


**Graph 7.2** Dose-response curves for RyR2<sup>WT</sup> and RYR2<sup>L433P</sup> of the [<sup>3</sup>H]ryanodine binding data (obtained as described in Graph 7.1) fitted with GraphPad Prism using four-parameter logistic model. Best-fit values shown in the table; n/a (non-applicable), ns (not significant). Statistical analysis performed on data where RYR2<sup>L433P</sup> results are normalised to its own maximum binding (100 μM Ca<sup>2+</sup>), right panel.

### 7.3.2 RyR2<sup>L433P</sup> calcium sensitivity remains unchanged in the presence of the BT4L fragment

In the study presented in Chapter 5, the co-expression of the BT4L fragment with RyR2<sup>WT</sup> promoted channel activation at sub-threshold Ca<sup>2+</sup> thus imitating the effect of arrhythmia-linked mutations. It was speculated that the increased activity of the channel in the presence of exogenous BT4L is due to the disruption of “endogenous” N-terminus self-association within the RyR2<sup>WT</sup> tetrameric assembly. Thus, it was next investigated whether the observed RyR2<sup>L433P</sup> channel dysfunction is due to defective N-terminal inter-subunit interactions. If the above hypothesis was correct, the presence of the exogenous (BT4L) N-terminus should have no effect on RyR2<sup>L433P</sup> function. Since these experiments were performed on cell homogenates as opposed to microsomal fractions (Chapter 5) for reasons explained in Section 7.2.1, the effect of the exogenous BT4L on RyR2<sup>WT</sup> was tested again. In agreement with the notion that N-terminus self-association is already disrupted in the mutated channel, the RyR2<sup>L433P</sup> calcium dose response curve did not significantly change in the

presence of the BT4L fragment (Graph 7.3, right panel). These observations are also in agreement with the substantially reduced interaction of the RyR2<sup>L433P</sup> mutant with the BT4L fragment as we showed earlier (Chapter 6). Notably, there was a significant left-shift of the dose-response curve for the wild-type RyR2 in the presence of the exogenous BT4L (RyR2<sup>WT</sup> EC<sub>50</sub>=470.9 nM Ca<sup>2+</sup> versus 280.6 nM Ca<sup>2+</sup> for RyR2<sup>WT</sup>/BT4L, p=0.0247) (Graph 7.3, left panel) which corroborated earlier findings obtained in [<sup>3</sup>H]ryanodine binding assay performed on microsomal fractions (Chapter 5). These results suggest that the disruption of RyR2 N-terminus self-association might underlie the mechanism by which the L433P mutation triggers channel dysfunction.



**Graph 7.3** Dose-response curves of [<sup>3</sup>H]ryanodine binding data for RyR2<sup>WT</sup> (left panel) and RyR2<sup>L433P</sup> (right panel) expressed alone or in combination with the BT4L fragment fitted with GraphPad Prism using four-parameter logistic model with bottom and top constrained to 0 and 1 respectively and normalised to each maximum binding obtained at 100 μM Ca<sup>2+</sup>. Best-fit values shown in the table; n/a (non-applicable), ns (not significant). Data shown as mean +/-SEM, n=5 for 100-250 nM and n=3 for 1-100 μM Ca<sup>2+</sup> each performed at least in duplicate

### 7.3.3 RyR2<sup>L433P</sup> channels dissociate into monomers upon sucrose density gradient centrifugation

The substantially reduced [<sup>3</sup>H]ryanodine binding of RyR2<sup>L433P</sup> under conditions of maximal activation prompted investigation into the oligomerisation properties of this mutant channel, since ryanodine requires RyR tetrameric assembly to bind. This was performed by sucrose density gradient centrifugation, a technique that separates proteins according to their size under non-denaturing conditions, thereby allowing protein oligomers to be retained. Indeed, wild-type RyR2 was almost exclusively present in “heavy” sucrose fractions between 23-31% implying that RyR2<sup>WT</sup> is retained as a tetramer (Figure 7.2, upper panel). The RyR2<sup>L433P</sup> distribution however did not follow the same pattern, i.e. the protein was in fact spread over almost the entire sucrose fractions (Figure 7.2, lower panel). Moreover, mutated channel seemed to be slightly enriched in “light” sucrose fractions most likely representing RyR2<sup>L433P</sup> monomer. This phenomenon was observed in three independent experiments. Cumulative data following densitometry analysis of protein distribution are presented in Graph 7.4. These findings imply that the presence of the L433P substitution considerably destabilises the channel and promotes subunit dissociation upon solubilisation and subsequent sucrose density gradient centrifugation.

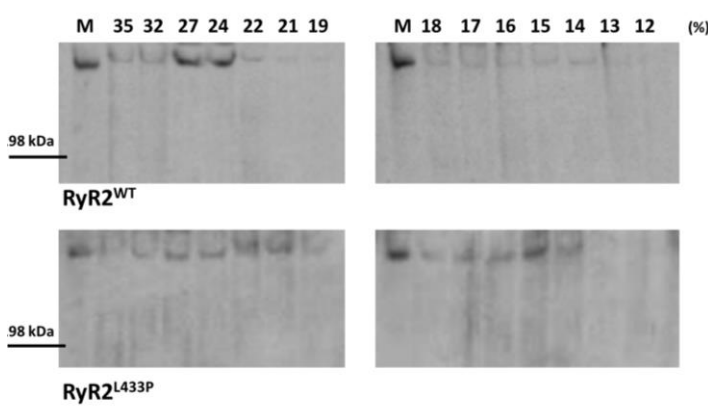
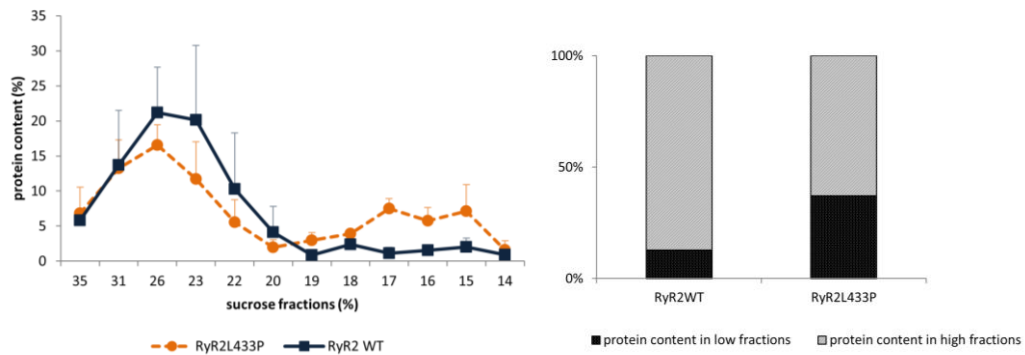


**Figure 7.2** Distribution of RyR2<sup>WT</sup> (upper panel) and RyR2<sup>L433P</sup> (lower panel) channels in fractions obtained following sucrose density gradient centrifugation. Sucrose concentration as indicated, M: microsomes (25 µg)



**Graph 7.4** Cumulative data following densitometry analysis ( $n=3$ ). Left panel: protein distribution in all sucrose fractions tested (14-35%) for RyR2<sup>WT</sup> and RyR2<sup>L433P</sup> (data presented as mean +/- SEM), right panel: relative protein content in high (20-35%) and low (14-19%) sucrose fractions for RyR2<sup>WT</sup> and RyR2<sup>L433P</sup>

### 7.3.4 Dantrolene increases tetramer stability

In follow-up experiments, it was tested whether dantrolene would reverse the destabilisation of the RyR2<sup>L433P</sup> tetramer. The rationale behind those experiments was based on the fact that dantrolene was able to rescue the reduced N-terminus self-association of the BT4L<sup>L433P</sup> fragment (Chapter 6). Remarkably, dantrolene promoted a substantial redistribution of RyR2<sup>L433P</sup> protein (Figure 7.3). In fact, dantrolene promoted a pattern almost identical to that observed for wild-type channels, i.e. reduced the spread of RyR2<sup>L433P</sup> and increased its presence concentration in “heavy” sucrose fractions. Cumulative data are summarised in Graph 7.4.

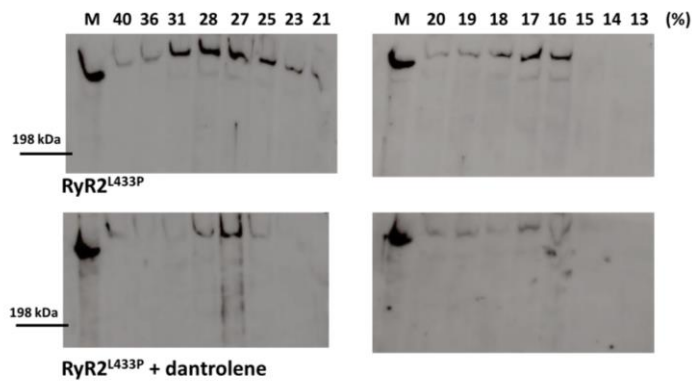
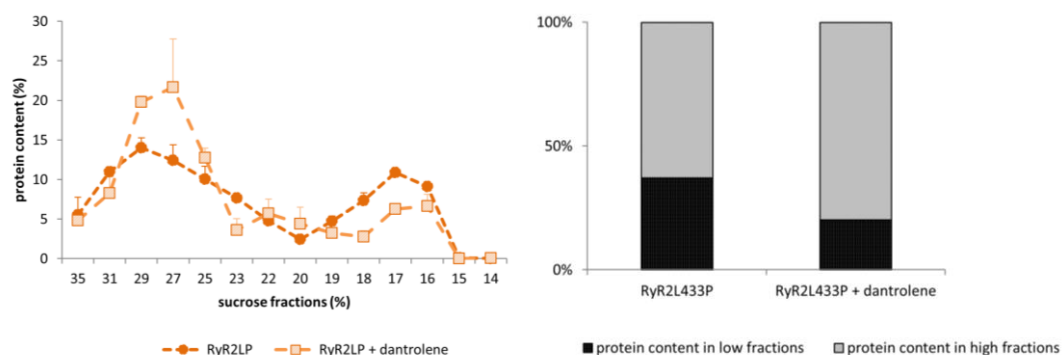


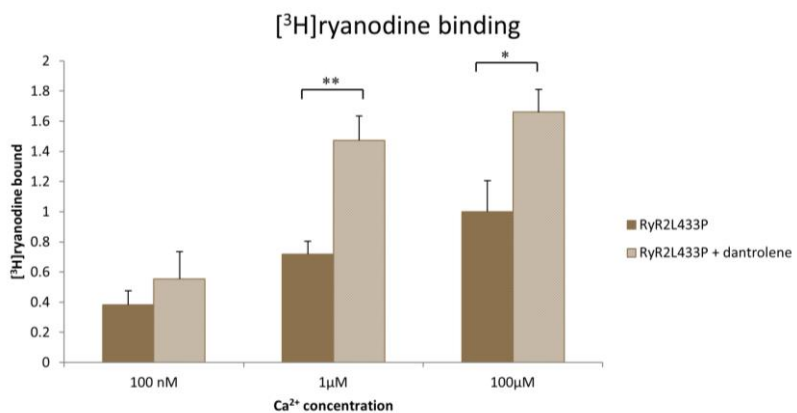
**Figure 7.3** Distribution of  $\text{RyR2}^{\text{L433P}}$  channels in the presence and absence of dantrolene (lower and upper panel respectively) in fractions obtained following sucrose density gradient centrifugation. Following cell homogenisation, 1  $\mu\text{M}$  dantrolene was included in all buffers used in the assay. Sucrose concentration as indicated, M: microsomes (25  $\mu\text{g}$ )



**Graph 7.5** Cumulative data following densitometry analysis ( $n=3$ ). Left panel: protein distribution in all sucrose fractions tested (14-35%) for  $\text{RyR2}^{\text{L433P}}$  in the presence and absence of dantrolene (data presented as mean +/- SEM), right panel: relative protein content in high (20-35%) and low (14-19%) sucrose fractions for  $\text{RyR2}^{\text{L433P}}$  (with and without dantrolene)

### 7.3.5 Dantrolene changes RyR<sup>L433P</sup> ryanodine binding profile

The substantial redistribution of RyR2<sup>L433P</sup> channels into “heavy” sucrose fractions in the presence of dantrolene suggests that dantrolene stabilises the RyR2<sup>L433P</sup> tetrameric assembly. It was earlier shown that RyR2<sup>L433P</sup> displays atypical calcium dependence of [<sup>3</sup>H]ryanodine binding (section 7.3.1) which was speculated to reflect reduced affinity for ryanodine due to the compromised tetrameric assembly of the mutant channel. Indeed, the findings from sucrose gradient centrifugation implied that RyR2<sup>L433P</sup> forms tetramers of decreased stability. Thus if the reduced [<sup>3</sup>H]ryanodine binding observed for RyR2<sup>L433P</sup> is directly correlated to the disrupted association between channel subunits, dantrolene should also increase [<sup>3</sup>H]ryanodine binding. Indeed, dantrolene promoted a substantial and statistically significant increase in [<sup>3</sup>H]ryanodine binding in the activating calcium range (1 and 100 μM) while it had a negligible effect at diastolic calcium (Graph 7.6).



**Graph 7.5** Graph illustrating the functional effect of dantrolene (1μM) on RyR2<sup>L433P</sup> as assessed by [<sup>3</sup>H] ryanodine binding. Results presented relative to the maximum binding obtained without the drug. Data shown as mean +/-SEM, n=3 each performed at least in duplicate, single and double asterisks indicate statistical significance at p<0.05 and p<0.01 respectively calculated using 2-tailed Student's t test

## 7.4 Discussion

Evidence that arrhythmia-associated mutations disrupt the self-association of the RyR2 N-terminus was presented in Chapter 6. In Chapter 5 it was shown that, in the full-length channel, a tight inter-subunit interaction of the N-terminus is likely to prevent its spontaneous activation at diastolic calcium levels. In this Chapter the effects of one particular missense mutation L433P were evaluated further in respect to RyR2 function and tetramer stability. It was shown that the exogenous BT4L fragment has no effect on [<sup>3</sup>H]ryanodine binding of RyR2<sup>L433P</sup> contrary to the hypersensitising effect it has on wild-type RyR2 (Graph 7.3). This finding supports the hypothesis that N-terminus self-association is already defective in the mutated channel and that defective interaction within this interface is most likely the mechanism by which the L433P mutation triggers channel dysfunction. In Chapter 6 it was shown that the presence of L433P in the full-length channel impairs its interaction with the BT4L fragment (Graph 6.8). Thus one might argue that the lack of functional effect on RyR2<sup>L433P</sup> might in fact result arise solely from the reduced association between the two. However, the cumulative data strongly imply that it is the pre-existing defect in the N-terminus self-interaction within the mutated channel that determines the BT4L failure to promote hypersensitisation of RyR2<sup>L433P</sup>. This notion is supported by the following findings: the presence of the L433P mutation impairs N-terminus self-association (Chapter 6), inter-subunit interactions within full-length RyR2<sup>L433P</sup> are compromised as shown by tetramer dissociation in sucrose density gradient centrifugation (Section 7.3.3). Moreover, based on data obtained in the yeast two-hybrid assay (Graph 6.4), one would expect the endogenous self-association of RyR2<sup>L433P</sup> N-terminus (i.e. homozygote scenario) to be much more compromised than formation of “mixed interaction” between the exogenous BT4L and endogenous N-terminus. This is further supported by the observations that although reduced, the interaction between BT4L and RyR2<sup>L433P</sup> still takes place as assessed in sub-cellular fractionation experiments (Section 6.3.5).

The molecular mechanism of channel dysfunction was further investigated in [<sup>3</sup>H]ryanodine binding assays. Quite unexpectedly, RyR2<sup>L433P</sup> channels displayed substantially reduced ryanodine binding (Graph 7.1). Notably, similar observations were made for some of the disease-associated RyR1 mutants expressed in

heterologous systems as homotetramers (Gao et al. 2000; Du et al. 2004). Further analysis of these mutants in cell based assays revealed a substantially reduced calcium sensitivity, which was restored upon co-expression with the wild-type protein (Du et al. 2004). Thus, the inability to obtain a considerable increase in ryanodine binding for RyR2<sup>L433P</sup> channels within systolic calcium range might reflect their inability to respond to calcium. However, in the course of this study, it was determined that RyR2<sup>L433P</sup> channels exhibit remarkably reduced stability of tetramers which dissociate upon solubilisation and sucrose density gradient centrifugation (Figure 7.2, Graph 7.4). This is a novel observation that was not previously reported for other arrhythmia-associated mutations and one that has paramount implications on the interpretation of the functional data obtained in this study. [<sup>3</sup>H]ryanodine binding assay is an indirect measurement of channel activity as ryanodine binds preferentially to the open-state channel. The assay is valid under the assumption that a given mutation does not affect high-affinity ryanodine binding site and/or does not impair a tetrameric arrangement as there is a single high-affinity ryanodine-binding site per RyR tetramer (Pessah and Zimanyi 1991). This is clearly not the case for RyR2<sup>L433P</sup> as shown in sucrose density gradient centrifugation. Thus it is argued that the reduced [<sup>3</sup>H]ryanodine binding observed in this study for RyR2<sup>L433P</sup> is a consequence of compromised stability of RyR<sup>L433P</sup> oligomers and not reduced sensitivity to calcium activation. Moreover, when the RyR2<sup>L433P</sup> data are normalised to its own [<sup>3</sup>H]ryanodine maximum binding, it becomes apparent the L433P mutant is hypersensitive to calcium activation (Graph 7.2, right panel). Interestingly, the L433P mutation was also characterised by Jang and colleagues who failed to observe any significant shift in the calcium-dependence of [<sup>3</sup>H]ryanodine binding compared to the wild-type receptor but reported increased propensity for SOCIR and increased sensitivity to caffeine activation (Jiang et al. 2005).. On the other hand, Thomas and colleagues reported a desensitised response of this mutant to caffeine activation accompanied by an increase in the calcium release rate and prolonged calcium transient and loss of Ca<sup>2+</sup>-dependent inhibition (Thomas et al. 2004; Thomas et al. 2005). The reason for these discrepancies is unclear since all studies used HEK expression system, however the difference in mutation-induced effects might be species-dependent (human versus mouse in Jiang study).

Notably, dantrolene was shown to promote the stability of RyR2<sup>L433P</sup> tetramers (Figure 7.3, Graph 7.5). Moreover, in agreement with the notion that decreased ryanodine binding observed for the mutant channel reflects an altered tetrameric arrangement, dantrolene also increased ryanodine binding at calcium concentrations that are known to mediate channel activation (Graph 7.6). Therefore when the tetramer is stabilised by dantrolene the ability of ryanodine binding is restored which implies that RyR2<sup>L433P</sup> does not display desensitised response to calcium. These results also suggest that the mutant channel might be hypersensitive to calcium-mediated activation as presented in the right panel in Graph 7.2, a feature that is obscured by the limitations of the experimental technique used.

The extreme impact of this mutation in the experimental setting of this study might be due to the fact that RyR2<sup>L433P</sup> channels were investigated mimicking a “homozygous” scenario, which is not the case in human patients. Thus, the severity of the L433P mutation is most likely masked in the heterozygous scenario and by additional compensating mechanisms present in the native environment of cardiomyocytes. A discrepancy between data obtained from heterologous expression systems and those obtained in the context of a muscle cell has been observed by others. Notably, some of the CCD-linked RyR1 mutations, exhibited a desensitised response in the native environment of skeletal muscle (Avila and Dirksen 2001; Avila *et al.* 2001a), however upon heterologous expression in HEK293 cells it recapitulated a common leaky-channel phenotype characteristic for most MH/CCD mutants (Lynch *et al.* 1999).

In conclusion, the L433P mutation appears to severely impair the stability of the RyR2 homotetramer which is most likely responsible for the functional impairment of this mutant. Dantrolene reverses mutation-triggered effects at both the structural and functional level. Based on the findings obtained earlier (Chapter 6) showing the ability of dantrolene to rescue mutation-induced decline in the N-terminus self-association, stabilisation of the N-terminus inter-subunit interface might be dantrolene’s primary mode of action. A number of evidence suggests that the RyR C-terminus is the primary oligomerisation determinant (Gao *et al.* 1997; Stewart *et al.* 2003). However, in the context of the data obtained in this study, i.e. dissociation of RyR2<sup>L433P</sup> tetramers, the RyR N-terminus might constitute an important oligomerisation determinant. Alternatively, the dissociation of the RyR2 tetramer

might not be a direct consequence of the reduced N-terminus self-association in RyR2<sup>L433P</sup> but rather reflect long distance alterations in the protein tertiary structure which affect oligomerisation determinants located elsewhere. Given the limitations of the experimental approach undertaken in this study, it is not possible to precisely determine underlying defects in RyR2<sup>L433P</sup> channels.

## 8 Closing remarks

The principal aim of this thesis was to characterise inter-subunit interactions involving the RyR2 N-terminus. This interaction was characterised biochemically in Chapter 3 and 4. The process of N-terminus self-association appears to be mediated by multiple sites. The two important oligomerisation determinants are located in the loops connecting strands  $\beta$ 8- $\beta$ 9 and  $\beta$ 20- $\beta$ 21, which according to the docking of the RyR1 N-terminus crystal structure into the cryo-EM map of the full-length receptor, reside at the inter-subunit interface (Tung et al. 2010). However, due to the limitations of the experimental approach undertaken, it was not feasible to determine the role of other potential sites of inter-subunit interaction. The technique used in this study, i.e. generation and testing of deletion mutants is mostly restricted to protein segments with known tertiary structure and is only able to determine the role of fragments which removal would not substantially change protein conformation. This means that the deletion within the loop is dictated by the relative distance of the preceding and the following secondary structure elements. Due to the latter, the role of the short loop connecting  $\beta$  strand 13 and 14 could not be explored while the former limited investigation to residues encompassing the published RyR1 N-terminus crystal structure. Moreover, the removal of some residues might have additional and impossible to predict consequences on the protein structure in spite of a careful and rationalized deletion design as it was observed when part of the  $\beta$ 20- $\beta$ 21 loop was removed. In such circumstances it is very difficult to attribute observed effects to the absence of a particular fragment, as global change of conformation will ultimately affect other oligomerisation determinants. In order to gain further insight into the role of additional inter-subunit contact sites in the N-terminus self-tetramerisation and to validate findings of this study, a complementary experimental technique would be highly valuable. In fact, an alternative approach involving the use of synthetic peptides encompassing putative inter-subunit contact sites and evaluation of their effects on BT4L tetramerisation properties has been already undertaken.

In the course of this study, it was also shown that N-terminus self-association is further stabilised by disulphide bonds most likely involving multiple cysteine residues with cysteine 361 being implicated in this process. However, disulphide bonds are not essential for oligomerisation as tetramers are also formed in conditions

precluding cysteine oxidation (reducing conditions). Moreover, it appears that oxidation process involves the formation of internal disulphide bonds (residing within a monomer). This finding calls for further investigation as it might be possible that disulphide bridges between cysteines within a single monomer rather than across subunits confers BT4L tetramers resistant to SDS. In order to explore this possibility, experiments using thiol-specific reagents with high molecular weight should be conducted. Moreover, additional efforts determining whether BT4L tetramers are in fact resistant to SDS rather than held by disulphide bonds, such as combined use of SDS, urea/guanidine chloride and salt, should be undertaken.

N-terminus self-association appears to be involved in the regulation of channel function. Inter-subunit interactions involving the RyR2 N-terminus were characterised functionally in Chapter 5. It was shown that stable N-terminus self-interaction within the full-length RyR2 is likely to prevent spontaneous activation of the channel at diastolic calcium levels. Notably, the disruption of the N-terminus self-association, which results in channel hypersensitivity, shares common features with the phenotype observed for recombinantly expressed RyR2 containing arrhythmia-associated mutations.

The role of the RyR2 N-terminus inter-subunit interaction in RyR2 pathology was investigated in Chapters 6 and 7. It was shown that the presence of arrhythmia-linked mutations compromises the ability of the RyR2 N-terminus to oligomerise, however this effect was not uniform and depended on the mutation itself. These findings suggest that defective N-terminus self-association might underlie the mechanism by which some of the CPVT/ARVD2 mutations promote RyR2 hyperactivity at diastolic calcium levels. This hypothesis was further tested in Chapter 7. It was shown that in the presence of an arrhythmia-linked mutation (L433P), endogenous N-terminus self-association in the full-length channel appears to be defective leading to the functional impairment. Although this observation is supported by a number of cumulative evidence, additional studies would be necessary to validate this hypothesis. In order to further verify postulated disruption of endogenous N-terminus interaction within the native channel by mutation and/or the exogenous BT4L fragment, calcium dependence of RyR2 ryanodine binding should be also performed in presence of BT4L containing arrhythmia-associated mutations. If the proposed hypothesis is

correct, the presence of the mutant fragment should not affect wild-type RyR2 activation profile.

This study also provided evidence that homotetramers formed by RyR2<sup>L433P</sup> exhibit compromised stability, which has profound implications on functional assays employed to study RyR channels *in vitro*. It must be pointed out that reduced tetramer stability would not only affect [<sup>3</sup>H]ryanodine binding, the method used in this study, but also other functional assays like electrophysiological single channel recordings, which require RyR2 channels purified using solubilisation and sucrose density gradient centrifugation. Notably, since defective tetrameric assembly of RyR2<sup>L433P</sup> impeded conclusive determination of channel functional impairment in the [<sup>3</sup>H]ryanodine binding assay (non-responsive versus hypersensitive phenotype), alternative techniques should be employed. Recombinant expression of this mutant in HEK293 cells followed by the evaluation of calcium-induced Ca<sup>2+</sup> transients should shed more light on this matter.

One of the more remarkable findings of this study is the ability of dantrolene to rescue the mutation-triggered effects at a clinically relevant concentration. This observation is in agreement with a number of recent reports showing that dantrolene might be an effective therapeutic agent in RyR2-associated disorders. Notably, results presented in this thesis provide new insights into dantrolene's mechanism of action which was previously proposed to involve stabilisation of N-terminal – central domain interactions (Kobayashi et al. 2009; Kobayashi et al. 2010; Uchinoumi et al. 2010; Suetomi et al. 2011). Findings reported here suggest that dantrolene's primary mode of action involves stabilisation of N-terminus self-association.

Dantrolene holds great promise for treatment of RyR2-associated disorders. It has a great advantage over other experimental compounds that regulate RyR as its safety has been proven during long clinical use of this compound in the management of MH episodes. More importantly, dantrolene has no effect on the wild-type RyR2 which has been confirmed in experiments performed in this work. This phenomenon is of particular significance for any potential clinical application of this drug in treatment of RyR2-assossiated disorders where a long-term dantrolene administration would be most likely required. Dantrolene supresses RyR1-mediated depolarisation-induced calcium release from SR (Szentesi et al. 2001) and the same effect of dantrolene on

the RyR2 function would be expected to result in a substantial decline of heart contractility, a particularly deleterious effect in patients with HF and ARVD2. However and in agreement with the notion that binding of dantrolene to RyR2 takes place only in particular settings, dantrolene was shown to prevent arrhythmogenic calcium release without compromising systolic function in heart failure (Maxwell et al. 2012).

The existence of dynamic cross-talk between structural/functional domains within RyR has been proposed to modulate channel activity and a number of such domains has been identified (Yamamoto et al. 2000; Yamamoto and Ikemoto 2002a; George et al. 2004; Gangopadhyay and Ikemoto 2006). This work further supports the notion that RyR is an allosteric protein where a number of critical domains are involved in the transmission of signals regulating channel function. The novel inter-subunit interaction characterised in this study further extends our understanding of the role of defective domain-domain interactions in RyR2 pathology and provide important insights into the mechanism of conformation-linked RyR2 dysfunction and the disruptive role of arrhythmia-associated mutations. The destabilisation of domain-domain interactions by arrhythmia-associated mutations have been long proposed to underlie the mechanism of RyR dysregulation (Oda et al. 2005; George et al. 2006; Uchinoumi et al. 2010). Moreover, a number of drugs including dantrolene, JTV519 and antioxidant agents, which were reported to rescue the disease phenotype, were proposed to exert their beneficial effects through stabilisation of domain-domain interfaces (Kobayashi et al. 2005; Yano et al. 2005; Mochizuki *et al.* 2007; Yamamoto et al. 2008). The study presented here provides evidence that stabilisation of RyR2 N-terminus self-oligomerisation might constitute another therapeutic approach against RyR2-associated disorders and thus become a novel target for the design of anti-arrhythmic drugs. However, CPVT/ARVD2-associated mutations are not restricted to the N-terminal portion of the protein thus it cannot be determined whether disruption of the N-terminal inter-subunit contact underlies a common mechanism of channel dysfunction. Rather, the results presented here complement findings reported by other groups where a number of additional domain-domain interfaces are involved in the tuning of RyR activity (Xiong et al. 2006; Hamada et al. 2007; Tateishi et al. 2009; Suetomi et al. 2011) . It is not possible to predict whether stabilisation of the N-terminal inter-subunit interaction will be an effective strategy

for RyR2 dysfunction observed in other arrhythmia-associated mutations located outside the N-terminus. In fact, correction of particular domain-domain interactions by JTV519 has been shown to be effective only for mutations occurring at particular loci (Liu et al. 2006; Suetomi et al. 2011).

The N-terminus inter-subunit interaction identified and characterised here provides important insights into the regulation of RyR2 function, however general limitations of this study should be considered. This work determined RyR2 N-terminus self-association biochemically and independent of other structural determinants present in the full-length channel. This is a clear disadvantage in respect to the extrapolation of this data to the full-length RyR. However, if the stabilisation of N-terminus self-association was to be an effective therapy for RyR2-associated disorders, a simple biochemical assay used in this study (chemical crosslinking) might be employed for a robust screening of potential anti-arrhythmic compounds. Moreover, this work determined functional and structural impairment of RyR<sup>L433P</sup> outside the cell in a homozygous scenario which does not represent a physiologically relevant setting. Thus the mechanism of channel dysfunction in the presence of arrhythmia-associated mutations and dantrolene rescue of disease phenotype requires further investigation. The role of N-terminus association in channel function should be evaluated in heterozygous scenario within the context of living cells and ideally within human cardiomyocytes where other cardiac-specific proteins are present. Current development in the generation of patient-specific iPSC-derived cardiomyocytes (Jung et al. 2012; Novak et al. 2012; Guo et al. 2013; Li et al. 2013) and advances in techniques allowing for *in vitro* site-specific incorporation of unnatural amino-acids combined with bioorthogonal labelling using FRET-compatible molecules (Ye et al. 2008; Huber et al. 2013; Naganathan et al. 2013) may provide new methodology to study the role of domain-domain interactions in RyR2 dysfunction in a more physiological setting.



# I Appendix: List of abbreviations

Ab antibody

AD activating domain

AF atrial fibrillation

BCA bicinchoninic acid

BSA bovine serum albumin

CaM calmodulin

CaMKII  $\text{Ca}^{2+}$ /calmodulin-dependent protein kinases II

CCD central core disease

CHAPS 3-[(3-cholamidopropyl)dimethylammonio]-1-propanesulfonate

CPVT catecholaminergic polymorphic ventricular tachycardia

Cryo-EM cryo-electron microscopy

CSQ calsequestrin

DCM dilated cardiomyopathy

DHPR dihydropyridine receptors

DMEM Dulbecco's Modified Eagle Medium

DMF *N,N*-dimethylformamide

DMSO dimethyl sulfoxide

DNA-BD DNA binding domain

Dpm decays per minute

DTT dithiothreitol

ECL enhanced luminescence

EDTA ethylenediaminetetraacetic acid  
EGTA ethylene glycol tetraacetic acid  
ER endoplasmic reticulum  
FBS foetal bovine serum  
FKBP FK506- Binding Protein  
FRET Förster resonance energy transfer  
GAL4 AD activating domain of GAL4 transcriptional activator  
GAL4 BD DNA binding domain of GAL4 transcriptional activator  
HEPES 2-[4-(2-hydroxyethyl)piperazin-1-yl]ethanesulfonic acid  
HPLC high performance/pressure liquid chromatography  
HRP horseradish peroxidase  
ICD implantable cardioverter-defibrillator  
IP<sub>3</sub>R inositol 1,4,5-trisphosphate receptor  
iPSC induced pluripotent stem cells  
LiAc lithium acetate  
LV left ventricle  
LZ leucine/isoleucine zipper  
MCS multi cloning site  
MCU mitochondrial calcium uniporter  
MH malignant hyperthermia  
MIR O-mannosyltransferases, IP<sub>3</sub>R and RyR domain  
NAADP nicotinic acid dinucleotide phosphate  
NCX sodium/calcium exchanger

NCLX sodium/calcium/lithium exchanger NEM N-ethylmaleimide

OD optical density

ONPG o-nitrophenyl- $\beta$ -D-galactopyranoside

PC phosphatidylcholine

PCR polymerase chain reaction

PIPES piperazine-N,N'-bis(2-ethanesulfonic acid)

PKA protein kinase A (cAMP-dependent protein kinase)

PMCA plasma membrane  $\text{Ca}^{2+}$ -ATPase

PP1 protein phosphatase 1

PP2A protein phosphatase 2A

PVDF polyvinylidene difluoride

RIH ryanodine receptor and IP<sub>3</sub>R homology domain

RyR ryanodine receptor

SB super broth

SD selective dropout medium

SDS sodium lauryl sulfate

SERCA sarco(endo)plasmic reticulum  $\text{Ca}^{2+}$ -ATPase SIDS sudden infant death syndrome

SNP single nucleotide polymorphism

SOCE store-operated  $\text{Ca}^{2+}$  entry

SPCA secretory pathway  $\text{Ca}^{2+}$ -ATPase

SPRY SP1A kinase of *Dictyostelium discoideum* and ryanodine receptor domain

SR sarcoplasmic reticulum (specialized compartment of ER in smooth and striated muscle)

STIM1 stromal interaction protein 1

TAE Tris-acetate-EDTA buffer

TBS Tris-buffered saline

TE Tris-EDTA buffer

TEMED N,N,N',N'-tetramethylethane-1,2-diamine

T<sub>m</sub> melting temperature

TPC two-pore channel

Tris 2-amino-2-hydroxymethyl-propane-1,3-diol

VGCC voltage-gated calcium channel

X-Gal 5-bromo-4-chloro-indolyl-β-D-galactopyranoside

YNB Yeast Nitrogen Base medium

YPD Yeast Extract Peptone Dextrose medium

## II Appendix: Bibliography

- Abulimiti, A., Fu, X., Gu, L., Feng, X. and Chang, Z. (2003). Mycobacterium tuberculosis Hsp16.3 nonamers are assembled and re-assembled via trimer and hexamer intermediates. *J Mol Biol* **326**:1013-1023.
- Aghdasi, B., Reid, M. B. and Hamilton, S. L. (1997a). Nitric oxide protects the skeletal muscle Ca<sup>2+</sup> release channel from oxidation induced activation. *J Biol Chem* **272**:25462-25467.
- Aghdasi, B., Zhang, J., Wu, Y., Reid, M. and Hamilton, S. (1997b). Multiple classes of sulfhydryls modulate the skeletal muscle Ca<sup>2+</sup> release channel. *J Biol Chem* **272**:3739-3748.
- Aizawa, Y., Mitsuma, W., Ikrar, T., Komura, S., Hanawa, H., Miyajima, S., Miyoshi, F. et al. (2007). Human cardiac ryanodine receptor mutations in ion channel disorders in Japan. *Int J Cardiol*. Vol. 116. Netherlands, pp. 263-265.
- Antos, C., Frey, N., Marx, S., Reiken, S., Gaburjakova, M., Richardson, J., Marks, A. et al. (2001). Dilated cardiomyopathy and sudden death resulting from constitutive activation of protein kinase a. *Circ Res* **89**:997-1004.
- Aracena-Parks, P., Goonasekera, S., Gilman, C., Dirksen, R., Hidalgo, C. and Hamilton, S. (2006). Identification of cysteines involved in S-nitrosylation, S-glutathionylation, and oxidation to disulfides in ryanodine receptor type 1. *J Biol Chem* **281**:40354-40368.
- Avila, G. and Dirksen, R. T. (2001). Functional effects of central core disease mutations in the cytoplasmic region of the skeletal muscle ryanodine receptor. *J Gen Physiol* **118**:277-290.
- Avila, G., O'Brien, J. J. and Dirksen, R. T. (2001a). Excitation-contraction uncoupling by a human central core disease mutation in the ryanodine receptor. *Proc Natl Acad Sci U S A* **98**:4215-4220.
- Avila, G., O'Connell, K. M. and Dirksen, R. T. (2003). The pore region of the skeletal muscle ryanodine receptor is a primary locus for excitation-contraction uncoupling in central core disease. *J Gen Physiol* **121**:277-286.
- Avila, G., O'Connell, K. M., Groom, L. A. and Dirksen, R. T. (2001b). Ca<sup>2+</sup> release through ryanodine receptors regulates skeletal muscle L-type Ca<sup>2+</sup> channel expression. *J Biol Chem* **276**:17732-17738.
- Bagattin, A., Veronese, C., Bauce, B., Wuyts, W., Settimi, L., Nava, A., Rampazzo, A. et al. (2004). Denaturing HPLC-based approach for detecting RYR2 mutations involved in malignant arrhythmias. *Clin Chem* **50**:1148-1155.

Bai, J. P., Surguchev, A., Bian, S., Song, L., Santos-Sacchi, J. and Navaratnam, D. (2010). Combinatorial cysteine mutagenesis reveals a critical intramonomer role for cysteines in prestin voltage sensing. *Biophys J* **99**:85-94.

Bannister, M., Hamada, T., Murayama, T., Harvey, P., Casarotto, M., Dulhunty, A. and Ikemoto, N. (2007). Malignant hyperthermia mutation sites in the Leu2442-Pro2477 (DP4) region of RyR1 (ryanodine receptor 1) are clustered in a structurally and functionally definable area. *Biochem J* **401**:333-339.

Bannister, M. L. and Ikemoto, N. (2006). Effects of peptide C corresponding to the Glu724-Pro760 region of the II-III loop of the DHP (dihydropyridine) receptor alpha1 subunit on the domain- switch-mediated activation of RyR1 (ryanodine receptor 1) Ca<sup>2+</sup> channels. *Biochem J* **394**:145-152.

Bauce, B., Rampazzo, A., Basso, C., Bagattin, A., Daliento, L., Tiso, N., Turrini, P. et al. (2002). Screening for ryanodine receptor type 2 mutations in families with effort-induced polymorphic ventricular arrhythmias and sudden death: early diagnosis of asymptomatic carriers. *J Am Coll Cardiol* **40**:341-349.

Beam, K. G., Adams, B. A., Niidome, T., Numa, S. and Tanabe, T. (1992). Function of a truncated dihydropyridine receptor as both voltage sensor and calcium channel. *Nature* **360**:169-171.

Beckmann, B. M., Wilde, A. A. and Kaab, S. (2008). Dual inheritance of sudden death from cardiovascular causes. *N Engl J Med*. Vol. 358. United States, pp. 2077-2078.

Bednar, R. A. (1990). Reactivity and pH dependence of thiol conjugation to N-ethylmaleimide: detection of a conformational change in chalcone isomerase. *Biochemistry* **29**:3684-3690.

Beigi, F., Gonzalez, D. R., Minhas, K. M., Sun, Q. A., Foster, M. W., Khan, S. A., Treuer, A. V. et al. (2012). Dynamic denitrosylation via S-nitrosoglutathione reductase regulates cardiovascular function. *Proc Natl Acad Sci U S A* **109**:4314-4319.

Belevych, A. E., Terentyev, D., Viatchenko-Karpinski, S., Terentyeva, R., Sridhar, A., Nishijima, Y., Wilson, L. D. et al. (2009). Redox modification of ryanodine receptors underlies calcium alternans in a canine model of sudden cardiac death. *Cardiovasc Res* **84**:387-395.

Bellinger, A., Reiken, S., Carlson, C., Mongillo, M., Liu, X., Rothman, L., Matecki, S. et al. (2009). Hypernitrosylated ryanodine receptor calcium release channels are leaky in dystrophic muscle. *Nat Med* **15**:325-330.

Bellinger, A., Reiken, S., Dura, M., Murphy, P., Deng, S., Landry, D., Nieman, D. et al. (2008). Remodeling of ryanodine receptor complex causes "leaky" channels: a molecular mechanism for decreased exercise capacity. *Proc Natl Acad Sci U S A* **105**:2198-2202.

Berge, K. E., Haugaa, K. H., Fruh, A., Anfinsen, O. G., Gjesdal, K., Siem, G., Oyen, N. *et al.* (2008). Molecular genetic analysis of long QT syndrome in Norway indicating a high prevalence of heterozygous mutation carriers. *Scand J Clin Lab Invest* **68**:362-368.

Berridge, M., Bootman, M. and Roderick, H. (2003). Calcium signalling: dynamics, homeostasis and remodelling. *Nat Rev Mol Cell Biol* **4**:517-529.

Berridge, M. J. (2012). Calcium signalling remodelling and disease. *Biochem Soc Trans* **40**:297-309.

Bers, D. M. (2002). Cardiac Na/Ca exchange function in rabbit, mouse and man: what's the difference? *J Mol Cell Cardiol* **34**:369-373.

Betzenhauser, M. J. and Marks, A. R. (2010). Ryanodine receptor channelopathies. *Pflugers Arch* **460**:467-480.

Bhat, M. B., Zhao, J., Takeshima, H. and Ma, J. (1997). Functional calcium release channel formed by the carboxyl-terminal portion of ryanodine receptor. *Biophys J* **73**:1329-1336.

Bhuiyan, Z. A., van den Berg, M. P., van Tintelen, J. P., Bink-Boelkens, M. T., Wiesfeld, A. C., Alders, M., Postma, A. V. *et al.* (2007). Expanding spectrum of human RYR2-related disease: new electrocardiographic, structural, and genetic features. *Circulation* **116**:1569-1576.

Bidasee, K. R., Xu, L., Meissner, G. and Besch, H. R., Jr. (2003). Diketopyridylryanodine has three concentration-dependent effects on the cardiac calcium-release channel/ryanodine receptor. *J Biol Chem* **278**:14237-14248.

Blayney, L., Zissimopoulos, S., Ralph, E., Abbot, E., Matthews, L. and Lai, F. (2004). Ryanodine receptor oligomeric interaction: identification of a putative binding region. *J Biol Chem* **279**:14639-14648.

Boehning, D. and Joseph, S. K. (2000). Direct association of ligand-binding and pore domains in homo- and heterotetrameric inositol 1,4,5-trisphosphate receptors. *Embo J* **19**:5450-5459.

Brandes, N., Schmitt, S. and Jakob, U. (2009). Thiol-based redox switches in eukaryotic proteins. *Antioxid Redox Signal* **11**:997-1014.

Brandt, N. R., Caswell, A. H., Brandt, T., Brew, K. and Mellgren, R. L. (1992). Mapping of the calpain proteolysis products of the junctional foot protein of the skeletal muscle triad junction. *J Membr Biol* **127**:35-47.

Brini, M., Manni, S., Pierobon, N., Du, G. G., Sharma, P., MacLennan, D. H. and Carafoli, E. (2005). Ca<sup>2+</sup> signaling in HEK-293 and skeletal muscle cells expressing recombinant ryanodine receptors harboring malignant hyperthermia and central core disease mutations. *J Biol Chem* **280**:15380-15389.

Bruno, A. M., Huang, J. Y., Bennett, D. A., Marr, R. A., Hastings, M. L. and Stutzmann, G. E. (2012). Altered ryanodine receptor expression in mild cognitive impairment and Alzheimer's disease. *Neurobiol Aging* **33**:1001.e1001-1006.

Bull, R. and Marengo, J. J. (1994). Calcium-dependent halothane activation of sarcoplasmic reticulum calcium channels from frog skeletal muscle. *Am J Physiol* **266**:C391-396.

Callaway, C., Seryshev, A., Wang, J. P., Slavik, K. J., Needleman, D. H., Cantu, C., 3rd, Wu, Y. et al. (1994). Localization of the high and low affinity [<sup>3</sup>H]ryanodine binding sites on the skeletal muscle Ca<sup>2+</sup> release channel. *J Biol Chem* **269**:15876-15884.

Castro, M. J. and Anderson, S. (1996). Alanine point-mutations in the reactive region of bovine pancreatic trypsin inhibitor: effects on the kinetics and thermodynamics of binding to beta-trypsin and alpha-chymotrypsin. *Biochemistry* **35**:11435-11446.

Catterall, W. A. (2000). Structure and regulation of voltage-gated Ca<sup>2+</sup> channels. *Annu Rev Cell Dev Biol* **16**:521-555.

Cerrone, M., Colombi, B., Santoro, M., di Barletta, M. R., Scelsi, M., Villani, L., Napolitano, C. et al. (2005). Bidirectional ventricular tachycardia and fibrillation elicited in a knock-in mouse model carrier of a mutation in the cardiac ryanodine receptor. *Circ Res* **96**:e77-82.

Chelu, M., Danila, C., Gilman, C. and Hamilton, S. (2004). Regulation of ryanodine receptors by FK506 binding proteins. *Trends Cardiovasc Med* **14**:227-234.

Chen, S. R., Airey, J. A. and MacLennan, D. H. (1993). Positioning of major tryptic fragments in the Ca<sup>2+</sup> release channel (ryanodine receptor) resulting from partial digestion of rabbit skeletal muscle sarcoplasmic reticulum. *J Biol Chem* **268**:22642-22649.

Chen, S. R., Ebisawa, K., Li, X. and Zhang, L. (1998). Molecular identification of the ryanodine receptor Ca<sup>2+</sup> sensor. *J Biol Chem* **273**:14675-14678.

Chen, S. R., Li, P., Zhao, M., Li, X. and Zhang, L. (2002). Role of the proposed pore-forming segment of the Ca<sup>2+</sup> release channel (ryanodine receptor) in ryanodine interaction. *Biophys J* **82**:2436-2447.

Chen, S. R. and MacLennan, D. H. (1994). Identification of calmodulin-, Ca(2+)-, and ruthenium red-binding domains in the Ca<sup>2+</sup> release channel (ryanodine receptor) of rabbit skeletal muscle sarcoplasmic reticulum. *J Biol Chem* **269**:22698-22704.

Cheng, W., Altafaj, X., Ronjat, M. and Coronado, R. (2005). Interaction between the dihydropyridine receptor Ca<sup>2+</sup> channel beta-subunit and ryanodine receptor type 1 strengthens excitation-contraction coupling. *Proc Natl Acad Sci U S A* **102**:19225-19230.

Cherednichenko, G., Ward, C. W., Feng, W., Cabrales, E., Michaelson, L., Samso, M., Lopez, J. R. *et al.* (2008). Enhanced excitation-coupled calcium entry in myotubes expressing malignant hyperthermia mutation R163C is attenuated by dantrolene. *Molecular Pharmacology* **73**:1203-1212.

Ching, L. L., Williams, A. J. and Sitsapesan, R. (2000). Evidence for Ca(2+) activation and inactivation sites on the luminal side of the cardiac ryanodine receptor complex. *Circ Res* **87**:201-206.

Choi, G., Kopplin, L. J., Tester, D. J., Will, M. L., Haglund, C. M. and Ackerman, M. J. (2004). Spectrum and frequency of cardiac channel defects in swimming-triggered arrhythmia syndromes. *Circulation* **110**:2119-2124.

Chopra, N., Yang, T., Asghari, P., Moore, E. D., Huke, S., Akin, B., Cattolica, R. A. *et al.* (2009). Ablation of triadin causes loss of cardiac Ca2+ release units, impaired excitation-contraction coupling, and cardiac arrhythmias. *Proc Natl Acad Sci U S A* **106**:7636-7641.

Collins, H. E., Zhu-Mauldin, X., Marchase, R. B. and Chatham, J. C. (2013). STIM1/Orai1-mediated SOCE: current perspectives and potential roles in cardiac function and pathology. *Am J Physiol Heart Circ Physiol* **305**:H446-458.

Cornea, R. L., Nitu, F., Gruber, S., Kohler, K., Satzer, M., Thomas, D. D. and Fruen, B. R. (2009). FRET-based mapping of calmodulin bound to the RyR1 Ca2+ release channel. *Proc Natl Acad Sci U S A* **106**:6128-6133.

Coronado, R., Ahern, C. A., Sheridan, D. C., Cheng, W., Carbonneau, L. and Bhattacharya, D. (2004). Functional equivalence of dihydropyridine receptor alpha1S and beta1a subunits in triggering excitation-contraction coupling in skeletal muscle. *Biol Res* **37**:565-575.

Creighton, W., Virmani, R., Kutys, R. and Burke, A. (2006). Identification of novel missense mutations of cardiac ryanodine receptor gene in exercise-induced sudden death at autopsy. *J Mol Diagn* **8**:62-67.

Cui, Y., Tae, H. S., Norris, N. C., Karunasekara, Y., Pouliquin, P., Board, P. G., Dulhunty, A. F. *et al.* (2009). A dihydropyridine receptor alpha1s loop region critical for skeletal muscle contraction is intrinsically unstructured and binds to a SPRY domain of the type 1 ryanodine receptor. *Int J Biochem Cell Biol* **41**:677-686.

Curran, J., Hinton, M. J., Rios, E., Bers, D. M. and Shannon, T. R. (2007). Beta-adrenergic enhancement of sarcoplasmic reticulum calcium leak in cardiac myocytes is mediated by calcium/calmodulin-dependent protein kinase. *Circ Res* **100**:391-398.

Cutler, M. J., Plummer, B. N., Wan, X., Sun, Q. A., Hess, D., Liu, H., Deschenes, I. *et al.* (2012). Aberrant S-nitrosylation mediates calcium-triggered ventricular arrhythmia in the intact heart. *Proc Natl Acad Sci U S A* **109**:18186-18191.

d'Amati, G., Bagattin, A., Bauce, B., Rampazzo, A., Autore, C., Basso, C., King, K. *et al.* (2005). Juvenile sudden death in a family with polymorphic ventricular

arrhythmias caused by a novel RyR2 gene mutation: evidence of specific morphological substrates. *Hum Pathol* **36**:761-767.

Dainese, M., Quarta, M., Lyfenko, A. D., Paolini, C., Canato, M., Reggiani, C., Dirksen, R. T. *et al.* (2009). Anesthetic- and heat-induced sudden death in calsequestrin-1-knockout mice. *Fasebj* **23**:1710-1720.

di Barletta, M. R., Viatchenko-Karpinski, S., Nori, A., Memmi, M., Terentyev, D., Turcato, F., Valle, G. *et al.* (2006). Clinical phenotype and functional characterization of CASQ2 mutations associated with catecholaminergic polymorphic ventricular tachycardia. *Circulation* **114**:1012-1019.

Diaz-Sylvester, P. L., Porta, M. and Copello, J. A. (2011). Modulation of cardiac ryanodine receptor channels by alkaline earth cations. *PLoS One* **6**:e26693.

Dirksen, R. T. and Avila, G. (2002). Altered ryanodine receptor function in central core disease: leaky or uncoupled Ca(2+) release channels? *Trends Cardiovasc Med* **12**:189-197.

Dirksen, R. T. and Avila, G. (2004). Distinct effects on Ca2+ handling caused by malignant hyperthermia and central core disease mutations in RyR1. *Biophys J* **87**:3193-3204.

Du, G. G., Khanna, V. K., Guo, X. and MacLennan, D. H. (2004). Central core disease mutations R4892W, I4897T and G4898E in the ryanodine receptor isoform 1 reduce the Ca2+ sensitivity and amplitude of Ca2+-dependent Ca2+ release. *Biochem J* **382**:557-564.

Du, G. G., Khanna, V. K. and MacLennan, D. H. (2000). Mutation of divergent region 1 alters caffeine and Ca(2+) sensitivity of the skeletal muscle Ca(2+) release channel (ryanodine receptor). *J Biol Chem* **275**:11778-11783.

Du, G. G. and MacLennan, D. H. (1998). Functional consequences of mutations of conserved, polar amino acids in transmembrane sequences of the Ca2+ release channel (ryanodine receptor) of rabbit skeletal muscle sarcoplasmic reticulum. *J Biol Chem* **273**:31867-31872.

Du, G. G. and MacLennan, D. H. (1999). Ca(2+) inactivation sites are located in the COOH-terminal quarter of recombinant rabbit skeletal muscle Ca(2+) release channels (ryanodine receptors). *J Biol Chem* **274**:26120-26126.

Du, G. G., Sandhu, B., Khanna, V. K., Guo, X. H. and MacLennan, D. H. (2002a). Topology of the Ca2+ release channel of skeletal muscle sarcoplasmic reticulum (RyR1). *Proc Natl Acad Sci U S A* **99**:16725-16730.

Du, X. J., Cole, T. J., Tenis, N., Gao, X. M., Kontgen, F., Kemp, B. E. and Heierhorst, J. (2002b). Impaired cardiac contractility response to hemodynamic stress in S100A1-deficient mice. *Mol Cell Biol* **22**:2821-2829.

Duarte, S. T., Oliveira, J., Santos, R., Pereira, P., Barroso, C., Conceicao, I. and Evangelista, T. (2011). Dominant and recessive RYR1 mutations in adults with core lesions and mild muscle symptoms. *Muscle Nerve* **44**:102-108.

Dulhunty, A. F., Curtis, S. M., Watson, S., Cengia, L. and Casarotto, M. G. (2004). Multiple actions of imperatoxin A on ryanodine receptors: interactions with the II-III loop "A" fragment. *J Biol Chem* **279**:11853-11862.

Dybкова, N., Sedej, S., Napolitano, C., Neef, S., Rokita, A. G., Hünlich, M., Brown, J. H. et al. (2011). Overexpression of CaMKII $\delta$ c in RyR2R4496C+/- knock-in mice leads to altered intracellular Ca<sup>2+</sup> handling and increased mortality. *J Am Coll Cardiol* **57**:469-479.

El-Hayek, R., Saiki, Y., Yamamoto, T. and Ikemoto, N. (1999). A postulated role of the near amino-terminal domain of the ryanodine receptor in the regulation of the sarcoplasmic reticulum Ca(2+) channel. *J Biol Chem* **274**:33341-33347.

Eltit, J. M., Ding, X., Pessah, I. N., Allen, P. D. and Lopez, J. R. (2013). Nonspecific sarcolemmal cation channels are critical for the pathogenesis of malignant hyperthermia. *Fasebj* **27**:991-1000.

Eu, J. P., Sun, J., Xu, L., Stamler, J. S. and Meissner, G. (2000). The skeletal muscle calcium release channel: coupled O<sub>2</sub> sensor and NO signaling functions. *Cell* **102**:499-509.

Fabiato, A. (1983). Calcium-induced release of calcium from the cardiac sarcoplasmic reticulum. *Am J Physiol* **245**:C1-14.

Farrell, E. F., Antaramian, A., Rueda, A., Gomez, A. M. and Valdivia, H. H. (2003). Sorcin inhibits calcium release and modulates excitation-contraction coupling in the heart. *J Biol Chem* **278**:34660-34666.

Fauconnier, J., Thireau, J., Reiken, S., Cassan, C., Richard, S., Matecki, S., Marks, A. et al. (2010). Leaky RyR2 trigger ventricular arrhythmias in Duchenne muscular dystrophy. *Proc Natl Acad Sci U S A*.

Feng, W., Liu, G., Allen, P. D. and Pessah, I. N. (2000). Transmembrane redox sensor of ryanodine receptor complex. *Journal of Biological Chemistry* **275**:35902-35907.

Feng, W., Liu, G., Xia, R., Abramson, J. J. and Pessah, I. N. (1999). Site-selective modification of hyperreactive cysteines of ryanodine receptor complex by quinones. *Molecular Pharmacology* **55**:821-831.

Fernández-Velasco, M., Rueda, A., Rizzi, N., Benitah, J. P., Colombi, B., Napolitano, C., Priori, S. G. et al. (2009). Increased Ca<sup>2+</sup> sensitivity of the ryanodine receptor mutant RyR2R4496C underlies catecholaminergic polymorphic ventricular tachycardia. *Circ Res* **104**:201-209, 212p following 209.

Ferreiro, A., Monnier, N., Romero, N. B., Leroy, J. P., Bonnemann, C., Haenggeli, C. A., Straub, V. *et al.* (2002). A recessive form of central core disease, transiently presenting as multi-minicore disease, is associated with a homozygous mutation in the ryanodine receptor type 1 gene. *Ann Neurol* **51**:750-759.

Fessenden, J. D., Chen, L., Wang, Y., Paolini, C., Franzini-Armstrong, C., Allen, P. D. and Pessah, I. N. (2001). Ryanodine receptor point mutant E4032A reveals an allosteric interaction with ryanodine. *Proc Natl Acad Sci U S A* **98**:2865-2870.

Fessenden, J. D., Feng, W., Pessah, I. N. and Allen, P. D. (2004). Mutational analysis of putative calcium binding motifs within the skeletal ryanodine receptor isoform, RyR1. *J Biol Chem* **279**:53028-53035.

Fields, S. and Song, O. (1989). A novel genetic system to detect protein-protein interactions. *Nature* **340**:245-246.

Flucher, B. E., Conti, A., Takeshima, H. and Sorrentino, V. (1999). Type 3 and type 1 ryanodine receptors are localized in triads of the same mammalian skeletal muscle fibers. *J Cell Biol* **146**:621-630.

Fomenko, D. E. and Gladyshev, V. N. (2002). CxxS: fold-independent redox motif revealed by genome-wide searches for thiol/disulfide oxidoreductase function. *Protein Science* **11**:2285-2296.

Fomenko, D. E. and Gladyshev, V. N. (2003). Identity and functions of CxxC-derived motifs. *Biochemistry* **42**:11214-11225.

Frank, K. F., Bolck, B., Ding, Z., Krause, D., Hattebuhr, N., Malik, A., Brixius, K. *et al.* (2005). Overexpression of sorcin enhances cardiac contractility in vivo and in vitro. *J Mol Cell Cardiol* **38**:607-615.

Franzini-Armstrong, C. (1999). The sarcoplasmic reticulum and the control of muscle contraction. *Faseb j* **13 Suppl 2**:S266-270.

Franzini-Armstrong, C., Protasi, F. and Ramesh, V. (1998). Comparative ultrastructure of Ca<sup>2+</sup> release units in skeletal and cardiac muscle. *Ann N Y Acad Sci* **853**:20-30.

Franzini-Armstrong, C., Protasi, F. and Ramesh, V. (1999). Shape, size, and distribution of Ca(2+) release units and couplons in skeletal and cardiac muscles. *Biophys J* **77**:1528-1539.

Fujii, J., Otsu, K., Zorzato, F., de Leon, S., Khanna, V. K., Weiler, J. E., O'Brien, P. J. *et al.* (1991). Identification of a mutation in porcine ryanodine receptor associated with malignant hyperthermia. *Science* **253**:448-451.

Futatsugi, A., Kuwajima, G. and Mikoshiba, K. (1995). Tissue-specific and developmentally regulated alternative splicing in mouse skeletal muscle ryanodine receptor mRNA. *Biochem J* **305 ( Pt 2)**:373-378.

Gaburjakova, M., Gaburjakova, J., Reiken, S., Huang, F., Marx, S., Rosemblit, N. and Marks, A. (2001). FKBP12 binding modulates ryanodine receptor channel gating. *J Biol Chem* **276**:16931-16935.

Galvan, D. L., Borrego-Diaz, E., Perez, P. J. and Mignery, G. A. (1999). Subunit oligomerization, and topology of the inositol 1,4, 5-trisphosphate receptor. *J Biol Chem* **274**:29483-29492.

Gangopadhyay, J. and Ikemoto, N. (2006). Role of the Met3534-Ala4271 region of the ryanodine receptor in the regulation of Ca<sup>2+</sup> release induced by calmodulin binding domain peptide. *Biophys J* **90**:2015-2026.

Gangopadhyay, J. and Ikemoto, N. (2008). Interaction of the Lys(3614)-Asn(3643) calmodulin-binding domain with the Cys(4114)-Asn(4142) region of the type 1 ryanodine receptor is involved in the mechanism of Ca<sup>2+</sup>/agonist-induced channel activation. *Biochem J* **411**:415-423.

Gangopadhyay, J. P. and Ikemoto, N. (2011). Aberrant interaction of calmodulin with the ryanodine receptor develops hypertrophy in the neonatal cardiomyocyte. *Biochem J* **438**:379-387.

Gao, L., Balshaw, D., Xu, L., Tripathy, A., Xin, C. and Meissner, G. (2000). Evidence for a role of the luminal M3-M4 loop in skeletal muscle Ca(2+) release channel (ryanodine receptor) activity and conductance. *Biophys J* **79**:828-840.

Gao, L., Tripathy, A., Lu, X. and Meissner, G. (1997). Evidence for a role of C-terminal amino acid residues in skeletal muscle Ca<sup>2+</sup> release channel (ryanodine receptor) function. *FEBS Lett* **412**:223-226.

George, C., Jundi, H., Thomas, N., Scoote, M., Walters, N., Williams, A. and Lai, F. (2004). Ryanodine receptor regulation by intramolecular interaction between cytoplasmic and transmembrane domains. *Mol Biol Cell* **15**:2627-2638.

George, C. H., Higgs, G. V. and Lai, F. A. (2003). Ryanodine receptor mutations associated with stress-induced ventricular tachycardia mediate increased calcium release in stimulated cardiomyocytes. *Circ Res* **93**:531-540.

George, C. H., Jundi, H., Walters, N., Thomas, N. L., West, R. R. and Lai, F. A. (2006). Arrhythmogenic mutation-linked defects in ryanodine receptor autoregulation reveal a novel mechanism of Ca<sup>2+</sup> release channel dysfunction. *Circ Res* **98**:88-97.

George, C. H., Rogers, S. A., Bertrand, B. M., Tunwell, R. E., Thomas, N. L., Steele, D. S., Cox, E. V. et al. (2007). Alternative splicing of ryanodine receptors modulates cardiomyocyte Ca<sup>2+</sup> signaling and susceptibility to apoptosis. *Circ Res* **100**:874-883.

Giannini, G., Conti, A., Mammarella, S., Scrobogna, M. and Sorrentino, V. (1995). The ryanodine receptor/calcium channel genes are widely and differentially expressed in murine brain and peripheral tissues. *J Cell Biol* **128**:893-904.

Gillard, E. F., Otsu, K., Fujii, J., Khanna, V. K., de Leon, S., Derdemezi, J., Britt, B. A. *et al.* (1991). A substitution of cysteine for arginine 614 in the ryanodine receptor is potentially causative of human malignant hyperthermia. *Genomics* **11**:751-755.

Girgenrath, T., Mahalingam, M., Svensson, B., Nitu, F. R., Cornea, R. L. and Fessenden, J. D. (2013). N-terminal and central segments of the type 1 ryanodine receptor mediate its interaction with FK506-binding proteins. *J Biol Chem* **288**:16073-16084.

Glover, L., Heffron, J. J. and Ohlendieck, K. (2004). Increased sensitivity of the ryanodine receptor to halothane-induced oligomerization in malignant hyperthermia-susceptible human skeletal muscle. *J Appl Physiol* **96**:11-18.

Gonzalez, D. R., Beigi, F., Treuer, A. V. and Hare, J. M. (2007). Deficient ryanodine receptor S-nitrosylation increases sarcoplasmic reticulum calcium leak and arrhythmogenesis in cardiomyocytes. *Proc Natl Acad Sci U S A* **104**:20612-20617.

Gonzalez, D. R., Treuer, A. V., Castellanos, J., Dulce, R. A. and Hare, J. M. (2010). Impaired S-nitrosylation of the ryanodine receptor caused by xanthine oxidase activity contributes to calcium leak in heart failure. *J Biol Chem* **285**:28938-28945.

Gorza, L., Vettore, S., Tessaro, A., Sorrentino, V. and Vitadello, M. (1997). Regional and age-related differences in mRNA composition of intracellular Ca(2+)-release channels of rat cardiac myocytes. *J Mol Cell Cardiol* **29**:1023-1036.

Grabner, M., Dirksen, R. T., Suda, N. and Beam, K. G. (1999). The II-III loop of the skeletal muscle dihydropyridine receptor is responsible for the Bi-directional coupling with the ryanodine receptor. *J Biol Chem* **274**:21913-21919.

Grande, A., Costas, C. and Benavente, J. (2002). Subunit composition and conformational stability of the oligomeric form of the avian reovirus cell-attachment protein sigmaC. *J Gen Virol* **83**:131-139.

Grunwald, R. and Meissner, G. (1995). Luminal sites and C terminus accessibility of the skeletal muscle calcium release channel (ryanodine receptor). *J Biol Chem* **270**:11338-11347.

Gu, L., Abulimiti, A., Li, W. and Chang, Z. (2002). Monodisperse Hsp16.3 nonamer exhibits dynamic dissociation and reassociation, with the nonamer dissociation prerequisite for chaperone-like activity. *J Mol Biol* **319**:517-526.

Guharoy, M. and Chakrabarti, P. (2007). Secondary structure based analysis and classification of biological interfaces: identification of binding motifs in protein-protein interactions. *Bioinformatics* **23**:1909-1918.

Guo, L., Coyle, L., Abrams, R., Kemper, R., Chiao, E. T. and Kolaja, K. L. (2013). Refining the Human iPSC-Cardiomyocyte Arrhythmic Risk (hCAR) Assessment Model. *Toxicol Sci*.

Guo, T., Cornea, R. L., Huke, S., Camors, E., Yang, Y., Picht, E., Fruen, B. R. *et al.* (2010). Kinetics of FKBP12.6 binding to ryanodine receptors in permeabilized cardiac myocytes and effects on Ca sparks. *Circ Res* **106**:1743-1752.

Gyorke, I., Hester, N., Jones, L. R. and Gyorke, S. (2004). The role of calsequestrin, triadin, and junctin in conferring cardiac ryanodine receptor responsiveness to luminal calcium. *Biophys J* **86**:2121-2128.

Hakamata, Y., Nakai, J., Takeshima, H. and Imoto, K. (1992). Primary structure and distribution of a novel ryanodine receptor/calcium release channel from rabbit brain. *FEBS Lett* **312**:229-235.

Hamada, T., Bannister, M. L. and Ikemoto, N. (2007). Peptide probe study of the role of interaction between the cytoplasmic and transmembrane domains of the ryanodine receptor in the channel regulation mechanism. *Biochemistry* **46**:4272-4279.

Hamada, T., Gangopadhyay, J., Mandl, A., Erhardt, P. and Ikemoto, N. (2009). Defective regulation of the ryanodine receptor induces hypertrophy in cardiomyocytes. *Biochem Biophys Res Commun* **380**:493-497.

Hamilton, S. and Serysheva, I. (2009). Ryanodine receptor structure: progress and challenges. *J Biol Chem* **284**:4047-4051.

Hasdemir, C., Aydin, H. H., Sahin, S. and Wollnik, B. (2008). Catecholaminergic polymorphic ventricular tachycardia caused by a novel mutation in the cardiac ryanodine receptor. *Anadolu Kardiyol Derg* **8**:E35-36.

Hasdemir, C., Priori, S. G., Overholt, E. and Lazzara, R. (2004). Catecholaminergic polymorphic ventricular tachycardia, recurrent syncope, and implantable loop recorder. *J Cardiovasc Electrophysiol* **15**:729.

Haugaa, K. H., Leren, I. S., Berge, K. E., Bathen, J., Loennechen, J. P., Anfinsen, O. G., Fruh, A. *et al.* (2010). High prevalence of exercise-induced arrhythmias in catecholaminergic polymorphic ventricular tachycardia mutation-positive family members diagnosed by cascade genetic screening. *Europace* **12**:417-423.

Hayashi, M., Denjoy, I., Extramiana, F., Maltret, A., Buisson, N. R., Lupoglazoff, J. M., Klug, D. *et al.* (2009). Incidence and risk factors of arrhythmic events in catecholaminergic polymorphic ventricular tachycardia. *Circulation* **119**:2426-2434.

Herrmann-Frank, A., Richter, M., Sarkozi, S., Mohr, U. and Lehmann-Horn, F. (1996). 4-Chloro-m-cresol, a potent and specific activator of the skeletal muscle ryanodine receptor. *Biochim Biophys Acta* **1289**:31-40.

Herron, T. J., Milstein, M. L., Anumonwo, J., Priori, S. G. and Jalife, J. (2010). Purkinje cell calcium dysregulation is the cellular mechanism that underlies catecholaminergic polymorphic ventricular tachycardia. *Heart Rhythm* **7**:1122-1128.

Hilliard, F. A., Steele, D. S., Laver, D., Yang, Z., Le Marchand, S. J., Chopra, N., Piston, D. W. *et al.* (2010). Flecainide inhibits arrhythmogenic Ca<sup>2+</sup> waves by open

state block of ryanodine receptor Ca<sup>2+</sup> release channels and reduction of Ca<sup>2+</sup> spark mass. *J Mol Cell Cardiol* **48**:293-301.

Hino, A., Yano, M., Kato, T., Fukuda, M., Suetomi, T., Ono, M., Murakami, W. *et al.* (2012). Enhanced binding of calmodulin to the ryanodine receptor corrects contractile dysfunction in failing hearts. *Cardiovasc Res* **96**:433-443.

Hsueh, C. H., Weng, Y. C., Chen, C. Y., Lin, T. K., Lin, Y. H., Lai, L. P. and Lin, J. L. (2006). A novel mutation (Arg169Gln) of the cardiac ryanodine receptor gene causing exercise-induced bidirectional ventricular tachycardia. *Int J Cardiol*. Vol. 108. Ireland, pp. 276-278.

Huber, T., Naganathan, S., Tian, H., Ye, S. and Sakmar, T. P. (2013). Unnatural amino acid mutagenesis of GPCRs using amber codon suppression and bioorthogonal labeling. *Methods Enzymol* **520**:281-305.

Hunt, D. J., Jones, P. P., Wang, R., Chen, W., Bolstad, J., Chen, K., Shimoni, Y. *et al.* (2007). K201 (JTV519) suppresses spontaneous Ca<sup>2+</sup> release and [<sup>3</sup>H]ryanodine binding to RyR2 irrespective of FKBP12.6 association. *Biochem J* **404**:431-438.

Hunton, D. L., Lucchesi, P. A., Pang, Y., Cheng, X., Dell'Italia, L. J. and Marchase, R. B. (2002). Capacitative calcium entry contributes to nuclear factor of activated T-cells nuclear translocation and hypertrophy in cardiomyocytes. *J Biol Chem* **277**:14266-14273.

Hurne, A. M., O'Brien, J. J., Wingrove, D., Cherednichenko, G., Allen, P. D., Beam, K. G. and Pessah, I. N. (2005). Ryanodine receptor type 1 (RyR1) mutations C4958S and C4961S reveal excitation-coupled calcium entry (ECCE) is independent of sarcoplasmic reticulum store depletion. *Journal of Biological Chemistry* **280**:36994-37004.

Hutlin, E. L., Jedrychowski, M. P., Elias, J. E., Goswami, T., Rad, R., Beausoleil, S. A., Villen, J. *et al.* (2010). A tissue-specific atlas of mouse protein phosphorylation and expression. *Cell* **143**:1174-1189.

Inan, S. and Wei, H. (2010). The cytoprotective effects of dantrolene: a ryanodine receptor antagonist. *Anesth Analg* **111**:1400-1410.

James, L. C., Keeble, A. H., Khan, Z., Rhodes, D. A. and Trowsdale, J. (2007). Structural basis for PRYSPRY-mediated tripartite motif (TRIM) protein function. *Proc Natl Acad Sci U S A* **104**:6200-6205.

Jiang, D., Jones, P. P., Davis, D. R., Gow, R., Green, M. S., Birnie, D. H., Chen, S. R. *et al.* (2010). Characterization of a novel mutation in the cardiac ryanodine receptor that results in catecholaminergic polymorphic ventricular tachycardia. *Channels (Austin)* **4**:302-310.

Jiang, D., Wang, R., Xiao, B., Kong, H., Hunt, D. J., Choi, P., Zhang, L. *et al.* (2005). Enhanced store overload-induced Ca<sup>2+</sup> release and channel sensitivity to luminal

Ca<sup>2+</sup> activation are common defects of RyR2 mutations linked to ventricular tachycardia and sudden death. *Circ Res* **97**:1173-1181.

Jiang, D., Xiao, B., Li, X. and Chen, S. R. (2003). Smooth muscle tissues express a major dominant negative splice variant of the type 3 Ca<sup>2+</sup> release channel (ryanodine receptor). *J Biol Chem* **278**:4763-4769.

Jiang, D., Xiao, B., Yang, D., Wang, R., Choi, P., Zhang, L., Cheng, H. et al. (2004). RyR2 mutations linked to ventricular tachycardia and sudden death reduce the threshold for store-overload-induced Ca<sup>2+</sup> release (SOICR). *Proc Natl Acad Sci U S A* **101**:13062-13067.

Jiang, D., Xiao, B., Zhang, L. and Chen, S. R. (2002a). Enhanced basal activity of a cardiac Ca<sup>2+</sup> release channel (ryanodine receptor) mutant associated with ventricular tachycardia and sudden death. *Circ Res* **91**:218-225.

Jiang, M. T., Lokuta, A. J., Farrell, E. F., Wolff, M. R., Haworth, R. A. and Valdivia, H. H. (2002b). Abnormal Ca<sup>2+</sup> release, but normal ryanodine receptors, in canine and human heart failure. *Circ Res* **91**:1015-1022.

Jones, P., Meng, X., Xiao, B., Cai, S., Bolstad, J., Wagenknecht, T., Liu, Z. et al. (2008). Localization of PKA phosphorylation site, Ser(2030), in the three-dimensional structure of cardiac ryanodine receptor. *Biochem J* **410**:261-270.

Jung, C. B., Moretti, A., Mederos y Schnitzler, M., Iop, L., Storch, U., Bellin, M., Dorn, T. et al. (2012). Dantrolene rescues arrhythmogenic RYR2 defect in a patient-specific stem cell model of catecholaminergic polymorphic ventricular tachycardia. *EMBO Mol Med* **4**:180-191.

Kang, G., Giovannone, S. F., Liu, N., Liu, F. Y., Zhang, J., Priori, S. G. and Fishman, G. I. (2010). Purkinje cells from RyR2 mutant mice are highly arrhythmogenic but responsive to targeted therapy. *Circ Res* **107**:512-519.

Kannankeril, P., Mitchell, B., Goonasekera, S., Chelu, M., Zhang, W., Sood, S., Kearney, D. et al. (2006). Mice with the R176Q cardiac ryanodine receptor mutation exhibit catecholamine-induced ventricular tachycardia and cardiomyopathy. *Proc Natl Acad Sci U S A* **103**:12179-12184.

Kashimura, T., Briston, S. J., Trafford, A. W., Napolitano, C., Priori, S. G., Eisner, D. A. and Venetucci, L. A. (2010). In the RyR2(R4496C) mouse model of CPVT, β-adrenergic stimulation induces Ca waves by increasing SR Ca content and not by decreasing the threshold for Ca waves. *Circ Res* **107**:1483-1489.

Kilpatrick, B. S., Eden, E. R., Schapira, A. H., Futter, C. E. and Patel, S. (2013). Direct mobilisation of lysosomal Ca<sup>2+</sup> triggers complex Ca<sup>2+</sup> signals. *J Cell Sci* **126**:60-66.

Kim, E., Youn, B., Kemper, L., Campbell, C., Milting, H., Varsanyi, M. and Kang, C. (2007). Characterization of human cardiac calsequestrin and its deleterious mutants. *J Mol Biol* **373**:1047-1057.

Kimlicka, L., Lau, K., Tung, C. C. and Van Petegem, F. (2013). Disease mutations in the ryanodine receptor N-terminal region couple to a mobile intersubunit interface. *Nat Commun* **4**:1506.

Kimura, T., Lueck, J. D., Harvey, P. J., Pace, S. M., Ikemoto, N., Casarotto, M. G., Dirksen, R. T. *et al.* (2009). Alternative splicing of RyR1 alters the efficacy of skeletal EC coupling. *Cell Calcium* **45**:264-274.

Kimura, T., Nakamori, M., Lueck, J. D., Pouliquin, P., Aoike, F., Fujimura, H., Dirksen, R. T. *et al.* (2005). Altered mRNA splicing of the skeletal muscle ryanodine receptor and sarcoplasmic/endoplasmic reticulum Ca<sup>2+</sup>-ATPase in myotonic dystrophy type 1. *Hum Mol Genet* **14**:2189-2200.

Kimura, T., Pace, S. M., Wei, L., Beard, N. A., Dirksen, R. T. and Dulhunty, A. F. (2007). A variably spliced region in the type 1 ryanodine receptor may participate in an inter-domain interaction. *Biochem J* **401**:317-324.

Knollmann, B. C. (2009). New roles of calsequestrin and triadin in cardiac muscle. *J Physiol* **587**:3081-3087.

Knollmann, B. C., Chopra, N., Hlaing, T., Akin, B., Yang, T., Ettenson, K., Knollmann, B. E. *et al.* (2006). Casq2 deletion causes sarcoplasmic reticulum volume increase, premature Ca<sup>2+</sup> release, and catecholaminergic polymorphic ventricular tachycardia. *J Clin Invest* **116**:2510-2520.

Kobayashi, S., Bannister, M., Gangopadhyay, J., Hamada, T., Parness, J. and Ikemoto, N. (2005). Dantrolene stabilizes domain interactions within the ryanodine receptor. *J Biol Chem* **280**:6580-6587.

Kobayashi, S., Yamamoto, T., Parness, J. and Ikemoto, N. (2004). Antibody probe study of Ca<sup>2+</sup> channel regulation by interdomain interaction within the ryanodine receptor. *Biochem J* **380**:561-569.

Kobayashi, S., Yano, M., Suetomi, T., Ono, M., Tateishi, H., Mochizuki, M., Xu, X. *et al.* (2009). Dantrolene, a therapeutic agent for malignant hyperthermia, markedly improves the function of failing cardiomyocytes by stabilizing interdomain interactions within the ryanodine receptor. *J Am Coll Cardiol* **53**:1993-2005.

Kobayashi, S., Yano, M., Uchinoumi, H., Suetomi, T., Susa, T., Ono, M., Xu, X. *et al.* (2010). Dantrolene, a therapeutic agent for malignant hyperthermia, inhibits catecholaminergic polymorphic ventricular tachycardia in a RyR2(R2474S<sup>+/</sup>) knock-in mouse model. *Circ J* **74**:2579-2584.

Kohno, M., Yano, M., Kobayashi, S., Doi, M., Oda, T., Tokuhisa, T., Okuda, S. *et al.* (2003). A new cardioprotective agent, JTV519, improves defective channel gating of ryanodine receptor in heart failure. *Am J Physiol Heart Circ Physiol* **284**:H1035-1042.

Kolb, M. E., Horne, M. L. and Martz, R. (1982). Dantrolene in human malignant hyperthermia. *Anesthesiology* **56**:254-262.

Kouwen, T. R., Andréll, J., Schrijver, R., Dubois, J. Y., Maher, M. J., Iwata, S., Carpenter, E. P. *et al.* (2008). Thioredoxin A active-site mutants form mixed disulfide dimers that resemble enzyme-substrate reaction intermediates. *J Mol Biol* **379**:520-534.

Krebs, J. and Michalak, M. (2007). Calcium: A Matter of Life or Death Preface. *Calcium: a Matter of Life or Death* **41**:XVII-XVII.

Kushnir, A., Shan, J., Betzenhauser, M. J., Reiken, S. and Marks, A. R. (2010). Role of CaMKII $\delta$  phosphorylation of the cardiac ryanodine receptor in the force frequency relationship and heart failure. *Proc Natl Acad Sci U S A* **107**:10274-10279.

Lahat, H., Pras, E., Olander, T., Avidan, N., Ben-Asher, E., Man, O., Levy-Nissenbaum, E. *et al.* (2001). A missense mutation in a highly conserved region of CASQ2 is associated with autosomal recessive catecholamine-induced polymorphic ventricular tachycardia in Bedouin families from Israel. *Am J Hum Genet* **69**:1378-1384.

Lai, F. A., Misra, M., Xu, L., Smith, H. A. and Meissner, G. (1989). The ryanodine receptor-Ca $^{2+}$  release channel complex of skeletal muscle sarcoplasmic reticulum. Evidence for a cooperatively coupled, negatively charged homotetramer. *J Biol Chem* **264**:16776-16785.

Laitinen, P. J., Brown, K. M., Piippo, K., Swan, H., Devaney, J. M., Brahmbhatt, B., Donarum, E. A. *et al.* (2001). Mutations of the cardiac ryanodine receptor (RyR2) gene in familial polymorphic ventricular tachycardia. *Circulation* **103**:485-490.

Laitinen, P. J., Swan, H. and Kontula, K. (2003). Molecular genetics of exercise-induced polymorphic ventricular tachycardia: identification of three novel cardiac ryanodine receptor mutations and two common calsequestrin 2 amino-acid polymorphisms. *Eur J Hum Genet* **11**:888-891.

Lamb, G. D. and Posterino, G. S. (2003). Effects of oxidation and reduction on contractile function in skeletal muscle fibres of the rat. *J Physiol* **546**:149-163.

Lamb, G. D., Posterino, G. S., Yamamoto, T. and Ikemoto, N. (2001). Effects of a domain peptide of the ryanodine receptor on Ca $^{2+}$  release in skinned skeletal muscle fibers. *Am J Physiol Cell Physiol* **281**:C207-214.

Lanner, J. T., Georgiou, D. K., Joshi, A. D. and Hamilton, S. L. (2010). Ryanodine receptors: structure, expression, molecular details, and function in calcium release. *Cold Spring Harb Perspect Biol* **2**:a003996.

Laver, D. R. and Honen, B. N. (2008). Luminal Mg $^{2+}$ , a key factor controlling RYR2-mediated Ca $^{2+}$  release: cytoplasmic and luminal regulation modeled in a tetrameric channel. *J Gen Physiol* **132**:429-446.

Laver, D. R., Honen, B. N., Lamb, G. D. and Ikemoto, N. (2008). A domain peptide of the cardiac ryanodine receptor regulates channel sensitivity to luminal Ca<sup>2+</sup> via cytoplasmic Ca<sup>2+</sup> sites. *Eur Biophys J* **37**:455-467.

Lee, C. W., Lee, E. H., Takeuchi, K., Takahashi, H., Shimada, I., Sato, K., Shin, S. Y. et al. (2004). Molecular basis of the high-affinity activation of type 1 ryanodine receptors by imperatoxin A. *Biochem J* **377**:385-394.

Lee, E. H. and Allen, P. D. (2007). Homo-dimerization of RyR1 C-terminus via charged residues in random coils or in an alpha-helix. *Exp Mol Med* **39**:594-602.

Leenhardt, A., Denjoy, I. and Guicheney, P. (2012). Catecholaminergic polymorphic ventricular tachycardia. *Circ Arrhythm Electrophysiol* **5**:1044-1052.

Leenhardt, A., Lucet, V., Denjoy, I., Grau, F., Ngoc, D. D. and Coumel, P. (1995). Catecholaminergic polymorphic ventricular tachycardia in children. A 7-year follow-up of 21 patients. *Circulation* **91**:1512-1519.

Lehnart, S. E., Wehrens, X. H., Laitinen, P. J., Reiken, S. R., Deng, S. X., Cheng, Z., Landry, D. W. et al. (2004). Sudden death in familial polymorphic ventricular tachycardia associated with calcium release channel (ryanodine receptor) leak. *Circulation* **109**:3208-3214.

Leong, P. and MacLennan, D. H. (1998a). A 37-amino acid sequence in the skeletal muscle ryanodine receptor interacts with the cytoplasmic loop between domains II and III in the skeletal muscle dihydropyridine receptor. *J Biol Chem* **273**:7791-7794.

Leong, P. and MacLennan, D. H. (1998b). The cytoplasmic loops between domains II and III and domains III and IV in the skeletal muscle dihydropyridine receptor bind to a contiguous site in the skeletal muscle ryanodine receptor. *J Biol Chem* **273**:29958-29964.

Li, P. and Chen, S. R. (2001). Molecular basis of Ca(2)+ activation of the mouse cardiac Ca(2)+ release channel (ryanodine receptor). *J Gen Physiol* **118**:33-44.

Li, S., Chen, G. and Li, R. A. (2013). Calcium Signaling of Human Pluripotent Stem Cell-Derived Cardiomyocytes. *J Physiol*.

Liang, X., Chen, K., Fruen, B., Hu, J., Ma, J., Hu, X. and Parness, J. (2009). Impaired interaction between skeletal ryanodine receptors in malignant hyperthermia. *Integr Biol (Camb)* **1**:533-539.

Liu, G., Abramson, J. J., Zable, A. C. and Pessah, I. N. (1994). Direct evidence for the existence and functional role of hyperreactive sulfhydryls on the ryanodine receptor-triadin complex selectively labeled by the coumarin maleimide 7-diethylamino-3-(4'-maleimidylphenyl)-4-methylcoumarin. *Mol Pharmacol* **45**:189-200.

Liu, N., Colombi, B., Memmi, M., Zissimopoulos, S., Rizzi, N., Negri, S., Imbriani, M. et al. (2006). Arrhythmogenesis in catecholaminergic polymorphic ventricular

tachycardia: insights from a RyR2 R4496C knock-in mouse model. *Circ Res* **99**:292-298.

Liu, N., Denegri, M., Ruan, Y., Avelino-Cruz, J. E., Perissi, A., Negri, S., Napolitano, C. *et al.* (2011a). Short communication: flecainide exerts an antiarrhythmic effect in a mouse model of catecholaminergic polymorphic ventricular tachycardia by increasing the threshold for triggered activity. *Circ Res* **109**:291-295.

Liu, N., Ruan, Y., Denegri, M., Bachetti, T., Li, Y., Colombi, B., Napolitano, C. *et al.* (2011b). Calmodulin kinase II inhibition prevents arrhythmias in RyR2(R4496C+/-) mice with catecholaminergic polymorphic ventricular tachycardia. *J Mol Cell Cardiol* **50**:214-222.

Liu, Z., Wang, R., Tian, X., Zhong, X., Gangopadhyay, J., Cole, R., Ikemoto, N. *et al.* (2010). Dynamic, inter-subunit interactions between the N-terminal and central mutation regions of cardiac ryanodine receptor. *J Cell Sci* **123**:1775-1784.

Liu, Z., Wang, R., Zhang, J., Chen, S. and Wagenknecht, T. (2005). Localization of a disease-associated mutation site in the three-dimensional structure of the cardiac muscle ryanodine receptor. *J Biol Chem* **280**:37941-37947.

Liu, Z., Zhang, J., Li, P., Chen, S. and Wagenknecht, T. (2002). Three-dimensional reconstruction of the recombinant type 2 ryanodine receptor and localization of its divergent region 1. *J Biol Chem* **277**:46712-46719.

Liu, Z., Zhang, J., Wang, R., Wayne Chen, S. and Wagenknecht, T. (2004). Location of divergent region 2 on the three-dimensional structure of cardiac muscle ryanodine receptor/calcium release channel. *J Mol Biol* **338**:533-545.

Lobo, P. and Van Petegem, F. (2009). Crystal structures of the N-terminal domains of cardiac and skeletal muscle ryanodine receptors: insights into disease mutations. *Structure* **17**:1505-1514.

Lokuta, A. J., Meyers, M. B., Sander, P. R., Fishman, G. I. and Valdivia, H. H. (1997). Modulation of cardiac ryanodine receptors by sorcin. *J Biol Chem* **272**:25333-25338.

Ludtke, S., Serysheva, I., Hamilton, S. and Chiu, W. (2005). The pore structure of the closed RyR1 channel. *Structure* **13**:1203-1211.

Lynch, P. J., Tong, J., Lehane, M., Mallet, A., Giblin, L., Heffron, J. J., Vaughan, P. *et al.* (1999). A mutation in the transmembrane/luminal domain of the ryanodine receptor is associated with abnormal Ca<sup>2+</sup> release channel function and severe central core disease. *Proc Natl Acad Sci U S A* **96**:4164-4169.

Löhn, M., Jessner, W., Fürstenau, M., Wellner, M., Sorrentino, V., Haller, H., Luft, F. C. *et al.* (2001). Regulation of calcium sparks and spontaneous transient outward currents by RyR3 in arterial vascular smooth muscle cells. *Circ Res* **89**:1051-1057.

MacDonnell, S. M., Garcia-Rivas, G., Scherman, J. A., Kubo, H., Chen, X., Valdivia, H. and Houser, S. R. (2008). Adrenergic regulation of cardiac contractility does not involve phosphorylation of the cardiac ryanodine receptor at serine 2808. *Circ Res* **102**:e65-72.

MacLennan, D. H. and Zvaritch, E. (2011). Mechanistic models for muscle diseases and disorders originating in the sarcoplasmic reticulum. *Biochim Biophys Acta* **1813**:948-964.

Marinov, B. S., Olojo, R. O., Xia, R. and Abramson, J. J. (2007). Non-thiol reagents regulate ryanodine receptor function by redox interactions that modify reactive thiols. *Antioxid Redox Signal* **9**:609-621.

Marjamaa, A., Laitinen-Forsblom, P., Lahtinen, A. M., Viitasalo, M., Toivonen, L., Kontula, K. and Swan, H. (2009). Search for cardiac calcium cycling gene mutations in familial ventricular arrhythmias resembling catecholaminergic polymorphic ventricular tachycardia. *BMC Med Genet* **10**:12.

Marjamaa, A., Laitinen-Forsblom, P., Wronska, A., Toivonen, L., Kontula, K. and Swan, H. (2011). Ryanodine receptor (RyR2) mutations in sudden cardiac death: studies in extended pedigrees and phenotypic characterization in vitro. *Int J Cardiol* **147**:246-252.

Marx, S., Reiken, S., Hisamatsu, Y., Gaburjakova, M., Gaburjakova, J., Yang, Y., Rosemblit, N. et al. (2001a). Phosphorylation-dependent regulation of ryanodine receptors: a novel role for leucine/isoleucine zippers. *J Cell Biol* **153**:699-708.

Marx, S. O., Gaburjakova, J., Gaburjakova, M., Henrikson, C., Ondrias, K. and Marks, A. R. (2001b). Coupled gating between cardiac calcium release channels (ryanodine receptors). *Circ Res* **88**:1151-1158.

Marx, S. O., Ondrias, K. and Marks, A. R. (1998). Coupled gating between individual skeletal muscle Ca<sup>2+</sup> release channels (ryanodine receptors). *Science* **281**:818-821.

Marx, S. O., Reiken, S., Hisamatsu, Y., Jayaraman, T., Burkhoff, D., Rosemblit, N. and Marks, A. R. (2000). PKA phosphorylation dissociates FKBP12.6 from the calcium release channel (ryanodine receptor): defective regulation in failing hearts. *Cell* **101**:365-376.

Marziali, G., Rossi, D., Giannini, G., Charlesworth, A. and Sorrentino, V. (1996). cDNA cloning reveals a tissue specific expression of alternatively spliced transcripts of the ryanodine receptor type 3 (RyR3) calcium release channel. *FEBS Lett* **394**:76-82.

Masumiya, H., Wang, R., Zhang, J., Xiao, B. and Chen, S. R. (2003). Localization of the 12.6-kDa FK506-binding protein (FKBP12.6) binding site to the NH<sub>2</sub>-terminal domain of the cardiac Ca<sup>2+</sup> release channel (ryanodine receptor). *J Biol Chem* **278**:3786-3792.

Mathur, N., Sood, S., Wang, S., van Oort, R. J., Sarma, S., Li, N., Skapura, D. G. *et al.* (2009). Sudden infant death syndrome in mice with an inherited mutation in RyR2. *Circ Arrhythm Electrophysiol* **2**:677-685.

Maxwell, J. T., Domeier, T. L. and Blatter, L. A. (2012). Dantrolene prevents arrhythmogenic Ca<sup>2+</sup> release in heart failure. *Am J Physiol Heart Circ Physiol* **302**:H953-963.

Medeiros-Domingo, A., Bhuiyan, Z. A., Tester, D. J., Hofman, N., Bikker, H., van Tintelen, J. P., Mannens, M. M. *et al.* (2009). The RYR2-encoded ryanodine receptor/calcium release channel in patients diagnosed previously with either catecholaminergic polymorphic ventricular tachycardia or genotype negative, exercise-induced long QT syndrome: a comprehensive open reading frame mutational analysis. *J Am Coll Cardiol* **54**:2065-2074.

Medzihradszky, K. F., Campbell, J. M., Baldwin, M. A., Falick, A. M., Juhasz, P., Vestal, M. L. and Burlingame, A. L. (2000). The characteristics of peptide collision-induced dissociation using a high-performance MALDI-TOF/TOF tandem mass spectrometer. *Anal Chem* **72**:552-558.

Meissner, G., Rios, E., Tripathy, A. and Pasek, D. A. (1997). Regulation of skeletal muscle Ca<sup>2+</sup> release channel (ryanodine receptor) by Ca<sup>2+</sup> and monovalent cations and anions. *J Biol Chem* **272**:1628-1638.

Meli, A. C., Refaat, M. M., Dura, M., Reiken, S., Wronska, A., Wojciak, J., Carroll, J. *et al.* (2011). A novel ryanodine receptor mutation linked to sudden death increases sensitivity to cytosolic calcium. *Circ Res* **109**:281-290.

Meng, X., Xiao, B., Cai, S., Huang, X., Li, F., Bolstad, J., Trujillo, R. *et al.* (2007). Three-dimensional localization of serine 2808, a phosphorylation site in cardiac ryanodine receptor. *J Biol Chem* **282**:25929-25939.

Meyers, M. B., Fischer, A., Sun, Y. J., Lopes, C. M., Rohacs, T., Nakamura, T. Y., Zhou, Y. Y. *et al.* (2003). Sorcin regulates excitation-contraction coupling in the heart. *J Biol Chem* **278**:28865-28871.

Mikoshiba, K. (2007). IP3 receptor/Ca<sup>2+</sup> channel: from discovery to new signaling concepts. *J Neurochem* **102**:1426-1446.

Milting, H., Lukas, N., Klauke, B., Korfer, R., Perrot, A., Osterziel, K. J., Vogt, J. *et al.* (2006). Composite polymorphisms in the ryanodine receptor 2 gene associated with arrhythmogenic right ventricular cardiomyopathy. *Cardiovasc Res* **71**:496-505.

Mochizuki, M., Yano, M., Oda, T., Tateishi, H., Kobayashi, S., Yamamoto, T., Ikeda, Y. *et al.* (2007). Scavenging free radicals by low-dose carvedilol prevents redox-dependent Ca<sup>2+</sup> leak via stabilization of ryanodine receptor in heart failure. *J Am Coll Cardiol* **49**:1722-1732.

Monkawa, T., Miyawaki, A., Sugiyama, T., Yoneshima, H., Yamamoto-Hino, M., Furuichi, T., Saruta, T. *et al.* (1995). Heterotetrameric complex formation of inositol 1,4,5-trisphosphate receptor subunits. *J Biol Chem* **270**:14700-14704.

Monnier, N., Marty, I., Faure, J., Castiglioni, C., Desnuelle, C., Sacconi, S., Estournet, B. *et al.* (2008). Null mutations causing depletion of the type 1 ryanodine receptor (RYR1) are commonly associated with recessive structural congenital myopathies with cores. *Hum Mutat* **29**:670-678.

Monnier, N., Procaccio, V., Stieglitz, P. and Lunardi, J. (1997). Malignant-hyperthermia susceptibility is associated with a mutation of the alpha 1-subunit of the human dihydropyridine-sensitive L-type voltage-dependent calcium-channel receptor in skeletal muscle. *Am J Hum Genet* **60**:1316-1325.

Moore, C. P., Rodney, G., Zhang, J. Z., Santacruz-Toloza, L., Strasburg, G. and Hamilton, S. L. (1999). Apocalmodulin and Ca<sup>2+</sup> calmodulin bind to the same region on the skeletal muscle Ca<sup>2+</sup> release channel. *Biochemistry* **38**:8532-8537.

Morgan, R. O., Martin-Almedina, S., Iglesias, J. M., Gonzalez-Florez, M. I. and Fernandez, M. P. (2004). Evolutionary perspective on annexin calcium-binding domains. *Biochim Biophys Acta* **1742**:133-140.

Muik, M., Schindl, R., Fahrner, M. and Romanin, C. (2012). Ca(2+) release-activated Ca(2+) (CRAC) current, structure, and function. *Cell Mol Life Sci* **69**:4163-4176.

Murayama, T., Kurebayashi, N., Oba, T., Oyamada, H., Oguchi, K., Sakurai, T. and Ogawa, Y. (2011). Role of amino-terminal half of the S4-S5 linker in type 1 ryanodine receptor (RyR1) channel gating. *J Biol Chem* **286**:35571-35577.

Murayama, T., Oba, T., Hara, H., Wakebe, K., Ikemoto, N. and Ogawa, Y. (2007). Postulated role of interdomain interaction between regions 1 and 2 within type 1 ryanodine receptor in the pathogenesis of porcine malignant hyperthermia. *Biochem J* **402**:349-357.

Murayama, T., Oba, T., Kobayashi, S., Ikemoto, N. and Ogawa, Y. (2005). Postulated role of interdomain interactions within the type 1 ryanodine receptor in the low gain of Ca<sup>2+</sup>-induced Ca<sup>2+</sup> release activity of mammalian skeletal muscle sarcoplasmic reticulum. *Am J Physiol Cell Physiol* **288**:C1222-1230.

Murayama, T. and Ogawa, Y. (1996). Properties of RyR3 ryanodine receptor isoform in mammalian brain. *J Biol Chem* **271**:5079-5084.

Murayama, T. and Ogawa, Y. (1997). Characterization of type 3 ryanodine receptor (RyR3) of sarcoplasmic reticulum from rabbit skeletal muscles. *J Biol Chem* **272**:24030-24037.

Naganathan, S., Ye, S., Sakmar, T. P. and Huber, T. (2013). Site-specific epitope tagging of G protein-coupled receptors by bioorthogonal modification of a genetically encoded unnatural amino acid. *Biochemistry* **52**:1028-1036.

Nakai, J., Dirksen, R. T., Nguyen, H. T., Pessah, I. N., Beam, K. G. and Allen, P. D. (1996). Enhanced dihydropyridine receptor channel activity in the presence of ryanodine receptor. *Nature* **380**:72-75.

Nakai, J., Imagawa, T., Hakamat, Y., Shigekawa, M., Takeshima, H. and Numa, S. (1990). Primary structure and functional expression from cDNA of the cardiac ryanodine receptor/calcium release channel. *FEBS Lett* **271**:169-177.

Nakai, J., Ogura, T., Protasi, F., Franzini-Armstrong, C., Allen, P. D. and Beam, K. G. (1997). Functional nonequality of the cardiac and skeletal ryanodine receptors. *Proc Natl Acad Sci U S A* **94**:1019-1022.

Nakai, J., Sekiguchi, N., Rando, T. A., Allen, P. D. and Beam, K. G. (1998a). Two regions of the ryanodine receptor involved in coupling with L-type Ca<sup>2+</sup> channels. *J Biol Chem* **273**:13403-13406.

Nakai, J., Tanabe, T., Konno, T., Adams, B. and Beam, K. G. (1998b). Localization in the II-III loop of the dihydropyridine receptor of a sequence critical for excitation-contraction coupling. *J Biol Chem* **273**:24983-24986.

Nishio, H., Iwata, M., Tamura, A., Miyazaki, T., Tsuboi, K. and Suzuki, K. (2008). Identification of a novel mutation V2321M of the cardiac ryanodine receptor gene of sudden unexplained death and a phenotypic study of the gene mutations. *Leg Med (Tokyo)* **10**:196-200.

Novak, A., Lorber, A., Itskovitz-Eldor, J. and Binah, O. (2012). Modeling Catecholaminergic Polymorphic Ventricular Tachycardia using Induced Pluripotent Stem Cell-derived Cardiomyocytes. *Rambam Maimonides Med J* **3**:e0015.

Numa, S., Tanabe, T., Takeshima, H., Mikami, A., Niidome, T., Nishimura, S., Adams, B. A. et al. (1990). Molecular insights into excitation-contraction coupling. *Cold Spring Harb Symp Quant Biol* **55**:1-7.

Nyegaard, M., Overgaard, M. T., Sondergaard, M. T., Vranas, M., Behr, E. R., Hildebrandt, L. L., Lund, J. et al. (2012). Mutations in calmodulin cause ventricular tachycardia and sudden cardiac death. *Am J Hum Genet* **91**:703-712.

Oda, T., Yang, Y., Nitu, F. R., Svensson, B., Lu, X., Fruen, B. R., Cornea, R. L. et al. (2013). In cardiomyocytes, binding of unzipping peptide activates ryanodine receptor 2 and reciprocally inhibits calmodulin binding. *Circ Res* **112**:487-497.

Oda, T., Yano, M., Yamamoto, T., Tokuhisa, T., Okuda, S., Doi, M., Ohkusa, T. et al. (2005). Defective regulation of interdomain interactions within the ryanodine receptor plays a key role in the pathogenesis of heart failure. *Circulation* **111**:3400-3410.

Ondrias, K., Marx, S. O., Gaburjakova, M. and Marks, A. R. (1998). FKBP12 modulates gating of the ryanodine receptor/calcium release channel. *Ann N Y Acad Sci* **853**:149-156.

Ono, K. and Iijima, T. (2010). Cardiac T-type Ca(2+) channels in the heart. *J Mol Cell Cardiol* **48**:65-70.

Ono, M., Yano, M., Hino, A., Suetomi, T., Xu, X., Susa, T., Uchinoumi, H. et al. (2010). Dissociation of calmodulin from cardiac ryanodine receptor causes aberrant Ca(2+) release in heart failure. *Cardiovasc Res* **87**:609-617.

Palty, R., Hershfinkel, M. and Sekler, I. (2012). Molecular identity and functional properties of the mitochondrial Na+/Ca2+ exchanger. *J Biol Chem* **287**:31650-31657.

Paolini, C., Fessenden, J. D., Pessah, I. N. and Franzini-Armstrong, C. (2004). Evidence for conformational coupling between two calcium channels. *Proc Natl Acad Sci U S A* **101**:12748-12752.

Park, H., Park, I. Y., Kim, E., Youn, B., Fields, K., Dunker, A. K. and Kang, C. (2004). Comparing skeletal and cardiac calsequestrin structures and their calcium binding: a proposed mechanism for coupled calcium binding and protein polymerization. *J Biol Chem* **279**:18026-18033.

Park, I. Y., Kim, E. J., Park, H., Fields, K., Dunker, A. K. and Kang, C. (2005). Interaction between cardiac calsequestrin and drugs with known cardiotoxicity. *Mol Pharmacol* **67**:97-104.

Patel, S. and Brailoiu, E. (2012). Triggering of Ca2+ signals by NAADP-gated two-pore channels: a role for membrane contact sites? *Biochem Soc Trans* **40**:153-157.

Patel, S., Ramakrishnan, L., Rahman, T., Hamdoun, A., Marchant, J. S., Taylor, C. W. and Brailoiu, E. (2011). The endo-lysosomal system as an NAADP-sensitive acidic Ca(2+) store: role for the two-pore channels. *Cell Calcium* **50**:157-167.

Patterson, R. L., Boehning, D. and Snyder, S. H. (2004). Inositol 1,4,5-trisphosphate receptors as signal integrators. *Annu Rev Biochem* **73**:437-465.

Paul-Pletzer, K., Yamamoto, T., Bhat, M., Ma, J., Ikemoto, N., Jimenez, L., Morimoto, H. et al. (2002). Identification of a dantrolene-binding sequence on the skeletal muscle ryanodine receptor. *J Biol Chem* **277**:34918-34923.

Paul-Pletzer, K., Yamamoto, T., Ikemoto, N., Jimenez, L., Morimoto, H., Williams, P., Ma, J. et al. (2005). Probing a putative dantrolene-binding site on the cardiac ryanodine receptor. *Biochem J* **387**:905-909.

Perez, C. F., Mukherjee, S. and Allen, P. D. (2003). Amino acids 1-1,680 of ryanodine receptor type 1 hold critical determinants of skeletal type for excitation-contraction coupling. Role of divergence domain D2. *J Biol Chem* **278**:39644-39652.

Perfetto, L., Gherardini, P. F., Davey, N. E., Diella, F., Helmer-Citterich, M. and Cesareni, G. (2013). Exploring the diversity of SPRY/B30.2-mediated interactions. *Trends Biochem Sci* **38**:38-46.

Pessah, I. N. and Zimanyi, I. (1991). Characterization of multiple [<sup>3</sup>H]ryanodine binding sites on the Ca<sup>2+</sup> release channel of sarcoplasmic reticulum from skeletal and cardiac muscle: evidence for a sequential mechanism in ryanodine action. *Mol Pharmacol* **39**:679-689.

Petrotchenko, E., Pasek, D., Elms, P., Dokholyan, N., Meissner, G. and Borchers, C. (2006). Combining fluorescence detection and mass spectrometric analysis for comprehensive and quantitative analysis of redox-sensitive cysteines in native membrane proteins. *Anal Chem* **78**:7959-7966.

Petrotchenko, E. V., Yamaguchi, N., Pasek, D. A., Borchers, C. H. and Meissner, G. (2011). Mass spectrometric analysis and mutagenesis predict involvement of multiple cysteines in redox regulation of the skeletal muscle ryanodine receptor ion channel complex. *Res Rep Biol* **2011**:13-21.

Porta, M., Diaz-Sylvester, P. L., Neumann, J. T., Escobar, A. L., Fleischer, S. and Copello, J. A. (2012). Coupled gating of skeletal muscle ryanodine receptors is modulated by Ca<sup>2+</sup>, Mg<sup>2+</sup>, and ATP. *Am J Physiol Cell Physiol* **303**:C682-697.

Porter Moore, C., Zhang, J. and Hamilton, S. (1999). A role for cysteine 3635 of RYR1 in redox modulation and calmodulin binding. *J Biol Chem* **274**:36831-36834.

Posterino, G. S., Cellini, M. A. and Lamb, G. D. (2003). Effects of oxidation and cytosolic redox conditions on excitation-contraction coupling in rat skeletal muscle. *J Physiol* **547**:807-823.

Postma, A. V., Denjoy, I., Kamblock, J., Alders, M., Lupoglazoff, J. M., Vaksman, G., Dubosq-Bidot, L. *et al.* (2005). Catecholaminergic polymorphic ventricular tachycardia: RYR2 mutations, bradycardia, and follow up of the patients. *J Med Genet*. Vol. 42. England, pp. 863-870.

Priori, S. G. and Chen, S. R. (2011). Inherited dysfunction of sarcoplasmic reticulum Ca<sup>2+</sup> handling and arrhythmogenesis. *Circ Res* **108**:871-883.

Priori, S. G., Napolitano, C., Memmi, M., Colombi, B., Drago, F., Gasparini, M., DeSimone, L. *et al.* (2002). Clinical and molecular characterization of patients with catecholaminergic polymorphic ventricular tachycardia. *Circulation* **106**:69-74.

Priori, S. G., Napolitano, C., Tiso, N., Memmi, M., Vignati, G., Bloise, R., Sorrentino, V. *et al.* (2001). Mutations in the cardiac ryanodine receptor gene (hRyR2) underlie catecholaminergic polymorphic ventricular tachycardia. *Circulation* **103**:196-200.

Protasi, F., Franzini-Armstrong, C. and Allen, P. D. (1998). Role of ryanodine receptors in the assembly of calcium release units in skeletal muscle. *J Cell Biol* **140**:831-842.

Protasi, F., Paolini, C., Nakai, J., Beam, K. G., Franzini-Armstrong, C. and Allen, P. D. (2002). Multiple regions of RyR1 mediate functional and structural interactions

with alpha(1S)-dihydropyridine receptors in skeletal muscle. *Biophys J* **83**:3230-3244.

Qin, J., Valle, G., Nani, A., Chen, H., Ramos-Franco, J., Nori, A., Volpe, P. *et al.* (2009). Ryanodine receptor luminal Ca<sup>2+</sup> regulation: swapping calsequestrin and channel isoforms. *Biophys J* **97**:1961-1970.

Qin, J., Valle, G., Nani, A., Nori, A., Rizzi, N., Priori, S. G., Volpe, P. *et al.* (2008). Luminal Ca<sup>2+</sup> regulation of single cardiac ryanodine receptors: insights provided by calsequestrin and its mutants. *J Gen Physiol* **131**:325-334.

Ramachandran, S., Chakraborty, A., Xu, L., Mei, Y., Samsó, M., Dokholyan, N. V. and Meissner, G. (2013). Structural determinants of skeletal muscle ryanodine receptor gating. *J Biol Chem* **288**:6154-6165.

Ramachandran, S., Serohijos, A. W., Xu, L., Meissner, G. and Dokholyan, N. V. (2009). A structural model of the pore-forming region of the skeletal muscle ryanodine receptor (RyR1). *PLoS Comput Biol* **5**:e1000367.

Rodney, G. G., Wilson, G. M. and Schneider, M. F. (2005). A calmodulin binding domain of RyR increases activation of spontaneous Ca<sup>2+</sup> sparks in frog skeletal muscle. *J Biol Chem* **280**:11713-11722.

Rotem, D., Mason, A. and Bayley, H. (2010). Inactivation of the KcsA potassium channel explored with heterotetramers. *J Gen Physiol* **135**:29-42.

Roux-Buisson, N., Cacheux, M., Fourest-Lievin, A., Fauconnier, J., Brocard, J., Denjoy, I., Durand, P. *et al.* (2012). Absence of triadin, a protein of the calcium release complex, is responsible for cardiac arrhythmia with sudden death in human. *Hum Mol Genet* **21**:2759-2767.

Sacherer, M., Sedej, S., Wakula, P., Wallner, M., Vos, M. A., Kockskamper, J., Siegler, P. *et al.* (2012). JTV519 (K201) reduces sarcoplasmic reticulum Ca(2)(+) leak and improves diastolic function in vitro in murine and human non-failing myocardium. *Br J Pharmacol* **167**:493-504.

Saito, A., Inui, M., Radermacher, M., Frank, J. and Fleischer, S. (1988). Ultrastructure of the calcium release channel of sarcoplasmic reticulum. *J Cell Biol* **107**:211-219.

Sambrook, J., Fritsch, E. F. E. F. and Maniatis, T. (1989). Molecular cloning : a laboratory manual. New York: Cold Spring Harbor Laboratory Press.

Samso, M., Feng, W., Pessah, I. N. and Allen, P. D. (2009). Coordinated movement of cytoplasmic and transmembrane domains of RyR1 upon gating. *Plos Biology* **7**:e85.

Samsó, M. and Wagenknecht, T. (2002). Apocalmodulin and Ca<sup>2+</sup>-calmodulin bind to neighboring locations on the ryanodine receptor. *J Biol Chem* **277**:1349-1353.

- Schug, Z. T. and Joseph, S. K. (2006). The role of the S4-S5 linker and C-terminal tail in inositol 1,4,5-trisphosphate receptor function. *J Biol Chem* **281**:24431-24440.
- Sedej, S., Heinzel, F. R., Walther, S., Dybkova, N., Wakula, P., Groborz, J., Gronau, P. et al. (2010). Na<sup>+</sup>-dependent SR Ca<sup>2+</sup> overload induces arrhythrogenic events in mouse cardiomyocytes with a human CPVT mutation. *Cardiovasc Res* **87**:50-59.
- Sencer, S., Papineni, R. V., Halling, D. B., Pate, P., Krol, J., Zhang, J. Z. and Hamilton, S. L. (2001). Coupling of RYR1 and L-type calcium channels via calmodulin binding domains. *J Biol Chem* **276**:38237-38241.
- Seo, M. D., Velamakanni, S., Ishiyama, N., Stathopoulos, P. B., Rossi, A. M., Khan, S. A., Dale, P. et al. (2012). Structural and functional conservation of key domains in InsP<sub>3</sub> and ryanodine receptors. *Nature* **483**:108-112.
- Serysheva, I., Hamilton, S., Chiu, W. and Ludtke, S. (2005). Structure of Ca<sup>2+</sup> release channel at 14 Å resolution. *J Mol Biol* **345**:427-431.
- Serysheva, I., Ludtke, S., Baker, M., Cong, Y., Topf, M., Eramian, D., Sali, A. et al. (2008). Subnanometer-resolution electron cryomicroscopy-based domain models for the cytoplasmic region of skeletal muscle RyR channel. *Proc Natl Acad Sci U S A* **105**:9610-9615.
- Sharma, M. R., Jeyakumar, L. H., Fleischer, S. and Wagenknecht, T. (2006). Three-dimensional visualization of FKBP12.6 binding to an open conformation of cardiac ryanodine receptor. *Biophys J* **90**:164-172.
- Sharma, P., Ishiyama, N., Nair, U., Li, W., Dong, A., Miyake, T., Wilson, A. et al. (2012). Structural determination of the phosphorylation domain of the ryanodine receptor. *FEBS J* **279**:3952-3964.
- Shtifman, A., Ward, C., Yamamoto, T., Wang, J., Olbinski, B., Valdivia, H., Ikemoto, N. et al. (2002). Interdomain interactions within ryanodine receptors regulate Ca<sup>2+</sup> spark frequency in skeletal muscle. *J Gen Physiol* **119**:15-32.
- Sikkel, M. B., Collins, T. P., Rowlands, C., Shah, M., O'Gara, P., Williams, A. J., Harding, S. E. et al. (2013a). Flecainide reduces Ca(2+) spark and wave frequency via inhibition of the sarcolemmal sodium current. *Cardiovasc Res* **98**:286-296.
- Sikkel, M. B., Collins, T. P., Rowlands, C., Shah, M., O'Gara, P., Williams, A. J., Harding, S. E. et al. (2013b). Triple mode of action of flecainide in catecholaminergic polymorphic ventricular tachycardia: reply. *Cardiovasc Res*. Vol. 98. England, pp. 327-328.
- Sitsapesan, R. and Williams, A. J. (1990). Mechanisms of caffeine activation of single calcium-release channels of sheep cardiac sarcoplasmic reticulum. *J Physiol* **423**:425-439.

Snyder, H. R., Jr., Davis, C. S., Bickerton, R. K. and Halliday, R. P. (1967). 1-[(5-arylfurylidene)amino]hydantoins. A new class of muscle relaxants. *J Med Chem* **10**:807-810.

Spoerner, M., Herrmann, C., Vetter, I. R., Kalbitzer, H. R. and Wittinghofer, A. (2001). Dynamic properties of the Ras switch I region and its importance for binding to effectors. *Proc Natl Acad Sci U S A* **98**:4944-4949.

Stange, M., Xu, L., Balshaw, D., Yamaguchi, N. and Meissner, G. (2003). Characterization of recombinant skeletal muscle (Ser-2843) and cardiac muscle (Ser-2809) ryanodine receptor phosphorylation mutants. *J Biol Chem* **278**:51693-51702.

Stewart, R., Zissimopoulos, S. and Lai, F. (2003). Oligomerization of the cardiac ryanodine receptor C-terminal tail. *Biochem J* **376**:795-799.

Stoynova, L., Solórzano, R. and Collins, E. D. (2004). Generation of large deletion mutants from plasmid DNA. *Biotechniques* **36**:402-404, 406.

Suarez, J., Belke, D. D., Gloss, B., Dieterle, T., McDonough, P. M., Kim, Y. K., Brunton, L. L. et al. (2004). In vivo adenoviral transfer of sorcin reverses cardiac contractile abnormalities of diabetic cardiomyopathy. *Am J Physiol Heart Circ Physiol* **286**:H68-75.

Suetomi, T., Yano, M., Uchinoumi, H., Fukuda, M., Hino, A., Ono, M., Xu, X. et al. (2011). Mutation-linked defective interdomain interactions within ryanodine receptor cause aberrant  $\text{Ca}^{2+}$  release leading to catecholaminergic polymorphic ventricular tachycardia. *Circulation* **124**:682-694.

Sun, J., Xin, C., Eu, J. P., Stamler, J. S. and Meissner, G. (2001a). Cysteine-3635 is responsible for skeletal muscle ryanodine receptor modulation by NO. *Proc Natl Acad Sci U S A* **98**:11158-11162.

Sun, J., Xu, L., Eu, J., Stamler, J. and Meissner, G. (2001b). Classes of thiols that influence the activity of the skeletal muscle calcium release channel. *J Biol Chem* **276**:15625-15630.

Sun, J., Xu, L., Eu, J. P., Stamler, J. S. and Meissner, G. (2003). Nitric oxide, NOC-12, and S-nitrosoglutathione modulate the skeletal muscle calcium release channel/ryanodine receptor by different mechanisms. An allosteric function for O<sub>2</sub> in S-nitrosylation of the channel. *J Biol Chem* **278**:8184-8189.

Sun, Q. A., Hess, D. T., Nogueira, L., Yong, S., Bowles, D. E., Eu, J., Laurita, K. R. et al. (2011). Oxygen-coupled redox regulation of the skeletal muscle ryanodine receptor-Ca<sup>2+</sup> release channel by NADPH oxidase 4. *Proc Natl Acad Sci U S A* **108**:16098-16103.

Sutko, J. L., Airey, J. A., Welch, W. and Ruest, L. (1997). The pharmacology of ryanodine and related compounds. *Pharmacol Rev* **49**:53-98.

Sy, R. W., Gollob, M. H., Klein, G. J., Yee, R., Skanes, A. C., Gula, L. J., Leong-Sit, P. *et al.* (2011). Arrhythmia characterization and long-term outcomes in catecholaminergic polymorphic ventricular tachycardia. *Heart Rhythm* **8**:864-871.

Szentesi, P., Collet, C., Sarkozi, S., Szegedi, C., Jona, I., Jacquemond, V., Kovacs, L. *et al.* (2001). Effects of dantrolene on steps of excitation-contraction coupling in mammalian skeletal muscle fibers. *J Gen Physiol* **118**:355-375.

Szilágyi, A., Grimm, V., Arakaki, A. K. and Skolnick, J. (2005). Prediction of physical protein-protein interactions. *Phys Biol* **2**:S1-16.

Tae, H., Casarotto, M. G. and Dulhunty, A. F. (2009a). Ubiquitous SPRY domains and their role in the skeletal type ryanodine receptor. *Eur Biophys J* **39**:51-59.

Tae, H., Wei, L., Willemse, H., Mirza, S., Gallant, E. M., Board, P. G., Dirksen, R. T. *et al.* (2011). The elusive role of the SPRY2 domain in RyR1. *Channels (Austin)* **5**:148-160.

Tae, H. S., Norris, N. C., Cui, Y., Karunasekara, Y., Board, P. G., Dulhunty, A. F. and Casarotto, M. G. (2009b). Molecular recognition of the disordered dihydropyridine receptor II-III loop by a conserved spry domain of the type 1 ryanodine receptor. *Clin Exp Pharmacol Physiol* **36**:346-349.

Takeshima, H., Nishimura, S., Matsumoto, T., Ishida, H., Kangawa, K., Minamino, N., Matsuo, H. *et al.* (1989). Primary structure and expression from complementary DNA of skeletal muscle ryanodine receptor. *Nature* **339**:439-445.

Tanabe, T., Beam, K. G., Adams, B. A., Niidome, T. and Numa, S. (1990). Regions of the skeletal muscle dihydropyridine receptor critical for excitation-contraction coupling. *Nature* **346**:567-569.

Tang, Y., Tian, X., Wang, R., Fill, M. and Chen, S. R. (2012). Abnormal termination of Ca<sup>2+</sup> release is a common defect of RyR2 mutations associated with cardiomyopathies. *Circ Res* **110**:968-977.

Tanna, B., Welch, W., Ruest, L., Sutko, J. L. and Williams, A. J. (1998). Interactions of a reversible ryanoid (21-amino-9alpha-hydroxy-ryanodine) with single sheep cardiac ryanodine receptor channels. *J Gen Physiol* **112**:55-69.

Tateishi, H., Yano, M., Mochizuki, M., Suetomi, T., Ono, M., Xu, X., Uchinoumi, H. *et al.* (2009). Defective domain-domain interactions within the ryanodine receptor as a critical cause of diastolic Ca<sup>2+</sup> leak in failing hearts. *Cardiovasc Res* **81**:536-545.

Taylor, C. W. and Tovey, S. C. (2010). IP(3) receptors: toward understanding their activation. *Cold Spring Harb Perspect Biol* **2**:a004010.

Terentyev, D., Györke, I., Belevych, A. E., Terentyeva, R., Sridhar, A., Nishijima, Y., de Blanco, E. C. *et al.* (2008a). Redox modification of ryanodine receptors contributes to sarcoplasmic reticulum Ca<sup>2+</sup> leak in chronic heart failure. *Circ Res* **103**:1466-1472.

Terentyev, D., Kubalova, Z., Valle, G., Nori, A., Vedamoorthyrao, S., Terentyeva, R., Viatchenko-Karpinski, S. *et al.* (2008b). Modulation of SR Ca release by luminal Ca and calsequestrin in cardiac myocytes: effects of CASQ2 mutations linked to sudden cardiac death. *Biophys J* **95**:2037-2048.

Tester, D. J., Arya, P., Will, M., Haglund, C. M., Farley, A. L., Makielski, J. C. and Ackerman, M. J. (2006). Genotypic heterogeneity and phenotypic mimicry among unrelated patients referred for catecholaminergic polymorphic ventricular tachycardia genetic testing. *Heart Rhythm* **3**:800-805.

Tester, D. J., Dura, M., Carturan, E., Reiken, S., Wronska, A., Marks, A. R. and Ackerman, M. J. (2007). A mechanism for sudden infant death syndrome (SIDS): stress-induced leak via ryanodine receptors. *Heart Rhythm* **4**:733-739.

Tester, D. J., Kopplin, L. J., Creighton, W., Burke, A. P. and Ackerman, M. J. (2005a). Pathogenesis of unexplained drowning: new insights from a molecular autopsy. *Mayo Clin Proc* **80**:596-600.

Tester, D. J., Kopplin, L. J., Will, M. L. and Ackerman, M. J. (2005b). Spectrum and prevalence of cardiac ryanodine receptor (RyR2) mutations in a cohort of unrelated patients referred explicitly for long QT syndrome genetic testing. *Heart Rhythm* **2**:1099-1105.

Tester, D. J., Spoon, D. B., Valdivia, H. H., Makielski, J. C. and Ackerman, M. J. (2004). Targeted mutational analysis of the RyR2-encoded cardiac ryanodine receptor in sudden unexplained death: a molecular autopsy of 49 medical examiner/coroner's cases. *Mayo Clin Proc* **79**:1380-1384.

Thomas, N. L., George, C. H. and Lai, F. A. (2004). Functional heterogeneity of ryanodine receptor mutations associated with sudden cardiac death. *Cardiovasc Res* **64**:52-60.

Thomas, N. L., Lai, F. A. and George, C. H. (2005). Differential Ca<sup>2+</sup> sensitivity of RyR2 mutations reveals distinct mechanisms of channel dysfunction in sudden cardiac death. *Biochem Biophys Res Commun* **331**:231-238.

Timerman, A. P., Wiederrecht, G., Marcy, A. and Fleischer, S. (1995). Characterization of an exchange reaction between soluble FKBP-12 and the FKBP.ryanodine receptor complex. Modulation by FKBP mutants deficient in peptidyl-prolyl isomerase activity. *J Biol Chem* **270**:2451-2459.

Tiso, N., Stephan, D. A., Nava, A., Bagattin, A., Devaney, J. M., Stanchi, F., Larderet, G. *et al.* (2001). Identification of mutations in the cardiac ryanodine receptor gene in families affected with arrhythmogenic right ventricular cardiomyopathy type 2 (ARVD2). *Hum Mol Genet* **10**:189-194.

Treves, S., Pouliquin, R., Moccagatta, L. and Zorzato, F. (2002). Functional properties of EGFP-tagged skeletal muscle calcium-release channel (ryanodine

receptor) expressed in COS-7 cells: sensitivity to caffeine and 4-chloro-m-cresol. *Cell Calcium* **31**:1-12.

Tung, C. C., Lobo, P. A., Kimlicka, L. and Van Petegem, F. (2010). The amino-terminal disease hotspot of ryanodine receptors forms a cytoplasmic vestibule. *Nature* **468**:585-588.

Tunwell, R. E., Wickenden, C., Bertrand, B. M., Shevchenko, V. I., Walsh, M. B., Allen, P. D. and Lai, F. A. (1996). The human cardiac muscle ryanodine receptor-calcium release channel: identification, primary structure and topological analysis. *Biochem J* **318** (Pt 2):477-487.

Uchinoumi, H., Yano, M., Suetomi, T., Ono, M., Xu, X., Tateishi, H., Oda, T. et al. (2010). Catecholaminergic polymorphic ventricular tachycardia is caused by mutation-linked defective conformational regulation of the ryanodine receptor. *Circ Res* **106**:1413-1424.

Voss, A. A., Lango, J., Ernst-Russell, M., Morin, D. and Pessah, I. N. (2004). Identification of hyperreactive cysteines within ryanodine receptor type 1 by mass spectrometry. *Journal of Biological Chemistry* **279**:34514-34520.

Wang, H., Viatchenko-Karpinski, S., Sun, J., Györke, I., Benkusky, N. A., Kohr, M. J., Valdivia, H. H. et al. (2010). Regulation of myocyte contraction via neuronal nitric oxide synthase: role of ryanodine receptor S-nitrosylation. *J Physiol* **588**:2905-2917.

Wang, J. P., Needleman, D. H. and Hamilton, S. L. (1993). Relationship of low affinity [3]ryanodine binding sites to high affinity sites on the skeletal muscle Ca<sup>2+</sup> release channel. *J Biol Chem* **268**:20974-20982.

Wang, J. P., Needleman, D. H., Seryshev, A. B., Aghdasi, B., Slavik, K. J., Liu, S. Q., Pedersen, S. E. et al. (1996). Interaction between ryanodine and neomycin binding sites on Ca<sup>2+</sup> release channel from skeletal muscle sarcoplasmic reticulum. *J Biol Chem* **271**:8387-8393.

Wang, R., Chen, W., Cai, S., Zhang, J., Bolstad, J., Wagenknecht, T., Liu, Z. et al. (2007). Localization of an NH(2)-terminal disease-causing mutation hot spot to the "clamp" region in the three-dimensional structure of the cardiac ryanodine receptor. *J Biol Chem* **282**:17785-17793.

Wang, R., Zhang, L., Bolstad, J., Diao, N., Brown, C., Ruest, L., Welch, W. et al. (2003). Residue Gln4863 within a predicted transmembrane sequence of the Ca<sup>2+</sup> release channel (ryanodine receptor) is critical for ryanodine interaction. *J Biol Chem* **278**:51557-51565.

Wang, R., Zhong, X., Meng, X., Koop, A., Tian, X., Jones, P. P., Fruen, B. R. et al. (2011). Localization of the dantrolene binding sequence near the FKBP binding site in the three-dimensional structure of the ryanodine receptor. *J Biol Chem*.

Watanabe, H., Chopra, N., Laver, D., Hwang, H. S., Davies, S. S., Roach, D. E., Duff, H. J. *et al.* (2009). Flecainide prevents catecholaminergic polymorphic ventricular tachycardia in mice and humans. *Nat Med* **15**:380-383.

Watanabe, H., Steele, D. S. and Knollmann, B. C. (2011). Mechanism of antiarrhythmic effects of flecainide in catecholaminergic polymorphic ventricular tachycardia. *Circ Res*. Vol. 109. United States, pp. 712-713.

Wehrens, X., Lehnart, S., Reiken, S., van der Nagel, R., Morales, R., Sun, J., Cheng, Z. *et al.* (2005). Enhancing calstabin binding to ryanodine receptors improves cardiac and skeletal muscle function in heart failure. *Proc Natl Acad Sci U S A* **102**:9607-9612.

Wehrens, X., Lehnart, S., Reiken, S., Vest, J., Wronska, A. and Marks, A. (2006). Ryanodine receptor/calcium release channel PKA phosphorylation: a critical mediator of heart failure progression. *Proc Natl Acad Sci U S A* **103**:511-518.

Wehrens, X. H., Lehnart, S. E., Huang, F., Vest, J. A., Reiken, S. R., Mohler, P. J., Sun, J. *et al.* (2003). FKBP12.6 deficiency and defective calcium release channel (ryanodine receptor) function linked to exercise-induced sudden cardiac death. *Cell* **113**:829-840.

Weinert, C., Grütter, C., Roschitzki-Voser, H., Mittl, P. R. and Grütter, M. G. (2009). The crystal structure of human pyrin b30.2 domain: implications for mutations associated with familial Mediterranean fever. *J Mol Biol* **394**:226-236.

Weiss, R. G., O'Connell, K. M., Flucher, B. E., Allen, P. D., Grabner, M. and Dirksen, R. T. (2004). Functional analysis of the R1086H malignant hyperthermia mutation in the DHPR reveals an unexpected influence of the III-IV loop on skeletal muscle EC coupling. *Am J Physiol Cell Physiol* **287**:C1094-1102.

Welch, W., Rheault, S., West, D. J. and Williams, A. J. (2004). A model of the putative pore region of the cardiac ryanodine receptor channel. *Biophys J* **87**:2335-2351.

Williams, G. S., Boyman, L., Chikando, A. C., Khairallah, R. J. and Lederer, W. J. (2013). Mitochondrial calcium uptake. *Proc Natl Acad Sci U S A* **110**:10479-10486.

Witcher, D. R., McPherson, P. S., Kahl, S. D., Lewis, T., Bentley, P., Mullinnix, M. J., Windass, J. D. *et al.* (1994). Photoaffinity labeling of the ryanodine receptor/Ca<sup>2+</sup> release channel with an azido derivative of ryanodine. *J Biol Chem* **269**:13076-13079.

Woo, J. S., Imm, J. H., Min, C. K., Kim, K. J., Cha, S. S. and Oh, B. H. (2006). Structural and functional insights into the B30.2/SPRY domain. *EMBO J* **25**:1353-1363.

Wright, N. T., Prosser, B. L., Varney, K. M., Zimmer, D. B., Schneider, M. F. and Weber, D. J. (2008). S100A1 and calmodulin compete for the same binding site on ryanodine receptor. *J Biol Chem* **283**:26676-26683.

Wright, N. T., Varney, K. M., Ellis, K. C., Markowitz, J., Gitti, R. K., Zimmer, D. B. and Weber, D. J. (2005). The three-dimensional solution structure of Ca(2+)-bound S100A1 as determined by NMR spectroscopy. *J Mol Biol* **353**:410-426.

Wu, Y., Aghdasi, B., Dou, S., Zhang, J., Liu, S. and Hamilton, S. (1997). Functional interactions between cytoplasmic domains of the skeletal muscle Ca2+ release channel. *J Biol Chem* **272**:25051-25061.

Xia, R., Stangler, T. and Abramson, J. J. (2000). Skeletal muscle ryanodine receptor is a redox sensor with a well defined redox potential that is sensitive to channel modulators. *Journal of Biological Chemistry* **275**:36556-36561.

Xiao, B., Masumiya, H., Jiang, D., Wang, R., Sei, Y., Zhang, L., Murayama, T. et al. (2002). Isoform-dependent formation of heteromeric Ca2+ release channels (ryanodine receptors). *J Biol Chem* **277**:41778-41785.

Xiao, B., Zhong, G., Obayashi, M., Yang, D., Chen, K., Walsh, M. P., Shimoni, Y. et al. (2006). Ser-2030, but not Ser-2808, is the major phosphorylation site in cardiac ryanodine receptors responding to protein kinase A activation upon beta-adrenergic stimulation in normal and failing hearts. *Biochem J* **396**:7-16.

Xiao, J., Tian, X., Jones, P. P., Bolstad, J., Kong, H., Wang, R., Zhang, L. et al. (2007). Removal of FKBP12.6 does not alter the conductance and activation of the cardiac ryanodine receptor or the susceptibility to stress-induced ventricular arrhythmias. *J Biol Chem* **282**:34828-34838.

Xiong, L., Newman, R., Rodney, G., Thomas, O., Zhang, J., Persechini, A., Shea, M. et al. (2002). Lobe-dependent regulation of ryanodine receptor type 1 by calmodulin. *J Biol Chem* **277**:40862-40870.

Xiong, L., Zhang, J., He, R. and Hamilton, S. (2006). A Ca2+-binding domain in RyR1 that interacts with the calmodulin binding site and modulates channel activity. *Biophys J* **90**:173-182.

Xu, L., Eu, J. P., Meissner, G. and Stamler, J. S. (1998a). Activation of the cardiac calcium release channel (ryanodine receptor) by poly-S-nitrosylation. *Science* **279**:234-237.

Xu, L. and Meissner, G. (1998). Regulation of cardiac muscle Ca2+ release channel by sarcoplasmic reticulum luminal Ca2+. *Biophys J* **75**:2302-2312.

Xu, L., Tripathy, A., Pasek, D. A. and Meissner, G. (1998b). Potential for pharmacology of ryanodine receptor/calcium release channels. *Ann N Y Acad Sci* **853**:130-148.

Xu, L., Tripathy, A., Pasek, D. A. and Meissner, G. (1999). Ruthenium red modifies the cardiac and skeletal muscle Ca(2+) release channels (ryanodine receptors) by multiple mechanisms. *J Biol Chem* **274**:32680-32691.

Xu, X., Yano, M., Uchinoumi, H., Hino, A., Suetomi, T., Ono, M., Tateishi, H. *et al.* (2010). Defective calmodulin binding to the cardiac ryanodine receptor plays a key role in CPVT-associated channel dysfunction. *Biochem Biophys Res Commun* **394**:660-666.

Yamaguchi, N., Prosser, B. L., Ghassemi, F., Xu, L., Pasek, D. A., Eu, J. P., Hernandez-Ochoa, E. O. *et al.* (2011). Modulation of sarcoplasmic reticulum Ca<sup>2+</sup> release in skeletal muscle expressing ryanodine receptor impaired in regulation by calmodulin and S100A1. *Am J Physiol Cell Physiol* **300**:C998-c1012.

Yamaguchi, N., Takahashi, N., Xu, L., Smithies, O. and Meissner, G. (2007). Early cardiac hypertrophy in mice with impaired calmodulin regulation of cardiac muscle Ca release channel. *J Clin Invest* **117**:1344-1353.

Yamaguchi, N., Xu, L., Evans, K. E., Pasek, D. A. and Meissner, G. (2004). Different regions in skeletal and cardiac muscle ryanodine receptors are involved in transducing the functional effects of calmodulin. *J Biol Chem* **279**:36433-36439.

Yamaguchi, N., Xu, L., Pasek, D. A., Evans, K. E. and Meissner, G. (2003). Molecular basis of calmodulin binding to cardiac muscle Ca(2+) release channel (ryanodine receptor). *J Biol Chem* **278**:23480-23486.

Yamamoto, T., El-Hayek, R. and Ikemoto, N. (2000). Postulated role of interdomain interaction within the ryanodine receptor in Ca(2+) channel regulation. *J Biol Chem* **275**:11618-11625.

Yamamoto, T. and Ikemoto, N. (2002a). Peptide probe study of the critical regulatory domain of the cardiac ryanodine receptor. *Biochem Biophys Res Commun* **291**:1102-1108.

Yamamoto, T. and Ikemoto, N. (2002b). Spectroscopic monitoring of local conformational changes during the intramolecular domain-domain interaction of the ryanodine receptor. *Biochemistry* **41**:1492-1501.

Yamamoto, T., Yano, M., Xu, X., Uchinoumi, H., Tateishi, H., Mochizuki, M., Oda, T. *et al.* (2008). Identification of target domains of the cardiac ryanodine receptor to correct channel disorder in failing hearts. *Circulation* **117**:762-772.

Yamazaki, H., Chan, J., Ikura, M., Michikawa, T. and Mikoshiba, K. (2010). Tyr-167/Trp-168 in type 1/3 inositol 1,4,5-trisphosphate receptor mediates functional coupling between ligand binding and channel opening. *J Biol Chem* **285**:36081-36091.

Yamazawa, T., Takeshima, H., Shimuta, M. and Iino, M. (1997). A region of the ryanodine receptor critical for excitation-contraction coupling in skeletal muscle. *J Biol Chem* **272**:8161-8164.

Yang, D., Pan, Z., Takeshima, H., Wu, C., Nagaraj, R. Y., Ma, J. and Cheng, H. (2001). RyR3 amplifies RyR1-mediated Ca(2+)-induced Ca(2+) release in neonatal mammalian skeletal muscle. *J Biol Chem* **276**:40210-40214.

Yang, T., Ta, T. A., Pessah, I. N. and Allen, P. D. (2003). Functional defects in six ryanodine receptor isoform-1 (RyR1) mutations associated with malignant hyperthermia and their impact on skeletal excitation-contraction coupling. *J Biol Chem* **278**:25722-25730.

Yang, Z., Ikemoto, N., Lamb, G. D. and Steele, D. S. (2006). The RyR2 central domain peptide DPc10 lowers the threshold for spontaneous Ca<sup>2+</sup> release in permeabilized cardiomyocytes. *Cardiovasc Res* **70**:475-485.

Yano, M., Kobayashi, S., Kohno, M., Doi, M., Tokuhisa, T., Okuda, S., Suetsugu, M. et al. (2003). FKBP12.6-mediated stabilization of calcium-release channel (ryanodine receptor) as a novel therapeutic strategy against heart failure. *Circulation* **107**:477-484.

Yano, M., Okuda, S., Oda, T., Tokuhisa, T., Tateishi, H., Mochizuki, M., Noma, T. et al. (2005). Correction of defective interdomain interaction within ryanodine receptor by antioxidant is a new therapeutic strategy against heart failure. *Circulation* **112**:3633-3643.

Ye, S., Kohrer, C., Huber, T., Kazmi, M., Sachdev, P., Yan, E. C., Bhagat, A. et al. (2008). Site-specific incorporation of keto amino acids into functional G protein-coupled receptors using unnatural amino acid mutagenesis. *J Biol Chem* **283**:1525-1533.

Yin, C., Blayney, L. and Lai, F. (2005a). Physical coupling between ryanodine receptor-calcium release channels. *J Mol Biol* **349**:538-546.

Yin, C., Han, H., Wei, R. and Lai, F. (2005b). Two-dimensional crystallization of the ryanodine receptor Ca<sup>2+</sup> release channel on lipid membranes. *J Struct Biol* **149**:219-224.

Yin, C. and Lai, F. (2000). Intrinsic lattice formation by the ryanodine receptor calcium-release channel. *Nat Cell Biol* **2**:669-671.

Yuchi, Z., Lau, K. and Van Petegem, F. (2012). Disease mutations in the ryanodine receptor central region: crystal structures of a phosphorylation hot spot domain. *Structure* **20**:1201-1211.

Zha, X.-m., Wang, R., Collier, D. M., Snyder, P. M., Wemmie, J. A. and Welsh, M. J. (2009). Oxidant regulated inter-subunit disulfide bond formation between ASIC1a subunits. *Proceedings of the National Academy of Sciences of the United States of America* **106**:3573-3578.

Zhang, H., Zhang, J., Danila, C. and Hamilton, S. (2003a). A noncontiguous, intersubunit binding site for calmodulin on the skeletal muscle Ca<sup>2+</sup> release channel. *J Biol Chem* **278**:8348-8355.

Zhang, J., Liu, Z., Masumiya, H., Wang, R., Jiang, D., Li, F., Wagenknecht, T. et al. (2003b). Three-dimensional localization of divergent region 3 of the ryanodine

receptor to the clamp-shaped structures adjacent to the FKBP binding sites. *J Biol Chem* **278**:14211-14218.

Zhang, J. Z., Wu, Y., Williams, B. Y., Rodney, G., Mandel, F., Strasburg, G. M. and Hamilton, S. L. (1999). Oxidation of the skeletal muscle Ca<sup>2+</sup> release channel alters calmodulin binding. *Am J Physiol* **276**:C46-53.

Zhao, F., Li, P., Chen, S. R., Louis, C. F. and Fruen, B. R. (2001). Dantrolene inhibition of ryanodine receptor Ca<sup>2+</sup> release channels. Molecular mechanism and isoform selectivity. *J Biol Chem* **276**:13810-13816.

Zhao, M., Li, P., Li, X., Zhang, L., Winkfein, R. J. and Chen, S. R. (1999). Molecular identification of the ryanodine receptor pore-forming segment. *J Biol Chem* **274**:25971-25974.

Zhou, H., Jungbluth, H., Sewry, C. A., Feng, L., Bertini, E., Bushby, K., Straub, V. et al. (2007). Molecular mechanisms and phenotypic variation in RYR1-related congenital myopathies. *Brain* **130**:2024-2036.

Zhou, Q., Wang, Q., Meng, X., Shu, Y., Jiang, T., Wagenknecht, T., Yin, C. et al. (2008). Structural and functional characterization of ryanodine receptor-natrin toxin interaction. *Biophys J* **95**:4289-4299.

Zhu, L., Zhong, X., Chen, S. R., Banavali, N. and Liu, Z. (2013). Modeling a ryanodine receptor N-terminal domain connecting the central vestibule and the corner clamp region. *J Biol Chem* **288**:903-914.

Zhu, X., Ghanta, J., Walker, J. W., Allen, P. D. and Valdivia, H. H. (2004). The calmodulin binding region of the skeletal ryanodine receptor acts as a self-modulatory domain. *Cell Calcium* **35**:165-177.

Zissimopoulos, S. and Lai, F. (2005a). Central domain of the human cardiac muscle ryanodine receptor does not mediate interaction with FKBP12.6. *Cell Biochem Biophys* **43**:203-219.

Zissimopoulos, S. and Lai, F. (2005b). Interaction of FKBP12.6 with the cardiac ryanodine receptor C-terminal domain. *J Biol Chem* **280**:5475-5485.

Zissimopoulos, S. and Lai, F. A. (2007). Ryanodine receptor structure, function and pathophysiology. In: Krebs, J. and Michalak, M. (eds.) *Calcium: A Matter of Life and Death*. 2007 Elsevier B.V.

Zissimopoulos, S., Seifan, S., Maxwell, C., Williams, A. J. and Lai, F. A. (2012). Disparities in the association of the ryanodine receptor and the FK506-binding proteins in mammalian heart. *J Cell Sci* **125**:1759-1769.

Zissimopoulos, S., Thomas, N. L., Jamaluddin, W. W. and Lai, F. A. (2009). FKBP12.6 binding of ryanodine receptors carrying mutations associated with arrhythmogenic cardiac disease. *Biochem J* **419**:273-278.

Zorzato, F., Fujii, J., Otsu, K., Phillips, M., Green, N. M., Lai, F. A., Meissner, G. *et al.* (1990). Molecular cloning of cDNA encoding human and rabbit forms of the Ca<sup>2+</sup> release channel (ryanodine receptor) of skeletal muscle sarcoplasmic reticulum. *J Biol Chem* **265**:2244-2256.

Zorzato, F., Scutari, E., Tegazzin, V., Clementi, E. and Treves, S. (1993). Chlorocresol: an activator of ryanodine receptor-mediated Ca<sup>2+</sup> release. *Mol Pharmacol* **44**:1192-1201.

Zvaritch, E., Kraeva, N., Bombardier, E., McCloy, R. A., Depreux, F., Holmyard, D., Kraev, A. *et al.* (2009). Ca<sup>2+</sup> dysregulation in Ryr1(I4895T/wt) mice causes congenital myopathy with progressive formation of minicores, cores, and nemaline rods. *Proc Natl Acad Sci U S A* **106**:21813-21818.